EVALUATION OF PORTLAND CEMENT CONCRETE CONTAINING RECLAIMED ASPHALT PAVEMENT FOR PAVEMENT APPLICATIONS

A Dissertation

by

XIJUN SHI

Submitted to the Office of Graduate and Professional Studies of
Texas A&M University
in partial fulfillment of the requirements for the degree of

DOCTOR OF PHILOSOPHY

Chair of Committee,	Dan Zollinger
Co-Chair of Committee,	Anol Mukhopadhyay
Committee Members,	Robert Lytton
	Zachary Grasley
	Vikram Kinra
Head of Department,	Robin Autenrieth

May 2018

Major Subject: Civil Engineering

ABSTRACT

Potential challenges associated with depletion of good aggregate sources and management of excess reclaimed asphalt pavement (RAP) stockpiles increasingly motivate use of RAP in portland cement concrete (PCC) as a coarse aggregate replacement. A number of the existing works on use of RAP in PCC for pavement applications only focused on testing mechanical properties of PCC containing RAP (RAP-PCC). The findings addressing other significant aspects, such as durability, failure mechanism, fracture properties, and pavement performance evaluation, are limited; approach to formulate RAP-PCC mixture with minimum strength reduction is not available from the previous work. The lack of a good understanding of RAP-PCC's behavior and its impact on pavement performance has hindered the implementation of RAP-PCC pavement in the field, and consequently may result in missing an opportunity for a potential good approach to use RAP.

Various aspects including mechanical properties, durability, microstructures, crack pattern, fracture properties, and pavement evaluation related to the use of RAP-PCC for pavement applications were comprehensively evaluated through robust experimental, analytical, and simulative approaches. The mechanical properties and durability of the RAP-PCC were tested through an extensive experimental program, followed by sufficient discussions of the results. An effective method using the total asphalt volumetric fraction to determine the optimum RAP replacement level in a RAP-PCC mixture was developed. The microstructures and crack pattern in the RAP-PCC system were subsequently investigated through several advanced techniques in order to provide scientific evidence and explanation for the RAP-PCC's behaviors observed in the lab. The fracture properties of the RAP-PCC were experimentally determined

through an innovative approach using specimens with semi-circular bending geometry. Finally, evaluation of the performance of rigid pavements containing RAP-PCC was carried out.

Based on the findings from this dissertation, RAP-PCC is a construction material with higher ductility and better fracture properties relative to conventional PCC. It meets the increasing need for sustainability and therefore should be greatly advocated. Although there may still be concerns on implementing single-lift pavement made of RAP-PCC at present, use of RAP-PCC as a bottom lift in a two-lift PCC pavement could be an alternative way to maximize the RAP usage with little compromise of pavement performance.

DEDICATION

To my wife, Xuan Zhou; my parents, Hantang Shi and Xiulan Shi; my parents-in-law, Hongyong Zhou and Shihong Jia

ACKNOWLEDGEMENTS

I would like to express my deepest appreciation to my committee chairs, Professor Dan Zollinger and Dr. Anol Mukhopadhyay, for their continued support and encouragement. It is not only their profound knowledge, but also their diligence, precision, and whole academic ethic, which guide and motivate me to overcome difficulties in this research. Without their assistance, this dissertation could not have been possible. I also owe many thanks to my committee members, Professor Robert Lytton, Professor Zachary Grasley and Professor Vikram Kinra, for their invaluable insight for this research.

I would like to acknowledge my research teammates, Dr. Kai-wei Liu, Younho Rew, Mengge Yuan, Chuhao Liu, Yunxing Lu, Jinmoe Kwon, Chong Suk Shin, Jiacheng Sheng, and Ryan George; they have spent a great deal of time assisting me with lab-related work. I also sincerely appreciate my friends from the Zachry Department of Civil Engineering at Texas A&M University for their continued assistance and encouragement. I will never forget the journey we shared during the past several years.

A special thanks to Professor John Dempsey from Clarkson University for his patiently and appropriately answering my questions regarding the derivation of the stress intensity factor and the crack opening displacement for the SCB geometry. A thanks also goes to Dr. Joshua Hogancamp for helping me with the mortar ring tests.

This research could not have been possible without the support from several facilities at Texas A&M University. The Materials Lab at Zachry Department of Civil Engineering allowed me to produce concrete specimens. The High-bay Structural and Materials Testing Lab helped me produce high quality concrete mechanical property testing data. The McNew Lab of Texas

A&M Transportation Institute provided me with testing equipment for various aggregate and asphalt tests. I appreciate all the assistance provided by the lab staff: Rick Canatella, Dave Dillon, Charlie Droddy, Matthew Potter and Ramiro Vanoye-Trevino.

I would like to take this opportunity to express my sincere gratitude to Professor Yunlong Zhang. Professor Zhang recruited me to Texas A&M University; he has provided invaluable guidance and support to me during my entire study at Texas A&M University.

Finally, I am extremely thankful for all the love, support, and patience from my family. This dissertation is dedicated to my family.

CONTRIBUTORS AND FUNDING SOURCES

CONTRIBUTORS

Faculty Committee Recognition

This work was supervised by a dissertation committee consisting of Professor Dan Zollinger (advisor), Dr. Anol Mukhopadhyay (co-advisor), Professor Robert Lytton, Professor Zachary Grasley of the Zachry Department of Civil Engineering, and Professor Vikram Kinra of the Department of Aerospace Engineering.

Student/Advisor Contributions

All work for the dissertation was completed by the student, under the advisement of Professor Dan Zollinger and Dr. Anol Mukhopadhyay of the Zachry Department of Civil Engineering.

FUNDING SOURCES

This work was made possible in part by the Texas Department of Transportation under research project number 0-6855 and by the Oklahoma Department of Transportation under research project number 2278. Dr. Anol Mukhopadhyay served as the principal investigator for both of the research projects.

The contents of this work are solely the responsibility of the author and do not necessarily represent the official views of the sponsors.

TABLE OF CONTENTS

LIST OF FIGURES

Page

LIST OF TABLES

Page

CHAPTER I

INTRODUCTION

I.1 BACKGROUND

Aggregate cost often comprises 20-30% of the material cost in concrete pavement. There is some concern that the days of having unlimited supplies of high quality virgin aggregates for concrete paving have gone (Hu et al. 2014). Many of the good aggregate sources have been depleted, resulting in a continuous increase in aggregate cost. The increase in aggregate cost is largely attributed to higher energy consumption during aggregate production and transportation together with higher expense to regulate the environment related issues (Hu et al. 2014). Due to the shortage of local aggregates as well as a chance to avail lowest bid price, contractors have been increasingly motivated to use recycled aggregate materials such as recycled concrete aggregate (RCA) and RAP to produce PCC. While the use of RCA in PCC has been extensively studied in the lab and successfully implemented in the field, the production of PCC containing RAP is still considered a relatively new but promising area, which attracts both industrial and academic interests.

Other motivations for utilization of RAP in PCC are related to the reduction of quantities of RAP stockpiles (Mukhopadhyay and Shi 2017b; Shi et al. 2017) (Figure 1). RAP is a material recycled from exiting HMA pavements. Over 90 percent of U.S. highways and roads are constructed with HMA (Copeland 2011). The Federal highway administration estimates that 100 million tons of HMA are milled each year (MAPA 2007). The increasing maintenance and rehabilitation actions of HMA pavement along with the restricted use of RAP in making new HMA generate excess RAP in some states. According to the latest asphalt pavement industry

survey on recycled materials and warm-mix asphalt usage (Hansen and Copeland 2017), the possession of excess RAP has been reported by 88% of U.S contractors, and the total estimated amount of RAP stockpiled nationwide was 85.1 million tons at the end of 2015. The expanding RAP stockpiling not only consumes more space and money, but also poses a threat to both environment and public safety.

Figure 1 RAP stockpile

With the increasing demands of sustainability, developing strategies for a better utilization of recycled material have become a hotter and hotter topic in the United States. A successful use of RAP in PCC not only saves money in purchasing and transporting virgin aggregates, but also reduces virgin aggregate consumption and pollutions related to quarrying and processing of natural aggregate. Additionally, the use of RAP to make PCC facilitates disposing excess RAP and avoids the challenges caused by RAP stockpiling.

While the lab-based research on the use of RAP to make PCC can probably date back to the 1970s and considerable amounts of effort haven been continuously made around the world in

the past 40 years to research RAP-PCC (Al-Oraimi et al. 2009; Berry et al. 2013; Brand et al. 2012; Delwar et al. 1997; Dumitru et al. 1999; Hassan et al. 2000; Huang et al. 2005; Kolias 1996; Mathias et al. 2004; Mukhopadhyay and Shi 2017b; Okafor 2010; Patankar and Williams 1970; Singh et al. 2017; Tia et al. 2012), the use of RAP in PCC has not yet been studied in a comprehensive manner for pavement applications. Most of the existing works published in the literature have only focused on testing mechanical properties of RAP-PCC with a very limited amount of findings addressing other aspects, such as failure mechanisms, fracture properties, and pavement performance evaluation of RAP-PCC. The pessimism about the use of RAP-PCC for pavement applications in some existing literature largely comes from the findings that the addition of RAP in PCC yielded a significant reduction in the mixture strength (especially compressive strength); no research has been carried out to systematically investigate the actual effect of RAP altered PCC properties on rigid pavement performance (both JPCP and CRCP). The inadequate characterization of RAP-PCC strengths only tends to underrate the performance of the pavement containing RAP-PCC. In fact, the reduced modulus, and improved ductility and fracture properties of RAP-PCC could potentially provide some benefits for the pavement, but such benefits have not been assessed yet. In addition, approach to formulate RAP-PCC mixture with minimum strength reductions is missing from the previous work. The lack of good understanding of RAP-PCC's behavior and its impact on pavement performance has hindered the implementation of RAP-PCC pavement in the field, and consequently may result in missing an opportunity for a potential good approach to use of RAP.

I.2 SCOPE AND OBJECTIVES

This dissertation presents an extensive study on evaluation of RAP-PCC to some extent through innovative approaches. It aids in filling the gaps of missing knowledge in RAP-PCC research through a better characterization of RAP-PCC. The utility of the improved characterization is manifested via a comprehensive analysis of the performance of rigid pavement containing RAP-PCC. Apparently, the use of RAP in HMA might still be a contractor's first consideration for the time being, which is mainly due indirectly that there is still a lack of experience and knowledge in producing RAP-PCC pavements. In this dissertation, several RAP samples from different Texas sources covering a wide range of gradation, rock type and asphalt content were collected, characterized and mixed into PCC. An extensive characterization of the RAP-PCC was carried out from different aspects such as mechanical properties, durability, and fracture properties. The microstructures and crack pattern in the RAP-PCC system have been investigated as well for a better interpretation of the RAP altered PCC properties. Subsequently, a detailed pavement evaluation on pavement distresses associated with both JPCP (fatigue and faulting) and CRCP (punchout) was conducted. Field data from evaluating the pavements built with RCA incorporated PCC (RCA-PCC) from the pavement sections in Oklahoma was used to assess the findings in the evaluation of RAP-PCC pavement. RCA-PCC is analogical to RAP-PCC because both manifest reduced MOE and increased coefficient of thermal expansion (CoTE) and ductility.

I.3 DISSERTATION ORGANIZATION

Chapter I introduces the backgrounds of this topic. The motivations of use RAP in PCC are clearly stated. The objectives and the organization of this dissertation are subsequently presented.

Chapter II reviews the relevant literature covering different aspects of this topic. The area of the missing research and the gaps in knowledge are identified. The specific goal and methodology of this dissertation are discussed.

Chapter III presents the experimental program of this dissertation. The testing procedures to characterize different RAP-PCC properties covering mechanical, durability and fracture aspects are described. The application of some micro-analytical techniques such as petrographic study using thin section specimens, SEM, and X-ray imaging analysis to explain the RAP-PCC's behaviors is introduced.

Chapter IV provides an extensive analysis and discussion of the testing results obtained from the experimental program. The effect of RAP on a wide range of PCC's properties is summarized and assessed. The potential influence of the RAP altered PCC property on pavement performance is discussed at the end of the chapter.

Chapter V evaluates the performance of rigid pavement containing RAP-PCC through the application of several pavement evaluation tools. The pros and cons of use of RAP in PCC for pavement application are discussed. Field data from evaluating single-lift concrete pavement built with RCA incorporated PCC (RCA-PCC) from both JPCP and CRCP pavement sections in Oklahoma was used to assess the findings.

Finally, Chapter VI concludes the findings of this research. Some important future work is mentioned as well.

CHAPTER II

LITERATURE REVIEW*

A detailed literature review was carried out in this chapter to identify the gaps of knowledge and the areas of further research related to the application of RAP-PCC for pavement applications. An attempt has been made to review the relevant publications addressing a wide range of aspects including mix design and fresh properties, mechanical properties, durability, microstructures, crack pattern, fracture properties, and pavement design of this topic. The key findings from the existing publications are summarized below.

II.1 REUSE OF RAP

RAP is generated when asphalt pavements are removed for reconstruction, resurfacing or to obtain access to buried utilities (Chesner et al. 1998). RAP contains mainly aggregate with adhering aged asphalt film and can be successfully reused for new construction. Unfractionated RAP usually contains more fines than natural aggregate due to generation of uncontrolled fines in the milling and crushing process. RAP can be typically obtained by cold milling or ripping followed by crushing. The RAP obtained from milling is generally finer and denser than that from ripping and crushing (Chesner et al. 1998). This large amount of fines in the RAP is likely to result in reduction in the load bearing capacity of a mix. As a result, it is often not recommended for constructing the parts of road that are crucial to the road's loading-bearing ability using RAP with large amount of fines (Robinson et al. 2004). The presence of aged

*Part of the contents in this chapter is reprinted with permission from:
Validation of RAP and/or RAS in Hydraulic Cement Concrete: Technical Report, by Mukhopadhyay, A., and Shi, X., 2017, Texas A&M Transportation Institute, Texas. Copyright [2017] by Texas A&M Transportation Institute.

asphalt also limits the RAP usage. Generally, the asphalt content of RAP ranges between 3 and 7 percent by weight (Robinson et al. 2004). Asphalt becomes stiffer with time when exposed to atmospheric factors as light constituents of asphalt volatilize and oxidize; the aged asphalt might have a higher rutting resistance but is usually more vulnerable to cracking. In order to mitigate this issue, asphalt recycling agents have been often added to RAP to restore aged asphalt to desired properties (Kandhal and Mallick 1998). Besides, RAP can be collected from various sources, whose properties can vary significantly depending on service life and ambient environment of the old pavement. Usually, RAP collected from most wearing surface exhibits relatively high viscosity. The large variability of the RAP properties add additional difficulty in the reuse of RAP.

II.2 RESTRICTED USE OF RAP IN HMA AND BASE

Hansen and Copeland (2017) conducted surveys of RAP usage in the United States. Their results show that the bulk of RAP is used in HMA or warm-mix asphalt (WMA) as being the optimal use. Besides the HMA/WMA application, RAP can also be used in base and cold mix application. RAP has been landfilled as well, but those amounts are fairly small (Figure 2).

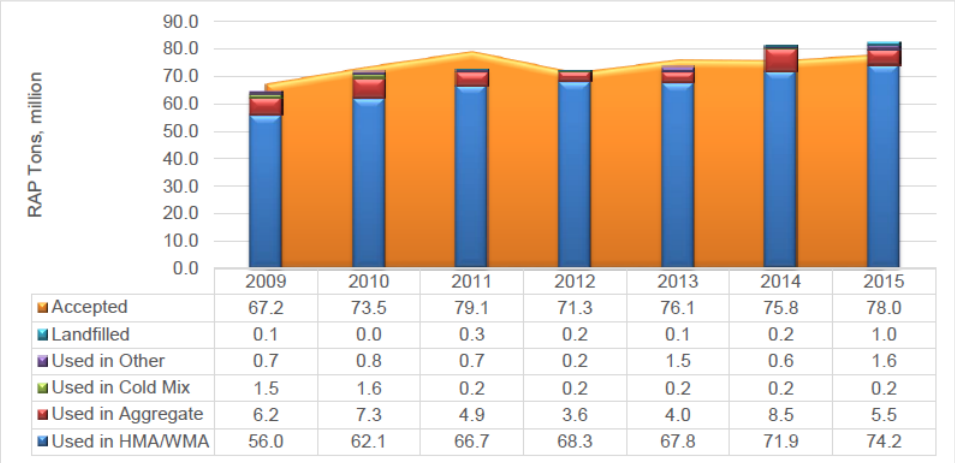

	2009	2010	2011	2012	2013	2014	2015
Accepted	67.2	73.5	79.1	71.3	76.1	75.8	78.0
Landfilled	0.1	0.0	0.3	0.2	0.1	0.2	1.0
Used in Other	0.7	0.8	0.7	0.2	1.5	0.6	1.6
Used in Cold Mix	1.5	1.6	0.2	0.2	0.2	0.2	0.2
Used in Aggregate	6.2	7.3	4.9	3.6	4.0	8.5	5.5
Used in HMA/WMA	56.0	62.1	66.7	68.3	67.8	71.9	74.2

Figure 2 Comparison of tons of RAP accepted and tons of RAP used or landfilled (million tons), 2009-2015 (Reprinted from Hansen and Copeland 2017)

Although RAP has been routinely used in HMA, most departments of transportation (DOTs) only allow the RAP fraction in the HMA up to 20 percent. The addition of RAP into a HMA mixture can alter the mixture properties significantly. While no problems with mixing and compacting asphalt concrete mixture with RAP were found (Yamada et al. 1987), adding RAP increased void in mineral aggregate and void filled with asphalt (Daniel and Lachance 2005). Based on Li et al. (2008), asphalt concrete containing RAP had higher dynamic modulus than the control with a greater influence at high temperature. The major concern which limits the use of RAP in HMA is that incorporation of high amounts of RAP may result in an "overly stiff" mixture. The "overly stiff" mixture not only can exhibit serious low-temperature cracking problems but also may crack prematurely when pavement is experiencing high deflections (Copeland 2011). Another issue of using RAP in HMA is related to producing low quality asphalt binder blends (i.e. virgin and RAP asphalt). The blended asphalt binder is more problematic especially when a high amount of RAP asphalt is introduced or RAP is blended with polymer modified binder (Copeland 2011). The restricted use of RAP in HMA has caused further RAP stockpiling.

Use of RAP as an unbound base material might be a potential construction strategy to reduce the volume of RAP stockpiles and facilitate sustainability. However, there are some challenges as well. When RAP percentage is high (more than 50%), the blended material might manifest unacceptably low shear strength, resulting in a larger pavement deformation (Dong and Huang 2013). In addition, the time-temperature dependency and large variation of RAP properties add more difficulty in ensuring the quality of base. Besides, putting RAP in an unbound base layer possibly poses an environmental risk due to leaching of chemicals. Although organic compounds do not leach from typical RAP, heavy metals such as chromium, lead, and barium are sometimes detected (Townsend 1998). Lead can exist in old RAP sources as a result of the traffic accidents and vehicle emissions. Pavements can be contaminated during gas spills since lead has been used in leaded gasoline and in crankcase oil for many years. Therefore, including RAP in a bonded material (such as PCC) might be the most environmentally friendly option. Due to the aforementioned concerns, most states only allow a partial use of RAP and require RAP to be blended with virgin aggregates in the base. According to McGarrah (2007), 50% is considered a common maximum percentage for including RAP in an unbound base.

II.3 USE OF RAP IN PCC

Lab-based research on the use of RAP in the manufacture of PCC probably dates back to the 1970s, followed by considerable amounts of effort around the world in the past 40 years (Al-Oraimi et al. 2009; Berry et al. 2013; Brand et al. 2012; Delwar et al. 1997; Dumitru et al. 1999; Hassan et al. 2000; Huang et al. 2005; Kolias 1996; Mathias et al. 2004; Mukhopadhyay and Shi 2017b; Okafor 2010; Patankar and Williams 1970; Singh et al. 2017; Tia et al. 2012). A recently growing interest in exploring alternative ways to use RAP has already motivated several state

transportation agencies to support projects related to use of RAP in making PCC (Berry et al. 2013; Brand et al. 2012; Mukhopadhyay and Shi 2017b; Tia et al. 2012). In 2012, Tia et al. (2012) from the University of Florida evaluated the mechanical properties of the RAP incorporated PCC. The research team selected four types of RAP to replace both coarse aggregates and fine aggregates in the conventional concrete mix covering a wide range of RAP replacement level (20%, 40%, 70% and 100%). The state of Illinois routinely fractionates RAP and forms coarse and fine stockpiles. While the fine RAP has been widely used in HMA, a numerous amount of coarse RAP stockpiles remain untouched, generating large disposal costs. The Illinois State Toll Highway Authority funded a study to evaluate the application of the coarse fractionated RAP in a cement-slag-fly ash ternary blend up to 50% replacement (Brand 2012). Another investigation was performed in the state of Montana. Berry et al. (2013) used a statistical experimental design procedure to formulate RAP-PCC mixtures. Two RAP-PCC mix designs were finalized and evaluated: One mix contained 50% of fine RAP and 100% of coarse RAP (they named as HR mix), and the other had 25% fine RAP and 50% coarse RAP in the concrete (named as HS mix). In 2017, the Texas A&M Transportation Institute completed a Texas DOT funded project (0-6855) titled *Validation of RAP and/or RAS in Hydraulic Cement Concrete.* In this project, the PCC mixtures containing coarse RAP up to 40% were extensively evaluated from different aspects (Mukhopadhyay and Shi 2017a; Mukhopadhyay and Shi 2017b). Some relevant findings from the existing publications on use of RAP in PCC for this research are summarized below.

II.4 FRESH AND HARDENED PROPERTIES OF RAP-PCC

II.4.1 Mix Design and Fresh Properties

Effects of RAP on Combined Aggregate Gradation

The gradation of RAP is often very different from the gradation of the original virgin aggregate used to make HMA. RAP gradation depends on the production process and the ambient environmental conditions of the original pavement. For a better gradation control, RAP is often fractionated into different stockpiles for different purposes. For example, the Illinois State Toll Highway Authority reprocessed their RAP to produce both coarse RAP and fine RAP stockpiles. They used a 4.75 mm sieve to separate the fine and coarse fractions. The coarse fraction underwent an additional screening by using a 12.5 mm or 15.6 mm sieve to remove the larger-size agglomerated particles and produce the coarse RAP (Brand et al. 2012). Usually, the portions of the intermediate (particles passing the 9.5 mm sieve and retained on the 2.36 mm sieve) and coarse (particles retained on 9.5 mm sieve) fractions in RAP are much higher than those in virgin concrete coarse aggregate. Based on the papers published by Huang et al. (2006) and Al-Oraimi et al. (2009), the coarse RAP is usually finer than the coarse limestone while the fine RAP is coarser than the sand, as shown in Figure 3 and Figure 4.

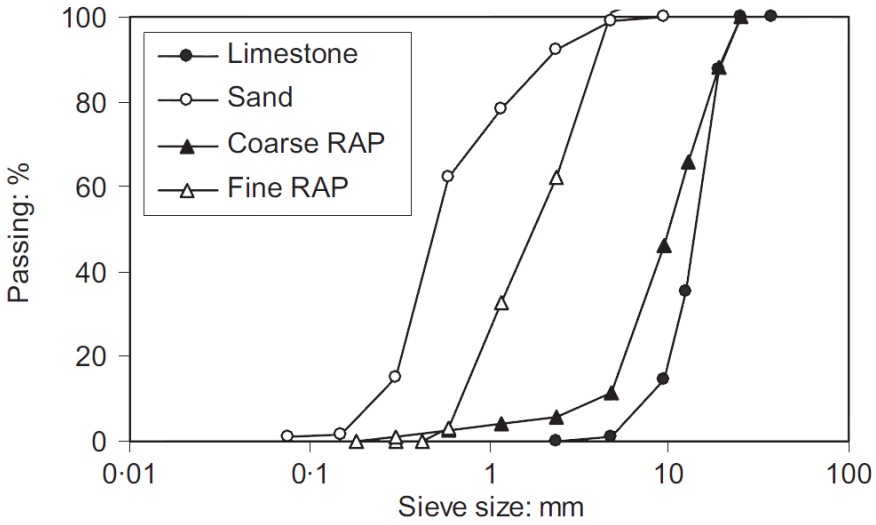

Figure 3 Gradations of limestone coarse aggregate, sand, and RAP materials (Reprinted from Huang et al. 2006)

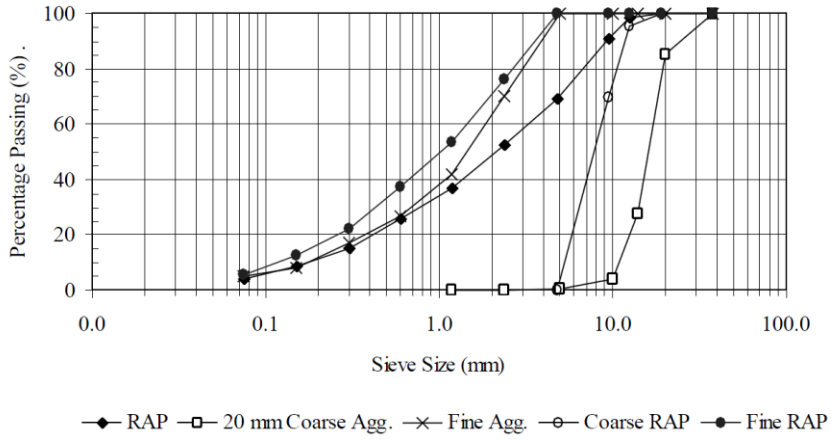

Figure 4 Gradations of different aggregate and RAP materials (Reprinted from Al-Oraimi et al. 2009)

Table 1 presents the results of the sieve analysis of the RAP samples collected in Texas by Zhou et al. (2011). The coarse RAP contained 47.5 percent of intermediate aggregate, and the binder content of the coarse RAP was much lower than that of the fine RAP. Because of containing a large fraction of the intermediate aggregates, the coarse RAP material can be used

to optimize concrete aggregate gradation, since most of the conventional concrete is gap-graded with a limited amount of intermediate aggregate particle sizes. Based on a detailed synthesis study (Richardson 2005), the potential benefits resulted from an optimized aggregate gradation can be significant. Richardson (2005) pointed out that the use of a more well-graded aggregate blend would result in less paste and reduced concrete shrinkage, greater strengths, better pumpability, and enhanced finishability. He also mentioned "well-graded mixtures tend not to have as many problems as gap-graded mixes in terms of pavement edge slump, segregation during vibration, finishing, raveling at joints, and wear resistance." According to Kim and Won (2008), the optimized aggregate gradation led to 9% higher flexural strength than a gap gradation. The reduction in shrinkage and coefficient of thermal expansion was also reported. Appendix A provides an overview of the approaches to optimize concrete aggregate gradation, among which the Shilstone's approach is highlighted and credited.

Table 1 Dry sieve analysis of the RAP samples collected in Texas (Reprinted from Zhou et al. 2011)

Sieve size (mm)	Ranges of cumulative % passing of RAP samples			
	TxDOT owned stockpiles, unfractionated RAP	Contractor owned stockpiles, crushed RAP	Contractor owned stockpile, crushed coarse RAP	Contractor owned stockpile, crushed fine RAP
19	100.0	100.0	100.0	100.0
12.5	97.7–99.2	98.1–98.4	97.5	99.8
9.5	91.4–92.0	91.4–92.7	84.5	98.8
4.75	65.1–72.2	67.5–74.5	54.5	85.2
2.36	45.0–46.8	46.5–56.3	37.0	58.7
1.18	32.9–35.0	35.0–44.3	26.2	45.2
0.6	24.6–28.1	28.3–34.2	19.8	38.0
0.3	18.0–19.4	22.3–24.0	14.5	28.1
0.15	11.8–12.0	13.1–15.8	7.5	15.1
0.075	7.5–7.6	8.1–11.6	3.6	7.5
Asphalt content (%)	5.4–7.9	4.4–5.3	2.8	5.3

There are very few existing studies on evaluation of the feasibility of using RAP to achieve optimized or enhanced aggregate gradation in PCC. Tia et al. (2012) selected four Florida DOT approved RAP and used a 4.75 mm sieve to fractionate the RAP into coarse and fine fractions. The virgin aggregates (both the coarse and fine) in the PCC mixtures were replaced by the selected RAP materials at replacement levels of 0 percent, 20 percent, 40 percent, 70 percent, and 100 percent. They evaluated the combined aggregate gradation based on the Shilstone's mix design optimization approach and made the following conclusions:

- Adding RAP with an adequate amount of intermediate size particles facilitated the improvement of a combined aggregate gradation
- The fineness modulus increased with an increasing amount of RAP
- The coarseness factor (CF), individual percent retained (IPR), and 0.45 power chart analysis suggested 40 percent RAP as the optimum level of replacement.

However, this research did not present any direct evidence of benefits resulted from the enhanced aggregate gradation with the addition of RAP.

Properties of Fresh Concrete

Properties of fresh concrete are of great importance because they are directly related to the choice of equipment for handling and consolidation and significantly affect the properties of hardened concrete. The effect of RAP on the properties fresh concrete is presented below.

Slump

Slump is an indicator of concrete workability. The addition of RAP into concrete caused a significant reduction in slump according to the most investigators (Al-Oraimi et al. 2009; Delwar et al. 1997; Huang et al. 2005; Okafor 2010; Tia et al. 2012). The higher the amount of RAP in the mixture, the lower the slump is. Huang et al. (2005) found coarse RAP aggregate has

less negative effect on concrete workability than fine RAP aggregate. This observation was likely due to a higher asphalt content in the fine RAP than the coarse RAP. Interestingly enough, they also reported that the mixture made with both coarse and fine RAP had a higher slump than the control mixture. Other than Huang et al. (2005), some researches also produced RAP-PCC mixtures with higher slumps compared to the control (Hossiney et al. 2010; Shi et al. 2017; Singh et al. 2017).

Percent Air Voids and Unit Weight

The addition of RAP into concrete appeared not to have a significant impact on percent air voids (Hossiney et al. 2010; Huang et al. 2005), but the decrease in unit weight was apparent (Al-Oraimi et al. 2009; Delwar et al. 1997; Tia et al. 2012). The decrease in unit weight is reasonable because asphalt is lighter compared to normal aggregate.

II.4.2 Mechanical Properties

Mechanical properties of hardened concrete are major indicators to manifest the feasibility of using RAP as an aggregate replacement in PCC. The mechanical properties of RAP-PCC mixtures have been extensively studied in the past. Those mechanical properties include compressive strength (CS), modulus of elasticity (MOE), flexural strength/modulus of rupture (MOR) and splitting tensile strength (STS). This section presents a detailed review of the RAP-PCC's mechanical properties.

Compressive Strength

Compressive strength is one of the most commonly used parameters to characterize concrete's quality. A number of studies have been conducted, which invariably concluded that the addition of RAP would reduce concrete's compressive strength (Al-Oraimi et al. 2009; Berry et al. 2013; Brand et al. 2012; Delwar et al. 1997; Hassan et al. 2000; Hossiney et al. 2010;

Huang et al. 2005; Katsakou and Kolias 2007; Mathias et al. 2004; Mukhopadhyay and Shi 2017b; Okafor 2010; Shi et al. 2017; Singh et al. 2017; Tia et al. 2012; Topcu and Isikdag 2009). Huang et al. (2005) evaluated the concrete mixtures made with different sized RAP and concluded that use of coarse RAP caused less reduction in compressive strength than fine RAP (Figure 5). Okafor (2010) replaced all of the virgin coarse aggregate with the coarse RAP but did not include any fine RAP in his study. He tested the compressive strengths of the mixtures with different water/cement (w/c) ratio. He believed that RAP-PCC could hardly yield a compressive strength exceeding 25 MPa because of the strength limit in asphalt-mortar bond (Figure 6). As shown in Figure 7, Hossiney et al. (2010) investigated the effects of the RAP replacement level (both the coarse and fine RAP replacement) on concrete compressive strength. Their results showed that concrete with higher amounts of RAP would have lower compressive strength. The findings reported by Tia et al. (2012) include: 1) the trend of strength development was similar between the RAP-PCC and the plain PCC and 2) the concrete mixtures with 100 percent RAP replacement (both coarse and fine) exhibited around 70 percent reduction in compressive strength. The project conducted in Illinois replaced virgin coarse aggregate with up to 50 percent of coarse RAP (Brand et al. 2012). Despite of the findings that the compressive strength of the mixture decreased by 39 percent for the 50 percent RAP replacement level, the research team still believed up to 50 percent of coarse RAP incorporation in a PCC mixture can be feasible to meet the Illinois DOT strength requirements for pavement applications. The research funded by the Montana DOT successfully produced RAP-PCC with a compressive strength that met the specification as well (Berry et al. 2013). They were able to allow a high amount of RAP and still met the strength specification because they used a control mix design which had a relatively high compressive strength (i.e., low w/cm and high cementitious content).

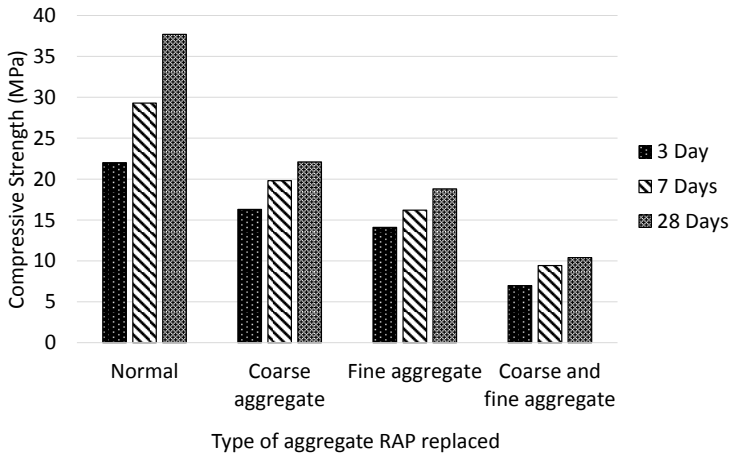

Figure 5 Effect of aggregate size on compressive strength (Re-plotted from Huang et al. 2005)

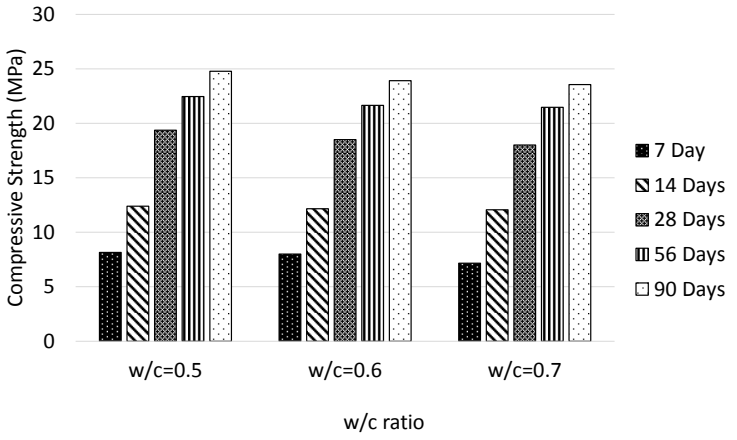

Figure 6 Effect of w/c ratio on compressive strength (Re-plotted from Okafor 2010)

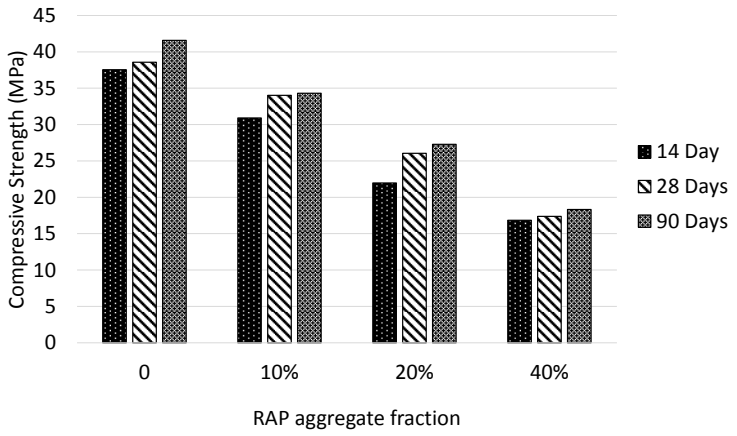

Figure 7 Effect of RAP aggregate fraction on compressive strength (Re-plotted from Hossiney et al. 2010)

Modulus of Rupture

Flexural strength, or modulus of rupture, is a measure of concrete tensile strength in an indirect manner. Similarly, all of the existing investigations showed that RAP-PCC has reduced MOR relative to the control. According to Katsakou and Kolias (2007) and Shi et al. (2017), the rate of reduction in flexural strength (reduction of strength versus RAP replacement level) was slower than the rate of reduction in the corresponding compressive strength for RAP-PCC. Similar to the compressive strength observations, Huang et al. (2005) found that introducing coarse RAP aggregates caused less reduction in flexural strength than fine RAP aggregates. The maximum reduction was reported as 50 percent when 100 percent of the virgin aggregates (both coarse and fine) were replaced by the RAP according to Tia et al. (2012). Both the Illinois Tollway project and the Montana DOT project obtained RAP-PCC with qualified flexural strengths (Berry et al. 2013; Brand et al. 2012).

Splitting Tensile Strength

Splitting tensile strength is an indirect measurement of concrete tensile strength, and is about 15% higher than the measurement from a direct tension test (Neville 1995). Tia et al. (2012) concluded that the STS of the RAP-PCC decreased with an increase of the RAP fraction in the mixture. A maximum reduction of 60 percent in STS was obtained when they applied the 100% RAP replacement. Mathias et al. (2004) investigated the splitting tensile behavior of the RAP-PCC under different temperatures. The found the higher the temperature, the lower the STS, and temperature had more significant influence on strength reduction at a higher RAP content. From the Illinois project, the researchers obtained a 52 percent STS reduction when 50 percent of the coarse RAP was added (Brand et al. 2012).

Modulus of Elasticity

Because asphalt has much lower modulus than cement paste at room temperature, it is not surprising to see that most of the investigators obtained a lower MOE of PCC made with RAP compared with the controls (Al-Oraimi et al. 2009; Berry et al. 2013; Brand et al. 2012; Katsakou and Kolias 2007; Mathias et al. 2004; Shi et al. 2017; Tia et al. 2012; Topcu and Isikdag 2009). The effect of RAP on the MOE reduction is significant. According to Tia et al. (2012), the maximum reduction could be up to 70 percent when they compared the PCC made with 100 percent RAP aggregates with the control PCC at 90 days. According to another finding obtained by Brand et al. (2012), the addition of 50 percent of the coarse RAP reduced the MOE by 30 percent. Berry et al. (2013) reported a reduction of 46 percent in the MOE for their HR mix (100 percent coarse RAP replacement and 50 percent fine RAP replacement) and a reduction of 17 percent for their HS mix (50 percent coarse RAP replacement and 25 percent fine RAP replacement) at the age of 28 days by comparing the RAP-PCC with the control concrete.

Relationship between Mechanical Properties

Concrete compressive strength might be the easiest parameter to obtain in the lab and field. The American Concrete Institute (ACI) adopted equations to calculate other properties by using compressive strength despite the fact that these equations might not be very applicable to field mixtures. Based on the experimental results of the RAP-PCC mixtures, Tia et al. (2012) developed new equations to estimate properties of concrete made with RAP. Table 2 summarizes the equations for RAP concrete with comparisons of the ACI equations.

Table 2 Comparison between the ACI Equations and Tia et al. (2012) equations

Mechanical property	ACI equations for normal concrete	Tia et al. (2012) equations for RAP concrete	Feasibility of using ACI equations to predict RAP concrete
MOR	$\mathrm{MOR} = 7.5 \times f_c^{0.5}$	$\mathrm{MOR} = 9.25 \times f_c^{0.5}$	ACI equation underestimates the prediction of the RAP concrete
MOE	$\mathrm{MOE} = 57 \times f_c^{0.5}$	$\mathrm{MOE} = 54.665 \times f_c^{0.5}$	ACI equation overestimates the prediction of the RAP concrete
STS	$\mathrm{STS} = 6.7 \times f_c^{0.5}$	$\mathrm{STS} = 1.5623 \times f_c^{0.6791}$	No conclusion made by the authors

Applicable unit: fc-psi; MOR-psi; MOE-ksi; STS-psi

II.4.3 Other Pavement-related Properties

The effect of RAP on some other pavement related properties of PCC is reviewed. These reviewed pavement related properties include Poisson's ratio and CoTE. The addition of RAP should also alter PCC's thermal properties (i.e., thermal conductivity and heat capacity), but no existing data has been found from the existing publications.

Poisson's Ratio

Very limited information is available regarding the RAP-PCC Poisson's ratio results. The only available finding was reported by Tia et al. (2012):

- The Poisson's ratio increased when RAP percentage increased.

- The values for the PCC made with no RAP, intermediate RAP fraction (20 percent, 40 percent, and 70 percent), and high RAP fraction (100 percent) were between 0.20 and 0.25, close to 0.25, and between 0.25 and 0.30, respectively.
- Poisson's ratio increased with increased curing days.

CoTE

The only available CoTE data for RAP-PCC was also reported by Tia et al. (2012). They found that the addition of RAP would increase PCC's CoTE. The higher the RAP content, the higher the CoTE of the mixture.

II.5 DURABILITY

Durability is another important aspect that significantly affects PCC performance. It is very necessary to evaluate the mixture's durability such as freeze-thaw resistance, rapid chloride permeability, shrinkage, and abrasion resistance, especially when recycled material such as RAP is involved in the concrete. A review of the existing findings on the durability of RAP-PCC is presented subsequently.

II.5.1 Rapid Chloride Permeability

The amount of the existing results for the RAP-PCC rapid chloride penetration test is limited. Brand et al. (2012) conducted the rapid chloride penetration test for the ternary blended RAP-PCC mixtures based on the American Association of State Highway and Transportation Officials (AASHTO) T277. They concluded that replacing the virgin coarse aggregate with the fractionated coarse RAP at different replacement level yielded very similar rapid chloride permeability results. The level of the ion penetration ranged from very low to low for all the studied mixtures. Berry et al. (2013) reported the chloride permeability results for their HR and

HS mixes according to ASTM C1202. Based on their results, a moderate level of chloride ion penetrations was reported for both HR and HS mixes. From the comparison between the HR and the HS mix, it was concluded that a higher amount of RAP in the mix caused a higher chloride ion penetrability.

II.5.2 Freeze-thaw Resistance

According to Brand et al. (2012), the durability factor decreased with an increase of coarse RAP fraction. But still, all their results were above the limiting value of 80 in the AASHTO T161 specification. From their findings, the samples with 20 percent RAP content had similar freeze/thaw durability with the controls, but both the 35 percent and 50 percent coarse RAP-PCC mixtures experienced slightly greater reductions in durability factor and mass loss than the control. Berry et al. (2013) reported an averaged durability factor of 94 for the HR mix and a factor of 98 for the HS mix after 300 freeze/thaw cycles, while the control mix had a value of 100 with no loss of stiffness. Both of the mixes had less than 1 percent mass loss. The observation that the HR mix had a slightly smaller durability factor and a slightly higher mass loss indicated that a larger amount of RAP is likely to have a more significant reduction in the freeze/thaw resistance.

II.5.3 Abrasion Resistance

To evaluate the abrasion resistance of the RAP-PCC, Berry et al. (2013) first used a 10-kg load to abrade the surface of the HR and HS mixes according to ASTM C944. The resulting averaged mass loss turned out to be 0.3 g with a less than 1.0 mm wear depths for both cases. These results indicated that the RAP-PCC samples performed well, so a further investigation was conducted by using a 20-kg load. Again, little weight loss and wear depth were reported for both samples.

II.5.4 Shrinkage

The results from Topcu and Isikdag (2009) showed replacing all of the virgin aggregates with RAP resulted in a 40 percent increase in shrinkage. The authors interpreted this observation as a result of a less restraint in cement paste because of a lower MOE of the RAP-PCC. Tia et al. (2012) found, in general, the shrinkage of RAP-PCC under an air curing process increased when the RAP fraction increased. For the concrete undergoing a moist curing process, the RAP-PCC specimens showed a significant length change before 28 days, but the change after 28 days was small. Based on the results from Brand et al. (2012), there was no clear trend of length changes in free shrinkage. However, the ring shrinkage tests indicated that adding the coarse RAP reduced the restraint-induced shrinkage strains, suggesting the RAP-PCC might have less cracking potential. The investigations conducted in Montana showed that neither of the two mixes exhibited excessive deformations associated with shrinkage (Berry et al. 2013).

II.6 MICROSTRUCTURE

RAP contains aggregates partially or fully covered by aged asphalt films. The effect of the asphalt films on the development of the PCC's microstructural features is very important to interpret PCC's overall behaviors. A limited amount of literature on this topic is available. Sachet et al. (2013) examined the fractured surface of the RAP incorporated roller-compacted concrete using the scanning electron microscopy (secondary electron) and suggested an adhesion failure between the cement paste and RAP. Brand and Roesler (2017a) used the SEM-backscattered imaging technique followed by an image analysis to quantify the amount and distribution of detectable porosity, un-hydrated cement, and calcium hydroxide in the cement mortar containing fine RAP. They observed that the cement mortar containing fine RAP had

larger, more porous interfacial transition zone (ITZ) and believed this abnormal ITZ caused strength and modulus reductions. They also found the calcium hydroxide (CH) morphology was not significantly affected, but the presence of asphalt layer might have affected the CH growth.

Saïd et al. (2017) believed the adhesion between cement paste and RAP aggregate was poor by identifying a presence of voids between these two constituents from the SEM images. They used the Laboratoire Central des Ponts et Chaussées (LCPC) model to determine the adhesion and threshold parameters for the studied RAP-PCC materials and found the threshold parameter remained constant for all RAP contents while the adhesion parameter decreased with the increase of RAP content.

II.7 CRACK PATTERN

The crack pattern and failure mechanism of RAP-PCC were studied through a few investigations in the past. Huang et al. (2005) stated that the asphalt film coating of RAP aggregate particles facilitated the crack propagation along the asphalt film around RAP aggregate particles instead of passing through the aggregate, which resulted in an increase in energy dissipation through a longer and more tortuous crack pattern (Figure 8).

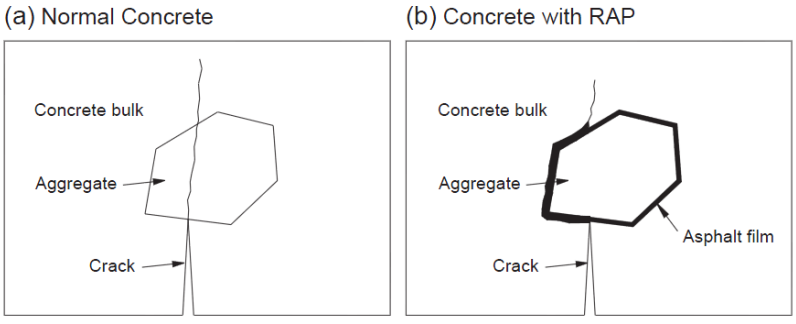

Figure 8 Crack propagation in concrete and concrete with RAP (Reprinted from Huang et al. 2005)

Brand and Roesler (2017a) believed that the strength and modulus reductions of cement mortar containing fine RAP were partially due to the existence of larger, more porous ITZ. In order to improve the cement-asphalt bond in the RAP-PCC system, they treated RAP with several types of chemical oxidative but the bonding improvement was not very significant. Based on the surface free energy measurement and visual inspections of the failure surface of the beam samples, they concluded that the asphalt cohesion failure was the dominating failure mode in the RAP-PCC system. Accordingly, the reductions of RAP-PCC's strength and modulus were contributed to a combined effect of the higher porosity in ITZ and the preferential asphalt cohesion failure (Brand and Roesler 2017b).

II.8 TOUGHNESS, DUCTILITY, AND FRACTURE PROPERTIES

Despite of strength reductions, portland cement concrete pavement containing RAP aggregates could still yield equivalent performance as the conventional PCCP based on the findings from some existing field demonstrations (Bentsen et al. 2013; Bergren and Britson 1977; Berry et al. 2015; Bilodeau et al. 2011; Gillen et al. 2012; Wojakowski 1998), the large scale slab test (Brand et al. 2014) and the slab load capacity analysis (Tia et al. 2012), as will be reviewed below. This inconsistency might be attributed to the size effect (Bažant and Oh 1983): the strength testing results from conventional lab sized specimens might not be applicable for pavement structure which has a larger scale. The size of pavement structure is within the application range of nonlinear fracture mechanics. Accordingly, the use of RAP-PCC fracture properties in addition to the conventional strength based criteria should be more effective to evaluate pavement performances. In the following sections, the two-parameter fracture model (TPFM) together with the existing experimental methods to evaluate concrete two-parameter

fracture properties (TPFP) is reviewed, followed by a presentation of some existing findings for the toughness, ductility and fracture properties of the RAP-PPC. Some of the additional concrete fracture mechanics theory relevant to this current work is reviewed in Appendix B.

II.8.1 Two-parameter Fracture Model by Jenq and Shah

Jenq and Shah (1985) proposed a two-parameter fracture model using the elastic response of concrete structures (Figure 9 (a)) based on the effective elastic crack approach. Their theory states that the crack mouth opening displacement can be divided into an elastic and an inelastic component:

$$\mathrm{CMOD_c} = \mathrm{CMOD_c^e} + \mathrm{CMOD_c^p} \tag{1}$$

The inelastic component can be separated from a loading and unloading procedure of the experiment (Figure 9 (b)), which is excluded from the calculation of the two-parameter fracture properties. The two parameters are the critical stress intensity factor, $\mathrm{K_{Ic}^s}$, and the critical crack tip opening displacement, $\mathrm{CTOD_c}$. Both of them are determined based on linear elastic fracture mechanics (LEFM) theory:

$$\mathrm{K_{Ic}^s} = \sigma_c\sqrt{\pi \mathrm{A_c}}\,\mathrm{g_1}\left(\frac{\mathrm{A_c}}{\mathrm{b}}\right) \tag{2}$$

$$\mathrm{CTOD_c} = \mathrm{CMOD_c^e}\,\mathrm{g_3}\left(\frac{\mathrm{A_c}}{\mathrm{b}}, \frac{\mathrm{A_0}}{\mathrm{a_c}}\right) \tag{3}$$

Where $\mathrm{A_c}$ is the critical effective elastic crack length, which can be solved for from Equation (4):

$$\mathrm{CMOD_c^e} = \frac{4\sigma_c \mathrm{A_c}}{\mathrm{E}}\,\mathrm{g_2}\left(\frac{\mathrm{A_c}}{\mathrm{b}}\right) \tag{4}$$

And $\mathrm{g_1}, \mathrm{g_2}, \mathrm{g_3}$ are all geometric functions.

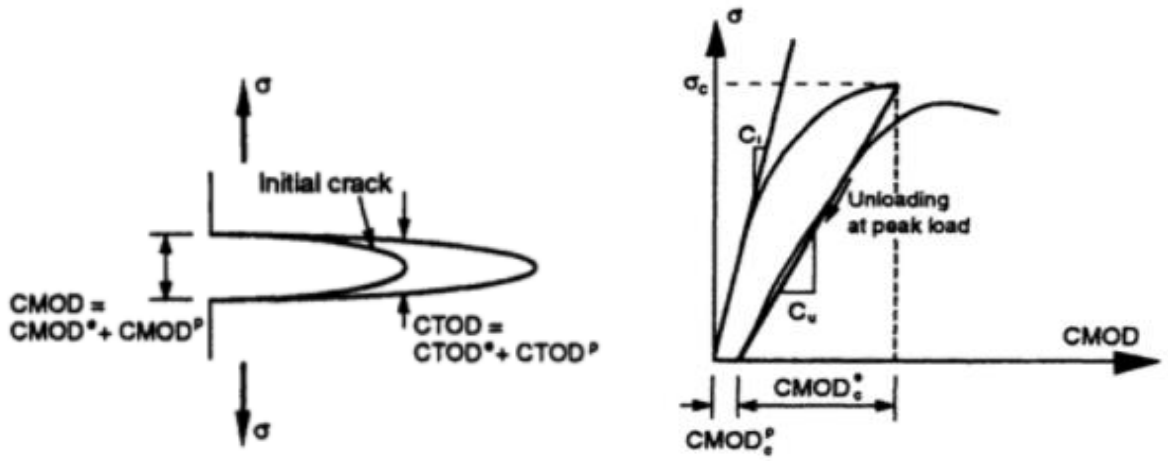

(a) Elastic and plastic fracture responses (b) Loading and unloading procedure

Figure 9 Two-parameter fracture properties model (Reprinted from Shah et al. 1995)

From the Jenq and Shah's theory, the two-parameter fracture properties are considered material properties; they are independent from the size and geometries of the structure. At the critical fracture of the material, the following two conditions need to be satisfied (Figure 10). This is the criteria of the two-parameter fracture model:

$$K_I = K_{Ic}^s \tag{5}$$

$$CTOD = CTOD_c \tag{6}$$

Where K_I and $CTOD$ are the stress intensity factor and the crack tip opening displacement, respectively. Both of them are functions of the applied load, structural geometry and size, and the crack length.

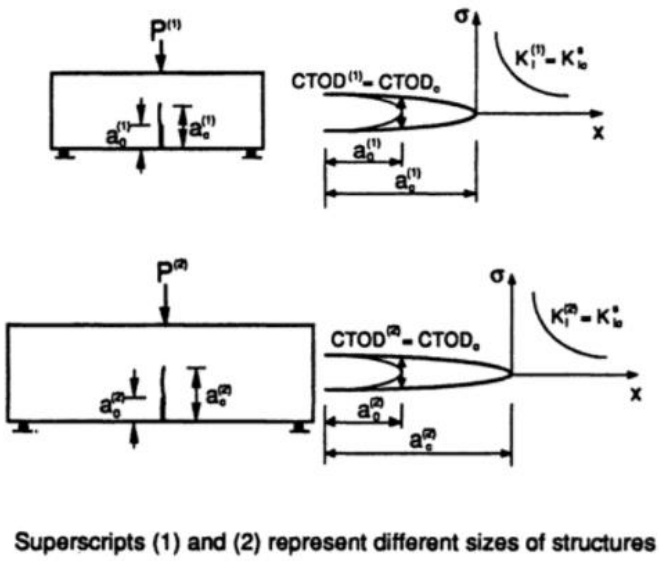

Figure 10 Two-parameter fracture model criteria (Reprinted from Shah et al. 1995)

With the K_{Ic}^{s} and $CTOD_c$ of a quasi-brittle material, some other material properties can be determined. Jenq and Shah (1985) introduced a material length, Q, which is expressed as:

$$Q = \left(\frac{E\ CTOD_c}{K_{Ic}^{s}}\right)^2 \tag{7}$$

Q is considered proportional to the size of the fracture process zone for a given material and can be used to quantify the material's brittleness (i.e., a higher Q indicates a more ductile material). The ranges of the Q were found to be 12.5-50 mm for hardened cement paste, 50-150 mm for mortar and 150-350 mm for concrete.

The theoretical tensile strength of a material can be estimated with the following equation (Shah et al. 1995):

$$f_t = 1.4705\frac{(K_{Ic}^{s})^2}{E\ CTOD_c} \tag{8}$$

John and Shah (1989) empirically related the two parameters with the compressive strength of conventional concrete:

$$K_{Ic}^{s} = 0.06(f_c')^{0.75} \quad (9)$$

$$CTOD_c = 0.00602(f_c')^{0.13} \quad (10)$$

$$E = 4785(f_c')^{0.5} \quad (11)$$

With K_{Ic}^{s} in $\sqrt{in.}$, $CTOD_c$ in in., E in psi, and f_c' in psi

The fracture behavior of concrete can be predicted using finite element methods. A cohesive zone model with a bilinear softening relation is usually used. The bilinear softening curve is shown in Figure 11.

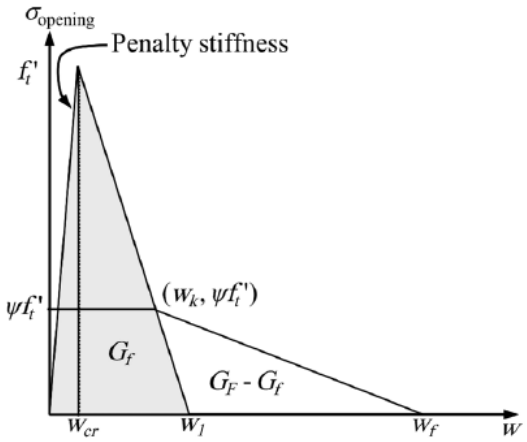

Figure 11 Cohesive zone model with a bilinear softening relation (Reprinted from Amirkhanian et al. 2015)

In the model, two energy parameters, namely the initial fracture energy G_f and the total fracture G_F are determined as:

$$G_f = \frac{(K_{Ic}^{s})^2}{E} \quad (12)$$

$$G_F = \frac{\int_0^{\delta_f} P d\delta}{BW} \quad (13)$$

Where δ_f is the ultimate load point displacement when the load P=0, B is the specimen thickness and W is the length of the uncracked ligament.

The location of the kink point in Figure 11 is determined as (Park et al. 2008):

$$w_k = CTOD_c \tag{14}$$

$$\psi = 1 - \frac{CTOD_c f_t}{2G_f} \tag{15}$$

The w_{cr} in Figure 11 is the crack opening displacement at the peak load, while w_f is the ultimate opening displacement:

$$w_1 = \frac{2G_f}{f_t} \tag{16}$$

$$w_f = \frac{2}{\psi f_t}[G_F - (1-\psi)G_f] \tag{17}$$

II.8.2 Existing Methods to Test Concrete TPFP through Various Geometries

RILEM Method Using a Three-point Bend Beam

The International Union of Laboratories and Experts in Construction Materials, System and Structures (RILEM) Technical Committee 89-FMT on Fracture Mechanics of Concrete-Test Method recommended to test concrete two-parameter fracture properties (K_{Ic}^s and $CTOD_c$) through a single edge notched beam (SEN(B)) (Figure 12). The recommendations on the dimensions of the concrete beam sample include (1) a span to depth ratio (S/b) of 4, (2) the initial notch-to-depth ratio of 1/3 and (3) the width of notch is less than 5 mm. The test requires a minimum of 4 specimens for each type of material.

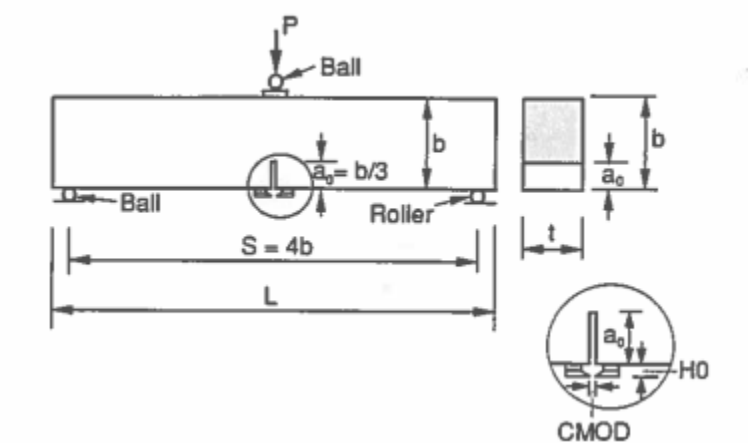

Figure 12 SEN(B) fracture test set-up (Reprinted from Shah et al. 1995)

A closed-loop testing machine using the CMOD as the control signal or a relatively stiff machine is required to ensure a stable failure of the sample. A clip-on gage or an LVDT is used for recording CMOD. The rate of the loading shall be controlled so that the peak load can be reached in about 5 minutes. The test follows the following procedures (Shah et al. 1995):

1. Load the specimen monotonically up to the maximum load
2. Manually release the load when it passes the maximum load and within 95% of the maximum load
3. When the applied load is reduced to zero, reload the specimen until sufficient data is recorded

Figure 13 shows a typical load-CMOD curve with the loading and unloading cycle. The modulus of elasticity, E, calculated from the loading portion of the curve is written (Brand et al. 2012):

$$E = \frac{6Sa_0g_2(a_0)}{C_i b^2 t} \tag{18}$$

Where C_i is the initial compliance calculated from the load-CMOD curve

t is the beam width

S is the span length

$g_2(a)$ is the geometric function of the crack length ratio $a = \frac{A}{D}$.

$$g_2(a) = 0.76 - 2.28a + 3.87a^2 - 2.04a^3 + \frac{0.66}{(1-a)^2} \quad (19)$$

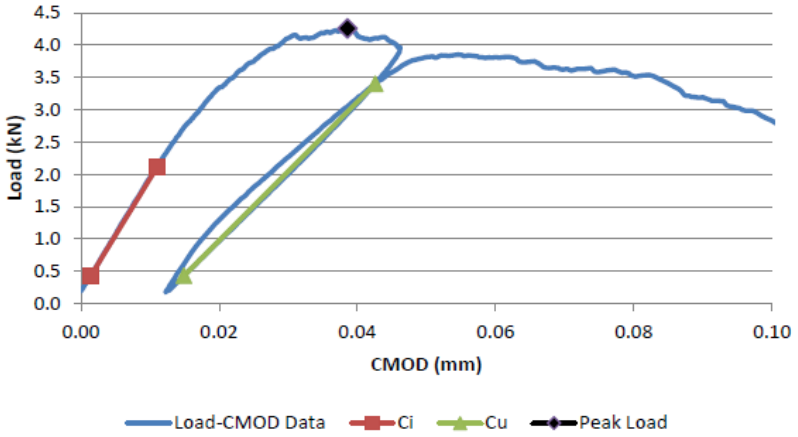

Figure 13 Typical load-CMOD curve (Reprinted from Brand et al. 2012)

From the unloading portion of the curve:

$$E = \frac{6Sa_0 g_2(a_c)}{C_u b^2 t} \quad (20)$$

By equating Equation (18) and (20), the value of the effective-elastic critical crack length ratio a_c can be solved with the following expression:

$$a_c = a_0 \frac{C_u}{C_i} \frac{g_2(a_0)}{g_2(a_c)} \quad (21)$$

The critical stress intensity factor is then calculated based on the LEFM theory:

$$K_{Ic}^s = 3(P_c + 0.5W_h) \frac{S\sqrt{\pi a_c} g_1(a_c)}{2b^2 t} \quad (22)$$

Where P_c is the peak load and

$$W_h = \frac{W_{h0} S}{L} \quad (23)$$

Where W_{h0} is the self-weight of the beam.

L is the beam length

The geometry function g_1 is written as:

$$g_1(a_c) = \frac{1.99 - (a_c)(1 - a_c)[2.15 - 3.93a_c + 2.70(a_c)^2]}{\sqrt{\pi}(1 + 2a_c)(1 - a_c)^{3/2}} \quad (24)$$

The critical crack tip opening, $CTOD_c$, is then calculated using Equation (25):

$$CTOD_c = \frac{6(P_c + 0.5W_h)Sa_c g_2(a_c)}{Eb^2 t}[(1 - \beta_0)^2 + (1.081 - 1.149a_c)(\beta_0 - \beta_0^2)]^{1/2} \quad (25)$$

Where $\beta_0 = \frac{A_0}{A_c}$

Amirkhanian et al. Method using a Disk-shaped Compact Tension Test

Analogous to the RILEM method, Amirkhanian et al. (2015) designed a test to characterize K_{Ic}^S and $CTOD_c$ of concrete using a disk-shaped compaction tension (DCT) geometry to overcome the difficulty of extracting beams from field. The test set-up is shown in Figure 14. This method uses a same loading and unloading procedure specified in the RILEM test. The modulus of elasticity of concrete is obtained in Equation (26):

$$E = \frac{2V_{CMOD}(a)}{C_{i,u} B} \quad (26)$$

Where

$$V_{CMOD}(a) = \frac{501.8a^3 + 2294a^2 + 4393a + 1384}{a^4 + 272.2a^3 - 139.8a^2 - 569.3a + 433.9} \quad (27)$$

And B is the specimen thickness

Similarly, the critical effective-elastic crack length ratio a_c can be solved for by assuming the equivalency of loading and unloading modulus of elasticity:

$$V_{CMOD}(a_c) = \frac{C_u}{C_i} V_{CMOD}(a_0) \tag{28}$$

The critical stress intensity factor and the critical crack tip opening displacement are calculated as:

$$K_{Ic}^{s} = \frac{P}{WB}\sqrt{W}F(a_c) \tag{29}$$

Where

$$F(a) = \frac{-1.498a^3 + 4.569a^2 - 1.078a + 0.113}{a^4 - 2.408a^3 + 1.717a^2 - 0.3467a + 0.0348} \tag{30}$$

$$CTOD_c = \frac{2PV_{CTOD}(a_c)}{BE} \tag{31}$$

Where

$$V_{CTOD}(a) = \frac{6.639a^3 - 3.209a^2 + 0.4169a - 0.006899}{a^4 - 2.429a^3 + 1.897a^2 - 0.5137a + 0.04504} \tag{32}$$

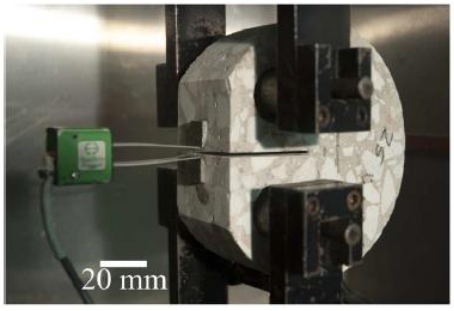

Figure 14 DCT fracture test set-up (Reprinted from Amirkhanian et al. 2015)

II.8.3 Toughness, Ductility, and Fracture Properties of RAP-PCC

Huang et al. (2005) demonstrated that the longer and more tortuous crack pattern could help dissipate more energy during the fracture in RAP-PCC. They also found that the RAP-PCC mixtures did not fail as abruptly as the control mixture under the splitting tensile test. It seems

that the RAP-PCC mixtures were capable to maintain the peak load longer while undergoing longer displacement (Figure 15). They then calculated the toughness of the materials by integrating the area under the splitting tensile load-deformation curve and found the toughness of the PCC containing coarse RAP only, fine RAP only, and both coarse and fine RAP was 1.9, 1.3 and 2.3 times of the control mixture after 14 day of moisture curing, respectively. Similarly, Tia et al. (2012) conducted the flexural beam tests to infer the toughness and ductility of the RAP-PCC mixtures. Although the concrete made with RAP failed at lower stress, the failure strain and the area under stress-strain curve increased with the increasing content of RAP. Hassan et al. (2000) and Su et al. (2014) verified the toughness improvement of RAP-PCC with the flexural test and Superpave indirect tensile strength test, respectively.

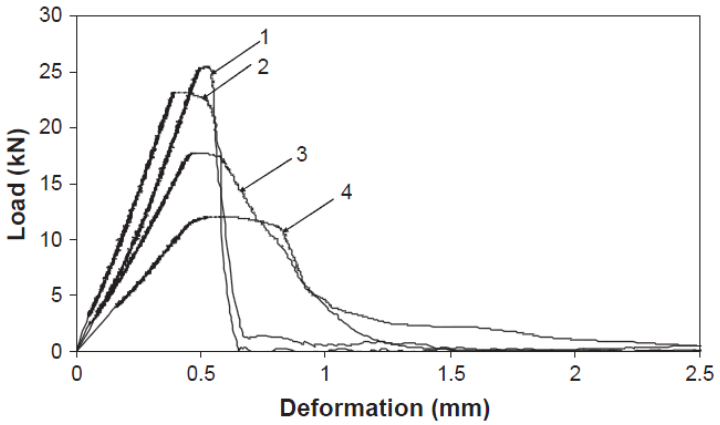

1. Control concrete; 2. Concrete containing 100% coarse RAP only; 3. Concrete containing 100% fine RAP only and 4. Concrete containing 100% coarse and fine RAP

Figure 15 Typical load deformation of concrete specimens under STS test at 14 days (Reprinted from Huang et al. 2005)

Not too much information regarding the fracture properties (i.e., stress intensity factor, crack opening displacement, fracture energies) of the RAP-PCC mixtures is available in the existing publications. The only two available reported results were both obtained from the RAP-

PCC mixtures using a cement-slag-fly ash ternary blend. Brand et al. (2012) tested the critical stress intensity factor (K_{Ic}^{s}), critical crack tip opening displacement ($CTOD_c$), and fracture energies (initial energy G_f total energy G_F) through the single-edge notch beam RAP-PCC specimens, while Amirkhanian et al. (2015) used the disk-shaped compact tension to characterize these fracture properties of the RAP-PCC. Both of the research concluded that the RAP-PCC had a slightly lower K_{Ic}^{s}, but similar $CTOD_c$ and fracture energies. Brand et al. (2014) then tested large-scale full-depth as well as two-lift RAP-PCC slabs (1.8m × 1.8m × 15cm) and observed that RAP-PCC slabs manifested similar to slightly higher flexural load capacity relative to the control slabs. They concluded this finding was possibly attributed to RAP-PCC's equivalent fracture properties.

II.9 PAVEMENT EVALUATION

The only relevant study to evaluate the effect of RAP on rigid pavement performance was found in Tia et al. (2012). Tia et al. (2012) performed a critical stress analysis based on a finite element elastic model named FEACONS. The analysis was performed by assuming a critical loading condition that a 22-kip (98 kN) axle load is applied at the middle of the slab when there is a +20°F (+11°C) temperature differential in the PCC slab. They concluded that the maximum tensile stress in a typical PCC pavement decreased with the increase of RAP content because of the reduced MOE. Despite of the reductions of the flexural strength of the RAP-PCC, the stress reduction turned out to be more pronounced as such the RAP-PCC slab showed a favorable stress/strength ratio.

Tia et al. (2012) subsequently carried out an analysis of failure load of concrete pavement slab using another finite element model ADINA. The results suggested that some of the slabs

containing RAP-PCC manifested higher load capacity relative to the control slab. They believed the higher toughness (area under a load-displacement curve of a flexural test) was the reason for the enhanced load capacity.

II.10 FIELD INVESTIGATION OF RAP-PCC PAVEMENTS

Because of the lab observations that adding RAP into PCC introduces a significant detrimental effect on mechanical properties, only a few field studies have been found from the exiting literature. Those existing field sections are reviewed below.

II.10.1 Single-lift Full-depth Pavement containing RAP-PCC

There are very few examples of making single-lift full-depth RAP-PCC field sections in the U.S, probably due to contractors' uncertainty of whether the RAP-PCC material can meet requirements (e.g., sufficient mechanical strength, adequate durability and acceptable surface characteristics) to make SLFD concrete pavements which can perform well, as well as a lack of extra bins to handle RAP aggregates in the pavement production. A peruse of literature review indicates that Montana might be the only state that had experience of building SLFD RAP-PCC pavement. In 2012, two demonstration sections with 25-cm RAP-PCC slabs using the HR mix (100% coarse RAP and 50% fine RAP replacement) for one section and the HS mix (50% coarse RAP and 25% fine RAP replacement) for the other section were placed at the MSU/WTI Transcend Research Facility. Material production and slab construction using conventional equipment were conducted successfully without any issues. None of the slabs from both the sections showed any observable damage (cracking or spalling), excessive shrinkage or curling during a two-year monitoring period (Berry et al. 2015). In 2010, the Illinois Toll Highway Authority constructed a 23-cm thick concrete slab containing 28 percent washed, coarse

fractionated RAP and overlaid by a 8-cm thick HMA as part of the Milwaukee Avenue ramp reconstruction. The RAP-PCC was produced with 389 kg/m^3 of cementitious content, including 79 percent of cement and 21 percent of fly ash. This innovative construction provided a viable way to enhance sustainability with no negative impacts on cost and performance (Bentsen et al. 2013).

II.10.2 Two-lift Pavement containing RAP-PCC

The use of RAP-PCC in the bottom lift can date back to the 1970s. Iowa State constructed a two-lift trial section with a 28-cm composite section (an 18-cm lower course and a 10-cm upper course). The lower course used RAP and recycled concrete aggregate as aggregate sources. Based on this field experience, the investigators believed that using existing concrete on reconstruction projects as an aggregate source can be feasible (Bergren and Britson 1977).

Kansas built a two-lift construction with RAP in placement of the intermediate sized well gravel at 15 percent of the total aggregate in the 18-cm bottom lift. The top lift was 8-cm and was placed with the standard control mixture. Until 2011, no major distresses were observed (Rao et al. 2013).

After building the RAP-PCC pavement with a HMA overlay, the Illinois Tollway built another two-lift composite concrete pavement containing dirty fractionated RAP. The pavement was placed on the Reagan Memorial Tollway (I-88) in 2012, and the total thickness was 28 cm. The contractor used a ternary concrete mixture with 35 percent supplementary cementitious material and 20 percent dirty fractionated RAP with an optimized aggregate gradation for the bottom lift, which was covered by a standard virgin aggregate non-ternary PCC as a top lift.

Some of the European countries such as Switzerland, Belgium, the Netherlands, France. Austria and Germany have applied the two-lift construction much more commonly than the U.S

(Rao et al. 2013). In Particular, Austria built the entire 322 km of A1 freeway with 10% RAP in the lower lift and the pavement was reported to perform well after 20 years (Rao et al. 2013). A unique roller compacted concrete with RAP and steel fibers has been designed and tested through an accelerated pavement testing and experimental field test section in France (Bilodeau et al. 2011). The studied fiber reinforced roller compacted concrete mixtures with RAP aggregates contained varying RAP percentage (0, 36%, and 70% by total dry mixture volume) and 25 kg/m^3 of hooked steel fiber. The accelerated pavement testing of the sections built with FRCC containing RAP after 2.3 million of the 65kN standard wheel load showed no significant structural damage caused by the addition of RAP (Nguyen et al. 2012).

It is worth noting that other than constructing pavement slabs, RAP-PCC has been used for some other low strength applications. For example, the Maine Department of Transportation blended portland cement, RAP milled from the highway, and virgin aggregates to reinforce and stabilize road shoulders adjacent to the existing old concrete slabs in 2001. This innovative method turned out to be very successful, provided the shoulder preservation and stabilization is a major concern of the design and the extra cost is considered worthwhile (Thompson 2007).

II.11 IMPLICATION TO CURRENT RESEARCH

A detailed review of literature indicates a number of the existing works only focused on testing the mechanical properties of RAP-PCC. The amount of the experimental data for the RAP-PCC's durability, microstructure, crack pattern, and fracture properties is very limited. Additionally, a comprehensive evaluation of effect of RAP on concrete pavement's performance has not yet been conducted. The areas of missing research and gaps in knowledge related to the use of RAP in PCC pavement application have been identified and presented in Table 3.

Table 3 Missing research of using RAP-PCC for pavement application.

Area	Missing research
Mechanical properties	• A systematic study on using RAP to achieve enhanced combined aggregate gradation to mitigate workability and strength reduction is warranted: replacing certain percentages of virgin coarse aggregate by coarse RAP with sufficient intermediate size particles may lead to producing dense-graded PCC and offer benefits (Richardson 2005). The possibility of obtaining enhanced aggregate gradation in PCC by adding RAP was mentioned in an earlier literature (Tia et al. 2012), but no related data was provided. • The previous researchers correlated percent RAP coated by asphalt (Moaveni et al. 2016) and RAP type (Brand and Roesler 2015) with RAP-PCC properties. More work is required to systematically establish the connections between RAP properties (such as binder content, percent agglomerated RAP, RAP minerology etc.) and RAP-PCC performance to facilitate the development RAP screening criteria used in PCC.
Durability	• Limited work showed RAP-PCC had no significant durability issues (Berry et al. 2013; Brand 2012). A more detailed durability study (especially long term durability) covering all applicable aspects is highly needed to verify whether RAP-PCC satisfy adequate durability requirements.
Microstructure	• Some work has been done on determining ITZ properties Brand and Roesler (2017a) and air void characteristics (Su et al. 2013) for RAP-PCC system. The use the findings from Brand and Roesler (2017a) to explain RAP-PCC microstructural features might not be convincing due to the nonrepresentativeness of the sample area (15-20 × 15-20 mm) and the use of mortar samples instead of concrete samples. A detailed study on ITZ properties and air void distribution using more representative samples is needed.
Crack pattern	• The asphalt cohesive failure was reported as a dominating failure mechanism in RAP-PCC based on visual inspection of beam samples and bonding energy calculation (Brand and Roesler 2017b). The application of some effective micro-analytical techniques to generate direct evidences of this phenomenon needs to be conducted. Crack patterns in RAP-PCC can be easily picked up under X-ray computed tomography (X-ray CT) analysis and petrographic analysis.
Fracture properties	• The existing fracture test method might be hard to perform. An effective method to test fracture properties of PCC along with the development of a fracture mechanics based pavement performance prediction approach is missing. • More data using RAP-PCC mixtures containing RAP from various sources needs to be generated to verify RAP-PCC has equivalent fracture properties relative to plain concrete.
Evaluation of RAP-PCC pavement performance	• Although Tia et al. (2012) did some work, their analysis was based on the RAP-PCC mixtures with both coarse and fine virgin aggregates replaced by RAP aggregates. Because of the high RAP replacement and use of fine RAP, their mixtures were much softer relative to the conventional PCC, which naturally yielded a much lower tensile stress in the simulated PCC slab. The favorable stress/strength of the RAP-PCC slab might not be valid in the field as using fine RAP to form paving mixture is considered impractical. Therefore, a more comprehensive study based on PCC containing coarse RAP only is needed to evaluate pavement performance.

To partially fill the gaps of research (identified in Table 3) and facilitate the implementation of RAP-PCC in the field, an extensive study on evaluation of RAP-PCC addressing various aspects has been conducted in this dissertation. A summary of the specific goal and methodology for different aspects of this research is shown in Table 4.

Table 4 Aims and methodology for different aspects of this research

Aspects	Specific goal & methodology
Mechanical properties	• Validate the previously published findings on mechanical properties (i.e., compressive strength, modulus of elasticity, flexural strength and, splitting tensile) of RAP-PCC • Develop an effective approach to determine the optimum RAP replacement level using the total asphalt volumetric fraction
Durability	• Verify RAP-PCC has adequate durability by performing relevant durability tests including freeze-thaw resistance, permeability, restrained shrinkage, and abrasion resistance tests.
Microstructures	• Investigate the effect of RAP on PCC's microstructures through the application of some micro-analytical techniques such as petrographic study using thin sections, X-ray CT and SEM imaging and analysis
Crack pattern	• Identify the weak zones of RAP-PCC by studying the actual crack pattern of the thin section specimens
Fracture properties	• Verify RAP-PCC has equivalent or even better fracture properties and ductility through an innovative fracture test using semi-circular bending specimens
Pavement design	• Carry out sensitivity analysis to evaluate influence of a wide range of PCC properties altered by the addition of RAP on both JPCP and CRCP performance

CHAPTER III

EXPERIMENTAL PROGRAM*

A number of the existing works only focused on testing the strengths and modulus of RAP-PCC, which naturally ignored some other properties (i.e., other pavement related properties, durability, and fracture properties) that would also significantly affect the performance of pavement containing RAP aggregates. Additionally, the microstructure and failure mechanism of the RAP-PCC have not been extensively studied. This chapter presents a comprehensive experimental program addressing various aspects of RAP-PCC properties.

III.1 MATERIALS CHARACTERIZATION

Since the focus of this research was to evaluate the feasibility of using RAP-PCC for pavement applications, all materials used in this research were selected on the basis of producing a typical class P concrete (paving mixture). A conventional TxDOT approved concrete paving mixture with a commonly used virgin coarse and fine aggregate was considered as a control mix. For the cement, a commercially available Type I/II cement made by TXI was used. A class F fly ash obtained from a fly ash limestone plant in Jewett, Texas was used. Table 5 lists the chemical composition of the studied fly ash. A typical mid-range water reducer and an air entraining agent were selected as chemical admixtures for this concrete paving mix. The virgin coarse aggregate (CA) was limestone with #4 (#57 in ASTM C33) gradation specified in the TxDOT standard specifications for construction and maintenance of highways, streets, and bridges

*Part of the contents in this chapter is reprinted with permission from:
Validation of RAP and/or RAS in Hydraulic Cement Concrete: Technical Report, by Mukhopadhyay, A., and Shi, X., 2017, Texas A&M Transportation Institute, Texas. Copyright [2017] by Texas A&M Transportation Institute.

(TxDOT 2014). Although the TxDOT standard specifications require the use of #2 or #3 coarse aggregate gradation for concrete pavement, it was decided to use #4 gradation based on the following reasons:

- Local coarse aggregate materials with #4 gradation were easily available
- There is a little difference between #3 and #4 gradations.
- Most of the published literature on RAP-PCC research used #4 gradation, and the use of the same gradation allowed the researchers to establish a comparative assessment effectively.

Some selective additional work using concrete made of #3 coarse aggregate gradation is presented in Appendix C. The differences in the results between RAP-PCC using #3 and #4 coarse aggregates were found to be negligible. The fine aggregate (FA) was a concrete natural siliceous sand with satisfied gradation requirements according to the specification. All the aggregates (both coarse and fine) and admixtures were provided by Kniferiver Inc., Bryan, Texas.

Table 5 Chemical composition of the fly ash

Composition	Content
SiO_2	53.46%
Al_2O_3	19.09%
Fe_2O_3	5.98%
MgO	2.92%
SiO_3	0.57%
Na_2O	0.48%
CaO	13.43%

RAP from six sources covering five Texas districts including Houston, Bryan, Amarillo, Childress, and San Antonio were collected. Table 6 lists the tests which were conducted for

material characterization for the collected RAP aggregates and virgin aggregates. Table 7 presents the results.

Table 6 Tests to characterize RAP and virgin aggregate materials

Test	Standard/procedure
Specific gravity	ASTM C127, ASTM C128
Absorption	ASTM C127, ASTM C128
Dry rodded unit weight	ASTM C29
Binder content	AASHTO T308
Gradation	ASTM C136

Table 7 Results of aggregate materials characterization

RAP/ VA ID	Description	Source	Binder content (%)	Dry rodded unit weight (kg/m^3)	Oven dry specific gravity	Absorption (%)
CA	Virgin coarse aggregate, #4 limestone	Limestone with minor chert particles	NA	1551	2.51	2.79
FA	Virgin fine aggregate, concrete sand	Siliceous river sand	NA	-	2.58	2.06
HOU_C	Coarse RAP collected from Houston District produced by SCC Asphalt in Houston, TX	Gravel made of mostly limestone with some siliceous particles	4.00	1335	2.41	2.61
BRY_C	Coarse (retained on a 2.36-mm sieve*) RAP collected from Bryan District produced by Kniferiver Inc., Bryan, TX.	Limestone with few siliceous particles (minor phase)	6.19	1373	2.36	1.78
BRY_F	Fine (passing a 2.36-mm sieve*) RAP collected from Bryan District produced by Kniferiver Inc., Bryan, TX	Limestone	8.96	-	2.07	6.87
AMA_C	Coarse RAP collected from Amarillo District produced by J Lee Milligan Inc., Amarillo, TX	Mostly siliceous gravel with some limestone particles	5.25	1255	2.40	1.89
SA_C1	Coarse (25 mm max size) RAP collected from San Antonio District produced by Dean Word company, New Braunfels, TX	Limestone	3.70	1470	2.43	1.77
SA_C2	Coarse (12.5 mm max size) RAP collected from San Antonio District produced by Dean Word company, New Braunfels, TX	Limestone	4.62	1425	2.33	2.69
CRS_F	Fine RAP collected from Childress District	Gravel	6.10	-	2.32	4.07

* Bryan RAP was a mixture of coarse, intermediate, and fine size particles. A 2.36-mm sieve was used to fractionate the RAP from Bryan District to yield coarse (BRY_C) and fine portions (BRY_F).

In Table 7, the identification of minerals present in the studied aggregates (both virgin and RAP aggregates) was conducted according to the ASTM C295. Thin sections using representative aggregate samples were prepared for all the studied aggregates. The thin sections were investigated using a transmitted light optical microscope (Figure 16) by following the guidelines in ASTM C295.

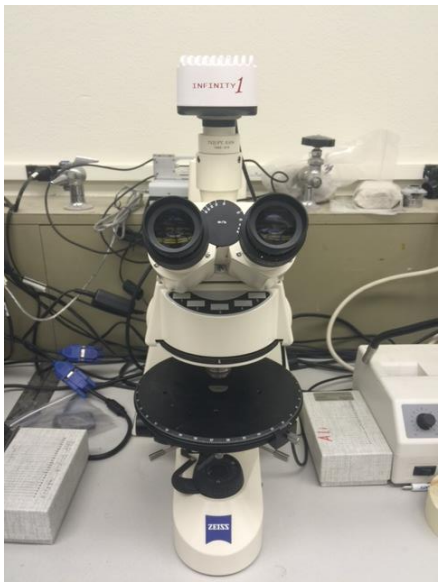

Figure 16 Transmitted light optical microscope

Table 8 lists the gradation of all the collected RAP aggregates and virgin aggregates (i.e., CA and FA). From Table 8, the HOU_C and AMA_C are RAP sources with a high amount of coarser size fraction. HOU_C and AMA_C happened to have similar gradation with the virgin coarse aggregate. The BRY is an un-fractionated RAP source that contains coarse, intermediate, and fine particles. A 2.36-mm sieve was used to remove the fine portion (labeled as BRY_F) and accumulated the coarse and intermediate particles only (labeled as BRY_C). The SA_C2 is another good source because it is well-graded and contains a large amount of intermediate particles but without fine particles. Since the intermediate sized portion of RAP is needed to fill the gap of a conventional gap aggregate gradation of concrete, it is anticipated that the use of BRY_C and SA_C2 RAPs would facilitate achieving concrete with enhanced aggregate gradation.

Table 8 Gradation for RAP materials and virgin aggregates (percent passing of each sieve size)

Sieve	Size (mm)	CA	FA	HOU_C	BRY (C+F)	AMA_C	SA_C1	SA_C2	CRS_F
1 1/2"	38.1	100	100	100	100	100	100	100	100
1"	25.4	99.7	100	100	100	100	99.9	100	100
3/4"	19	81	100	82	100	78	94	100	91
1/2"	12.5	42	100	38	90	44	78	99.9	85
3/8"	9.5	19	100	9	73	18	67	77	77
No. 4	4.75	5	96	2	42	4	39	12	49
No. 8	2.36	3	85	2	22	1	21	0	31
No. 16	1.18	0	74	0	9	0	14	0	21
No. 30	0.6	0	60	0	3	0	9	0	13
No. 50	0.3	0	15	0	1	0	8	0	5
No. 100	0.15	0	2	0	1	0	0	0	1
No. 200	0.075	0	0	0	1	0	0	0	0
Pan	0	0	0	0	0	0	0	0	0

Color coding: Coarse fraction; Intermediate fraction; Fine fraction; according to the Shilstone's classification

As mentioned in Chapter II, the strategy in this study was to replace a certain portion of virgin coarse aggregate in PCC mix by RAP with mainly coarse and intermediate size fractions. The inclusion of intermediate size fraction of RAP should facilitate achieving concrete with optimized or enhanced aggregate gradation, leading to a better workability and less reductions in mechanical properties. Based on the following reasons, it is decided to include any fine RAP (passing 2.36-mm sieve size) in this research:

- Based on the detailed literature review in Chapter II, it is widely accepted that adding fine RAP in PCC invariably causes significant reductions in workability and mechanical properties.
- Fine RAP contains higher amount of asphalt, which can be used to make new HMA mix more economically.

Four coarse RAPs (i.e., HOU_C, AMA_C, BRY_C, and SA_C2) were selected for the further material characterization (Table 9) followed by the detailed concrete testing. The selected coarse RAPs cover (i) a wide range of gradation and rock type, (ii) a wide range of asphalt binder content, and (iii) formation of two dense-graded RAP-PCC mixture series and two gap-

graded RAP-PCC mixtures series (presented later). Figure 17 shows a picture of the selected RAPs and Figure 18 presents their gradation. The HOU_C, AMA_C, BRY_C, and SA_C2 were renamed of as HOU, AMA, BRY, and SA in the remaining portions of this dissertation for the sake of convenience.

Table 9 Additional tests to characterize the selected RAP and virgin aggregates

Test	Standard/procedure
Shape and texture properties	Aggregate Imaging System (AIMS)
Asphalt binder extraction	AASHTO T164
Evaluation of the extracted asphalt grade	Dynamic shear modulus (DSR) test and bending beam rheometer (BBR) test in accordance with the Superpave PG grading system
Identifying minerals present in aggregate	Petrography (ASTM C295)

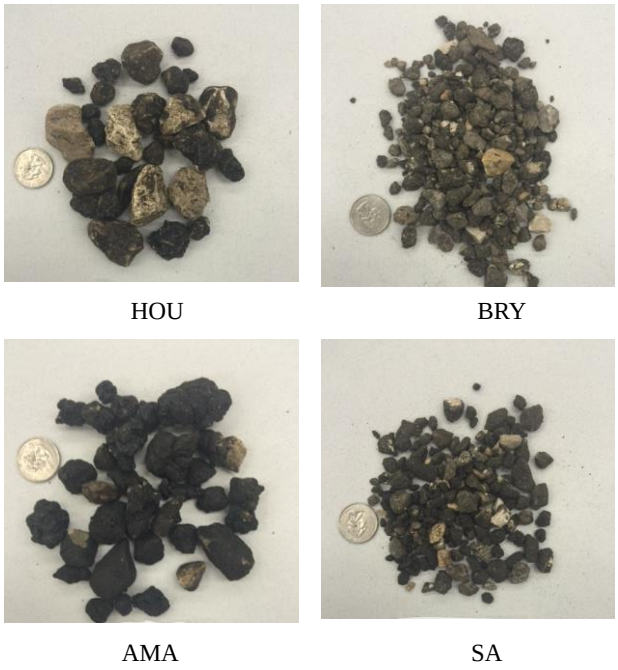

Figure 17 RAP materials used in RAP-PCC

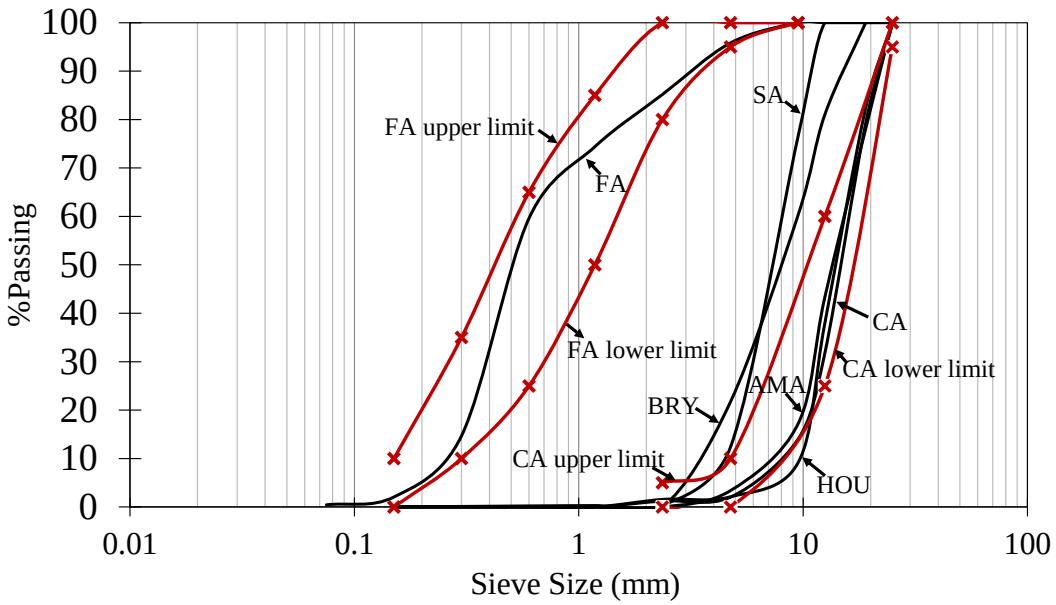

Figure 18 Gradation for the selected aggregates

The Aggregate Imaging System (AIMS) was used to characterize the shape and texture properties of the selected RAP materials and the virgin coarse aggregate. The device uses a variable magnification microscope-camera system and two different lighting configurations to capture aggregate images. With the images, the AIMS software applies a series of algorithms that objectively quantify aggregate shape properties such as angularity, surface texture, sphericity, flat and elongated distribution (Gates et al. 2011). Figure 19 shows the AIMS.

Table 10 shows the results for the HOU, BRY, AMA and SA. Table 10 indicates that the RAP materials have higher sphericity values and a lower amount of flat and elongation particles, compared to the virgin coarse aggregate. This finding indicates that adding RAP can be effective for achieving optimized aggregate gradation in a concrete mixture, because the intermediate particles must be rounded and should not be flat and elongated in order to make an effective dense graded concrete according to Richardson (2005). The SA is a crushed RAP, so it has the lowest sphericity and the highest flat and elongated distribution. It is noted that generally the

texture of RAP aggregates is much higher than the texture of CA. The mineralogy of BRY and HOU is similar to the mineralogy of CA, but their texture is totally different according to the AIMS results. Under an ongoing TxDOT project (0-6921), TTI is investigating this phenomenon. Based on the preliminary results, researchers observed that the texture data from AIMS is very sensitive to the color/shade of the aggregate particles and sometimes can lead to misleading results.

Figure 19 AIMS

Table 10 AIMS test results

Sample	Size (mm)	Angularity	Texture	Sphericity	Flat and Elongated Distribution (L/S>2:1)	Flat or Elongated Distribution (L/S>2:1)
CA	4.75	2344.4	78.8	0.70	58.9%	17.9%
HOU	4.75	2648.6	614.8	0.74	45.0%	13.3%
BRY	4.75	2324.6	543.9	0.77	25.0%	6.7%
AMA	4.75	2977.0	562.3	0.71	48.3%	5.2%
SA	4.75	2764.9	619.6	0.66	80.0%	30.0%

Aged asphalt binder was chemically extracted from the selected RAP aggregates based on the AASHTO T164 standard. The dynamic shear rheometer (DSR) test and bending beam

rheometer (BBR) test were performed to re-evaluate the extracted asphalt grade in accordance with the Superpave PG grading system (AI 2001). Figure 20 shows DSR device and the BBR device. Table 11 lists the test results. It is found that the AMA contains more agglomerated particles compared to the other three RAPs (Figure 21). Table 11 manifests that the AMA is softer at high temperature, which might be the reason for the formation of agglomerated particles in the AMA.

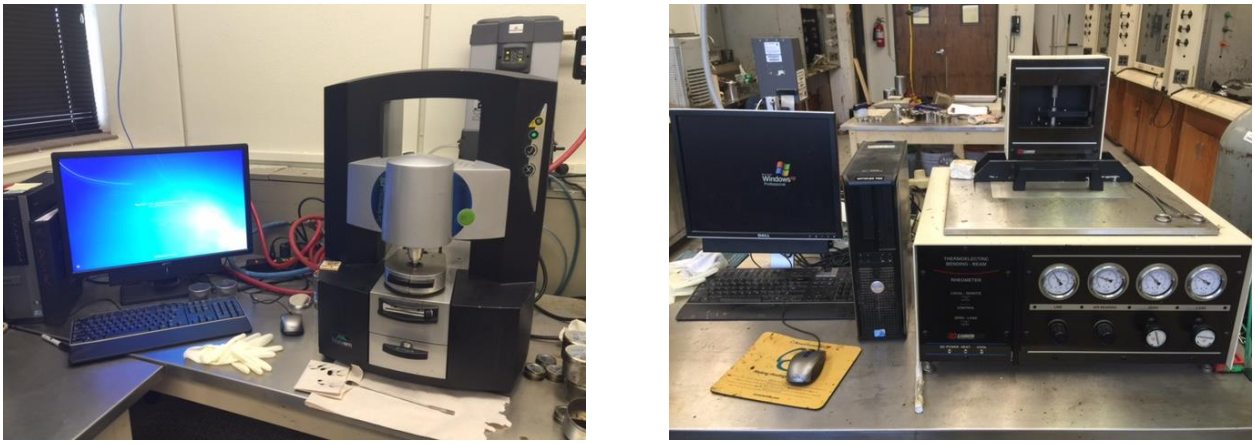

Figure 20 DSR (left) and BBR (right)

Table 11 RAP asphalt grade evaluation

RAP ID	DSR result	BBR result	PG grade
HOU	Passed @82°C, Failed @88°C	Passed @-6°C, Failed @ -12°C	PG 82-16
BRY	Passed @82°C, Failed @88°C	Passed @-12°C, Failed @-18°C	PG 82-22
AMA	Passed @76°C, Failed @82°C	Passed @-18°C, Failed @-24°C	PG 76-28
SA	Passed @ 88°C, Failed @ 96°C	Passed @ -12°C, Failed @ -18°C	PG 88-22

Figure 21 Agglomerated particles in AMA

III.2 MIX FORMULATION

A series of trial mixtures with 0.45 water/cementitious (w/cm) ratio and 389 kg/m^3 (656 lb/cy) cementitious content was initially designed because of the need to use a high w/cm and cementitious content to compensate the low workability and low strength of RAP-PCC, which was commonly reported from previously the published investigations. After a thorough assessment of the trial mixes (presented in Appendix D), a decision was made to reduce the w/cm to 0.40 and to decrease the cementitious content to 309 kg/m^3 (520 lb/cy) for the mixtures used for the detailed testing, because:

- In general, the slump values of the trial mixes were very high, which could cause potential segregation issues.
- The cementitious content of 309 kg/m^3 is higher than the common practice for a typical Class P concrete in Texas (The common practice for TxDOT Class P mix is to use a cementitious content that does not exceed 309 kg/m^3; a written approval needs to be obtained if the cementitious material exceeds 309 kg/m^3. The cementitious content can not exceed 415 kg/m^3 (700 lb/cy)).

Based on the hardened concrete property results of the trial mixtures, it is concluded that coarse RAP replacements up to 40 percent can be practically allowed with permissible reductions of different mechanical properties (e.g., different strengths) in comparison with the control concrete. Any higher amount (greater than 40 percent) led to significant reductions in mechanical properties in comparison with the control mixture, which might not be acceptable from a practical standpoint. As a result, the virgin coarse aggregate was replaced up to 40 percent by the selected RAPs (i.e., HOU, AMA, BRY, and SA) in the detailed testing program. The mix ID in this project was assigned with the following format:

w/cm_cementitious content*_coarse RAP replacement level+RAP type

*Since all the mixtures were designed according to the TxDOT specification, which uses the U.S customary units, the cementitious content in the mix ID was assigned as 520 (lb/cy).

Example: 0.40_520_40HOU represents a mix that has a 0.40 w/cm ratio, 520 lb/cy (309 kg/m3) cementitious content, and uses the HOU RAP to replace 40 percent of the virgin coarse aggregate. Table 12 presents the mix design for the 0.40_520 RAP-PCC mixtures.

Table 12 Mix designs for the concrete mixtures

Materials	0.40_520_REF	0.40_520_20HOU	0.40_520_40HOU	0.40_520_20AMA	0.40_520_40AMA	0.40_520_20BRY	0.40_520_40BRY	0.40_520_20SA	0.40_520_40SA	0.40_520_30BRY*	0.40_520_35SA*
Cement (kg/m^3)	247	247	247	247	247	247	247	247	247	247	247
Fly Ash (kg/m^3)	62	62	62	62	62	62	62	62	62	62	62
Virgin coarse aggregate (kg/m^3)	1058	825	604	842	628	830	611	846	635	734	688
Coarse RAP (kg/m^3)	0	206	403	202	400	208	408	196	393	296	344
FA (kg/m^3)	769	787	804	775	781	776	783	768	768	778	768
Water Reducer (ml/m^3)	402	402	402	402	402	402	402	402	402	402	402
Air Entraining Agent (ml/m^3)	60	60	60	60	60	60	60	60	60	60	60
Water (kg/m^3)	123	123	123	123	123	123	123	123	123	123	123

- Cement - Type I/II cement made by TXI® was used
- Class F fly ash (Sum of SiO_2, Al_2O_3 & Fe_2O_3=78.53%) - 20% replacement (weight) of cement as a common practice by TxDOT
- A typical mid-range water reducer (1.3 ml per 1 kg of cementitious materials) and an air entraining agent (0.2 ml per 1 kg of cementitious materials) were selected as commonly used chemical admixtures for TxDOT concrete paving projects

* The mechanical properties were tested for the 0.40_520_30BRY and the 0.40_520_35SA mixtures in order to validate the strengths and asphalt fraction relationship (presented later)

III.3 FRESH AND HARDENED PROPERTIES

The production of RAP-PCC was in accordance with the normal practice of making conventional concrete samples. Before mixing, all of the virgin aggregates and RAP materials were oven-dried and the moisture was compensated in the mix design based on the materials' absorption capacity. A 0.25 m^3 steel mixer and a 0.11 m^3 plastic mixer were used in combination. The RAP-PCC mixing procedure (Table 13) was developed based on the standard concrete mixing practice in the lab (ASTM C192). During the mixing and casting of the RAP-PCC, no abnormal observations were recorded.

Table 13 RAP-PCC mixing procedures

Step	Description
1	Batch all the ingredients
2	Batch the mixing water and add the water reducer and the air entraining agent into it
3	Place all of the coarse aggregates and the RAPs in the mixer
4	Mix 1 minute and let RAP distribute uniformly in the mixer
5	Add 1/3 of the prepared mixing water and mix for 30 seconds
6	Dump all the fine aggregate and the cementitious materials in the mixer, and add the rest of the mixing water and mix for 3 minutes
7	Stop mixing and let the concrete rest for 2 minutes
8	Mix 3 more minutes
9	Pour the concrete into the cart and carefully scrape out the cement paste and the cement mortar attached to the mixer

III.3.1 Fresh Properties

Immediately after finishing mixing concrete, the tests (Table 14) to determine fresh concrete properties were performed.

Table 14 Test methods to determine fresh concrete properties

Test	Standard
Slump	ASTM C143
Air content	ASTM C173

III.3.2 Mechanical Properties

Table 15 lists the tested hardened concrete properties. Specimens of varying dimensions for the determination of different hardened properties were cast. The molded specimens were placed inside a room with a temperature of 23°C for initial curing. After 24 hours, all the specimens were demolded and then immediately transported to a standard moist curing room at 23°C and 100% relative humidity.

Table 15 Test methods to determine mechanical properties

Test	Sample size (mm)	Duplicates	Mix	Curing age
Compressive strength (ASTM C39)	100×200 cylinder	3	0.40_520_REF 0.40_520_HOU mixture series 0.40_520_AMA mixture series 0.40_520_BRY mixture series 0.40_520_SA mixture series	7-day 28-day 56-day*
MOE (ASTM C469)	100×200 cylinder	3		
Flexural strength (ASTM C78)	150×150×500 beam	3		
STS (ASTM C496)	100×200 cylinder	3		

*The RAP-PCC made with AMA RAP showed higher strength reductions than the other RAP-PCC samples. Only 7-day and 28-day mechanical properties tests were conducted for the RAP-PCC made with AMA RAP. No 56-day MOE and STS for the RAP-PCC containing SA RAP were tested either.

Compressive Strength

Compressive strength is the most commonly used parameter to characterize hardened concrete property. It can be directly correlated with other concrete properties such as MOE, MOR, and STS. ASTM C39 specifies this test and the testing procedures were strictly followed. A MTS machine, which has a 1000-kN capacity, was used in the test. The test was performed at a controlled force mode (1.96 kN/sec). Figure 22 shows a picture of the compressive strength test.

Figure 22 Compressive strength test

MOE

MOE is another important material property for concrete and is directly related to stress and deflection development in pavement. The test was conducted in accordance with ASTM C469 using the 1000-kN MTS machine at a constant displacement rate of 0.0203 mm/sec. A ring attachment was used to hold two axial linear variable differential transformers (LVDTs) for displacement recording during the test. Figure 23 shows a picture of the MOE test.

Figure 23 MOE test

Flexural Strength/MOR

Concrete is a material which is strong in compression but weak in tension. The characterization of concrete tensile property is of great importance as it relates to crack initiation and propagation. A uniaxial direct tension test is the ideal test to evaluate concrete tensile property. However, such test is extremely hard to perform because of the brittle nature of cementitious concrete material. Therefore, flexural strength is widely used to present the tensile property of concrete in an indirect way. The flexural test was conducted using a simple beam with third-point loading method in accordance with ASTM C78. The test machine was a MTS machine with a 100-kN loading capacity. Figure 24 shows a picture of the MOR test.

Figure 24 MOR test

STS

Like the flexural test, STS is another indirect measurement of concrete tensile strength. One benefit of the STS test over the flexural test is that it uses cylinder specimen with a smaller dimension, which saves material and labor for sample preparation. The test was conducted followed by ASTM C496 using the 1000 kN MTS machine. Figure 25 shows a picture of the STS test.

Figure 25 STS test

III.3.3 Other Pavement Related Properties

Other than the strengths and stiffness of PCC material, the performance of rigid pavement also relies on the Poisson's Ratio, CoTE, and thermal properties (i.e., thermal conductivity and heat capacity) of PCC material. To ensure an accurate pavement evaluation (presented in Chapter V), all the required material property inputs of the plain PCC and RAP-PCC slab were directly acquired from the lab. A description of each testing procedure for these pavement related properties is presented below.

Table 16 Test methods to determine other properties

Test	Sample size (mm)	Duplicates	Mix	Curing age
Poisson's ratio (ASTM C39)	150×300 cylinder	3	0.40_520_REF 0.40_520_HOU mixture series 0.40_520_BRY mixture series	28-day
CoTE (ASTM C469)	100×178 cylinder	3		
Thermal properties (Hot disk approach)	100×50 disk	3		

Poisson's Ratio

Poisson's ratio of the studied mixtures was tested in accordance with ASTM C469. The test was conducted with 150 mm × 300 mm. cylinder specimens using an 1800-kN Tinius Olsen machine at a constant displacement rate of 1.3 mm/min. A similar ring attachment for testing MOE was used. The ring fixture was equipped with three radial LVDTs and three axial LVDTs in order to measure the displacement in both directions.

CoTE

The CoTE of PCC significantly affects rigid pavement's expansion and contraction characteristics. It is also an input for predicting slab curling and warping. The measurements made in this study followed the AASHTO T336 standard. Before the testing, the conventional 100 mm ×200 mm cylinder specimens were shortened to 178 mm in length, followed by a two-day period of conditioning in a lime-statured water storage tank at 23°C. During the test, the samples were placed in a water bath with controlled temperatures of 10°C and 50°C. A LVDT was mounted at the top of the testing specimen to record the length change of the specimen at 10°C and 50°C respectively. The CoTE of the specimen can be calculated subsequently using the recorded data for length change. Figure 26 shows a picture of the CoTE test.

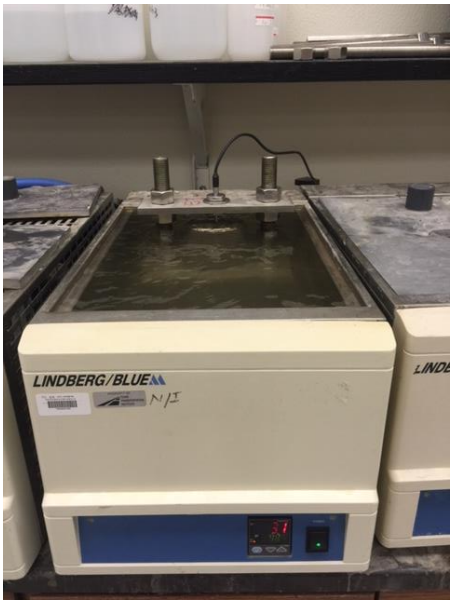

Figure 26 CoTE test

Thermal Properties

Concrete thermal properties (thermal conductivity and heat capacity) control the heat transfer within the pavement. Thermal conductivity measures how fast a material conducts heat, and heat capacity quantifies the amount of heat needed to raise a unit of material temperature. Both of the thermal conductivity and heat capacity are important inputs in calculating pavement temperature distribution and the induced temperature related responses. In this study, the thermal properties of the studied mixtures were determined using a hot disk thermal constants analyzer (model TPS-2500S) (Figure 27) according to the procedures described in the previously published works (Shi 2014; Shi et al. 2017; Shi et al. 2015). Each cylindrical specimen with 100 mm in diameter and 200 mm in length was sliced into four pieces in the transverse direction. During the test, the TPS 2500S sensor was sandwiched by two disk samples to record the temperature changes of the specimens and the thermal properties of the specimens were

automatically calculated by the software (Figure 27). For each type of the mixture, four disk samples yielded three data points.

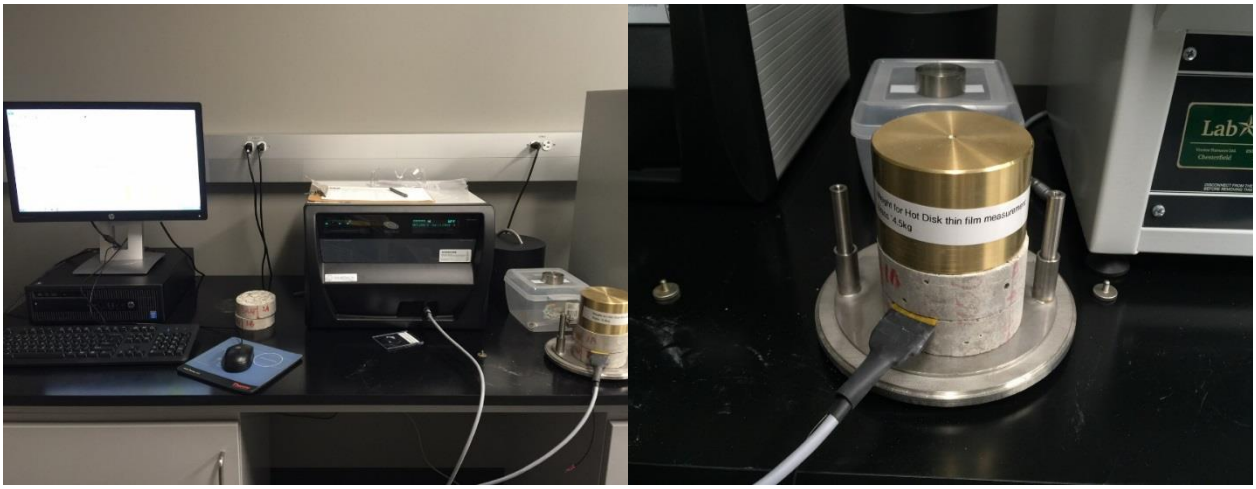

Figure 27 Thermal properties test

III.4 DURABILITY

The durability of the RAP-PCC mixtures was evaluated by carrying out some relevant durability testing such as freeze-thaw resistance testing, permeability testing, ring shrinkage testing, and abrasion resistance testing. A list of durability tests conducted in this study is shown in Table 17.

Table 17 Test methods to determine durability

Test	Approach	Sample size (mm)	Duplicates	Mix	Curing age (day)
Freeze-thaw resistance	ASTM C666	76 × 100 × 286 prism	3	0.40_520_REF 0.40_520_40HOU 0.40_520_40BRY 0.40_520_40SA	14
Permeability	Measuring concrete bulk electrical resistivity to correlate rapid chloride permeability	100 × 200	3	0.40_520_REF, 0.40_520_HOU mixture series 0.40_520_BRY mixture series	28
Restrained shrinkage	Concrete ring test (ASTM C1581)	See Table 18	4	0.40_520_REF, 0.40_520_40HOU, 0.40_520_40BRY	n.a
	Mortar ring test (Hogancamp and Grasley 2017)		4	REF-Mortar RAP-Mortar	n.a
Abrasion resistance	Revolving disk (ASTM C779)	300 × 300 × 100 slab	2	0.40_520_REF 0.40_520_40HOU 0.40_520_40BRY	28
	Rotating cutter (ASTM C944)	150 × 150 cylinder	2		28

III.4.1 Freeze-thaw Resistance

A direct freeze-thaw test by following ASTM C666 (Procedure A) was conducted. Only the RAP-PCC mixtures containing 40% RAP along with the control mixture were tested.

III.4.2 Permeability

Electrical resistivity measurements of the RAP-PCC mixtures were made in this study. The determined electrical resistivity was used to be correlated with the permeability of RAP-PCC mixture since several researches (Ramezanianpour et al. 2011; Riding et al. 2008; Wee et al. 2000) found a very strong correlation between the electrical resistivity and rapid chloride permeability (RCP).The electrical resistivity test was conducted using the Giatec RCON2 concrete bulk resistivity meter. Figure 28 shows a picture of the electrical resistivity test.

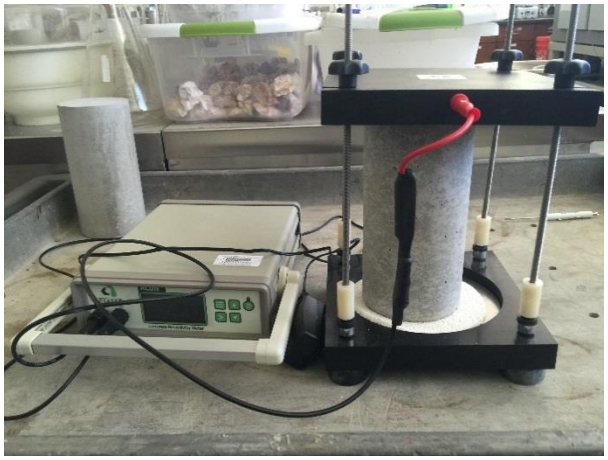

Figure 28 Electrical resistivity test

III.4.3 Ring Shrinkage

The restrained shrinkage of RAP-PCC was evaluated through two ring tests with different geometries. The concrete rings were initially tested according to ASTM C1581. However, none of the rings showed any cracking within a 28-day testing period (specified by ASMT C1581). A picture of the concrete ring test is shown in Figure 29.

Figure 29 Ring Test: concrete ring at age of 1 days (left) and at age of 28 days

It is suggested that a smaller ring geometry can accelerate the cracking process (Hogancamp and Grasley 2017), but the test only allows to use mortar samples due to the sample size limitation. A comparison of the two ring tests is tabulated in Table 18.

Table 18 Comparison of two ring tests

Test	Outer ring radius (mm)	Interior ring radius (mm)	Height (mm)	Steel thickness (mm)
Concrete test	202	165	150	13
Mortar test	76	56	57	3

The mix proportions of the mortar mixtures are shown in Table 19. The RAP-mortar rings were made of 100% fine RAP (i.e., BRY_F), while the REF-mortar rings were made of 100% virgin fine aggregate. The amount of the water, cementitious materials and fine aggregates remained same volumetric fractions as in the concrete mixture design. Pictures of mortar ring tests are presented in Figure 30.

Table 19 Mix design for the mortar mixtures

Materials	REF-mortar	RAP-mortar
Cement (kg/m^3)	467	467
Fly Ash (kg/m^3)	117	117
Virgin Fine Aggregate (kg/m^3)	1458	0
Fine RAP (kg/m^3)	0	1168
Water (kg/m^3)	234	234

Figure 30 Mortar ring test: a mortar ring after casting (left) and at the end of the testing period (right)

III.4.4 Abrasion Resistance

The abrasion resistance of RAP-PCC was evaluated through an innovative approach with a combined analysis of testing data from the revolving disk test (ASTM C779) and the rotating cutter test (ASTM C944). These two types of abrasion tests were used to provide different degree of abrasion by applying different shear stress on concrete surface. The procedure A of ASTM C779 uses an abrasion testing machine with three 60-mm diameter, cold rolled steel revolving disks. The disks are driven transversely along a circular path at 12 rpm while being individually rotating along their own axis at a speed of 280 rpm. A uniform total load of 22 N is applied on each abrading disk face and abrasive grit is continuously supplied by the abrasive dispenser during the test. ASTM C944 uses a rotating-cutter drill press to abrade concrete surface. The drill press is capable of holding and rotating the abrading cutter at a speed of 200 rpm and maintaining a normal force of 100 N on concrete surface. Pictures of these two abrasion tests are shown in Figure 31.

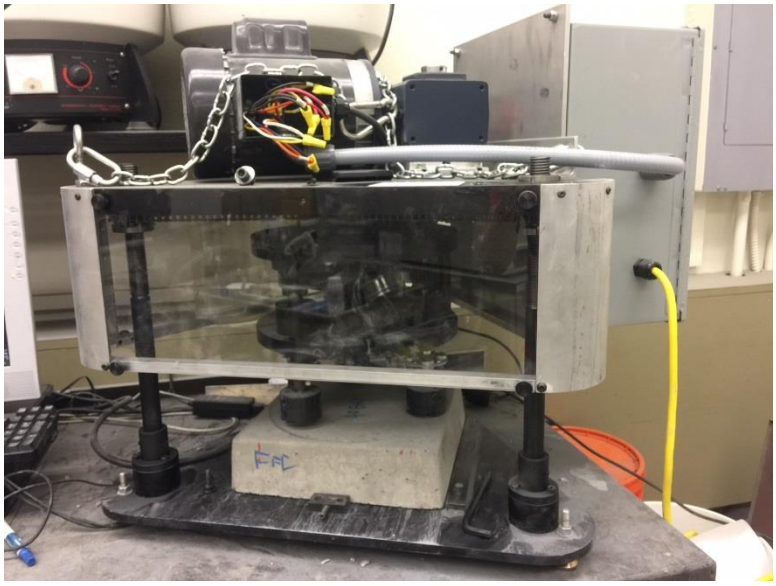

(a) Revolving disk approach, ASTM C779, procedure A

(b) Rotating cutter approach, ASTM C944

Figure 31 Abrasion tests

The RAP-PCC (i.e., the 0.40_520_40HOU and the 0.40_520_40BRY) and the reference (i.e., the 0.40_520_REF) samples were prepared and subjected to these two abrasion tests. During each of the two abrasion tests, a clamp style ammeter was used to record the electric current flowing into the driving motor. The total electric power (P) consumed by the abrasion machines during the test can be calculated as:

$$P = UI \tag{33}$$

Where

U= motor voltage (V)

I= the current flowing into motor (A)

The torque of the motor is then obtained in the following equation:

$$T = \frac{9.549 \times P \times \eta}{n} \tag{34}$$

Where

T= torque (Nm)

P= power (W)

η= motor efficiency

n= motor speed (rpm)

The manufacturing information for the driving motors is tabulated in Table 20.

Table 20 Manufacturing information for the driving motors

Method	Voltage (V)	Motor efficiency	Motor rpm	Inner radius of the wear (m)	Outer radius of the wear (m)	Abrading surface rpm
Revolving disk	110	69%	1725	0.075	0.1375	12 for the carrousel 280 for the revolving disks
rotating cutter	230	69%	1725	0.0105	0.0495	200

III.5 MICROSTRUCTURE

To overcome the limitations related to the previous RAP-PCC's microstructural studies (mentioned in Table 3), a petrographic analysis was carried out by observing thin section specimens made of RAP-PCC under the transmitted light optical microscope (ASTM C856). Comparing to the size of the SEM sample (15-20 × 15-20 mm), thin section specimen has a larger sample size (75 × 50 mm, around 25 μm thickness) and is supposed to provide a better insight of the microstructural features of the specimens. Hardened concrete specimens covering different RAP-PCC mixture types were sent to the National Petrographic Service Inc. in Houston for thin section preparation. Table 21 presents the information related to the mix design, specimen age, and sample selection. A blue dye was used during thin section preparation to highlight pores and cracks in cement paste matrix, aggregate particles, and ITZ. Therefore, pores and cracks were all highlighted by the blue color of the dye used for all the pictures provided in

Chapter IV. Some important microstructural investigations such as verification of presence of agglomerated RAP particles (i.e., RAP clumps), ITZ characterization, quantification of pores and identification of CH crystals' size and distribution were carried out. Limited evaluation of ITZ properties was performed using the SEM as well.

Table 21 Thin section information (intact samples)

Mix ID	Curing time	Sample selection
0.40_520_REF	28 days	A representative slice of concrete sample taken from a dedicated cylindrical (100 × 200 mm) concrete specimen for petrographic examination after 28 days of moist curing
0.40_520_40HOU	28 days	
0.40_520_40BRY	28 days	
0.40_520_40SA	28 days	

In addition to the petrographic technique, X-Ray CT was also used as an auxiliary tool for investigating RAP-PCC microstructures in this study. The X-ray CT is an advanced nondestructive testing technique to scan solid specimen and produces 3D images of all relevant features in the studied specimen through software reconstruction. The X-ray CT (Zeiss, model Xradia 520 Versa, Figure 32) used in this study has the capability to produce images with 50 micron resolution with a specimen of around 50 mm diameter. In this study, several 50 mm × 100 mm cylindrical specimens for some selective mixtures were made and underwent X-ray scans. The overall percent air void in the studied RAP-PCC mixtures was estimated based on an imaging analysis using the 3D reconstructed images. The selective mixtures were the control mix 0.40_520_REF, the RAP-PCC mixtures 0.40_520_40HOU, 0.40_520_40BRY and an additional RAP-PCC mixture with 100% RAP aggregates (i.e., all virgin coarse aggregate replaced by the BRY_C and all virgin fine aggregate replaced by the BRY_F). The RAP-PCC mixture with 100% RAP aggregates was labelled as 0.40_520_100BRY/100BRY.

Figure 32 Zeiss X-ray microscope Xradia 520 Versa

III.6 CRACK PATTERN

The most effective way to verify the weak zones in RAP-PCC is to study the actual crack pattern. After the intact cylindrical samples were X-ray CT scanned, indirect tensile loads were applied to the samples to mechanically induce cracks. Figure 33 presents a picture of the cracked samples. The cracked samples underwent another set of X-ray CT scans using the same scan recipe (i.e., same scan parameters) with the scans for the intact samples, and were then carefully wrapped and shipped to the National Petrographic Service Inc. for thin section preparation. The crack pattern in the RAP-PCC mixtures was investigated by both examining X-ray CT images and observing thin sections specimens under the optical microscope. Table 22 presents the information on the thin section samples for the crack pattern study.

(a) 0.40_520_REF

(b) 0.40_520_40HOU

(c) 0.40_520_40BRY

(d) 0.40_520_100BRY/100BRY

Figure 33 Cracked concrete samples

Table 22 Thin section information (cracked samples)

Mix ID	Curing time	Sample status when sent out
0.40_520_REF	14 day	Cracked
0.40_520_40HOU	14 day	Cracked
0.40_520_40BRY	14 day	Cracked
0.40_520_100BRY/100BRY	14 day	Cracked

III.7 FRACTURE PROPERTIES

In this dissertation, an innovative approach using specimens with semi-circular bending geometry was developed. The two-parameter fracture properties of the RAP-PCC mixtures were characterized and compared with the control mixture. Experimental and analytical procedures to determine RAP-PCC's TPFP are described subsequently.

III.7.1 Development of SCB Fracture Test

While the methods for testing two-parameter fracture properties of concrete have been established using a single edge notched beam (SEN(B)) and a DCT specimen respectively, neither of the tests is easy to perform: the SEN(B) uses large beam samples, which require a considerable amount of material and labor. Additionally, beam shaped specimens are hard to obtain from the field section. For the DCT sample, the complicated geometry causes tediousness and requires high accuracy in sample preparation. Accordingly, a simple but effective specimen geometry is heavily needed. Semi-circular bending specimen has been widely used to characterize asphalt concrete properties (Huang et al. 2005; Li and Marasteanu 2010; Wu et al. 2005). The geometry is simple to fabricate from both lab-made cylindrical samples and field cores; fracture tests for different fracture modes can be easily designed by changing the support locations and crack angles of the specimens as well (Mirsayar et al. 2017). This study has developed an innovative method using specimens with SCB geometry to characterize the concrete fracture properties in terms of K_{Ic}^{s} and $CTOD_c$. The design of experiment and calculation of K_{Ic}^{s} and $CTOD_c$ are presented below.

Sample Preparation and Testing Procedures

Concrete samples were produced in according to the normal practice of making conventional concrete in the lab. Cylindrical specimens of 150 mm in diameter and 300 mm in

length were cast and then cured in a standard moisture room with a temperature of 23°C and a relative humpty of 50% until a specific testing age. One day before the testing, the cylindrical specimens were cut into two half pieces along the diameter. For each half piece, 8 SCB specimens with a thickness of 38 mm were obtained. The samples made from both top and bottom portions of the cylinder were discarded to avoid potential segregation problems. Accordingly, 12 SCB specimens could be produced for each cylindrical specimen (Figure 34). A 3.0 mm wide notch was then made in the middle of each SCB sample using a table saw. Two notch lengths were chosen to evaluate the effect of the notch length in this study: one was 38 mm according to a previous study (Mirsayar et al. 2017), and the other was 12 mm by referring to the AASHTO TP105 standard method to determine the fracture energy of asphalt mixtures using the SCB geometry. Knife edges were then attached on the notched SCB specimen using a superglue. The knife edges would be used for mounting a clip-on gauge during the test. In the study, the bending span to specimen radius ratio (S/R) was selected as 1.6, which was the most commonly used value from the previous literature. Pictures of the notched SCB specimens are shown in Figure 35.

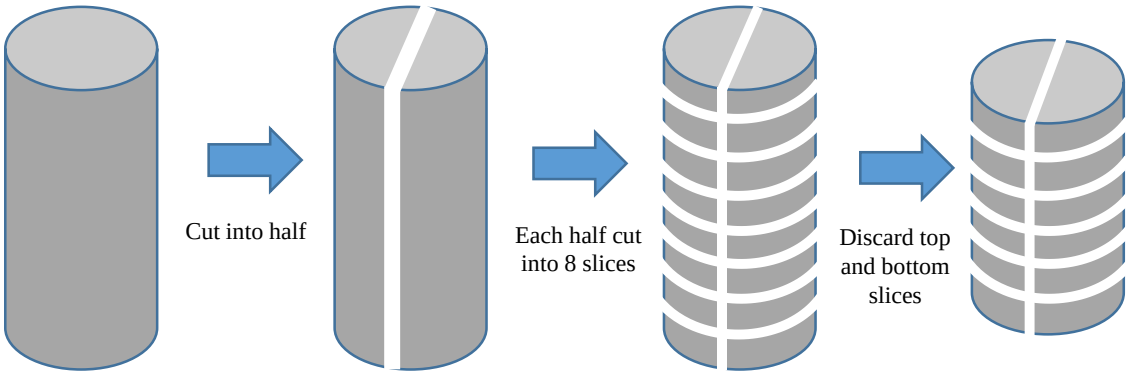

Figure 34 Production of 12 SCB specimens from one cylindrical specimen

(a) 38 mm long notch (b) 12 mm long notch

Figure 35 Pictures of the notched SCB specimens

A 100-kN MTS machine which has a high stiffness was used to carry out the test. The CMOD was recorded by a clip-on gauge. A picture of the test set-up is shown in Figure 36. Because the frame of the MTS is very stiff, the test was controlled with a constant movement of the crosshead at 0.05 mm/min instead of setting up a constant clip-on gauge extension rate. It was found that the specimens with the 12 mm notch had stable failures while those with the 38 mm notch showed a sudden drop after the peak load in the load-CMOD curve. Accordingly, the 12 mm notch is recommended for the 150 mm SCB specimen.

Figure 36 SCB fracture test set-up

The loading of the SCB specimen followed the same procedures in the RILEM method described in Section II.8.3. The testing procedure included a loading step and an unloading one in order to separate the elastic and inelastic portion of the measured CMOD: the SCB specimen was first loaded monotonically up to the peak load at a constant movement of the crosshead at 0.05 mm/min; as soon as the load reached the peak, an unloading step was applied at the same crosshead movement rate (0.05 mm/min). When the applied road reduced to zero, the specimen was reloaded until sufficient data was recorded.

Calculation of K_{Ic}^{s} and $CTOD_c$ based on LEFM

This section presents the details for getting the fracture properties $\mathrm{K_{Ic}^{s}}$ and $\mathrm{CTOD_c}$ from the measured SCB load-CMOD curve.

Weight Function Method

The weight function method is considered a versatile method to determine the stress intensity factor and the associated crack opening displacement. The weight function method states that once a two-dimensional elastic crack solution (reference solution) as a function of the crack length A for any loading condition is known, the stress intensity factor for the same geometry being subject to any other loading can be obtained (Wu and Carlsson 1991):

$$\mathrm{K(A)} = \frac{\mathrm{E'}}{\mathrm{K_r(A)}} \int_0^{\mathrm{A}} \sigma(\mathrm{Y}) \frac{\partial \mathrm{U_r(A,Y)}}{\partial \mathrm{A}} \mathrm{dY} \tag{35}$$

Here $\mathrm{E'} = \mathrm{E}$ for plane stress condition and $\mathrm{E'} = \frac{\mathrm{E}}{1-\upsilon^2}$ for plan strain condition

$\mathrm{K_r(A)}$ is the stress intensity factor for the reference solution

$\mathrm{U_r(A,Y)}$ is the crack face displacement for the reference solution

$\sigma(\mathrm{Y})$ is the crackline stress

For convenience, the non-dimensional notation is used for the studied semi-circular geometry (Figure 37):

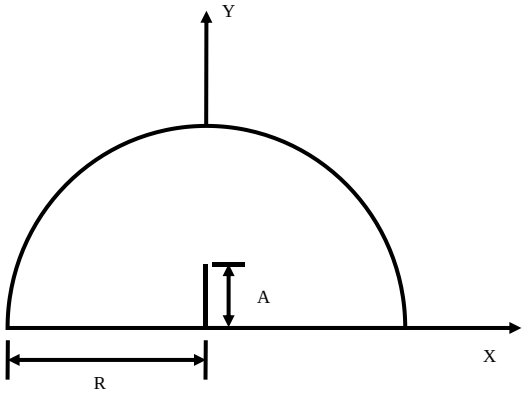

Figure 37 Semi-circular specimen

$$y = \frac{Y}{R} \tag{36}$$

$$a = \frac{A}{R} \tag{37}$$

$$u_r = \frac{U_r(A, Y)}{R} \tag{38}$$

Specifically,

$$f_r(a) = \frac{K_r(A)}{(\sigma\sqrt{\pi A})} \tag{39}$$

$$V_r(a) = \frac{E'}{\sigma A} U_r(A, 0) \tag{40}$$

Define

$$\frac{K(A)}{\sqrt{R}} = k(a) = \int_0^a \sigma(y) h_r(a, y) dy \tag{41}$$

In a non-dimensional form:

$$K(A) = f(a)\sigma\sqrt{\pi A R} \tag{42}$$

$$f(a) = \int_0^a \frac{\sigma(y)}{\sigma} \frac{h_r(a, y)}{\sqrt{\pi a}} dy \tag{43}$$

In which the weight function is expressed (Dempsey et al. 1995):

$$h_r(a,y) = \frac{1}{\sqrt{2\pi a}} \sum_{i-1}^{5} \mathcal{G}_i(a)\left(1-\frac{y}{a}\right)^{i-\left(\frac{3}{2}\right)}, y \le a \tag{44}$$

Where

$$\mathcal{G}_1(a) = 2.0 \tag{45}$$

$$\mathcal{G}_2(a) = \frac{6}{(1-a)} + \frac{105E(a)}{\sqrt{1-a}} + 4\frac{aF'(a)}{F(a)} - 30 \tag{46}$$

$$\mathcal{G}_3(a) = \frac{S_3(a)}{(1-a)^{3/2}} - \frac{26}{(1-a)} - \frac{455E(a)}{\sqrt{1-a}} - \frac{52aF'(a)}{3F(a)} + 86 \tag{47}$$

$$\mathcal{G}_4(a) = \frac{S_4(a)}{(1-a)^{3/2}} + \frac{154}{5(1-a)} + \frac{539E(a)}{\sqrt{1-a}} + \frac{308aF'(a)}{15F(a)} - \frac{434}{5} \tag{48}$$

$$\mathcal{G}_5(a) = \frac{S_5(a)}{(1-a)^{3/2}} - \frac{54}{5(1-a)} - \frac{189E(a)}{\sqrt{1-a}} - \frac{36aF'(a)}{5F(a)} + \frac{144}{5} \tag{49}$$

And

$$E(a) = \frac{3\pi\Phi(a) - V(a)}{8\sqrt{2}F(a)} \tag{50}$$

$$S_3(a) = \frac{35}{4\sqrt{2}}\left[3\pi F(a) - \frac{\hat{V}(a)}{F(a)}\right] \tag{51}$$

$$S_4(a) = \frac{7}{2\sqrt{2}}\left[-12\pi F(a) + 5\frac{\hat{V}(a)}{F(a)}\right] \tag{52}$$

$$S_5(a) = \frac{9}{4\sqrt{2}}\left[7\pi F(a) - 3\frac{\hat{V}(a)}{F(a)}\right] \tag{53}$$

$$\hat{V}(a) = (1+a)V(a) + a(1-a)V'(a) \tag{54}$$

The non-dimensional crack opening displacement is expressed as:

$$u(a,y) = \frac{\int_0^a k(s)h_r(s,y)ds}{E'} \tag{55}$$

The Reference Solution for Semi-circular Geometry

Based on a previous work using finite element method (Adamson et al. 1996), the reference solution for which a uniform crack face pressure is chosen can be obtained as below:

$$f_r(a) = \frac{F(a)}{(1-a)^{3/2}} \tag{56}$$

$$V_r(a) = \frac{V(a)}{(1-a)^2} \tag{57}$$

Where

$$F(s) = \sum_{i=0}^{7} \alpha_i s^i \tag{58}$$

$$V(s) = \sum_{i=0}^{7} \gamma_i s^i \tag{59}$$

The values for the coefficients α_i and γ_i are presented in Table 23.

Table 23 Values for the coefficients α_i and γ_i

i	0	1	2	3	4	5	6	7
α_i	1.1215	-1.1497	7.9753	-12.3914	6.4138	6.7957	-9.6846	3.1024
γ_i	2.9086	-4.3767	24.6551	-33.8874	64.2510	-83.8393	68.1176	-22.8548

The expression for $\Phi(a)$ for the SCB reference case is written:

$$\Phi(a) = \sum_{i=0}^{7} \kappa_i s^i \tag{60}$$

Where the coefficients κ_i ($i = 0,1, \ldots, 7$) are 0.6289, -1.081, 3.5188, -5.8425, 6.6906, -5.6382, 3.3323, and -0.9800, respectively.

Semi-circular Bending Crackline Stress

According to Adamson et al. (1996), the SCB crackline stress $\sigma(y)$ is expressed as:

$$\sigma(y) = \sigma_{SCB}\bar{\sigma}(y) = \sigma_{SCB} \sum_{i=0}^{N} c_i y^i \tag{61}$$

Where

$$\sigma_{SCB} = \frac{P}{BR} \tag{62}$$

The fitting coefficients are listed in Table 24 for different S/R.

Table 24 Values for the coefficients c_i

S/R	c_0	c_1	c_2	c_3	c_4
1.0	1.543	-7.720	16.443	-15.776	5.484
1.2	1.792	-7.227	12.026	-9.981	3.122
1.4	2.072	-7.155	9.090	-6.163	1.658
1.6	2.365	-7.086	5.959	-1.957	
1.8	2.702	-7.852	5.679	-1.443	
2.0	3.043	-8.503	5.153	-0.802	

Determination of K_{ic}^{s} and $CTOD_c$ from the Load-CMOD Curve

In the load-CMOD curve, the CMOD $\mathrm{w(A)} \equiv 2\mathrm{U(A,0)}$.

$$\mathrm{V(a)} = \frac{\mathrm{EBR}}{\mathrm{PA}}\mathrm{U(A,0)} = \frac{\mathrm{EBR}}{\mathrm{PA}}\frac{\mathrm{w(A)}}{2} \tag{63}$$

$$\frac{\mathrm{w(A)}}{\mathrm{P}} = \frac{2\mathrm{V(a)A}}{\mathrm{EBR}} \tag{64}$$

In the load-CMOD curve, the compliance C are calculated through the linear portion (within 10% and 40% of the peak load) of the loading and unloading step.

$$\mathrm{C} = \frac{\mathrm{w(A)}}{\mathrm{P}} \tag{65}$$

The modulus of elasticity is expressed as:

$$\mathrm{E} = \frac{\mathrm{V(a)A}}{\mathrm{BCR}} = \frac{2\mathrm{V(a)a}}{\mathrm{BC}} \tag{66}$$

Define $\mathrm{S(a)} = \mathrm{V(a)a}$,

$$\mathrm{E} = \frac{2\mathrm{S(a)}}{\mathrm{BC}} \tag{67}$$

Using the initial compliance $\mathrm{C_i}$ in the loading portion of the curve, the modulus of elasticity is written:

$$\mathrm{E} = \frac{2\mathrm{S(a_0)}}{\mathrm{BC_i}} \tag{68}$$

For the unloading compliance $\mathrm{C_u}$, the modulus of elasticity is written:

$$\mathrm{E} = \frac{2\mathrm{S(a_c)}}{\mathrm{BC_u}} \tag{69}$$

Assume E doesn't change during loading and unloading process:

$$\frac{2S(a_0)}{BC_l} = \frac{2S(a_c)}{BC_u} \tag{70}$$

$$S(a_c) = \frac{C_u}{C_l} S(a_0) \tag{71}$$

The effective-elastic cracking length ratio a_c can be easily determined through the Solver function in the Excel or using the numerical computing software such as Maple.

Once the a_c is determined, the critical fracture toughness is computed by:

$$K(A_c) = \sqrt{R}k(a_c) = \sqrt{R}\int_0^{a_c} \sigma(y)h_r(a_c, y)dy \tag{72}$$

And the critical cracking tip opening displacement is written as:

$$CTOD_c = 2U(a_c, a_0) = 2Ru(a_c, a_0) = \frac{2R}{E}\int_{a_0}^{a_c} k(s)h_r(s, a_0)ds \tag{73}$$

III.7.2 Fracture Test of RAP-PCC Mixtures

Three sets of SCB specimens covering the 0.40_520_REF, 0.40_520_40HOU and 0.40_520_40BRY mixtures were tested. For each mixture type, 6 SCB specimens with 12 mm notch length and 6 SCB specimens with 38 mm notch length were made from one 150 mm cylindrical specimen (R=75 mm). A list of the prepared of SCB specimens is presented in Table 25.

Table 25 Summary of SCB fracture test specimens

Mixture type	Sample ID	Curing age (day)	Thickness (mm)	Notch length (mm)
0.40_520_REF	REF 1-1	28	38.79	38
	REF 1-2	28	37.80	38
	REF 2-1	28	37.80	38
	REF 2-2	28	37.70	38
	REF 3-1	28	37.28	38
	REF 3-2	28	37.40	38
	REF 4-1	28	38.80	12
	REF 4-2	28	38.90	12
	REF 5-1	28	38.70	12
	REF 5-2	28	38.70	12
	REF 6-1	28	38.40	12
	REF 6-2	28	38.70	12
0.40_520_BRY	BRY 1-1	28	36.60	38
	BRY 1-2	28	36.50	38
	BRY 2-1	28	36.30	38
	BRY 2-2	28	35.90	38
	BRY 3-1	28	36.80	38
	BRY 3-2	28	36.70	38
	BRY 4-1	28	36.80	12
	BRY 4-2	28	37.00	12
	BRY 5-1	28	38.40	12
	BRY 5-2	28	38.60	12
	BRY 6-1	28	36.20	12
	BRY 6-2	28	36.20	12
0.40_520_HOU	HOU 1-1	28	36.40	38
	HOU 1-2	28	36.50	38
	HOU 2-1	28	35.90	38
	HOU 2-2	28	36.00	38
	HOU 3-1	28	36.30	38
	HOU 3-2	28	36.30	38
	HOU 4-1	28	36.46	12
	HOU 4-2	28	36.50	12
	HOU 5-1	28	34.80	12
	HOU 5-2	28	34.60	12
	HOU 6-1	28	36.30	12
	HOU 6-2	28	36.40	12

The fracture tests were conducted according to the testing procedure mentioned in 3.7.1. For each mixture type, 6 SCB specimens with 12 mm notch length (A/R=0.16) and 6 SCB specimens with 38 mm notch length (A/R=0.5) were initially prepared. However, several test results were discarded due to some unexpected errors during either the sample preparation or the test performing. Typical load-CMOD curves for the 38 mm notched specimen and the 12 mm

notched specimen are shown in Figure 38. It has been noted that most of the specimens with 12 mm notch suffered from a sudden failure after the peak load as such applying an unloading process when the loading was still within 95% of the maximum load was not possible. The unloading process usually occurred when the loading already dropped to less than half of the peak load (Figure 38 (b)). The violation of starting the unloading process when the load was still near the peak caused a higher unloading compliance, and consequently resulted in a higher calculated effective elastic crack length. As a result, the calculated values of K_{Ic}^{s} and $CTOD_c$ were higher than what they should be. Accordingly, the calculated values for K_{Ic}^{s}, $CTOD_c$, and G_f for all specimens with the 12 mm notch length were considered invalid. On the other hand, during the unstable failure of the 12 mm notched specimens, a considerable amount of energy was converted to the sound and heat energy, so the area under the load-load point displacement curve might overestimate the total fracture energy (G_F) of the specimen. With the aforementioned reasoning, the tested values for K_{Ic}^{s}, $CTOD_c$, G_f and G_F for the specimens with 12 mm initial notch length were not included in the further analysis in Chapter IV. Table 26 lists the results for all the SCB specimens. The abandoned data is clearly demonstrated with the color coding.

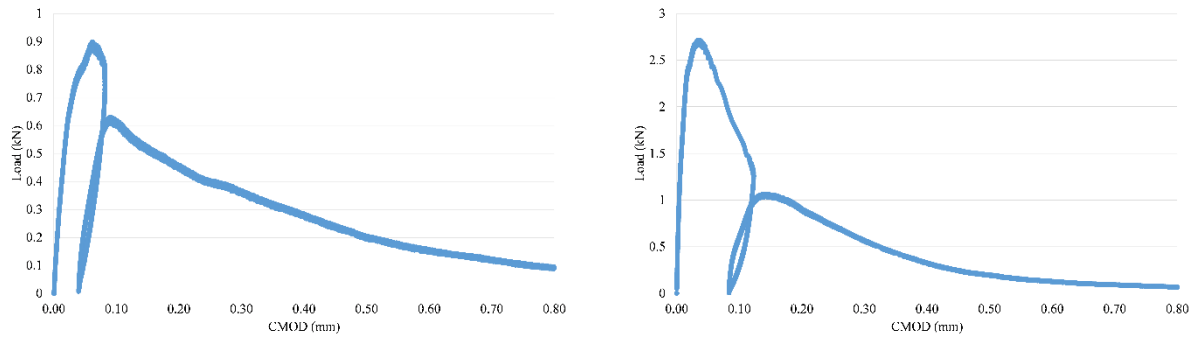

(a) 38 mm notch (HOU 1-1) (b) 12 mm notch (HOU 5-2)

Figure 38 Typical load-CMOD curve

Table 26 SCB fracture test results

Sample ID	Peak load (kN)	CMOD at the peak load (mm)	Modulus of elasticity (GPa)	K_{Ic}^{s} (MPa$\sqrt{m}$)	$CTOD_c$ (mm)	G_f (N/m)	G_F (N/m)
REF 1-1	0.9318	Knife edges drafting during the test					
REF 1-2	0.9837	0.023800	26.530	0.6060	0.00869	13.8414	69.9369
REF 2-1	0.9677	0.025065	25.527	0.6084	0.00933	14.5016	78.9607
REF 2-2	0.8420	0.024491	25.532	0.5338	0.00823	11.1598	95.1281
REF 3-1	1.0829	Knife edges drafting during the test					
REF 3-2	1.0617	0.028153	23.847	0.7099	0.01245	21.1302	92.7190
REF 4-1	2.6644	0.017997	37.613	Improper unloading, late unloading or no unloading during the test			
REF 4-2	3.2136	0.014776	30.956				
REF 5-1	4.2711	0.013644	32.598				
REF 5-2	3.4741	0.019028	33.520				
REF 6-1	3.5174	0.019581	21.448				
REF 6-2	3.1028	0.015883	25.944				
HOU 1-1	0.8987	0.062019	12.302	0.6093	0.02035	30.1745	115.2549
HOU 1-2	0.9218	0.049765	15.064	0.6213	0.01686	25.6214	96.4391
HOU 2-1	0.8559	0.045810	14.547	0.6613	0.02146	30.0622	69.1297
HOU 2-2	0.9272	0.030294	23.263	Improper unloading, late unloading or no unloading during the test			
HOU 3-1	0.7059	0.043163	11.989	0.4902	0.01724	20.0459	92.2181
HOU 3-2	0.9548	0.052272	17.366	0.6386	0.01482	23.4859	86.4393
HOU 4-1	Sample broken before the test						
HOU 4-2	3.0737	0.020007	21.456	Improper unloading, late unloading or no unloading during the test			
HOU 5-1	2.3597	0.030656	17.283				
HOU 5-2	2.7166	0.034788	14.506				
HOU 6-1	2.9695	0.024836	16.869				
HOU 6-2	2.6342	0.025759	16.150				
BRY 1-1	0.8828	0.039184	15.660	0.6646	0.01990	28.2044	118.4583
BRY 1-2	0.7982	0.051155	14.751	0.7340	0.02833	36.5229	73.4673
BRY 2-1	0.8506	0.054635	15.339	0.6745	0.02157	29.6595	93.8586
BRY 2-2	Sample broken before the test						
BRY 3-1	0.7903	0.041042	12.791	0.5779	0.02064	26.1146	139.9161
BRY 3-2	0.9339	0.063913	16.436	0.7183	0.03161	31.3885	118.6991
BRY 4-1	1.8789	0.020997	15.784	Improper unloading, late unloading or no unloading during the test			
BRY 4-2	3.2201	0.014460	27.604				
BRY 5-1	2.0912	0.025908	17.770				
BRY 5-2	3.1704	0.020845	26.074				
BRY 6-1	1.8801	0.025439	14.980				
BRY 6-2	2.1660	0.024757	20.230				

CHAPTER IV

ANALYSIS AND DISCUSSION OF THE TESTING RESULTS*

The analysis and discussion of the testing results obtained from Chapter III is presented below.

IV.1 USE OF RAP TO ENHANCE AGGREGATE GRADATION

IV.1.1 Enhanced Aggregate Gradation

Based on the literature review presented in Chapter III, replacing coarse virgin aggregate by coarse RAP aggregate with sufficient intermediate sized particles can create a combined aggregate gradation that approaches an optimized gradation. This is because HMA typically uses smaller sized aggregates than PCC, which makes RAP a rich source of intermediate particles; the intermediate particles are what conventional gap-graded concrete mixtures lack. Shilstone Sr (1990) initiated the optimized gradation mix design approach (reviewed in Appendix A). In his approach, the coarseness factor chart is used to optimize aggregate gradation. Figure 39(a) shows the coarseness factor chart for the studied mixtures. From Figure 39(a), since HOU and AMA have similar gradations with the virgin coarse aggregate (Figure 18), replacing the virgin coarse aggregate with either HOU or AMA does not significantly change the combined gradation. So, the plots of the 0.40_520_HOU mixture series, the 0.40_520_AMA mixture series, and the 0.40_520_REF are close to each other in the CF chart (close to the border between the well-

*Part of the contents in this chapter is reprinted with permission from:
Validation of RAP and/or RAS in Hydraulic Cement Concrete: Technical Report by Mukhopadhyay, A., and Shi, X., 2017, Texas A&M Transportation Institute, Texas. Copyright [2017] by Texas A&M Transportation Institute.
"Mix Design Formulation and Evaluation of Portland Cement Concrete Paving Mixtures Containing Reclaimed Asphalt Pavement." by Shi, X., Mukhopadhyay, A., and Liu, K.-W., 2017, *Construction and Building Materials*, 152, 756-768, Copyright [2017] by Elsevier Ltd.

graded region and the coarse gap-graded region). The combined gradations of the 0.40_520_BRY mixtures series and the 0.40_520_SA mixture series fall within the workability box (the 30 and 40 percent mixtures lie almost in the middle), indicating that these mixtures may be dense-graded PCC mixtures. Since the dense gradation is beneficial for concrete workability and mechanical properties, these two mixture series are anticipated to have better performance in terms of a better workability and less reductions in mechanical properties in comparison with the gap-graded RAP-PCC mixtures.

According to Shilestone (Shilstone Sr 1990), an ideal concrete aggregate gradation has a "haystack" shape on the individual percent retained chart. This concept has led to the development of some forms of "8-18 band" specification, which is used to force the gradation to become more of a haystack shape and get away a double humped one (Richardson 2005). The "8-18 band" specification generally requires to keep the individual retained percent between 8 and 18 percent for sieves #30 (0.6 mm) through the sieve one size below the normal maximum size. There is much discussion of the cons of the "8-18 band", though. One of the cons it that the "8-18 band" is sometimes too expensive to follow strictly as getting the fractions to fill the gaps is sometimes not practical or economical. Besides, in some locations this specification cannot be met because the native materials do not have the fraction available to meet the required gradation. Therefore, the "8-18 band" specification is considered a recommended tool but not a required one. In fact, experience has shown that a gradation which follows the 8-18 band does still not result in good concrete, and vice versa (Richardson 2005). The real significance of the "8-18 band" lies in the fact that it helps to design a well-graded aggregate blend that would not exhibit pronounced peaks and valleys. TxDOT modified the "8-18 band" specification and

formulated the designation Tex-470-A. According to the Tex-470-A, the combined percent retained gradations must meet the following criteria in the IPR chart.

- It must be within the upper and lower boundaries.
- The sum of the percent retained on the 2.36-mm sieve to the 0.6-mm sieve must not be less than 15 percent.
- The sum of the percent retained on the 0.6-mm sieve to the 0.75-mm sieve must be between 24 percent and 34 percent.

Figure 39(b) plots the percent retained charts for some of the RAP-PCC mixtures in this study. Both the TxDOT (black solid boundaries) and a conventional "8-18 band" (U.S. Air Force requirement, black dotted boundaries) requirements are shown in the same figure. Figure 39(b) indicates that the 0.40_520_40BRY and the 0.40_520_35SA mixtures can meet the requirements by TxDOT, while the REF, HOU and AMA mixture series have a peak at 12.5-mm sieve which exceeds the upper limit. The 0.40_520_40SA barely satisfies the TxDOT requirements as the percentage retained on the 4.75-mm sieve is slightly higher. In case of the "8-18 band" requirement, none of the designed mixtures in this study are qualified in a strict manner. However, for the RAP-PCC mixtures containing the RAP sources with a larger portion of intermediate particles (i.e., BRY and SA), the first peak on the coarser end of the curve can be significantly reduced. The most pronounced valley between the 9.5 mm and 2.36 mm sieve size (shown in the yellow box) could be mitigated as well. In fact, the U.S. Air Force requirement does not allow a significant valley, which is defined as one that has more than two sieve sizes between two peaks. Based on this definition, Figure 40 shows the 0.40_520_40BRY might be qualified as an enhanced mixture because the valley is not significant. The 0.40_520_REF and

the 0.40_520_40HOU are gap-graded because there are more than two sieve sizes are between two peaks.

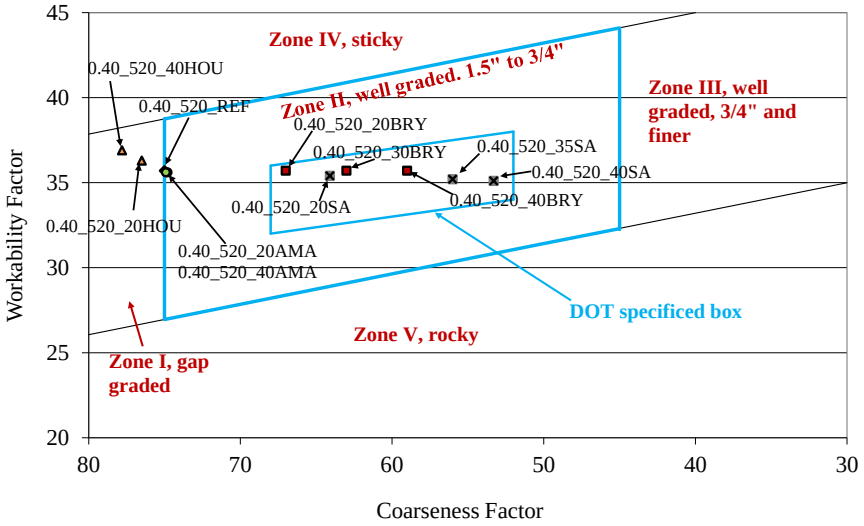

(a) CF chart

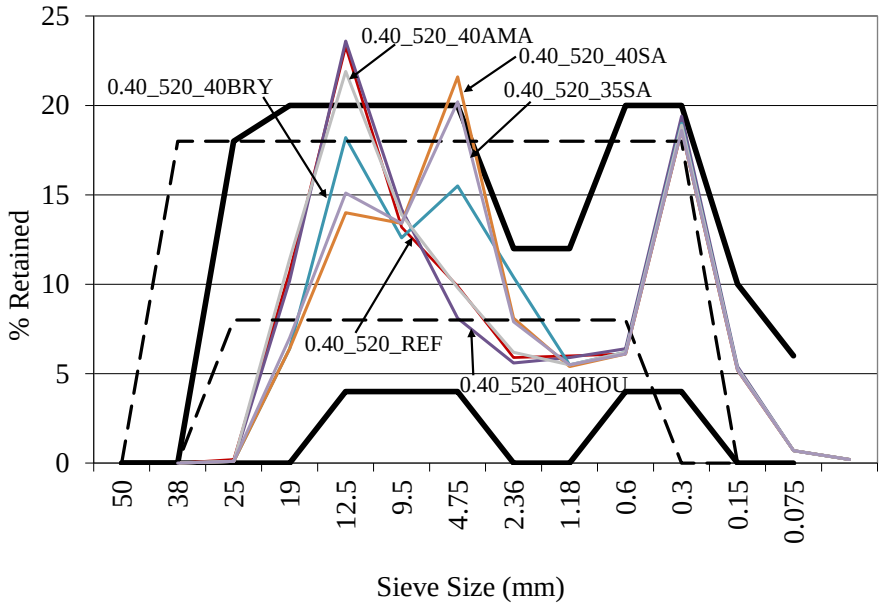

(b) Individual percent retained chart

Figure 39 Enhanced aggregate gradation analysis

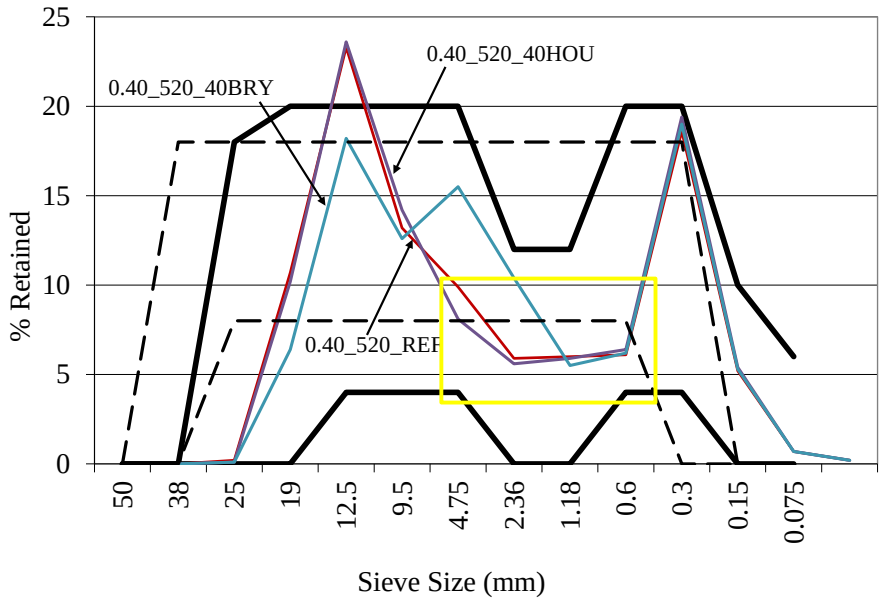

Figure 40 Demonstration of the dense-graded RAP-PCC and gap-graded RAP-PCC

From the aforementioned enhanced aggregate gradation analysis, it is concluded that the RAP-PCC mixtures containing HOU and AMA are gap-graded, while those containing BRY and SA are generally dense-graded or enhanced aggregate gradation. It is noted that a pronounced valley still exists at the 1.18-mm and 0.6-mm sieve sizes for the BRY and SA RAP-PCC. Despite of this valley, the 0.40_520_40BRY and the 0.40_520_SA mixture series are still considered dense-graded because they generally meet the specification in the IPR curve by TxDOT and the plots of these two mixture series all fall within the workability box in the CF chart. The presence of the valley in the combined percent retained curve is due to the fact that the sand used in this study lacks of the 0.6-mm sized particles and no RAP particles below 2.36-mm were added to fill the gap. Since the fine RAP contains a higher asphalt content, it is anticipated that the RAP-PCC containing fine RAP would have a more pronounced reduction in workability

and strengths, despite its aggregate gradation can be further optimized. Further research is needed to verify this assumption.

IV.1.2 Favorable RAP Gradation

The RAP samples were obtained directly from the HMA batching plants, so their gradations followed the specification controlling HMA production. It has been shown in Figure 39 that some RAP gradations yielded dense-graded RAP-PCC mixtures while the others could not. Therefore, it is crucial to make RAP stockpiles with a suitable gradation in order to facilitate producing RAP-PCC mixtures with enhanced aggregate gradation. In order to find a favorable RAP gradation corresponding to different RAP replacement levels, a Matlab code was developed. The favorable RAP gradation was determined so that the combined gradation yielded a position location which was closest to the middle point (CF=60, WF=35) of the workability box in the CF chart. Since the CF and WF calculation only requires the percentage passing values for the 9.5-mm sieve and 2.36-mm sieve, no requirements are needed for the other sieve sizes in the favorable RAP gradation by the CF chart. Table 27 tabulates a summary of the favorable RAP gradation for the various RAP replacement levels determined by the CF chart requirement.

Table 27 Favorable RAP gradations required by the CF chart

Replacement level	% Passing 9.5-mm Sieve	% Passing 2.36-mm Sieve	Corresponding CF	Corresponding WF
20%	100	0	60.1	36.5
25%	81	0	60.1	36.2
30%	71	0	60.0	35.7
35%	63	0	59.9	36.4
40%	58	0	59.8	35.7

After the computation of the percentage passing values for the 9.5-mm sieve and the 2.36-mm sieve, the percentage passing values for the other sieve sizes can be determined in

accordance with the TxDOT requirements of the IPR chart. This procedure can lead to multiple solutions. Table 28 lists examples of the favorable gradations for the corresponding RAP replacement level. Figure 41 shows the combined gradation using the favorable gradation at the corresponding replacement level. It is clearly indicated in Figure 41 the combined RAP-virgin aggregates gradations are much better than the control mix (i.e., the 0.40_520_REF) regarding mitigating both the peak at the 12.5-mm sieve size and the valley at the 2.36-mm sieve size. Except for the valley at the 1.18-mm size and 0.6-mm, the other sizes of the combined RAP-virgin aggregate blends met the "8-18 band" specification for all the replacement levels, which suggested that these RAP-virgin aggregate gradations are dense graded.

Table 28 Examples of the favorable RAP gradations (percent passing each sieve)

Replacement level	20%	25%	30%	35%	40%
25 mm	100	100	100	100	100
19 mm	100	100	100	100	100
12.5 mm	100	100	100	100	100
9.5 mm	100	81	71	63	58
4.75 mm	50	40	35	30	20
2.36 mm	0	0	0	0	0
1.18 mm	0	0	0	0	0
0.6 mm	0	0	0	0	0
0.3 mm	0	0	0	0	0
0.15 mm	0	0	0	0	0
0.075 mm	0	0	0	0	0
Pan	0	0	0	0	0

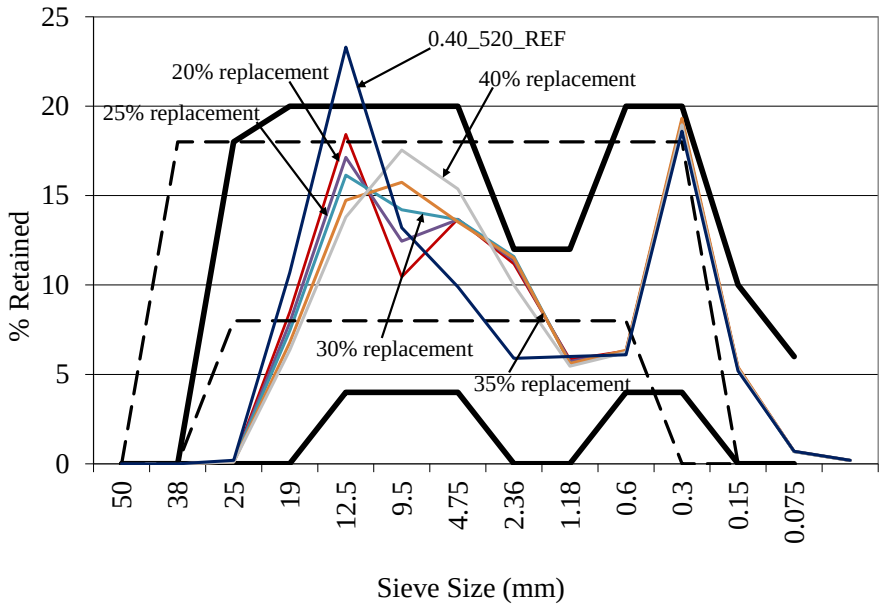

Figure 41 Combined gradation using favorable RAP gradations

Figure 42 plots the favorable gradations and the studied RAP gradations together. In Figure 42, BRY and SA are close to the favorable gradation curves of 30-40% replacement levels, indicating these two RAP gradations can produce dense aggregate gradation at the corresponding RAP replacement levels. For the HOU and AMA gradations, they are too far away from these favorable gradation curves, so they could not yield dense gradations. These conclusions match the results from the CF chart analysis (Figure 39).

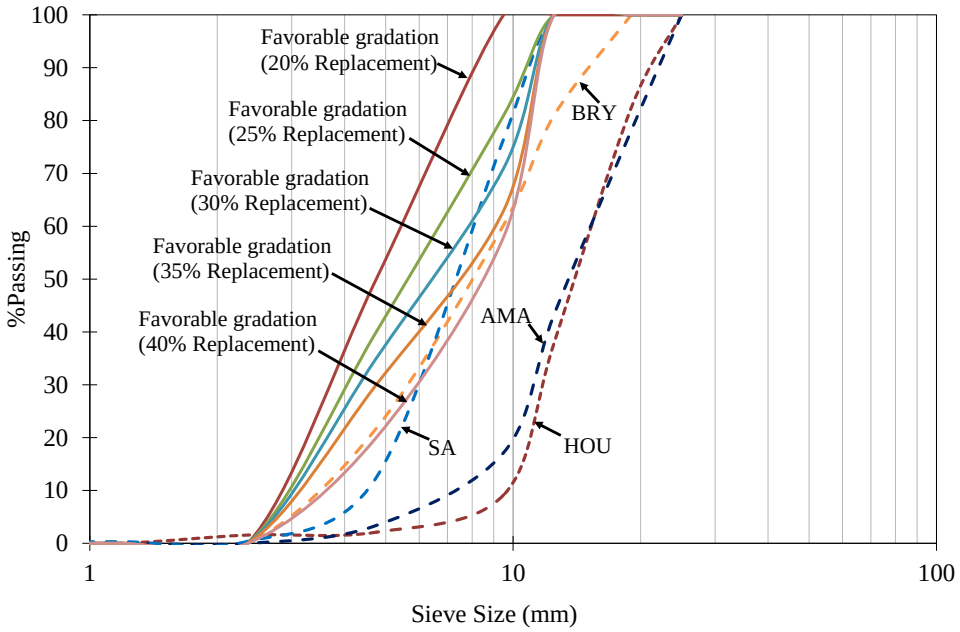

Figure 42 Comparison between the favorable gradations and tested RAP gradations

It is noted that the favorable gradations determined in this section are on the basis of the specific mix design for this dissertation using 0.40 w/cm ratio, 309 kg/m^3 cementitious content, #4 coarse limestone and the specific concrete sand. If the mix design changes, the favorable RAP gradation will also change. However, with the approach developed here, the favorable RAP gradations for different mix designs can be easily obtained.

IV.2 FRESH AND HARDENED PROPERTIES

IV.2.1 Fresh Properties

The slump test results in Figure 43(a) show that the addition of HOU or AMA slightly increased the slump, while adding BRY and SA reduced the slump, relative to the control mixture. However, the use of the slump values does not necessary reflect the workability of a PCC mixture (especially for RAP-PCC mixtures). Slump itself is only a measure of movement of

a 300 mm cone of fresh concrete, but workability is a reflection of the bulk displacement and overall sagging of a mixture. Figure 44 shows three problematic types of slump and one adequate one for the RAP-PCC mixtures in this study (including trial mixtures). Figure 44(a) indicates that when both of coarse and fine RAP are introduced in the PCC mixture at a high replacement level (>50%), the mixture would become inconsistent. The mixture lacks cohesion due to the poor shear resistance of the asphalt films of the RAP aggregates and therefore would suffer from a shear slump. When only the fine virgin aggregates are replaced by the fine RAP at a high replacement level (>50%) without adding excess water or cementitious materials, the mixture would look very dry and has very low movement (Figure 44(b)). These two types of slump again indicate that use of fine RAP to produce a workable class P concrete is not feasible. Figure 44 (c) shows a wet mixture which suffers from a collapse slump. This RAP-PCC mixture contains a high amount of coarse RAP (>50%), and the asphalt lubricating effect is the major reason for the high slump. This kind of mixture is anticipated to have segregation issues (refer to Appendix D). The observations of these three types of problematic mixtures validated the strategies of this study (i.e., use coarse RAP only, and limit the RAP replacement level within 50%). Figure 44(d) presents a picture of a workable RAP-PCC mixture produced in this study. In general, the mixtures designed from Table 12 fall into this category. It is also noted that the enhanced graded mixtures (the 0.40_520_BRY and the 0.40_520_SA series) indeed showed better workability compared to the gap-graded mixtures (the 0.40_520_REF, the 0.40_520_HOU and the 0.40_520_AMA series), as the gap-graded RAP-PCC mixtures appeared to be slightly too wetter (suggested by Figure 43(a)). In terms of air content, all the RAP-PCC samples showed lower air contents than the control mixture (Figure 43(b)).

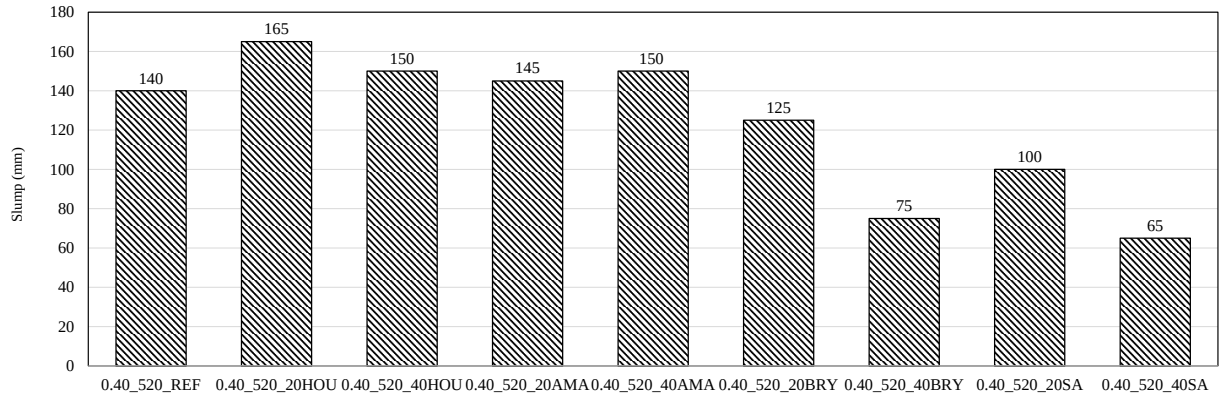

(a) Slump

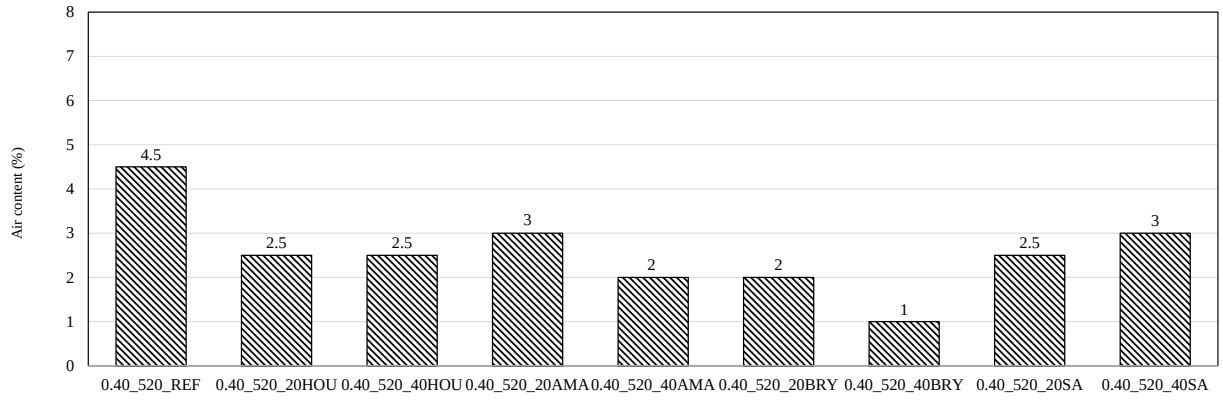

(b) Percent air content

Figure 43 Fresh properties of the studied RAP-PCC mixtures

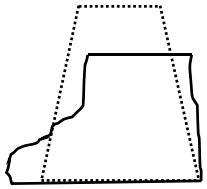

Mixture is not consistent or lack of cohesion

(a) RAP-PCC containg both coarse and fine RAP at a high replacement level (>50%)

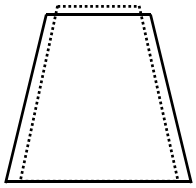

Concrete is too dry; almost has no fluidity

(b) RAP-PCC containing only fine RAP at a high replacement level (>50%)

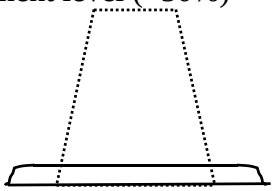

Concrete is too wet; can not hold together

(c) RAP-PCC containing only coarse RAP at a high replacemen level (>50%)

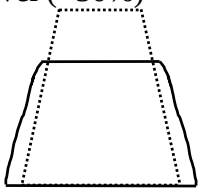

A consistent and flowable concrete mixture

(d) RAP-PCC containing only coarse RAP at a low replacement level (<50%)

Note: Applicable mix design: w/cm: 0.40-0.45; cementitious content: 309-389 kg/m^3

Figure 44 Interpretation of RAP-PCC slump tests

IV.2.2 Mechanical Properties

Mechanical Properties Testing Results

Compressive Strength

Figure 45 shows the average values of the CS, the percentage reduction of the CS of the RAP-PCC in comparison with the control mixture, and the rate of increase in the CS over time. The percentage reduction is defined as the strength difference between the RAP-PCC mixtures and the reference mixture normalized by the strength of the reference mixture. The results indicate that replacing the virgin aggregate with the SA had the least reduction in compressive strength, followed by BRY, HOU and AMA combinations. Since the mineralogy of HOU, BRY and SA stones are similar (mainly limestone), the main reason that the PCC containing BRY and SA had higher strength compared to the concrete containing HOU might be the enhanced

aggregate gradation. The AMA RAP-PCC manifested higher strength reduction compared to the other RAP-PCC mixtures. This is likely due to the higher amounts of agglomerated particles in the mixture based on visual evidence observed in broken specimen after testing. Figure 46 clearly shows there are agglomerated particles in the specimen. In terms of the rate of increase in the CS over time, there is no clear trend that could distinguish the RAP-PCC mixtures and the control mixture.

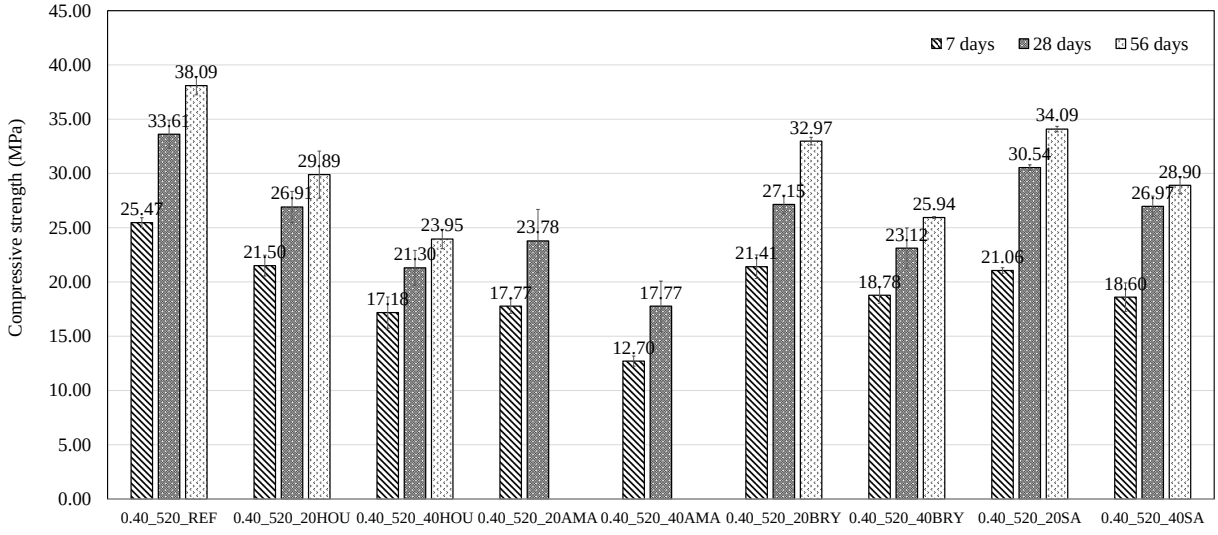

(a) Compressive strength

Figure 45 Compressive strength results

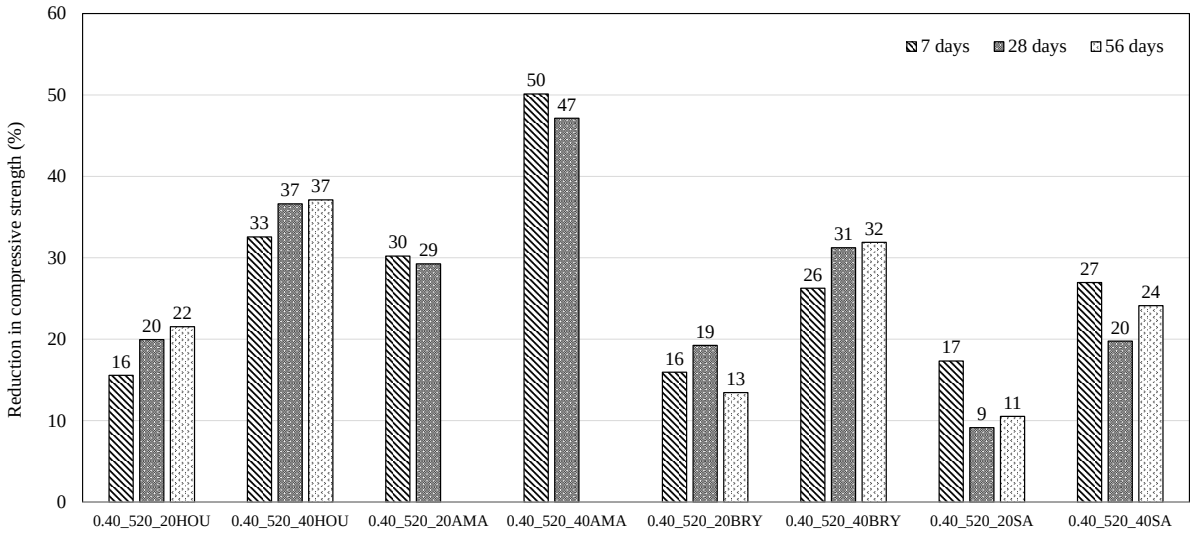

(b) Percentage reduction in comparison with the reference mix

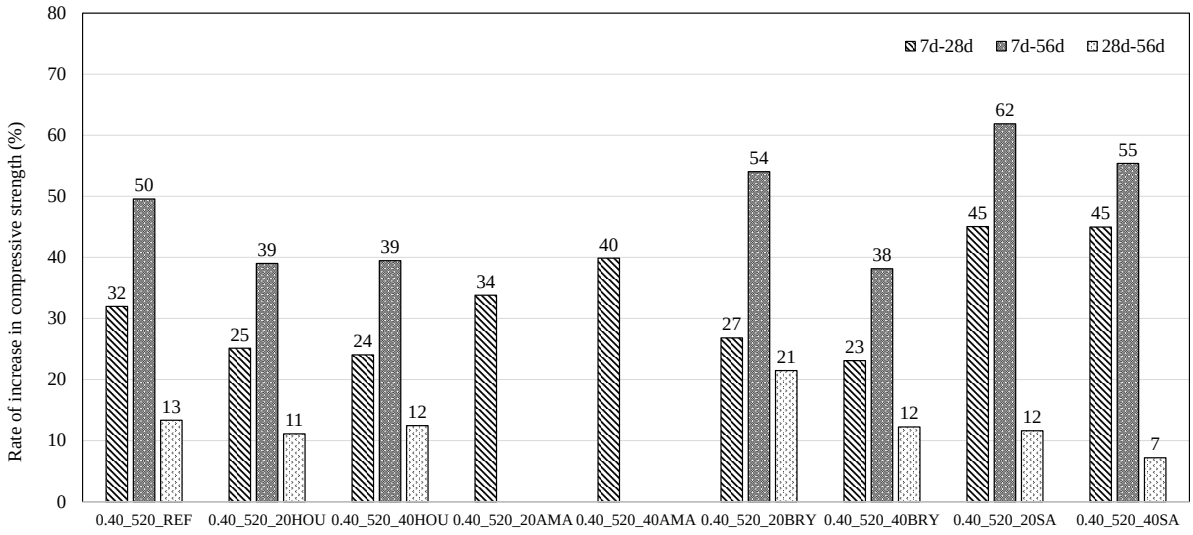

(c) Rate of increase over different time intervals

Figure 45 Continued

Figure 46 Agglomerated RAP particles from a cross section view of the 0.40_520_40AMA

MOE

Figure 47 shows the MOE results. The 0.4_520_20AMA samples had a slightly higher reduction than other RAP-PCC with 20% RAP replacement level, while the 0.40_520_40SA mixture showed the least MOE reduction among all the RAP-PCC with 40% RAP replacement level. Figure 47(c) shows that the samples for the 20 percent replacement level had similar rates of increase over time while the samples for the 40 percent replacement level tended to have higher rates compared to the reference mix, but the trends were not obvious.

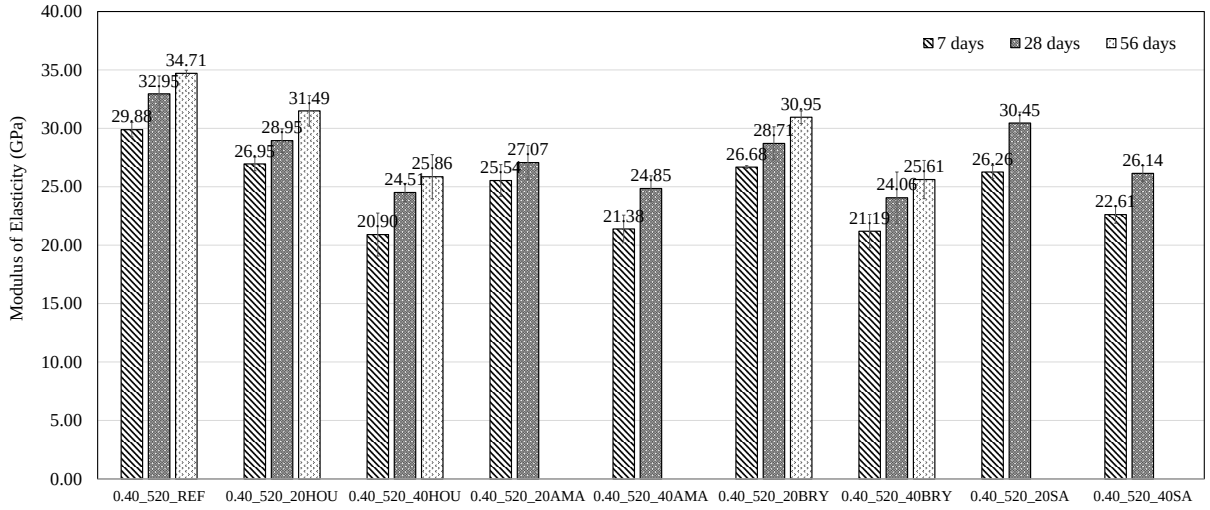

(a) MOE

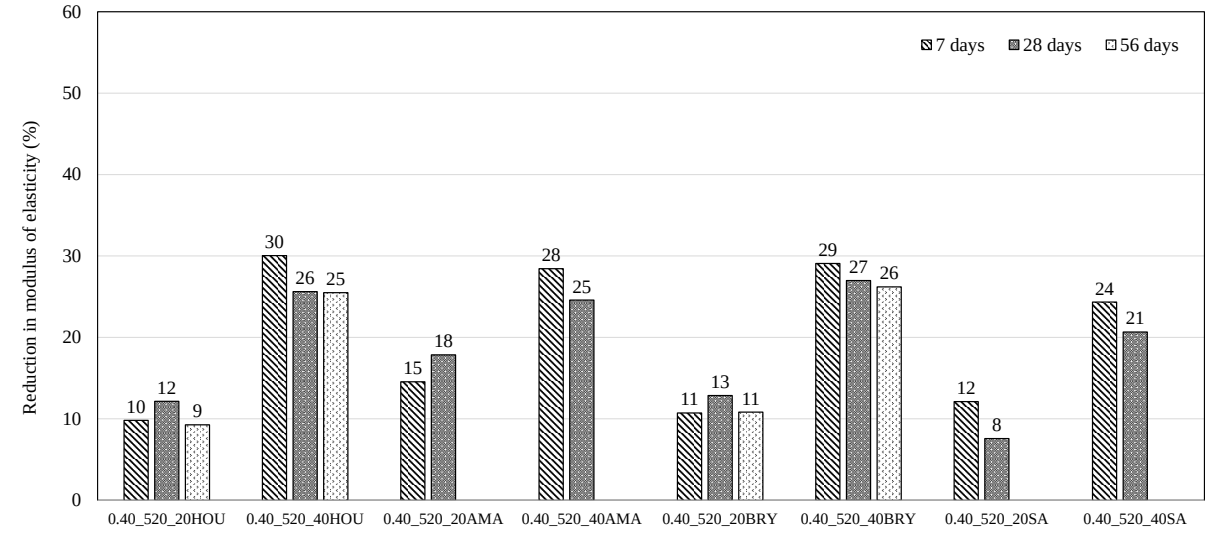

(b) Percentage reduction in comparison with the reference mix

Figure 47 MOE results

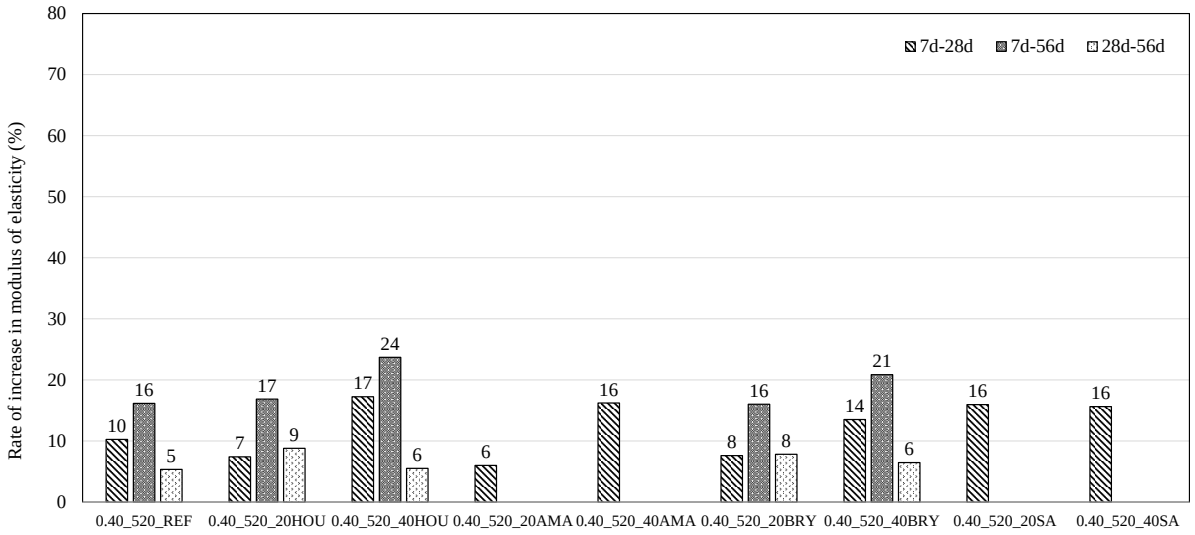

(c) Rate of increase over different time intervals

Figure 47 Continued

MOR

Figure 48 plots the average values of the MOR, the percentage reduction of the MOR in comparison with the control, and the rate of increase in the MOR over time. Based on the results obtained, the important observations are listed below:

- At 20 percent replacement level, the AMA RAP-PCC mixture show the highest percentage of reduction, while at 40 percent replacement level, the HOU RAP-PCC mixture had the highest reduction (Figure 48 (b)).
- The percentage reduction of the compressive strength (Figure 45(b)) is much higher than the percentage reduction of the MOR for all the RAP-PCC types.
- The dense-graded RAP-PCC (i.e., the 0.40_520_BRY and the 0.40_520_SA series) yielded obviously better results than the other two gap-graded RAP-PCC mixes (i.e., the

0.40_520_HOU and the 0.40_520_AMA), which again proved the benefit of the dense gradation mix design.

Interestingly enough, although the AMA RAP-PCC showed much higher reduction in compressive strength (Figure 45(b)), its rate of reduction level in MOR was close to the HOU RAP-PCC (Figure 48(b)). This finding suggests that the characteristics of the aggregate may play a less important role in determining flexural behavior of the RAP-PCC mixtures compared to its compressive behavior. The samples of 40 percent RAP replacement level showed a higher rate of increase over time compared to the samples of 20 percent RAP replacement level. The rate of increase of MOR for the mixes with 40 percent RAP replacement is higher than the control mix. However, the rate of increase of MOR for the mixtures with 20 percent RAP replacement is either little lower or comparable with the control mixture.

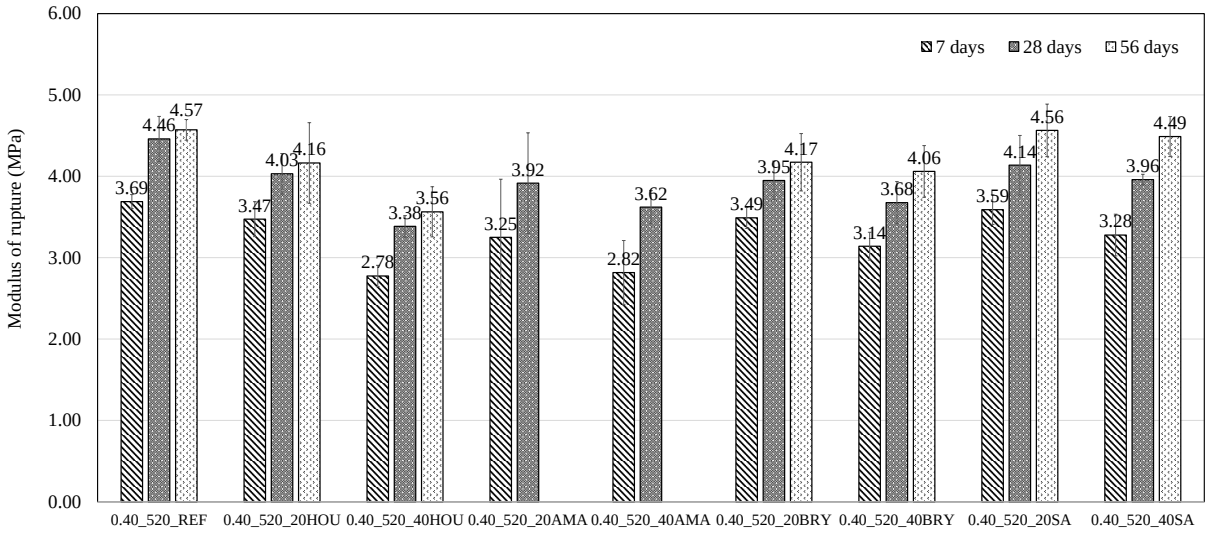

(a) MOR

Figure 48 MOR results

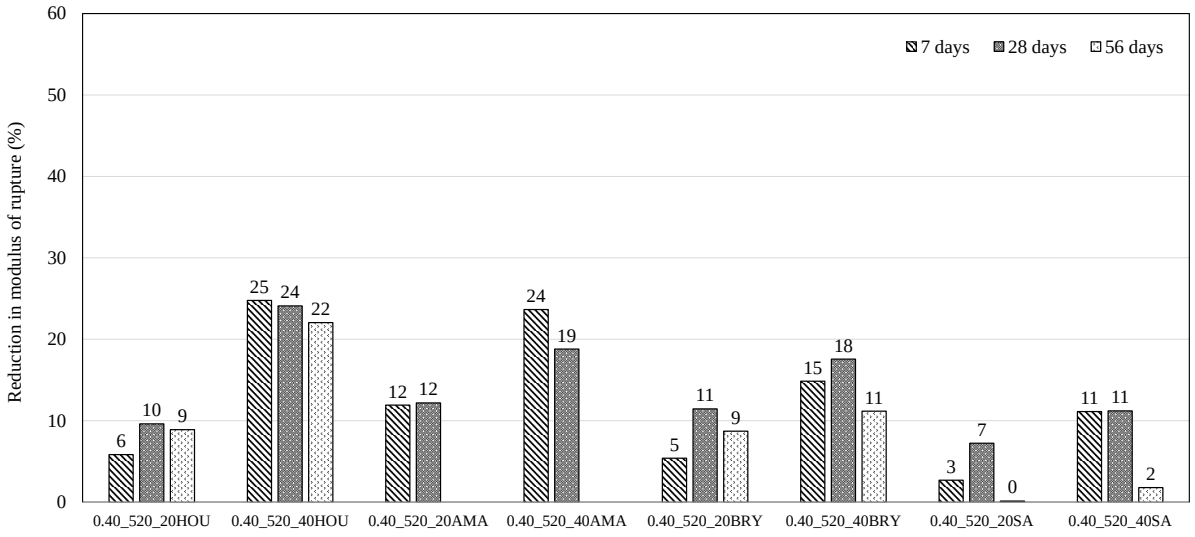

(b) Percentage reduction in comparison with the reference mix

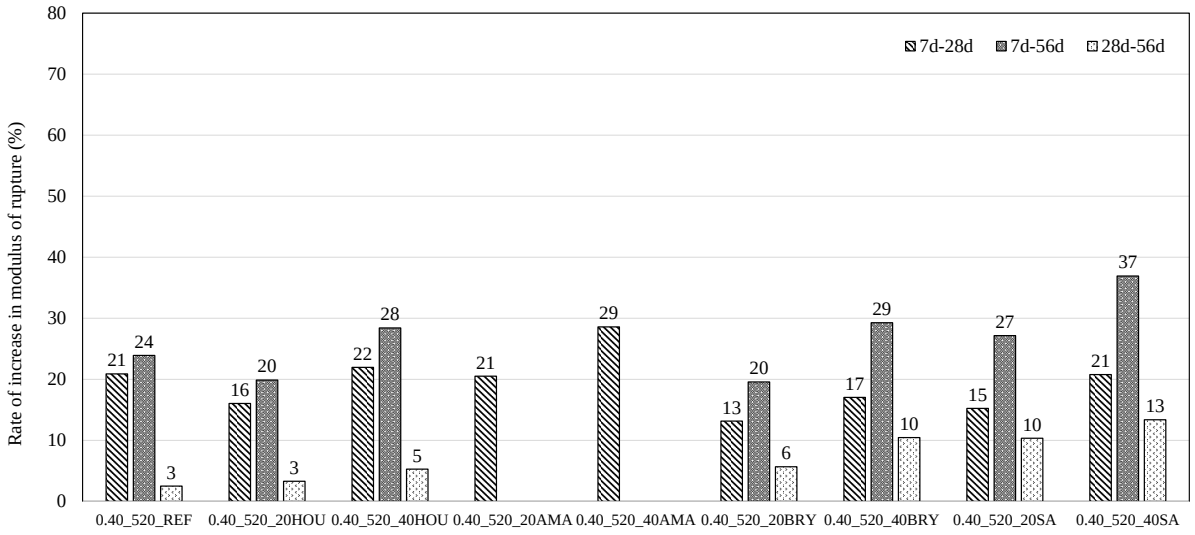

(c) Rate of increase over time

Figure 48 Continued

STS

Figure 49 presents the results for the STS of the PCC containing RAP. For the 20 percent replacement level, the strength reduction was small; the mixtures containing HOU, BRY and SA

RAP even had increased STS compared with the reference mixes. When 40 percent of RAP was added, the reduction became more obvious; the SA RAP-PCC yielded the highest STS, followed by the BRY RAP-PCC, the HOU RAP-PCC, and the AMA RAP-PCC. For the rate of increase over time, the RAP-PCC mixtures with 40% RAP generally had higher values compared to that for the reference mixture, while the mixtures with 20% RAP showed lower values.

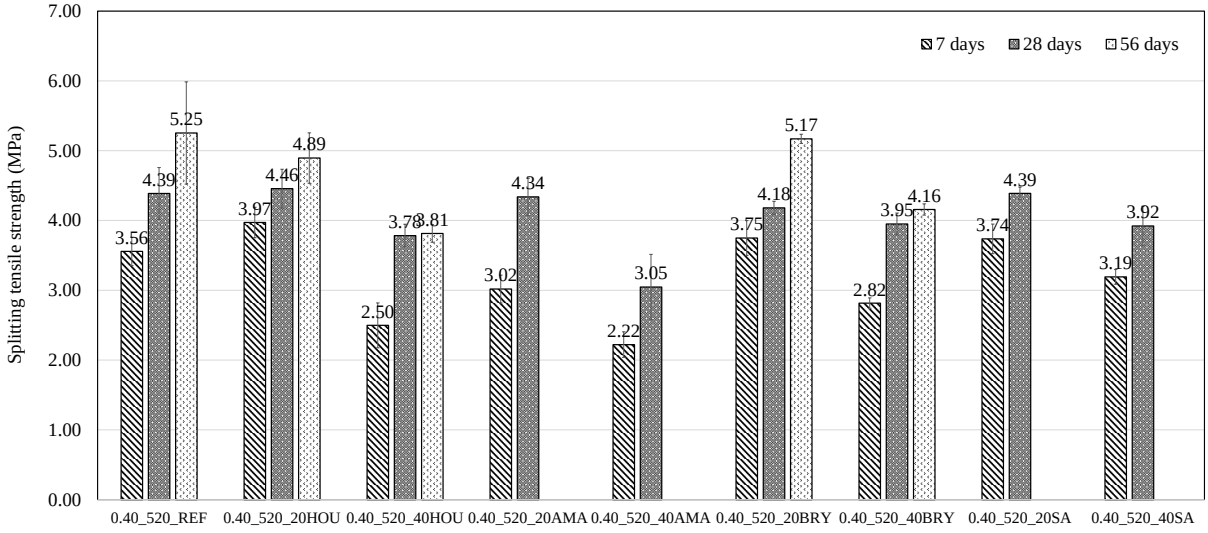

(a) STS

Figure 49 STS results

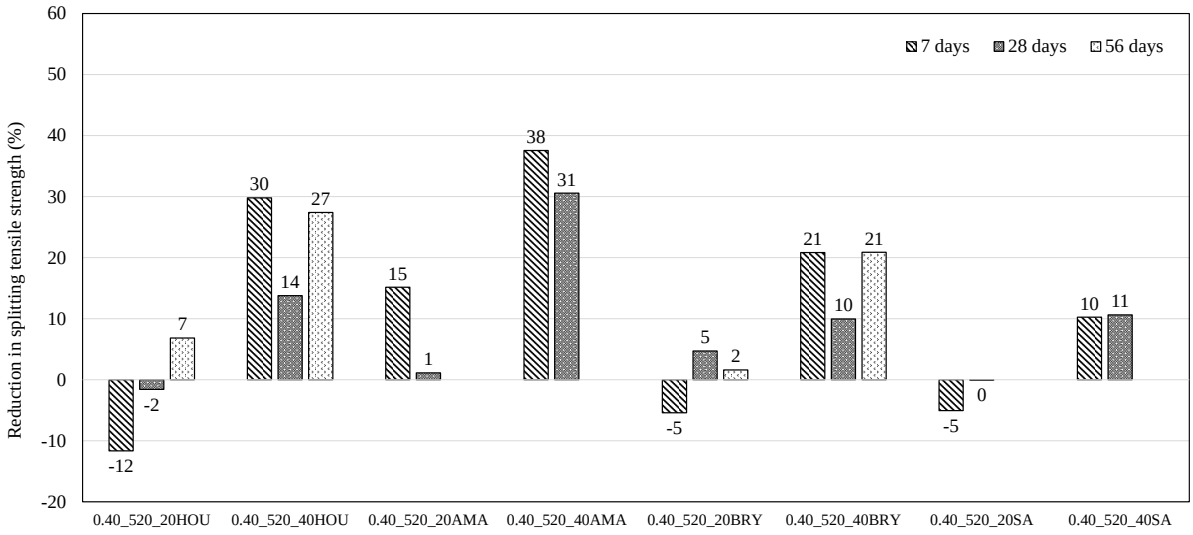

(b) Percentage reduction in comparison with the reference mix

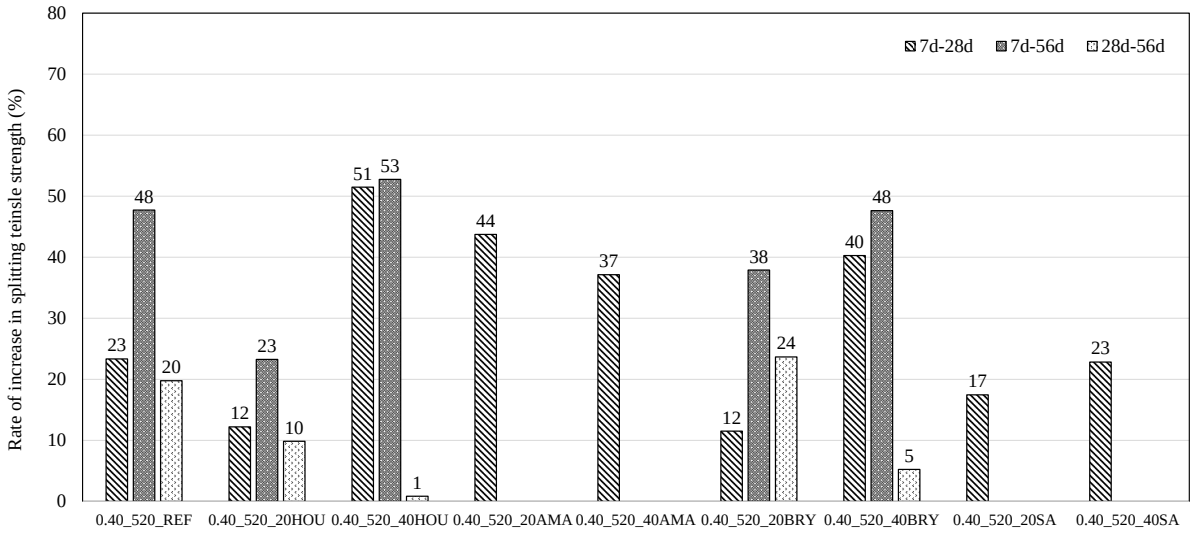

(c) Rate of increase over different time intervals

Figure 49 Continued

Analysis and Discussion of Mechanical Properties Test Results

Comparison between Different Strengths

The percentage reductions in different mechanical properties at 7-day, 28-day and 56-day for the studied RAP-PCC mixtures in comparison with the reference mixture are summarized in Figure 50. A negative percentage reduction indicates that the RAP-PCC has improved property. The 0.40_520_BRY and the 0.40_520_SA mixture series showed lower percentage reductions in mechanical properties than the PCC mixtures made of both HOU and AMA (more prominent with 40% replacement level than 20% replacement), which is believed to be resulted from the benefit of the dense gradation. In general, the AMA RAP mixtures showed the highest reductions, which is likely due to issues related to agglomeration of RAP particles mentioned earlier. In the most cases, the compressive strength showed the highest rate of reduction, while the flexural strength or the splitting tensile strength had the lowest reduction. Generally, the reduction in flexural strength was 5 to 28% less than the corresponding reduction in compressive strength. The trend of the rate of reduction was much clearer at higher curing ages and higher RAP replacement levels: the resulting reduction rates from high to low were the compressive strength, the modulus of elasticity, the flexural strength and the splitting tensile strength in general. The finding that RAP-PCC has a less reduction in tensile strength than in compressive strength is possibly explained as the matrix failure is more dominating under tension mode while the crushing of the matrix and aggregate leads to failure under compression. As in the RAP-PCC system, the aggregate bond is altered, so the effect of RAP on compressive properties is much more significant than that on tensile properties. This explanation also explains the previous finding that AMA RAP-PCC showed much higher reduction in compressive strength but its rate of reduction level in MOR was close to the HOU RAP-PCC. Another interesting finding is that

the results indicate that the inclusion of a small amount of RAP could possibly improve the concrete's splitting tensile strength, and this phenomenon occurred more frequently in the earlier ages of the RAP-PCC. This is because at the early age of the RAP-PCC, the cement paste has not gain sufficient strength (especially tensile strength) and is vulnerable to cracking, so adding RAP into the system may have little effect on composite strength. When the cement paste turns much stronger at 28-day, the asphalt layer and asphalt-cement interface behaved more as weak zones in the system, therefore the RAP replacement level becomes the dominating factor in determining the composite strength. This explanation also facilitates the explanation of a less reduction in the 7-day MOR compared to the 28-day MOR for the 20% replacement levels. This matches with the findings from a previous study (Brand and Roesler 2017a). A detailed research to study the nature of the asphalt layer and asphalt-cement in RAP-PCC is presented later in this chapter.

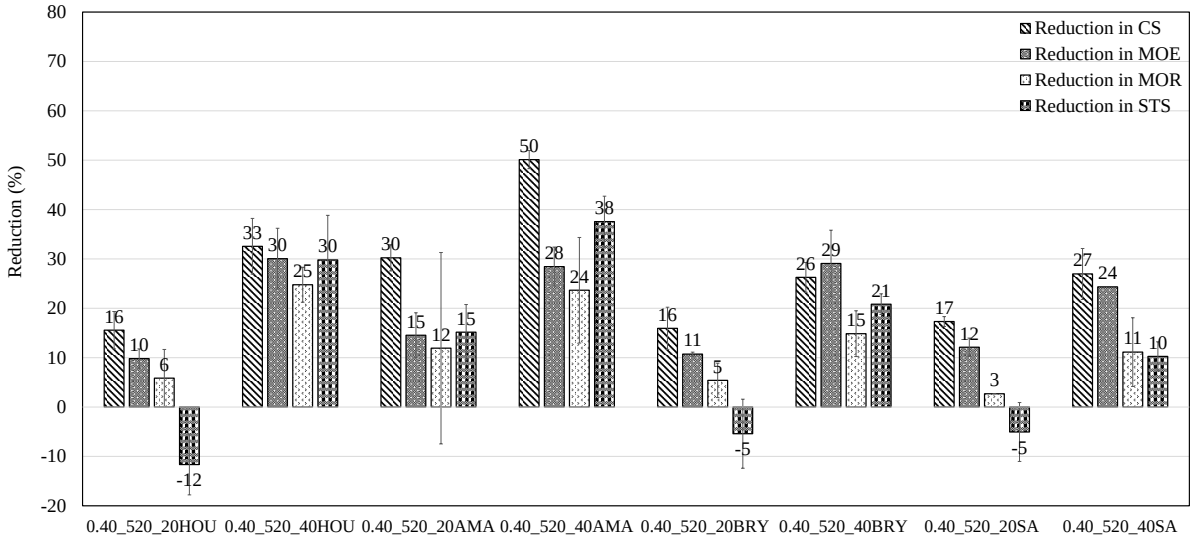

(a) 7 days

Figure 50 Comparison between different mechanical properties

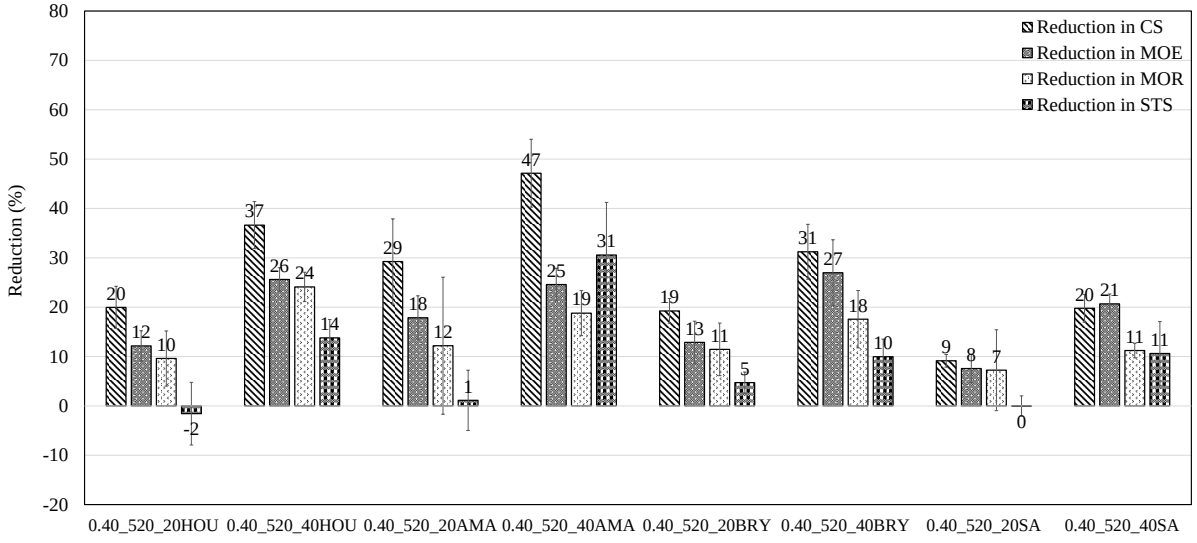

(b) 28 days

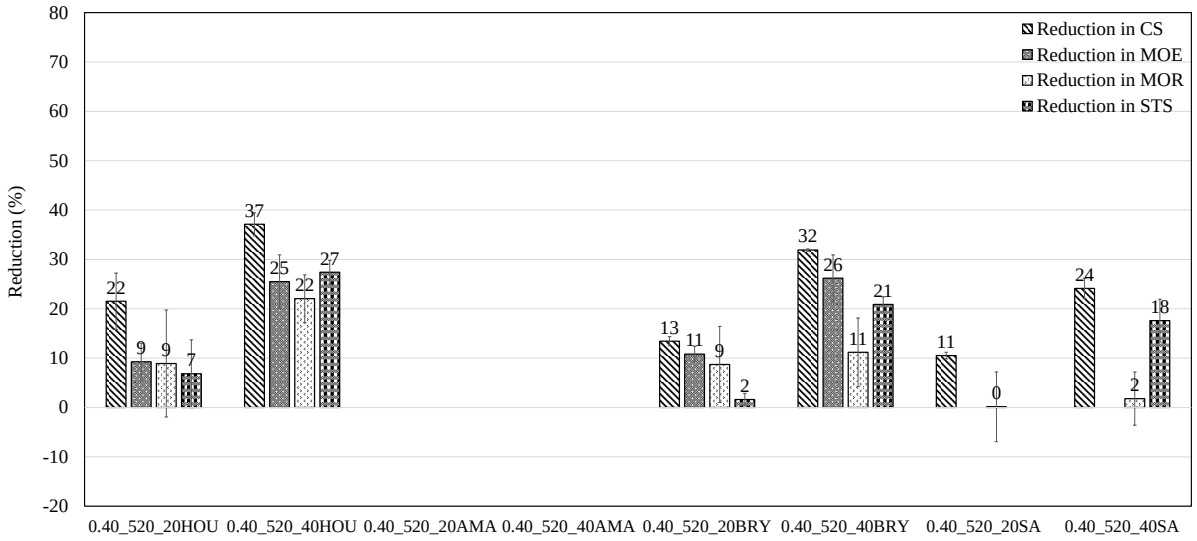

(c) 56 days

Figure 50 Continued

Modification of ACI Correlation Equations

Concrete compressive strength is the most widely tested concrete mechanical property because it is easy to perform. Its result also tends to have a lower coefficient of variance. The

American Concrete Institute (ACI) code 318 provides equations for predicting other mechanical properties such as MOR, MOE and STS from the measured compressive strength, but those equations are only applicable for conventional portland cement concrete (ACI 2008). Tia et al. (2012) have developed similar equations for the RAP-PCC combinations. Similar types of equations for the RAP-PCC system were developed based on the mean values of the tested mechanical properties of the studied mixtures. To increase the number of data and make the equations as general as possible, all of the data from both the 0.45_656 mixtures (presented in Appendix D) and the 0.40_520 mixtures were used. The correlations between the compressive strength and the other mechanical properties along with comparisons with the findings from other references are shown in Figure 51(The equations developed in this study adopted the US customary units in order to maintain the consistency with the ACI 318 equations for conventional PCC).

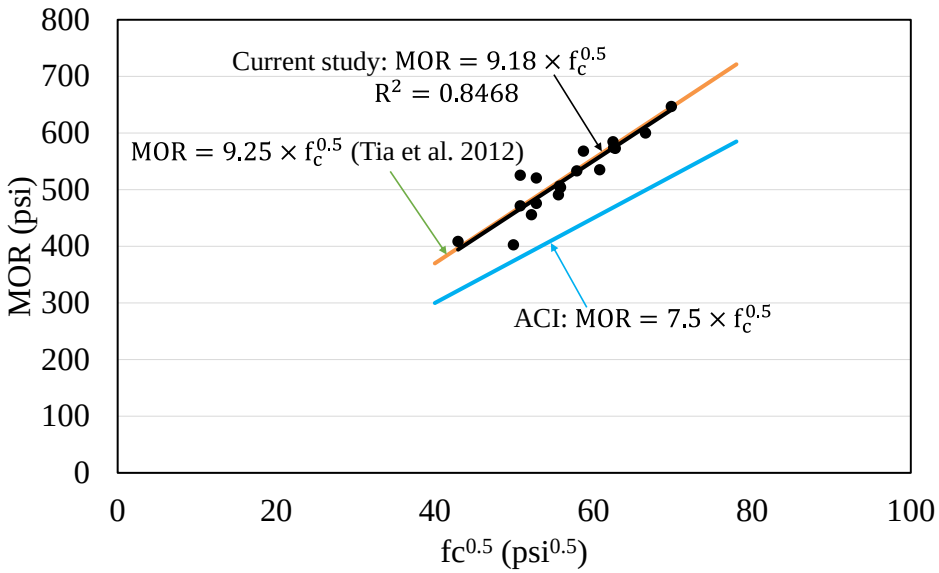

(a) Correlation between MOR and CS

Figure 51 Correlation between mechanical property and compressive strength

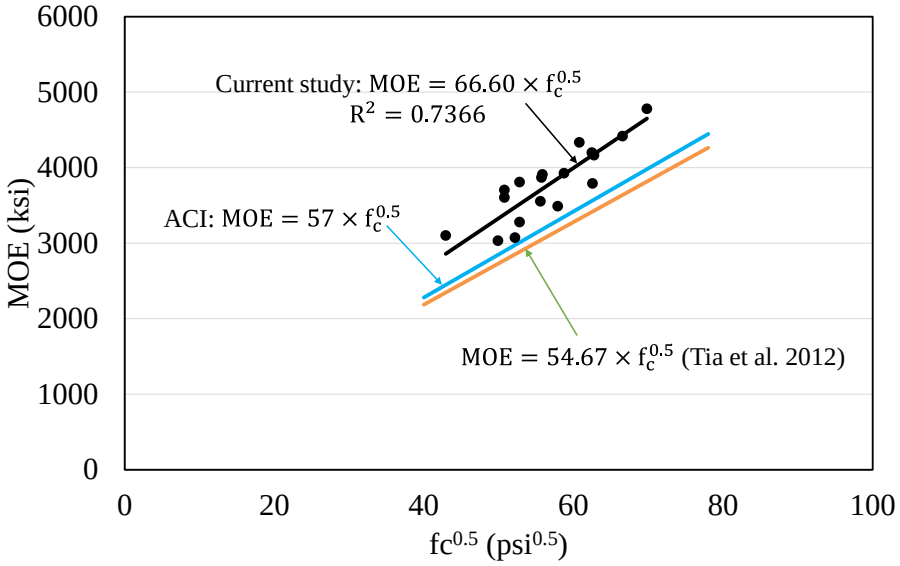

(b) Correlation between MOE and CS

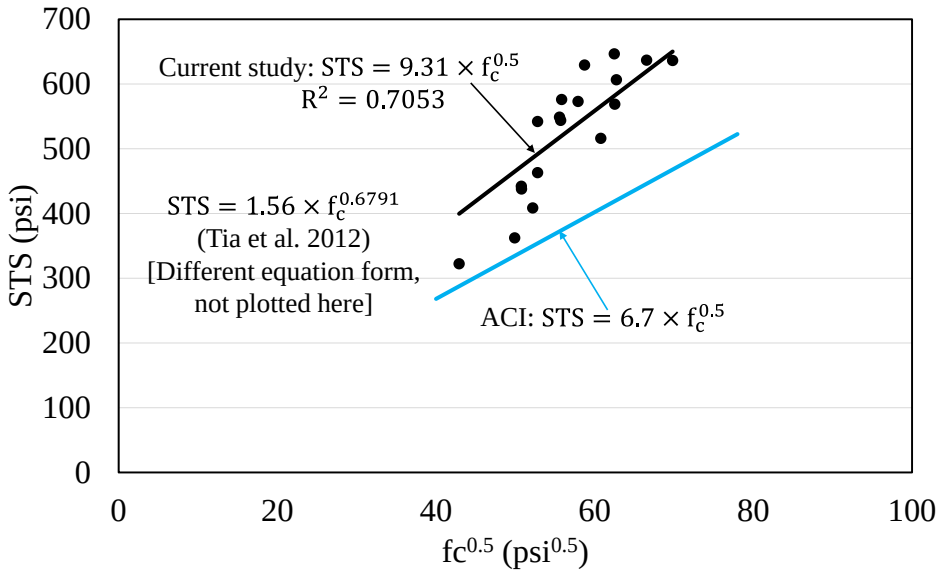

(c) Correlation between STS and CS

Figure 51 Continued

By comparing the equations developed in this study for the RAP-PCC system with the ACI equations for the conventional PCC, it is observed that the ACI equations underestimate the prediction of flexural strength, modulus of elasticity, splitting tensile strength of the studied RAP-PCC mixtures. A comparison between the equations in Tia et al. (2012) and the ACI equations shows that the ACI approach overestimates the modulus of elasticity but underestimates the flexural strength of RAP-PCC system. The inconsistency in the prediction of the modulus of elasticity between the equations developed by the two different studies for the RAP-PCC system might be explained as follows: in the work by Tia et al. (2012), both coarse and fine RAPs were used to make PCC mixtures, which may have resulted in much softer mixtures than the conventional PCC mixtures. The modified correlation between the CS and the MOR developed in this study is used later in this chapter for calculating the corresponding RAP-PCC compressive strength when a flexural strength is specified.

Relationship between Mechanical Properties and Asphalt Fraction

A regression analysis using the data obtained in this study was applied to describe the change of the RAP-PCC mechanical properties as a function of the asphalt fraction. Since the asphalt content varies with RAP types, a use of a total asphalt volumetric fraction (TAVF) is considered to be a more robust way than simply relying on RAP replacement level to quantify the amount of aged asphalt in the RAP-PCC mixtures. The TAVF (θ_g), defined as the volume fraction of the asphalt in the total aggregate mixture (including RAP aggregates), is computed using Equation (74).

$$\theta_g = \theta_l \times v \tag{74}$$

Where

θ_l= the volume fraction of the asphalt in the RAP.

θ_l can be calculated in Equation (75).

$$\theta_l = w \times G_{RAP}/G_b \quad (75)$$

w is the RAP asphalt content (weight fraction), determined by ASTM D6307.

G_b is the specific gravity of asphalt

G_{RAP} is the specific gravity of RAP

v= the RAP volume fraction. i.e., the volume fraction of the RAP in the total aggregate mixture.

Table 29 lists the mechanical properties and the TAVF for the studied mixtures.

Table 29 Summary of mechanical properties for different mixtures

Mix ID	TAVF (%)	7-day fc (MPa)	28-day fc (MPa)	7-day MOR (MPa)	28-day MOR (MPa)
0.40_520_REF	0	25.47	33.61	3.69	4.46
0.40_520_20HOU	1.080	21.50	26.90	3.47	4.03
0.40_520_40HOU	2.127	17.17	21.30	2.77	3.39
0.40_520_20AMA	1.425	17.77	23.78	3.25	3.92
0.40_520_40AMA	2.834	12.70	17.77	2.82	3.62
0.40_520_20BRY	1.653	21.41	27.14	3.49	3.95
0.40_520_30BRY	2.471	19.13	26.64	3.30	3.78
0.40_520_40BRY	3.285	18.78	23.12	3.14	3.67
0.40_520_20SA	1.327	21.06	30.54	3.59	4.14
0.40_520_35SA	2.323	19.22	27.92	3.16	4.26
0.40_520_40SA	2.655	18.60	26.97	3.28	3.96

Since the compressive and flexural strength requirements are the major criteria by different DOTs for specifying Class P concrete, only the relationships of (i) compressive strength versus TAVF and (ii) flexural strength versus TAVF, were used to develop regression equations. The regression equations, shown in Figure 52 and Figure 53, were developed using the averaged strength values from the mixtures with 0, 20% and 40% RAP replacement level for each RAP-PCC mixture type (Table 29). The 0.40_520_30BRY and the 0.40_520_35SA were used to validate the correlation based on the regression equations. As can be seen in Figure 52 and

Figure 53, the compressive strength and flexural strength show a strong linear relationship with the TAVF, and the compressive strength for the 0.40_520_35SA and the flexural strength for the 0.40_520_30BRY match well with the corresponding trend lines. This finding suggests testing two RAP replacement level (20% and 40% replacement are recommended here) together with the reference mixture data point can be considered as a reasonably good approximation to construct the relationship between the CS/MOR and TAVF. It is to be noted that the linearity may validate only within the range of the tested TAVF for these studied mixtures (i.e., 0-3.285). When the TAVF is higher (when higher RAP replacement level is used or/and fine RAP is introduced), the relationship between strengths and TAVF is generally nonlinear (Mukhopadhyay and Shi 2017b). A generalized relationship is then proposed in Figure 54. In Figure 54, the slope k is defined as the rate of deterioration. It represents how fast the addition of the RAP material negatively affects the strength. Obviously, a lower k is desired, because a lower k can allow more asphalt in the system before the properties become unacceptable. It is believed that k is largely related to the RAP quality and the mix design. The coefficient, b, is the intercept of the line with the y-axis, which should be close to the reference mixture property. The regression coefficients, k and b, for different RAP type are summarized in Table 30.

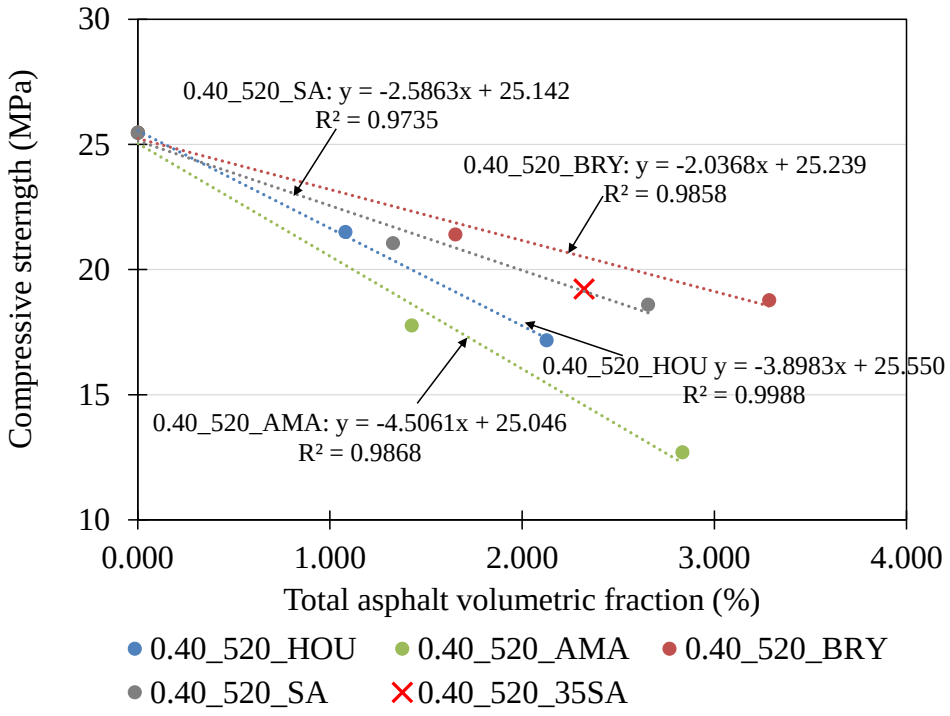

(a) 7 days

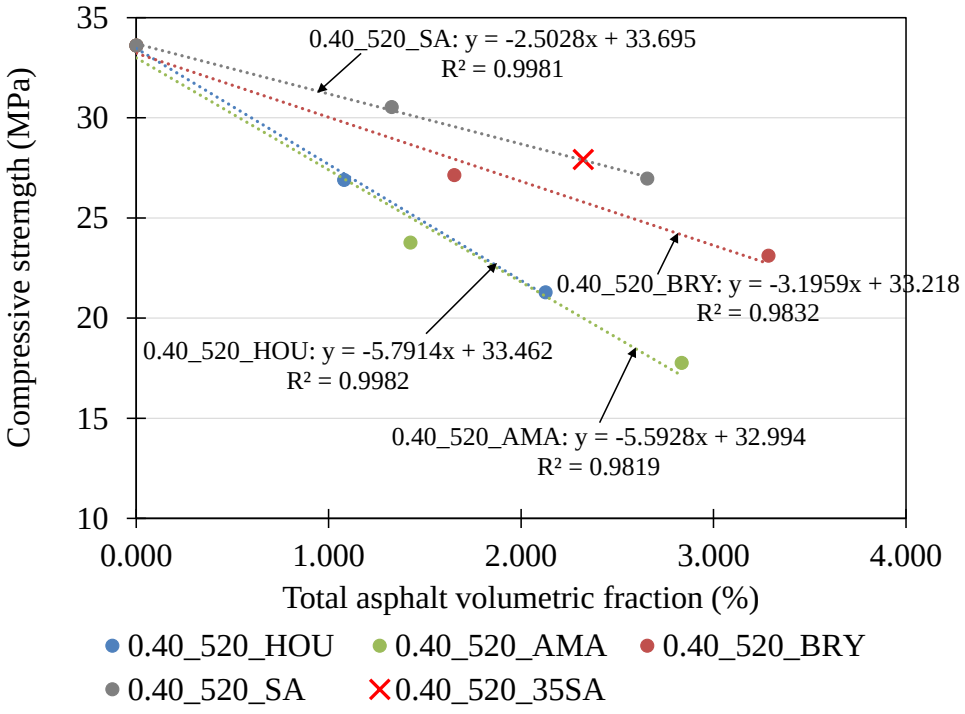

(b) 28 days

Figure 52 Correlations between asphalt fraction and compressive strength

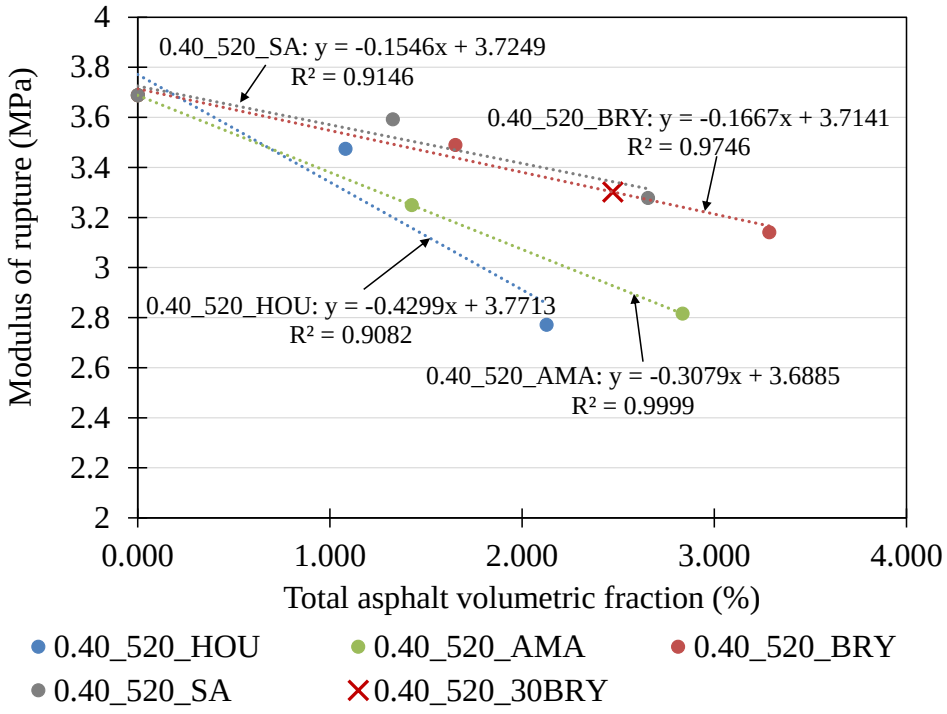

(a) 7 days

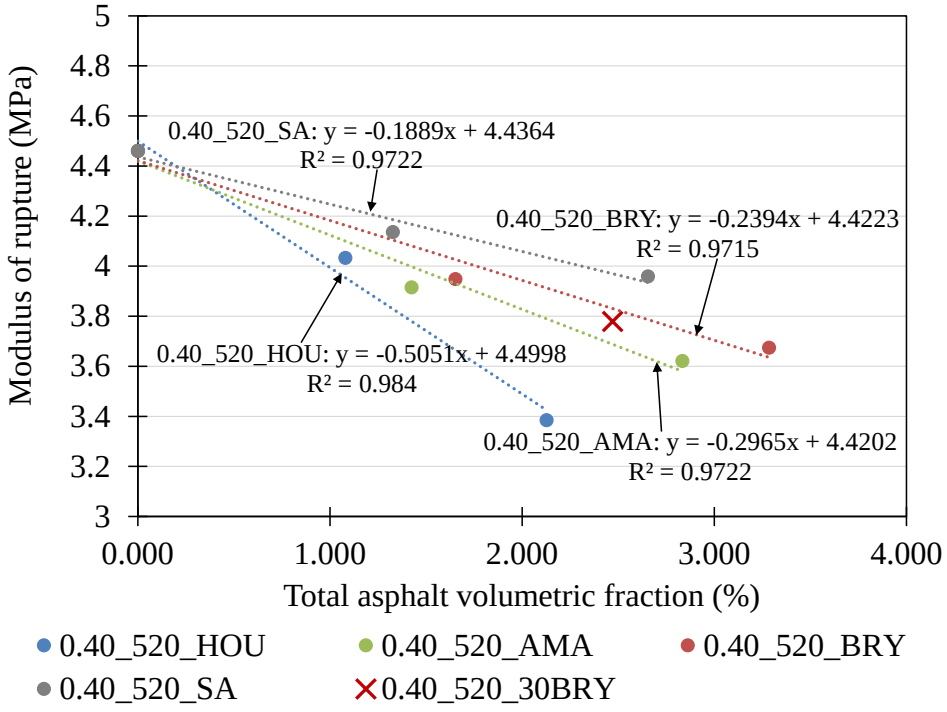

(b) 28 days

Figure 53 Correlations between asphalt fraction and modulus of rupture

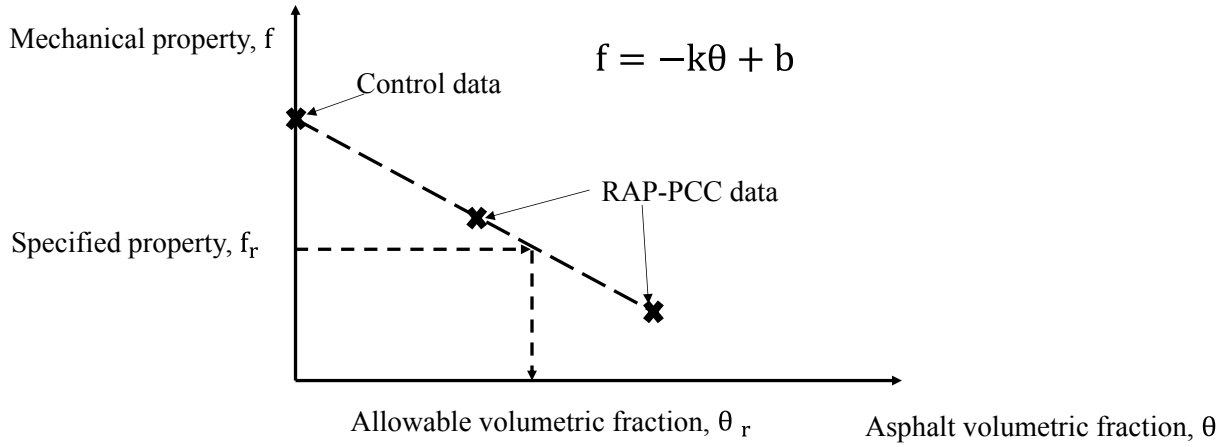

Figure 54 Correlations between the mechanical property-model

Table 30 Regression coefficients for different mixes

Mix ID	7-day fc'		28-day fc'		7-day MOR		28-day MOR	
	k (MPa)	b (MPa)	k (MPa)	b (MPa)	k (MPa)	b (MPa)	k (MPa)	b (MPa)
0.40_520_HOU	3.8983	25.550	5.7914	33.462	0.4299	3.7713	0.5051	4.4998
0.40_520_AMA	4.5061	25.046	5.5928	32.994	0.3079	3.6885	0.2965	4.4202
0.40_520_BRY	2.0368	25.239	3.1959	33.218	0.1667	3.7141	0.2394	4.4223
0.40_520_SA	2.5863	25.142	2.5028	33.695	0.1546	3.7249	0.1889	4.4364

The comparison among the workability results (Figure 43), the mechanical properties (Figure 50) and the enhanced aggregate gradation analysis (Figure 39) clearly demonstrates the benefit of using RAP to design dense-graded PCC. Table 30 shows that the dense-graded mixtures (i.e., 0.40_520_BRY and 0.40_520_SA mixture series) had much lower rate of deterioration for both compressive strength and flexural strength at both 7 and 28 curing ages compared to the gap-graded mixtures (i.e., 0.40_520_HOU and 0.40_520_AMA mixture series). Compared to the 0.40_520_HOU and the 0.40_520_AMA mixture series, the k values for the 0.40_520_BRY and the 0.40_520_SA mixture series were only approximately half. This finding

further indicates that the dense-graded RAP-PCC manifested higher mechanical properties than the gap-graded RAP-PCC.

Optimum RAP Replacement for Class P Concrete

The allowable TAVF can be easily found from the regression relationships (Table 30) when the allowable limit for the required strength (compressive or flexural strength) is given (Figure 54). The corresponding RAP replacement level can be back-calculated subsequently. Using the coefficients in Table 30, the allowable RAP replacement levels satisfying the TxDOT specification requirements were obtained and summarized in Table 31.

Table 31 Allowable RAP replacement level for different mixtures based on different criteria

TxDOT allowable values	7-day f_c': 22.06 MPa (3200 psi)	28-day f_c': 27.58 MPa (4000 psi)	7-day MOR: 3.10 MPa (450 psi)	28-day MOR: 3.93 MPa (570 psi)
0.40_520_HOU	16%	19%	29%	20%
0.40_520_AMA	9%	13%	27%	23%
0.40_520_BRY	18%	21%	44%	24%
0.40_520_SA	18%	36%	60%	40%

Table 31 indicates that the allowable AMA replacement level is much lower compared to the HOU RAP-PCC, BRY RAP-PCC and SA RAP-PCC if the compressive strength criteria are used. This is mainly due to the presence of greater number of agglomerated RAP particles in AMA RAP together with the high asphalt content of the AMA RAP. In addition, it has been indicated that the aggregate quality greatly impact the PCC's compressive strength. The slope of the linear regression line (k value) for the BRY RAP-PCC and the SA RAP-PCC were much smaller. As a result, their allowable amounts turn out to be higher than the gap-graded RAP-PCC mixtures. Based on the compressive strength criteria, the allowable replacement level satisfying

the 28-day requirement is higher than that satisfying the 7-days requirement for all the RAP-PCC cases. Based on the flexural strength, the trend is opposite. Therefore, assignment of a common replacement level can be explained as follows: with respect to the compressive strength in the TxDOT specification, the rate of increase from 7-day requirement (3200 psi) to 28-day requirement (4000 psi) is 25 percent. Figure 45(c) shows that the rate of increase of the RAP-PCC mixtures over the same time interval were higher or at least close to 25 percent. With a higher strength increase rate, the allowable replacement level at 28 days is expected to be higher than that at 7 days. However, for the flexural strength case, the rate of increase in the specification is 26.6 percent (from 450 psi to 570 psi), while most of the RAP-PCC mixtures showed a smaller rate of increase (Figure 48(c)), which leads to a lower (lower than 7 days replacement level) allowable replacement in 28 days.

The flexural strength is considered to be a more important and relevant parameter related to concrete pavement performance because concrete is weak in tension and its tensile strength counters stresses induced under traffic and environmental loading. Additionally, concrete fracture behavior is essentially controlled by its tensile strength (presented in later in this chapter). The TxDOT pavement design guide approves to use AASHTO 1993 and TxCRCP-ME to determine jointed plain concrete pavement and continuously reinforced concrete pavement (CRCP) slab thickness, respectively; both of these two design tools require 28-day flexural strength as a material input. Therefore, assigning replacement levels based on the flexural strength criteria may provide a simple approach. On the other hand, the RAP-PCC mixtures manifest a slower flexural strength growth over time than that required by the specification. Therefore meeting the 28-day flexural strength requirement would be considered a more conservative way to estimate the replacement level. Given that the 28-day flexural strength

requirement is 3.93MPa (570 psi), by applying the modified correlation equation for the RAP-PCC found in this study in Figure 51($MOR = 9.18 \times f_c'^{0.5}$ (unit: psi)), it is recommended to set the corresponding 28-day compressive strength requirement as 26.58MPa (3855 psi) for RAP-PCC mixtures, instead of directly using the original value for the conventional PCC (27.58 MPa, equal to 4000 psi).

IV.2.3 Other Pavement Related Properties

Poisson's Ratio

Figure 55 shows the Poisson's ratio results for the studied mixtures at 28-day moist curing age. The results indicate that incorporating RAP into concrete would slightly increase the Poisson's ratio. It is noted that the BRY RAP-PCC had higher Poisson's ratio compared to the HOU RAP-PCC, which suggested the higher the TAVF, the higher the Poisson's ratio of the RAP-PCC.

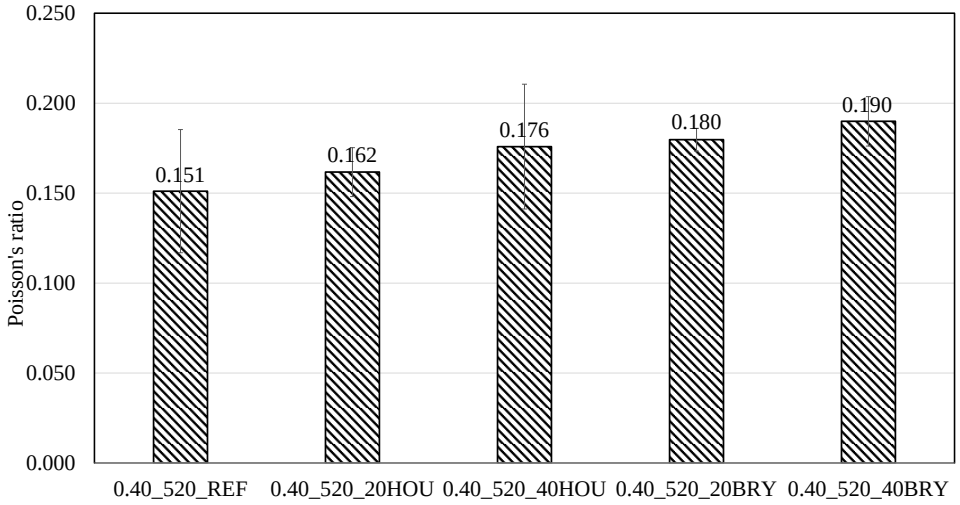

Figure 55 Poisson's ratio test results

CoTE

Figure 56 compares the CoTE results. All of the results are within the normal range of the value for PCC mixtures. However, all the RAP-PCC samples showed higher CoTE than the control sample. The higher the amount of RAP in the mixture, the higher the CoTE is. The material characterization results indicated that the virgin coarse aggregate and the BRY RAP are limestone particles, while the HOU RAP primarily contains limestone with some siliceous particles. Given that the aggregate minerology is similar, the change of CoTE is largely attributed to the asphalt binder in the RAP because the asphalt itself has a higher CoTE. Because of the higher TAVF, the BRY RAP-PCC had higher CoTE values than the HOU RAP-PCC with the same RAP replacement level.

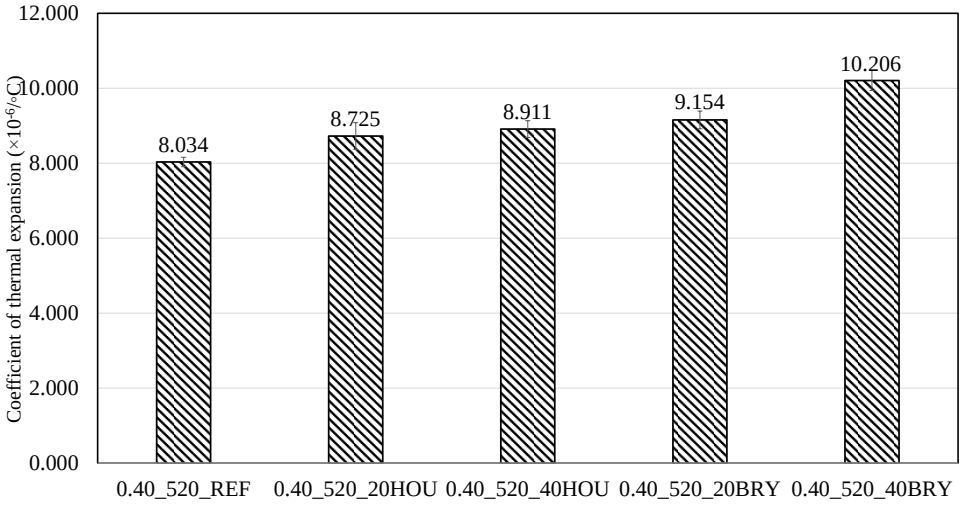

Figure 56 CoTE test results

Thermal Properties

The thermal conductivity and the heat capacity of the studied mixtures at 28-day curing age were tested. Figure 57 shows the results. From Figure 57(a), the thermal conductivity of RAP-PCC samples was lower than the plain PCC sample. This is reasonable because the asphalt is a more insulating material compared to aggregate and cement paste. Figure 57(b) shows that adding RAP into PCC reduced the heat capacity, but the trend was not clear.

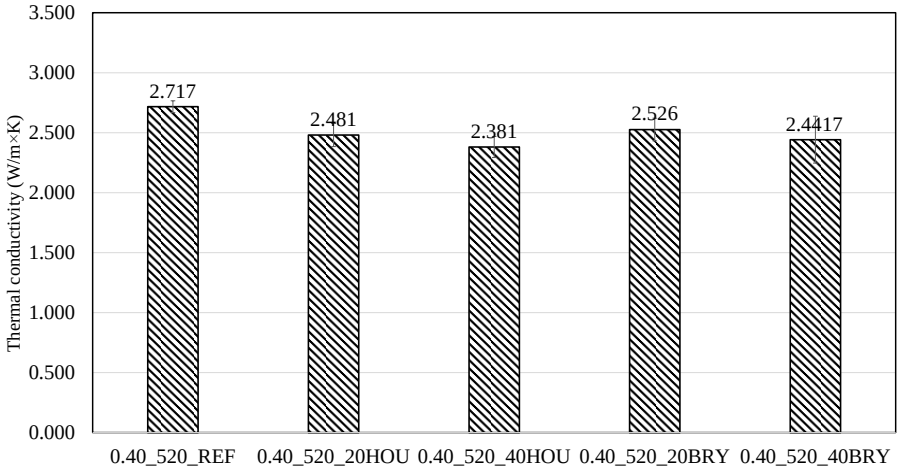

(a) Thermal conductivity

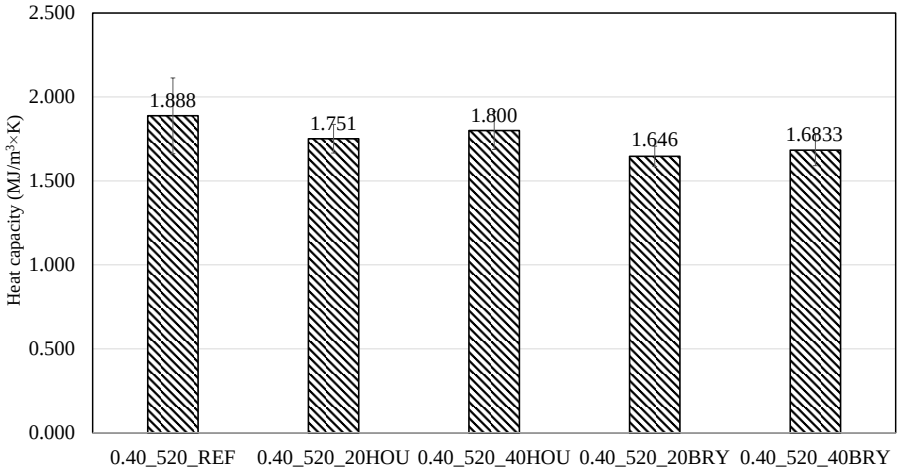

(b) Heat capacity

Figure 57 Thermal properties test results

RAP-PCC Properties VS TAVF

The previous work in this study showed that the asphalt content is the dominating factor affecting RAP-PCC's strengths; the TAVF is strongly correlated to RAP-PCC's strength such as the compressive strength and flexural strength. The averaged percent reduction for the additionally tested RAP-PCC properties is correlated with the TAVF in Figure 58. In Figure 58, a negative slope value means the addition of RAP increases the studied PCC property. Figure 58 suggests that other than the strength properties of RAP-PCC, the averaged value of some other properties of RAP-PCC can be correlated using the TAVF as well. These properties include Poisson's ratio, CoTE, and MOE (R^2>0.8).

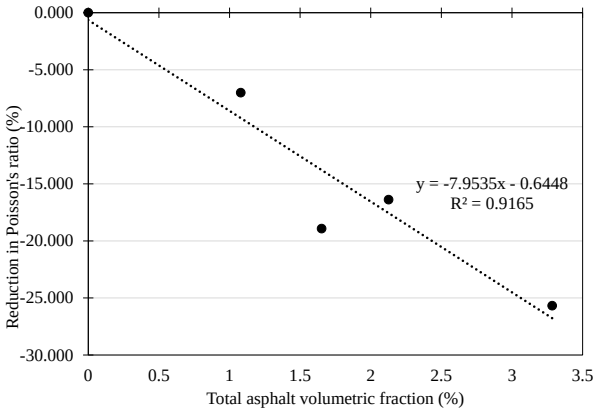

(a) Reduction in Poisson's ratio

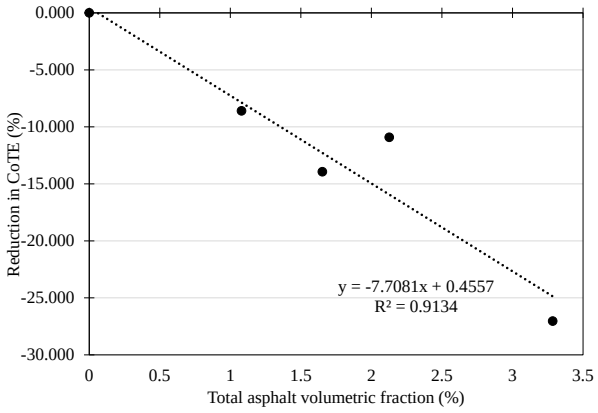

(b) Reduction in CoTE

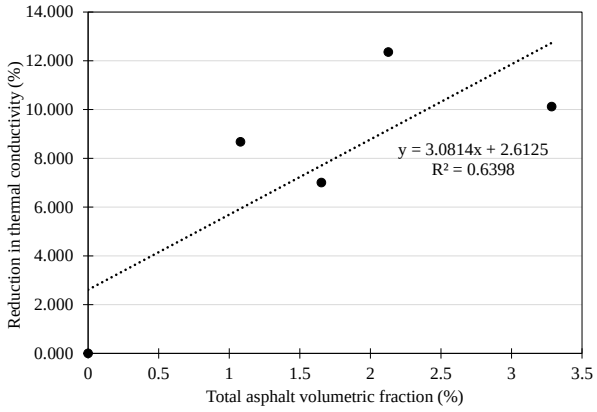

(c) Reduction in thermal conductivity

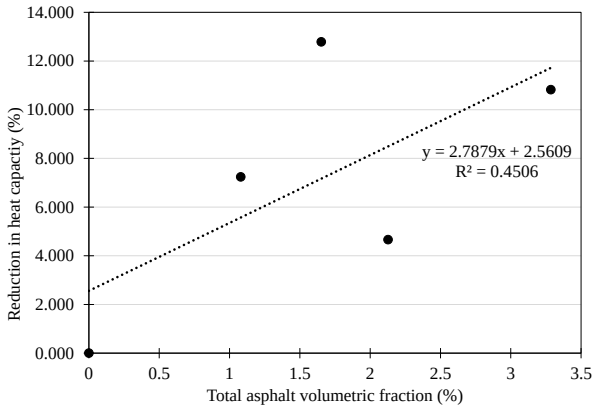

(d) Reduction in heat capacity

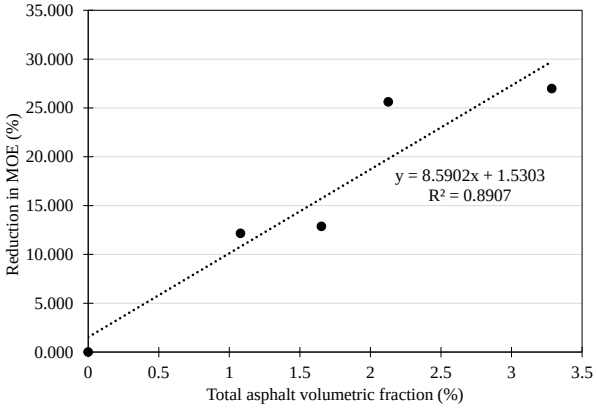

(e) Reduction in MOE

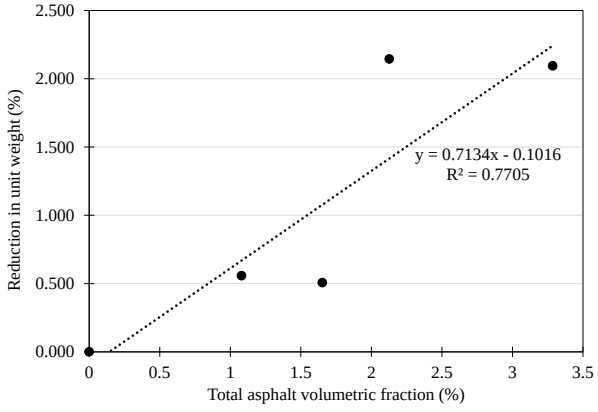

(f) Reduction in unit weight

Figure 58 Correlation between percent reduction and TAVF for different RAP-PCC properties

IV.3 DURABILITY

IV.3.1 Freeze-thaw Resistance

Figure 59 shows the freeze-thaw testing results. It is concluded that (i) the durability factors of all the tested mixtures did not drop below the limiting value of 80 after 300 freeze/thaw cycles, suggesting all the mixtures had adequate freeze-thaw resistance, (ii) all of the RAP-PCC mixtures had higher durability factors relative to the control sample, and (iii) the dense-graded RAP-PCC had higher durability factors than the gap-graded RAP-PCC. It has been reported that the reducing aggregate size is effective to control freeze-thaw damage in concrete (Gress et al. 2009). Since the dense-graded RAP-PCC has higher amounts of intermediate particles, the averaged aggregate size is reduced. Because of the reduced aggregate size, the dense-graded PCC-PCC could perform better than the gap-graded RAP-PCC under freeze-thaw cycles.

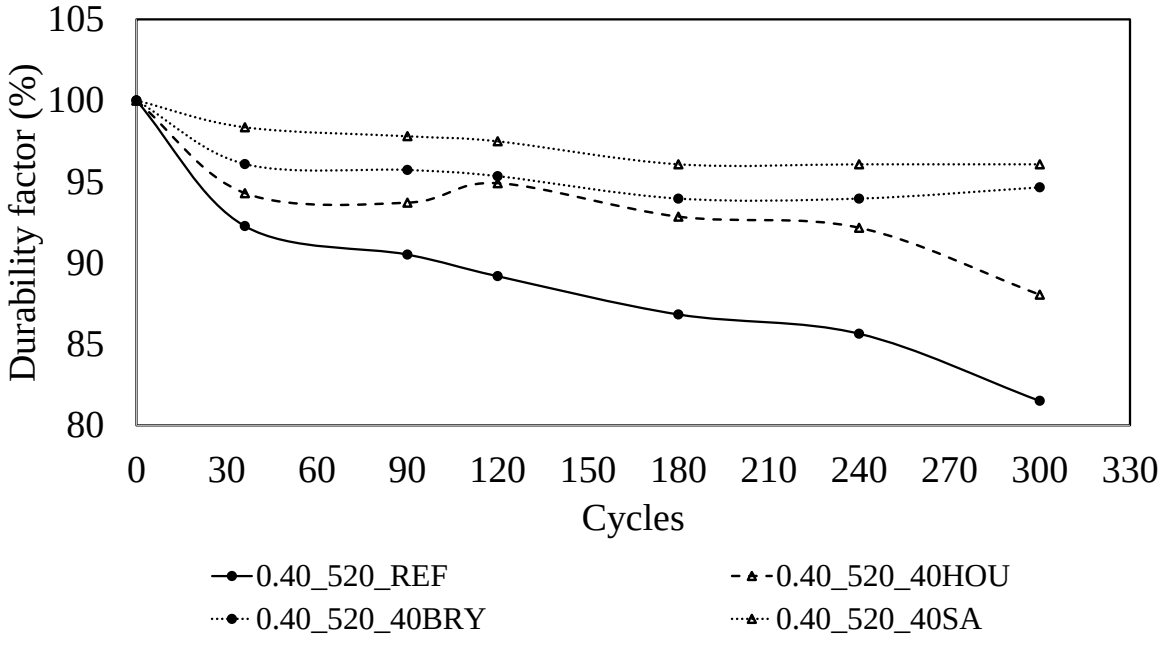

Figure 59 Freeze-thaw test results

The freeze-thaw testing results suggest that PCC made with RAP aggregates can have adequate freeze-thaw resistance. Therefore, there is no need to worry about the freeze-thaw problems of pavement built with RAP aggregates, especially in Texas where freeze-thaw damage is not a big concern.

IV.3.2 Permeability

Figure 60 shows the results for the electrical resistivity measurement of the concrete mixtures containing different types of RAP with varying replacement levels at the 56-day curing age. The results indicate that the resistivity values for all the studied concrete mixes were comparable. Table 32 shows the relationship chart between the bulk electrical resistivity and the rapid chloride permeability. All of the studied RAP-PCC mixtures along with the reference sample had low levels of chloride penetration. Accordingly, it is concluded that replacing a certain portion of virgin coarse aggregate by coarse RAP (i.e., ≤ 40 percent) seems not to introduce any significant change in permeability property of the concrete.

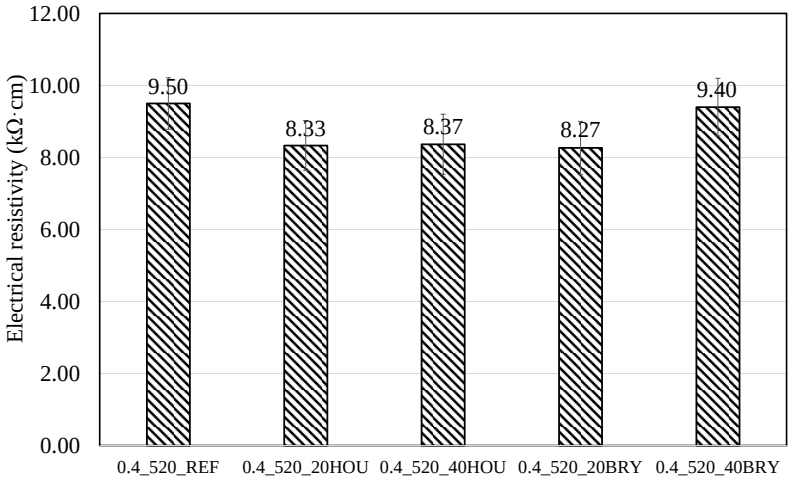

Figure 60 Electrical resistivity test results

Table 32 Relationship between electrical resistivity and the rapid chloride permeability (Reprinted from Smith 2006)

Chloride penetration Level	56-day rapid chloride permeability charge passed (coulombs)	28-day bulk electrical resistivity of saturated concrete (kΩ.cm)
High	>4000	<4
Moderate	2000–4000	4–8
Low	1000–2000	8–16
Very Low	100–1000	16–190
Negligible	<100	>190

IV.3.3 Ring Shrinkage

Concrete Test Results

Figure 61 presents the reasonably good data from concrete ring testing. The figure shows that the 0.40_520_40HOU mixture had a slightly higher amount of tensile strain than the reference mixture, while the 0.40_520_40BRY mixture had the lowest amount of tensile strain. The formation of any crack till 28 days of testing period was not observed visually in any of the ring specimens, nor was shown in the curve. This possibly suggests that replacing a certain portion of virgin coarse aggregate by coarse RAP up to 40% replacement level does not introduce shrinkage cracking in the RAP-PCC.

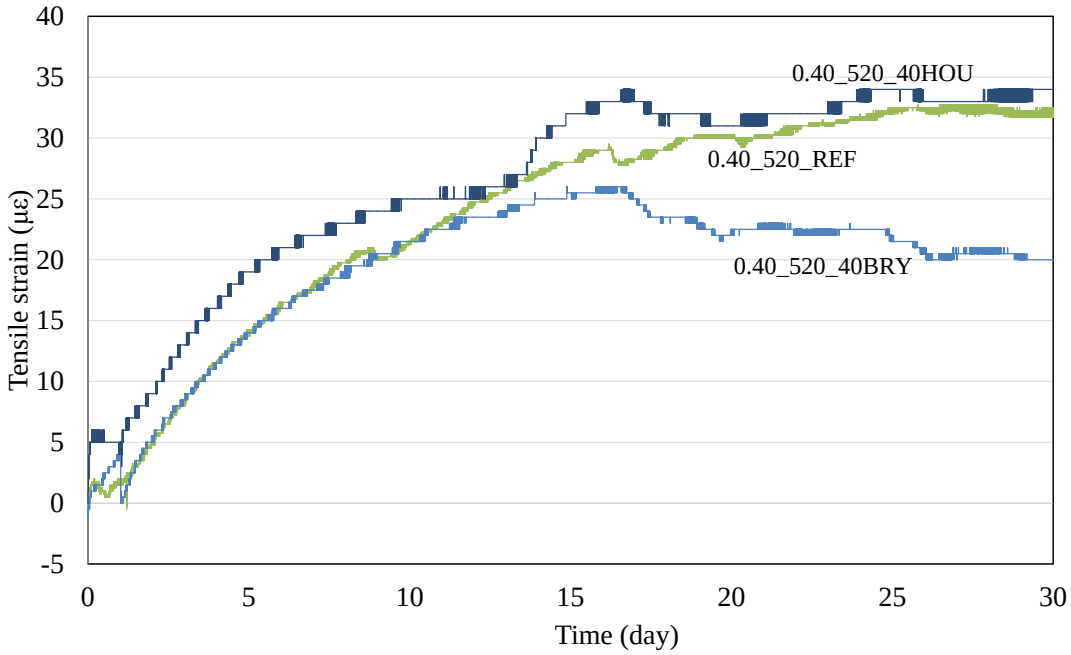

Figure 61 Concrete ring test results

Mortar Test Results

The results of four reference mortar samples and four RAP mortar samples are shown in Figure 62. Figure 62 clearly demonstrates that the RAP-mortar had a significantly different strain growth pattern. While the REF-mortar mixtures rapidly developed tensile strain until cracking, the slopes of the curve at the beginning stage were much smaller for the RAP-mortar. Moreover, the mortar specimens containing fine RAP showed noticeable ductile behaviors as all of the specimens maintained the peak strain for several days before finally cracked. It is also noted the cracking process for the RAP-mortar was not as abrupt as the REF-mortar, which suggests that microcracks might have been initiated and developed.

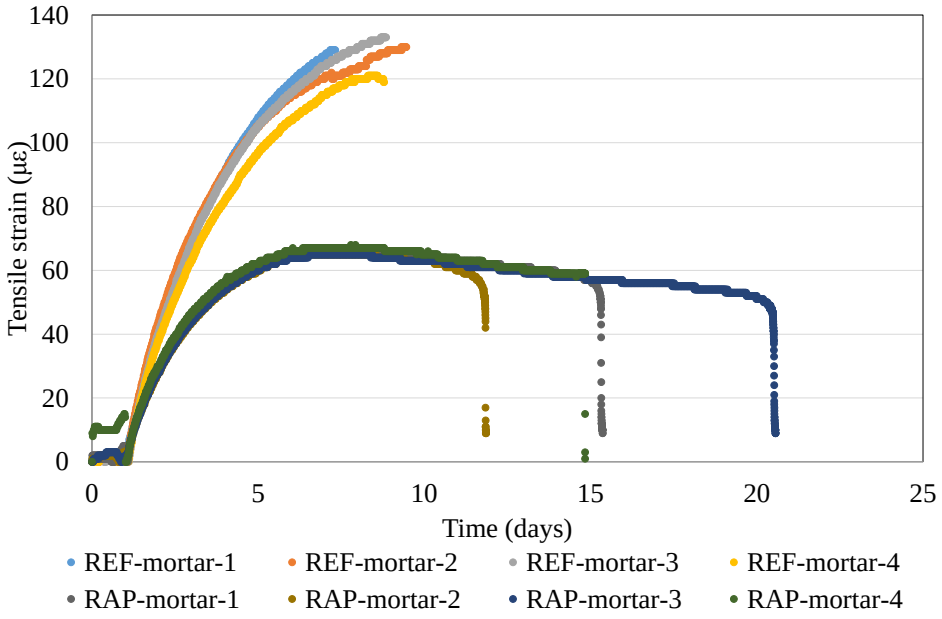

Figure 62 Mortar ring test results

Table 33 summarizes the time of cracking appearance for the REF-mortar specimens and the RAP-mortar specimens. Although the data for the RAP-mortar had a slightly higher coefficient of variance, the averaged time of cracking appearance for the RAP-mortar was considerably higher than that for the REF-mortar (almost twice). The lower elastic modulus and the higher viscoelasticity caused by the RAP addition are believed to create such difference for the ring cracking behavior of the RAP-mortar specimens relative to the REF-mortar specimens. With the ring testing data, the viscoelastic properties of the RAP-mortar can be extracted (Grasley and Matthew 2011). The unique characteristics of the cementitious material containing RAP (lower modulus and higher viscoelasticity) are anticipated to provide some benefits for concrete pavement such as improvement of crack potential and mitigation of corner lifting due to a higher creep.

Table 33 Time of cracking appearance for the ring test

Mixture type	Sample number	Time of cracking appearance	
REF-mortar	1	7.33	Ave: 8.62 COV: 11%
	2	9.47	
	3	8.86	
	4	8.80	
RAP-mortar	1	15.37	Ave: 15.6 COV: 23%
	2	11.84	
	3	20.53	
	4	14.83	

IV.3.4 Abrasion Resistance

During the abrasion tests, the abrading disk/cutter generated a circular wear path on the concrete surface. An effective shear stress term, τ, is proposed to quantify the average stress level on the abrading zone of concrete specimen (Figure 63).

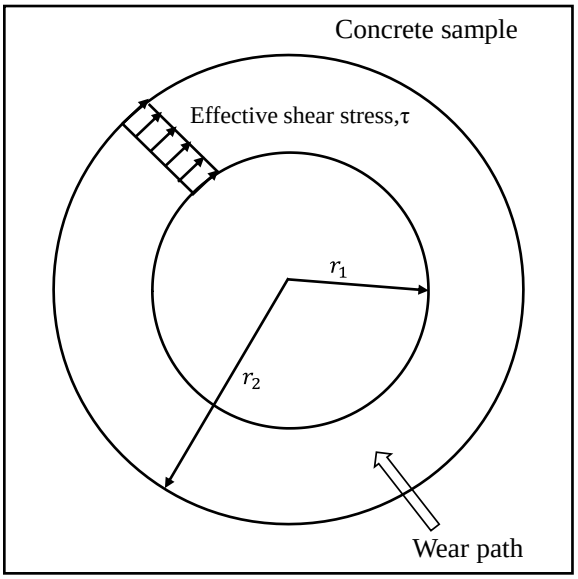

Figure 63 Effective shear stress

Based on the balance of moment, τ can determined in the following equation:

$$T = \int_{r_1}^{r_2} 2\tau\pi r^2 dr \tag{76}$$

The above equation yields:

$$\tau = \frac{3T}{2\pi(r_2^3 - r_1^3)} \tag{77}$$

Where

r_1= inner radius of the wear path

r_2= outer radius of the wear path

The stress/strength, R, of the concrete sample is then obtained:

$$R = \frac{\tau}{f_\tau} \tag{78}$$

Where f_τ= the shear strength of the material

Here, the shear strength of the tested materials is estimated by taking 50% of the flexural strength (Bari and Zollinger 2016):

$$f_\tau = 0.5MOR \tag{79}$$

The materials' shear strengths are presented in Table 34.

Table 34 Shear strengths of the tested mixtures

Mix ID	56-day shear strength (MPa)
0.40_520_REF	2.86
0.40_520_40HOU	1.78
0.40_520_40BRY	2.03

The averaged abrasion depth, D, is computed

$$D = \frac{\Delta V}{A} \tag{80}$$

Where

ΔV= loss of material in volume during the test (m^3), $\Delta V = \frac{\Delta m}{\rho}$

A= the abrading disk/cutter contact area (m^2), which equals to the area of wear path

A term, abrasion coefficient (c), is further defined to account for the velocity of the abrading surface. The use of c also can convert D into a dimensionless term.

$$c = \frac{D}{vt} \tag{81}$$

Where

v=the velocity of the abrading disk/cutter (m/s)

t= test time (s)

The abrasion testing results are summarized in Table 35.

Table 35 Test results for the abrasion tests

Mix ID	Method	Averaged amperage (A)	Abrasion time (mins)	Mass loss (g)
0.40_520_REF	Revolving disk	10.014	30	6.8
	Rotating cutter	6.152	10	3.7
0.40_520_40HOU	Revolving disk	9.909	30	9.4
	Rotating cutter	6.126	10	6.3
0.40_520_40BRY	Revolving disk	9.910	30	13.3
	Rotating cutter	6.076	10	8.4

The calculated parameters are shown in Table 36.

Table 36 Summary of the calculated parameters

Mix ID	Method	Torque (Nm)	Shear stress (Pa)	Stress/strength	Abrasion depth, D, ($\times 10^{-6}$ cm)	Abrasion coefficient, c, ($\times 10^{-8}$)
0.40_520_REF	Revolving disk	4.208	923	0.000404	95	3.548
	rotating cutter	5.405	21482	0.009399	789	56.668
0.40_520_40HOU	Revolving disk	4.163	913	0.000512	136	5.012
	rotating cutter	5.381	21389	0.012005	1391	98.603
0.40_520_40BRY	Revolving disk	4.164	913	0.00045	198	7.088
	rotating cutter	5.337	21215	0.01045	1831	131.403

It is assumed that the relationship between the abrasion coefficient, c, and the stress/strength, R, can be correlated with a linear equation:

$$c = mR + n \tag{82}$$

Where m, n are fitting coefficients

With the calculated abrasion coefficients and stress/strength ratios from the two abrasion tests along with the origin point (abrasion coefficient is 0 when the corresponding stress/strength is 0), a regression analysis was performed and the results are shown in Figure 64. It turned out that the assumption of a linear relationship between the abrasion coefficient and stress/strength is valid since all three fitting lines have a very high R^2 value. It is noted that the reference mixture has the lowest slope, followed by the 0.40_520_40HOU and the 0.40_520_40BRY. Since the 0.40_520_40BRY has the highest TAVF, it is concluded that the higher the asphalt volume content, the lower the abrasion resistance of the mixture.

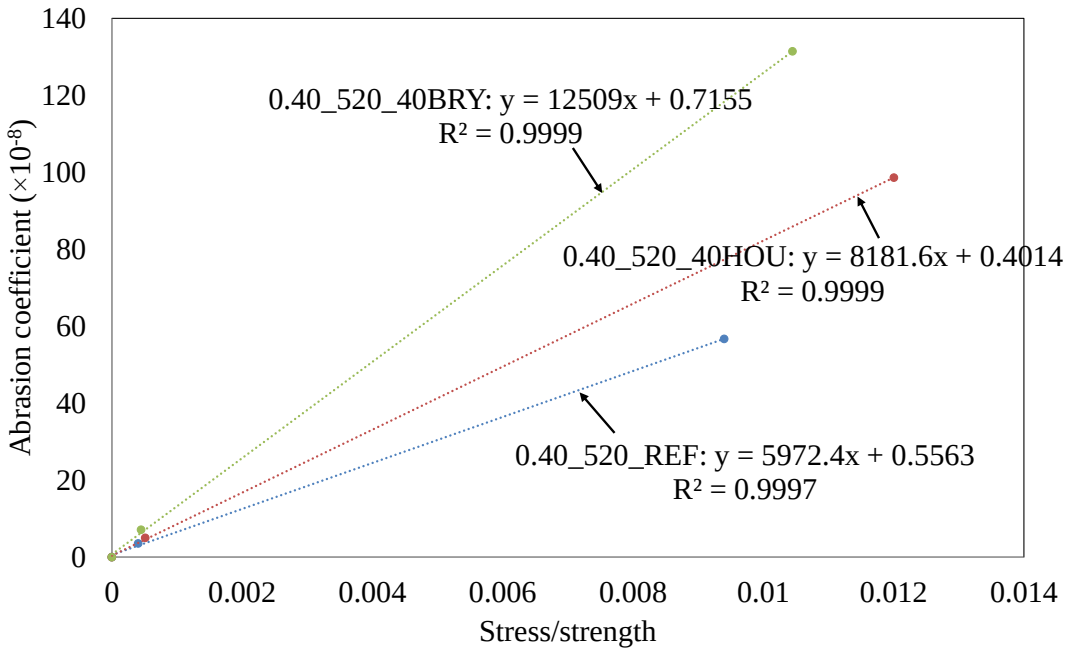

Figure 64 Regression analysis of abrasion coefficient and stress/strength

The regression relation between the abrasion coefficient and stress/strength can be used in prediction concrete pavement's life under dry erosion damage. According to Bari and Zollinger (2016), the erosion model is express as:

$$\%E = e^{-(\frac{\rho}{D_i})^{\alpha}} \tag{83}$$

Where %E = the percent of erosion

D_i= erosion damage

ρ, α = are the calibrations factors

The erosion damage is calculated as:

$$D_i = \sum \frac{N_i}{N_f} \tag{84}$$

Where

N_f= the ultimate load application to failure at a stress/strength R_j

For a dry abrasion condition, N_f can be derived from the following equations:

The allowable abrasion coefficient is written:

$$c(R_j) = \frac{D_{allowable}}{vt} \tag{85}$$

Where

$D_{allowable}$= allowable abrasion depth

v=the traffic speed

t=traffic load application time

Since vt equals to the ultimate total distance that a specific traffic load R_j travels, the ultimate load application might be defined as:

$$N_f(R_j) = \frac{vt}{\ell} \tag{86}$$

Where the effective relative stiffness:

$$\ell = \sqrt[4]{\frac{E_c h^3}{12k(1-\nu^2)}} \tag{87}$$

Where

E_c= Concrete modulus of elasticity,

h= slab thickness

k= modulus of the subgrade reaction

ν= Concrete Poisson's ratio

Therefore,

$$N_f(R_j) = \frac{D_{allowable}}{c(R_j)\ell} \tag{88}$$

Accordingly, the concrete pavement life can be predicted by following the steps as below:

1. Perform the dry abrasion resistance tests (i.e., ASTM C779 and ASTM C944)

2. Develop the correlation between the abrasion coefficient, c, and the stress/strength, R using the testing data
3. Numerically compute the induced stress/strength R_j for the traffic load classification j
4. Estimate the ultimate load application, N_f, by assigning a specific value for $D_{allowable}$
5. Calculate the erosion damage, D_i under a specific number of applications for the traffic load j
6. Evaluate the %E from falling weight deflectometer (FWD) data using a procedure described by Bari and Zollinger (2016)
7. Perform a regression analysis for the erosion model and obtain the calibrations factors

The freeze-thaw resistance of PCC can be probably related to the abrasion test as well. The reason behind is that when concrete undergoes freeze-thaw cycles, the water inside the concrete pores freezes and expands, causing shear on the material. The shear force is assumed to be analogical to the shear caused by the abrading surface, and is related with the abrasion test by a term freeze-thaw factor (FTF):

$$\mathrm{FTF} = \frac{\Delta \mathrm{m/cycle}_{\mathrm{abrasion}}}{\Delta \mathrm{m/cycle}_{\mathrm{freeze-thaw}}} \tag{89}$$

The FTF for the studied mixtures is shown in Table 37.

Table 37 FTF for the studied mixtures

Mix ID	$\Delta \mathrm{m/cycle}_{\mathrm{freeze-thaw}}$ (g/cycle)	$\Delta \mathrm{m/cycle}_{\mathrm{abrasion}}$ (g/cycle, revolving disk)	$\Delta \mathrm{m/cycle}_{\mathrm{abrasion}}$ (g/cycle, rotating cutter)	FTF (revolving disk)	FTF (rotating cutter)
0.40_520_REF	0.4834	0.0008	0.0018	0.0017	0.4834
0.40_520_40HOU	0.6918	0.0011	0.0032	0.0016	0.6918
0.40_520_40BRY	0.7036	0.0016	0.0042	0.0023	0.7036

With the calculated FTF, the effective shear stress in the specimens undergoing freeze-thaw testing together with the freeze-thaw life of the mixture can be reasonably estimated. A detailed discussion of this approach is not within the scope of this study.

IV.4 MICROSTRUCTURE

Concrete properties not only depend on the characteristics of the constituent materials (e.g., cement, fly ash, and aggregate) but also relate to the physical and chemical interaction between the ingredients. When concrete cures, it undergoes significant microstructural changes due to cement hydration, pozzolanic reaction, drying shrinkage, carbonation etc., and these changes have a profound effect on concrete mechanical properties and durability. The previous sections indicate that RAP-PCC has reduced strengths and stiffness. The mechanism that whether asphalt interacts with cement hydration and how asphalt alters the microstructural features in RAP-PCC are extremely important for a good understanding and interpretation of the previous observations. The findings from the RAP-PCC microstructural study is presented below.

IV.4.1 Verification of Presence of Agglomerated RAP

The presence of agglomerated RAP in different types of RAP-PCC samples was verified through the thin section observations. The formation of agglomerated RAP happened when several RAP aggregate particles stick to each other due to the presence of sticky asphalt binder around each RAP aggregate particle. The RAP agglomeration is a very common phenomenon in the RAP stockpiles, especially when the ambient temperature is high. The presence of agglomerated RAP in RAP-PCC causes weak zones in concrete, which is considered as one of the reasons for strength reductions in RAP-PCC (Singh et al. 2017).

AMA RAP had a significant amount of agglomerations, while the particles from the HOU, BRY, and SA RAP sources appeared to be cleaner and more separated based upon the visual observation. However, under the microscope observation, it is found that HOU RAP contains a considerable amount of agglomerated particles as well. One coarse HOU RAP particle, which appears to be a single one from the naked-eye observation, can consist of several small RAP particles (Figure 65). Figure 65 shows a typical agglomerated particle in the 0.40_520_40HOU thin section sample. The coarse agglomerated RAP contains three intermediate sized particles (2-3 mm) and a relatively large particle (at the lower right corner of the picture) along with some fine RAPs (several hundreds of μm) and entrapped voids. Figure 66 and Figure 67 present a detailed observation of the asphalt layer within the agglomerated RAP particles. The presence of fine aggregate particles and a large amount of voids (entrapped voids marked by blue dye) within the asphalt layer (Figure 66) are observed. In Figure 67, the thickness of the asphalt layer is around 500 μm, which contains several small fine particles. Because of the existence of small particles, the thickness of the asphalt layer varied considerably.

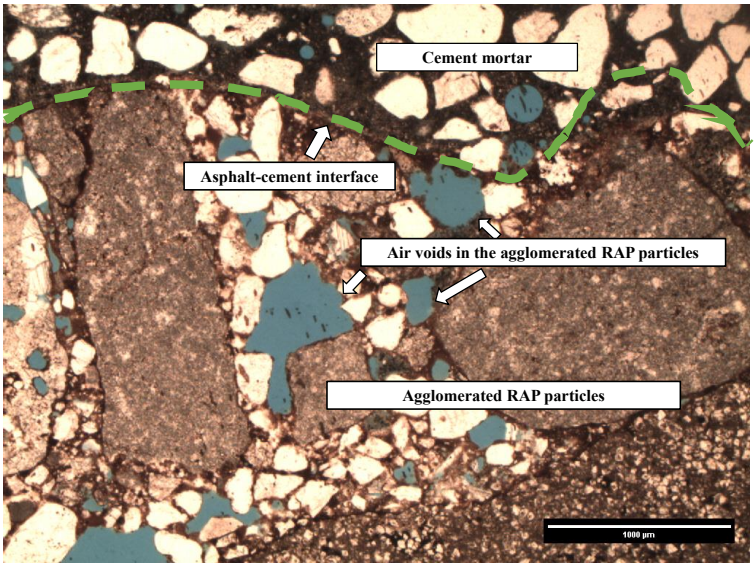

Figure 65 Agglomerated RAP particles in the 0.40_520_40HOU

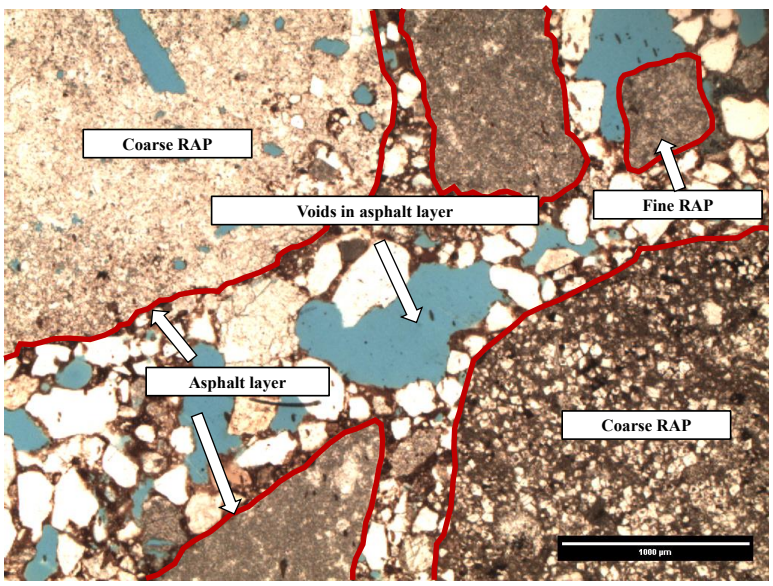

Figure 66 Another view of the same agglomerated RAP (the 0.40_520_40HOU)

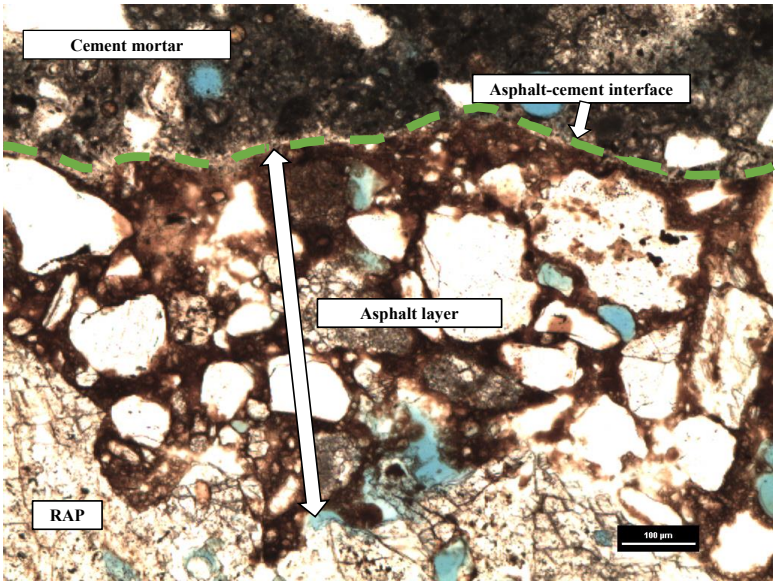

Figure 67 A view of the thick asphalt layer of the HOU RAP (the 0.40_520_40HOU)

Figure 68 shows a RAP in the 0.40_520_40BRY thin section specimen. Similar to the HOU RAP, some of the BRY RAP particles also contain asphalt layers with large amounts of fine particles. However, there are some RAP particles with a relatively thin and clean layer, as

can be seen in Figure 69. During the observation of the 0.40_520_40BRY sample, no big clumps were observed.

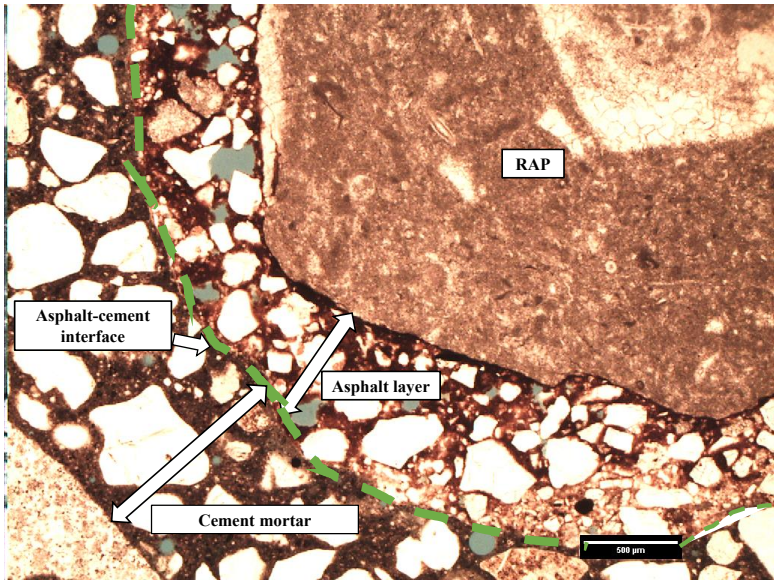

Figure 68 A view of the asphalt layer of the BRY RAP (the 0.40_520_40BRY)

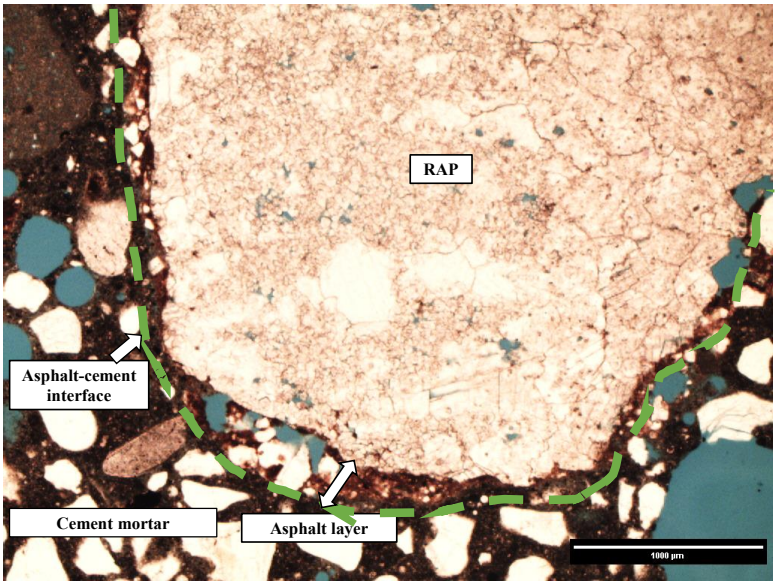

Figure 69 A relatively clean and thin asphalt layer in the 0.40_520_40BRY

The 0.40_520_40SA was then observed. Unlike HOU and BRY cases, the SA RAP has very thin asphalt layers, as can be seen in Figure 70 and Figure 71. The asphalt layer is also cleaner with fewer fine particles and voids. No big clumps have been found in the 0.40_520_40SA specimen.

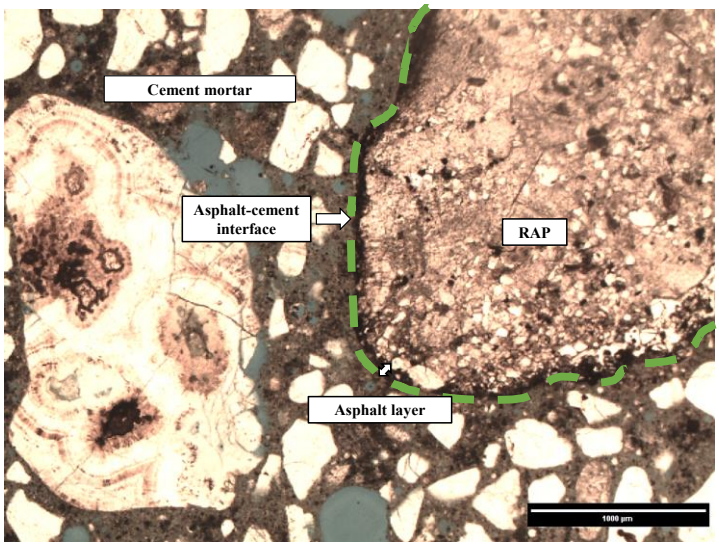

Figure 70 A thin RAP asphalt layer in the 0.40_520_40SA

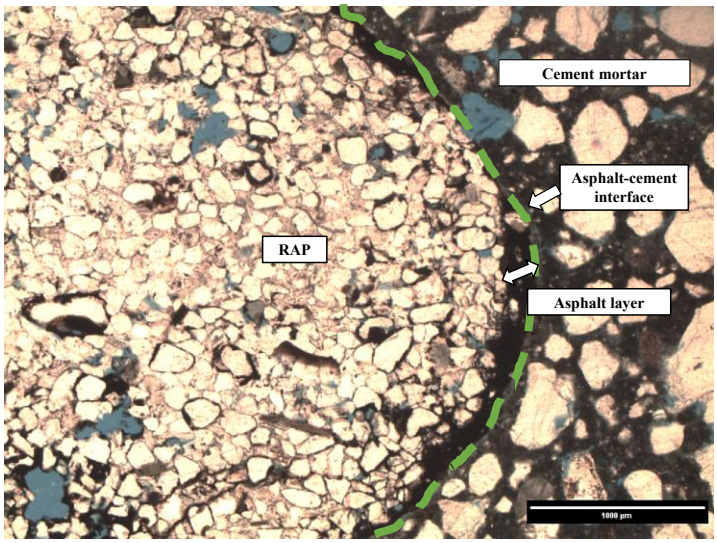

Figure 71 Another thin RAP asphalt layer in the 0.40_520_40SA

IV.4.2 ITZ Properties

In normal concrete, ITZ is a weak area where a crack is likely to propagate through. The weakness of ITZ is due to the following reasons (Bentur and Odler 1996; Maso 1980):

- The larger porosity
- The larger CH crystals and their preferential orientations

Based on the detailed observations on ITZ of different RAP-PCC thin section specimens, the ITZ of most of the RAP-PCC (especially those with higher levels of RAP replacement) is in general more porous than the ITZ of the reference concrete made of virgin aggregates, which can be shown in Figure 72 and Figure 73. In the pictures, a porous ITZ is manifested by a higher amount of blue dye impregnation. The higher the blue dye impregnation the higher the porosity is. Also, the ITZs in RAP-PCC show a higher degree of carbonation than that in reference concrete in general, which is another indirect evidence of porous nature of ITZ.

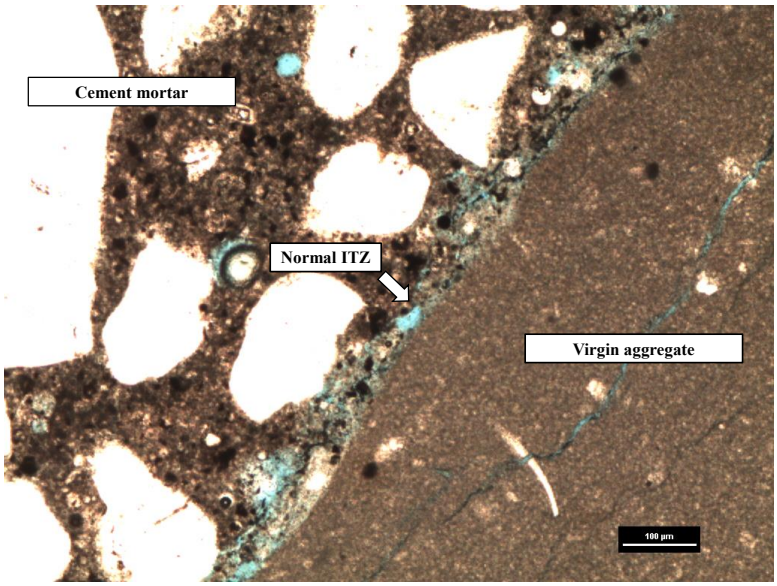

Figure 72 Normal ITZ in the 0.40_520_REF

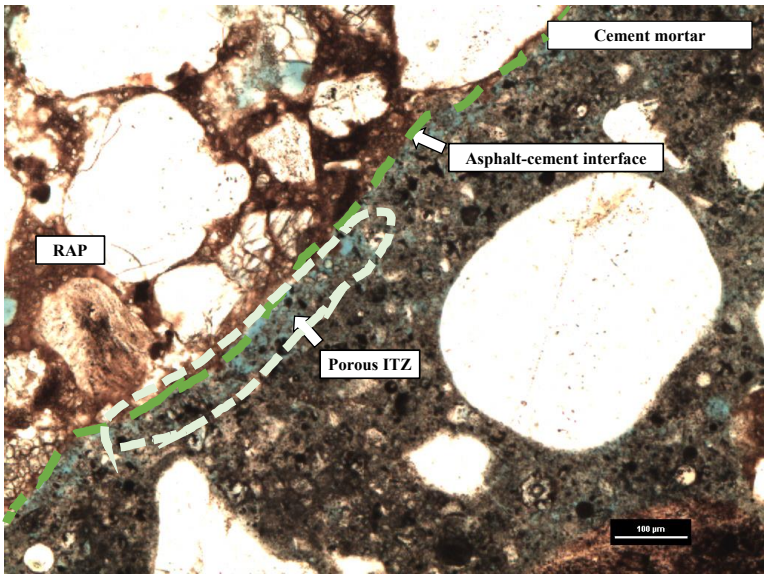

Figure 73 Porous ITZ in the 0.40_520_40HOU

The scanning electron microscope (SEM) was used to further investigate the ITZ property of the RAP-PCC. Figure 74 shows a comparison of an ITZ between a RAP and cement (yellow dash line) and an ITZ between a virgin aggregate and cement (red dash line). It is clearly indicated that the ITZ between the virgin coarse aggregate and cement mortar is much denser and well-formed than the ITZ between RAP and cement mortar.

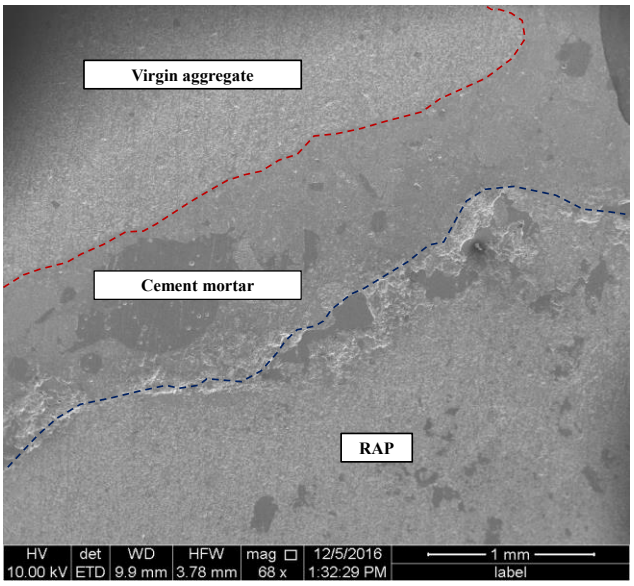

Figure 74 Comparison of normal ITZ and RAP ITZ (the 0.40_520_40SA)

IV.4.3 Size and Distribution of Pores

Petrographic Study Results

Observations of the thin section specimens indicated that RAP-PCCs are in general more porous than the reference sample. A combined effect of both entrapped air voids and capillary pores in the cement paste and ITZ was considered to define the porous nature of the RAP-PCC, which is described below:

- The presence of a greater number of larger voids in the cement mortar of RAP-PCC samples: Figure 75 shows the air void distribution of the reference sample. The cement mortar contains well-distributed air voids and most of them are entrained air (rounded shape) that were purposely introduced to reduce freeze-thaw damage. Figure 76 is an image taken with the 0.40_520_100BRY/100BRY sample. Compared to Figure 75, the sizes of the air voids are bigger, and entrapped air (irregular shape) can be found in a great number.

- Air voids exist in the thick RAP asphalt layer (Figure 66): Figure 77 presents an extremely porous area in the RAP asphalt layer. Although it is not known that whether these air voids were original in the RAP material or they were introduced by default during the sample preparation due to the stripping of the asphalt, it is clear that the thick asphalt layer is one of the weak zones in the RAP-PCC system.
- Air voids within those big RAP clumps (Figure 65).
- Porous ITZ in the RAP-PCC (Figure 73).

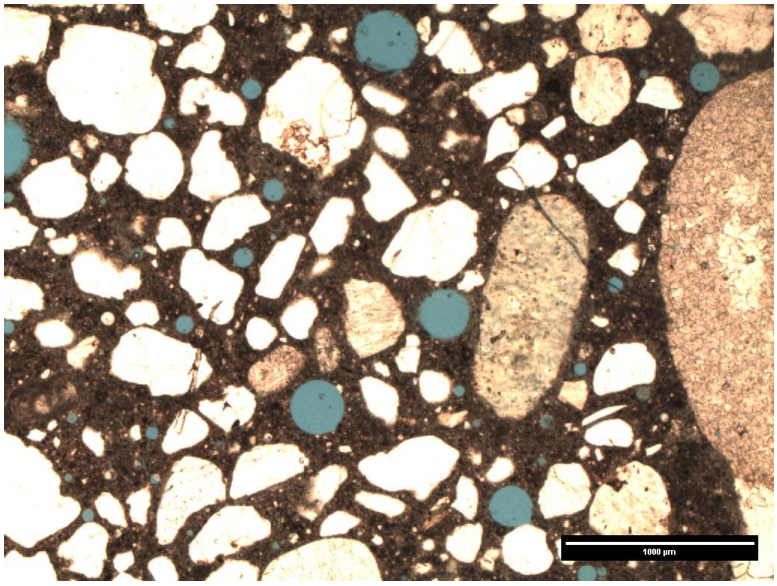

Figure 75 Air voids in the 0.40_520_REF

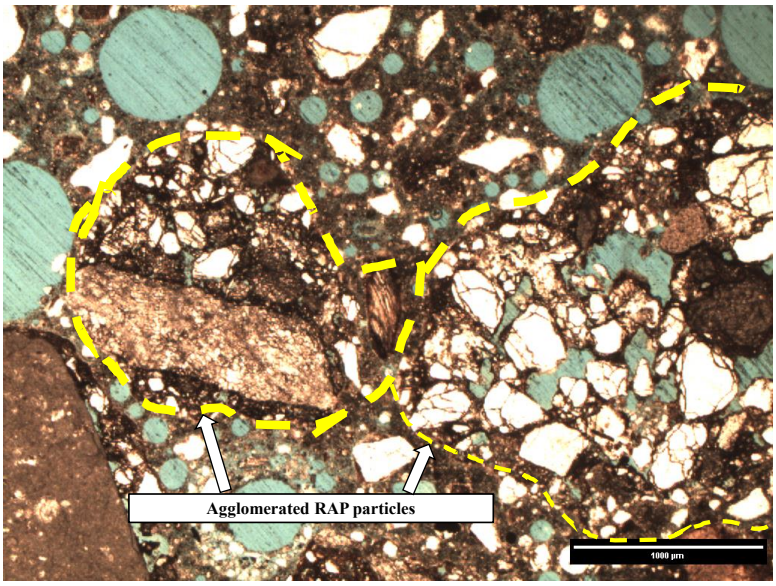

Figure 76 Air voids in the 0.40_520_100BRY/100BRY

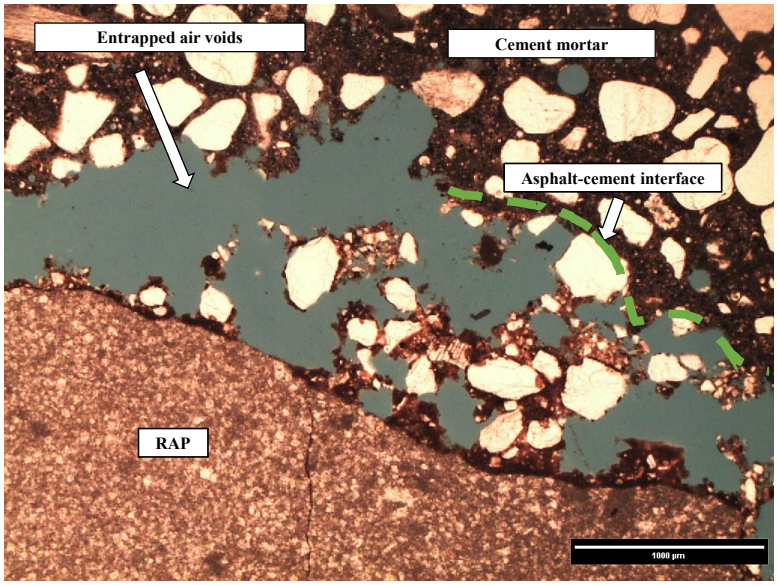

Figure 77 High amounts of air voids in the asphalt layer in the 0.40_520_40BRY

X-ray CT Results

The percent air void in the hardened concrete was estimated using the X-ray CT imaging followed by an analysis through the commercial software ORS Visual SI with the following steps:

1. An un-cracked 50 × 100 mm concrete sample was mounted to the sample stage.
2. The scan parameters were determined after a trial and error process to make sure the best X-ray CT images were achieved. The voxel size (the dimension of the smallest 3D element) was finally set as 53 μm. All the scan parameters were fixed for all of the samples.
3. After the X-ray scan was completed, the 3D reconstruction technique was applied to obtain a 3D structure of the sample. The raw tiff image sequence was then saved.
4. The image sequence was then loaded in the commercial software ORS Visual SI. In order to remove the sample edge effect, the first 100 and the last 100 images from the image sequence were removed.
5. The sample was then further trimmed and saved to ensure the full region of interest was within the sample.
6. The air void was segmented by properly setting the grey value range. Although that this process could be somewhat subjective, a good grey value threshold can be determined by comparing the segmented image.
7. The volume percent air void for the trimmed sample was then calculated by the software.

Table 38 summarizes the percent air void for different RAP-PCC and the reference PCC samples.

Table 38 Percent air void for different RAP-PCC mixtures

Sample ID	Grey value range	Percent air void
0.40_520_REF	12068	1.19%
0.40_520_40HOU	13607	2.09%
0.40_520_40BRY	9084	2.42%
0.40_520_40AMA	8642	3.17%
0.40_520_40SA	10155	1.46%
0.40_520_100BRY/100BRY	12873	7.31%

Table 38 indicates that the RAP-PCC specimens invariably had higher percentage air void than the reference PCC. The RAP-PCC containing 100 percent RAP aggregates had an extremely higher amount of air voids compared to the other samples. This high porosity was considered as one of the major reasons for serious strength reductions of the PCC containing RAP with high amounts. The 0.40_520_40AMA had higher percentage air void than the other samples with same RAP replacement level but different RAP type, which might contribute to the low compressive strength of the mixture to some extent. It is noted that the analysis was only able to estimate air voids larger than the resolution of the scan (53μm), therefore Table 38 underestimates the actual percent air voids in the mixtures.

IV.4.4 CH Size and Distribution

Based on a detailed petrographic examination, the CH size and distribution in the RAP-PCC system appeared to be comparable with the control concrete. Figure 78 presents the size and nature of distribution of a CH crystal in RAP-PCC under a microscope.

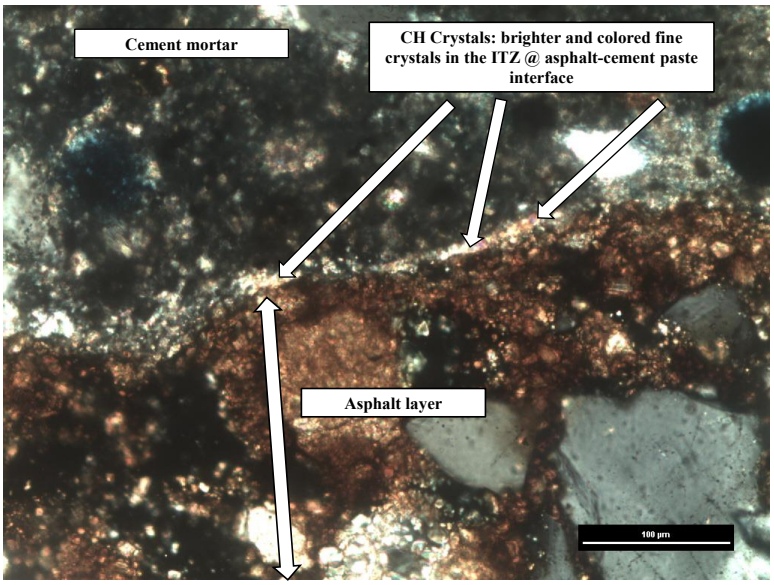

Figure 78 CH crystals at the asphalt-cement interface (the 0.40_520_40HOU)

IV.5 CRACK PATTERN

The crack patterns were studied under the optical microscope to directly investigate failure mechanism in RAP-PCC. Based on a detailed thin section observation, the following findings on the RAP-PCC failure mechanism were obtained:

- Asphalt cohesive failure (i.e., crack breaks through asphalt layer) is the primary failure mechanism in the RAP-PCC system. This can be verified by Figure 79 and Figure 80. The confirmation of asphalt cohesive failure in RAP-PCC manifested that the previously developed approaches of using TAVF to predict RAP-PCC's strengths can be effective.
- The big RAP clumps in the RAP-PCC system are the source of weak zones due to high porosity and high asphalt binder content. Figure 81 shows a typical crack passing an agglomerated RAP. Since AMA RAP and HOU RAP contain a higher amount of agglomerated particles, the finding from Section IV.2.2 that the rate of deterioration (k) of these two mixtures were much higher than that for the RAP-PCC mixtures containing

relatively clean and uniform RAPs (e.g., the BRY RAP-PCC and the SA RAP-PCC) can be reasonably explained.

- While asphalt cohesive failure is the primary failure mechanism in RAP-PCC, ITZ of RAP-PCC does not differ considerably in terms of CH size and distribution. However, the porous nature of RAP-PCC ITZ plays some role for crack propagation.
- The extremely high amounts of pores in PCC with high RAP replacement levels make crack initiation and propagation much more prevalent, which is again demonstrated by X-ray images presented later.

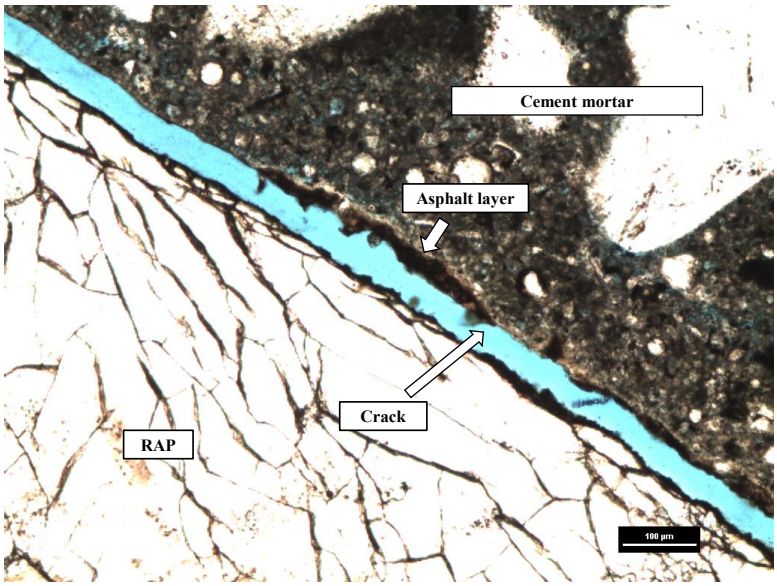

Figure 79 An example of asphalt cohesive failure (the 0.40_520_40HOU) (i.e., crack passing through the asphalt layer)

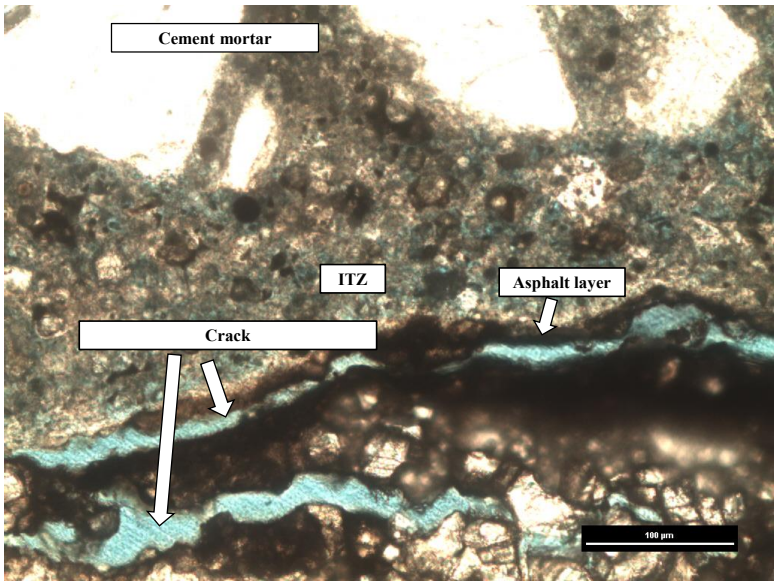

Figure 80 A close view of the asphalt cohesive failure (the 0.40_520_40HOU) (i.e., crack passing through the asphalt film)

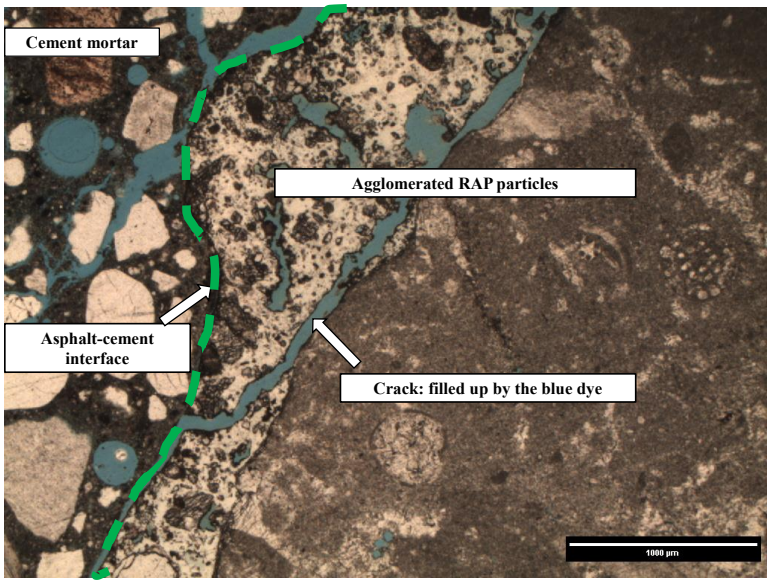

Figure 81 Crack propagates through the agglomerated RAP particle (the 0.40_520_40BRY)

The cracked samples (Figure 33) were scanned by the x-ray CT. Figure 82 to Figure 85 present the 3D structures of the cracked samples. Figure 82(a) shows a longitudinal crack in the 0.40_520_REF. The cross section (Figure 82(b)) indicates that the crack propagated through the

aggregate. For a conventional PCC, when ITZs are dense (in general ITZ between limestone coarse aggregate and cement paste is dense) and aggregate is relatively softer (e.g., the limestone used in this study), the aggregates would break during testing and crack propagates through the aggregates instead of passing through ITZ. On the contrary, for a weaker bond, cracks tend to pass through the bonding zone in the RAP-PCC (Figure 83, Figure 84 and Figure 85). Compared to a single longitudinal crack in 0.40_520_REF (Figure 82), all the RAP-PCC showed multiple cracks (the 0.40_520_40HOU even had transverse crack, Figure 83). Multiple cracks are often indication of a higher toughness and ductility. Furthermore, Figure 83 clearly shows a RAP clump in the sample, and the cracks tend to initiate and pass through the clumps. This again proved that the RAP clump is the weak zone in the RAP-PCC system and the percent agglomerated RAP should be strictly controlled to improve the performance of the RAP-PCC. For the 0.40_520_100BRY/100BRY sample in Figure 85, a very high porosity was observed. The high porosity facilitated cracking propagation.

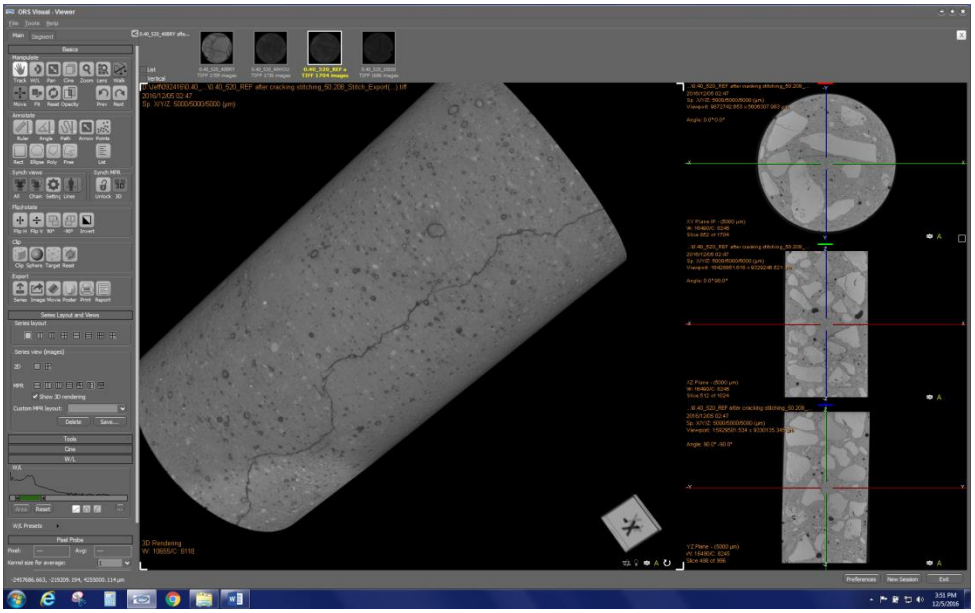

(a) Entire view

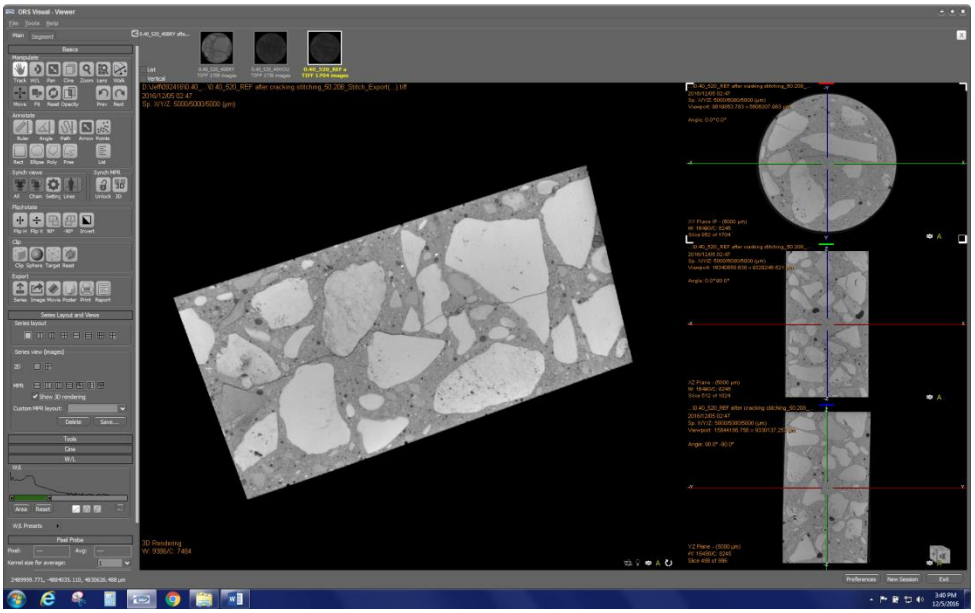

(b) Cross section

Figure 82 3D images for the cracked 0.40_520_REF

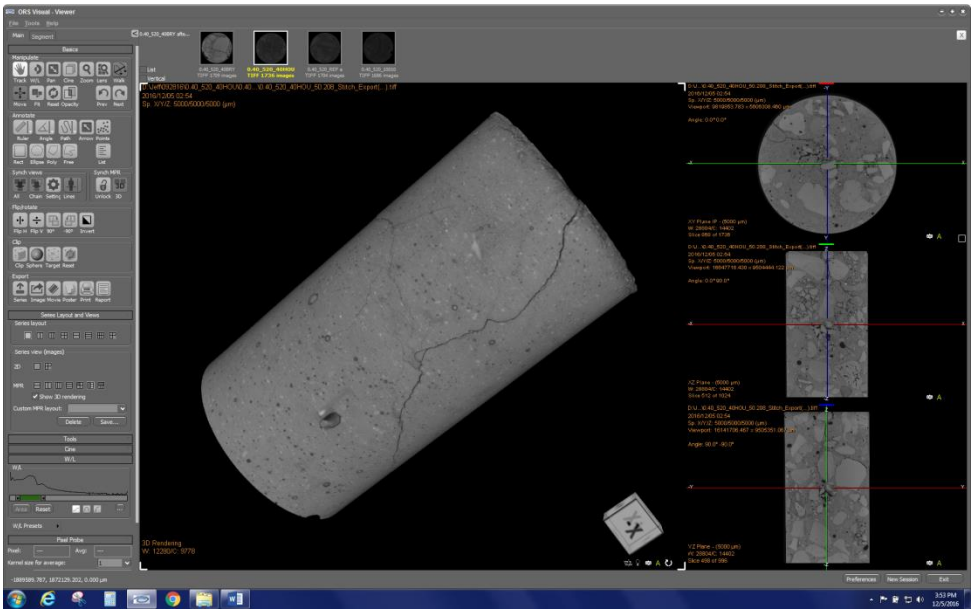

(a) Entire view

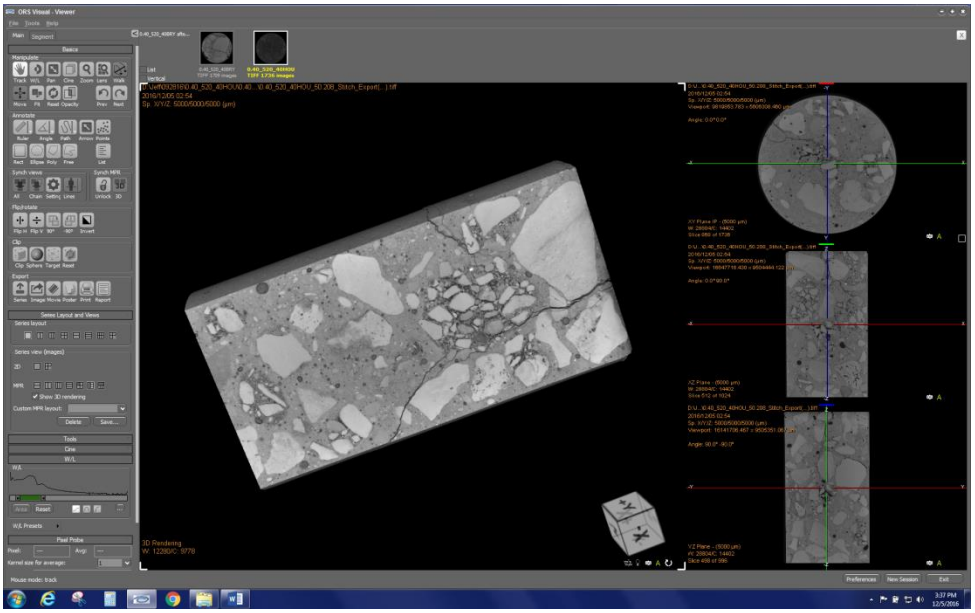

(b) Cross section

Figure 83 3D images of the cracked 0.40_520_40HOU

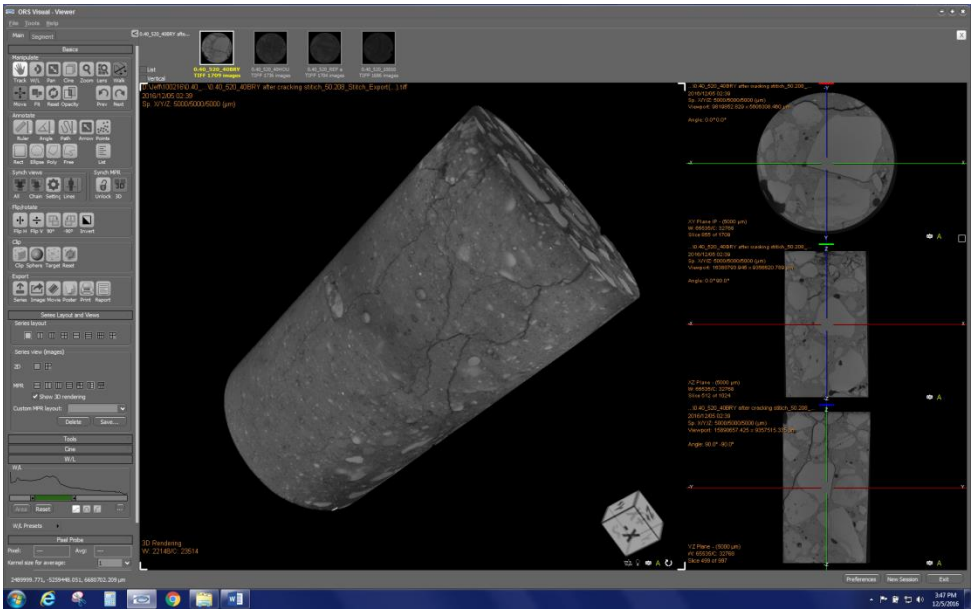

(a) Entire view

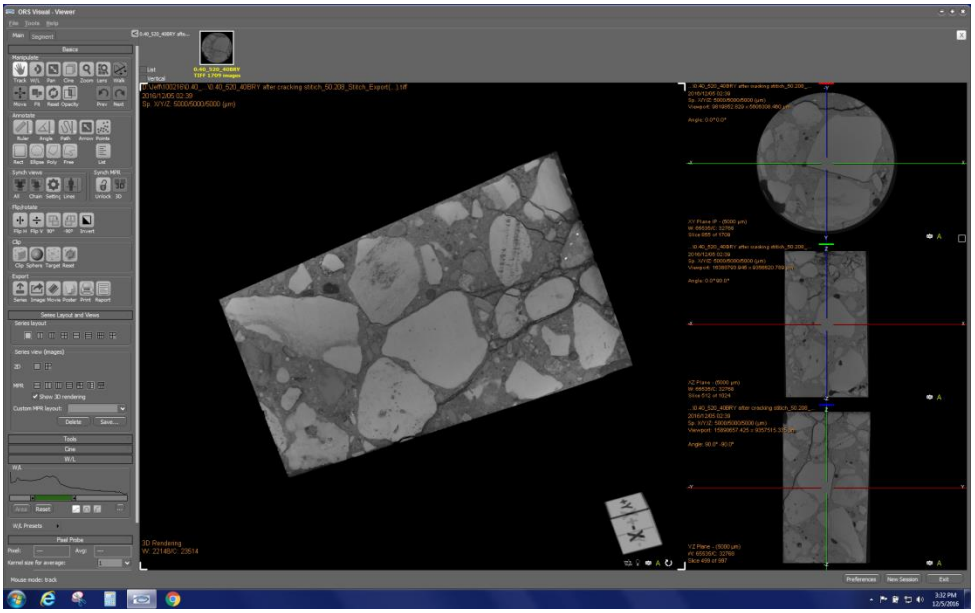

(b) Cross section

Figure 84 3D images of the cracked 0.40_520_40BRY

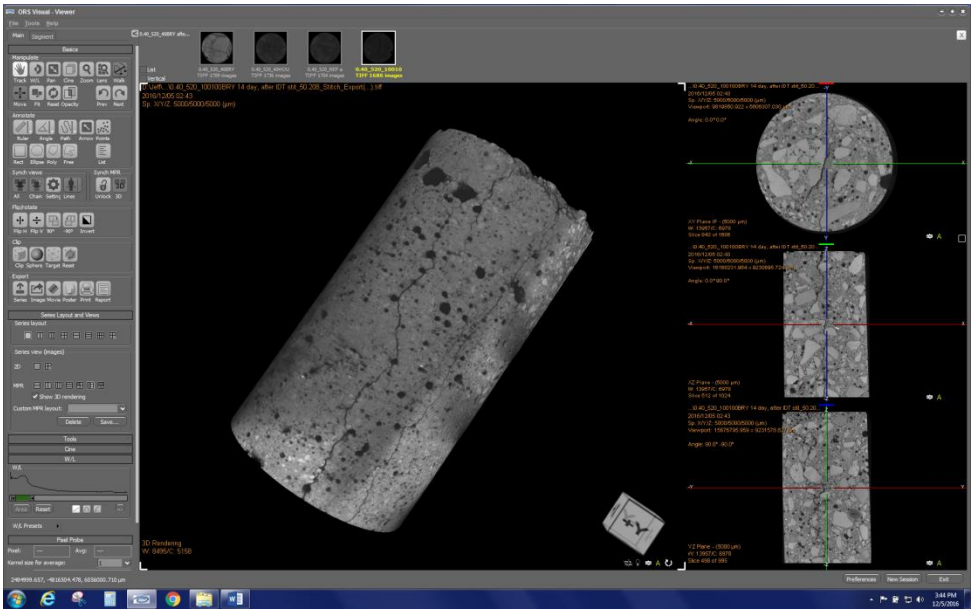

(a) Entire view

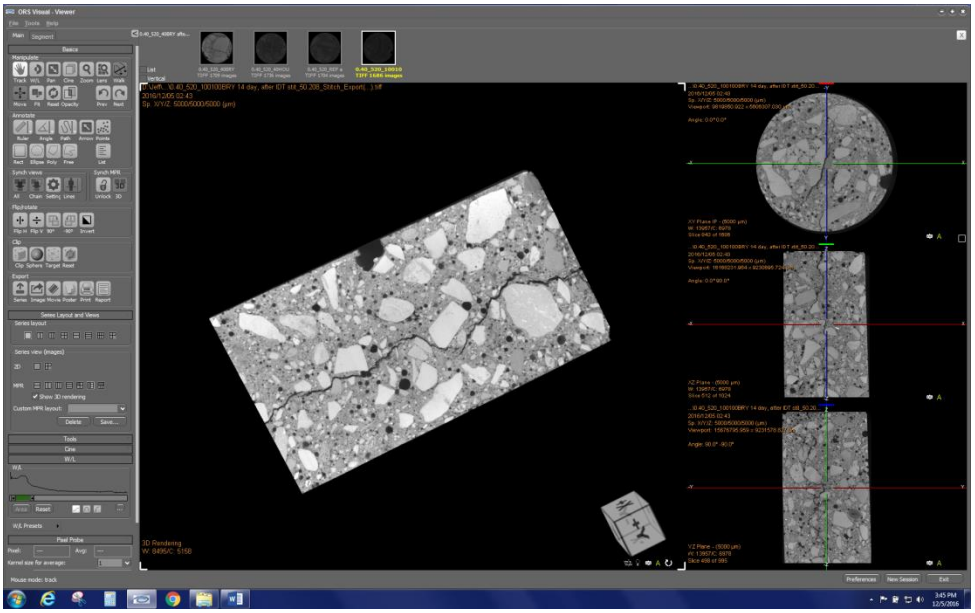

(b) Cross section

Figure 85 3D images of the cracked 0.40_520_100BRY/100BRY

IV.6 FRACTURE PROPERTIES

IV.6.1 Fracture Properties Testing Results

The peak load and the CMOD at the peak load for the SCB specimens with two notch lengths are shown in Figure 86 and Figure 87, respectively. The peak load of the plain PCC was higher than that for the RAP-PCC mixtures for both specimen types. By comparing the results between the 0.40_520_40HOU mixture and the 0.40_520_40BRY mixture, the PCC mixture containing HOU RAP showed higher load capacity. In the case of the CMOD at the peak load, all the RAP-PCC mixtures indicated higher values than the plain PCC, indicating that RAP-PCC is more ductile.

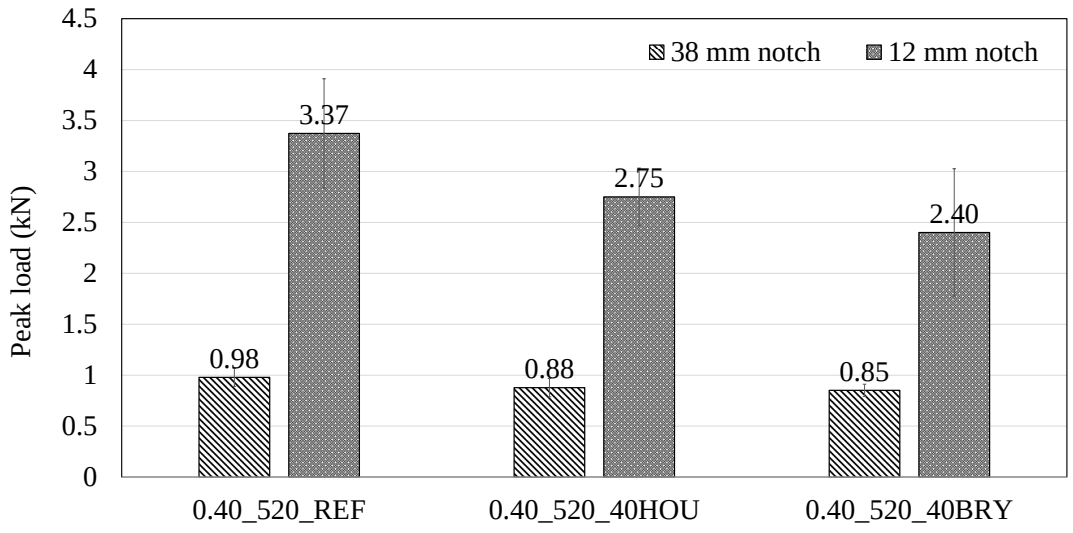

Figure 86 Comparison of peak load

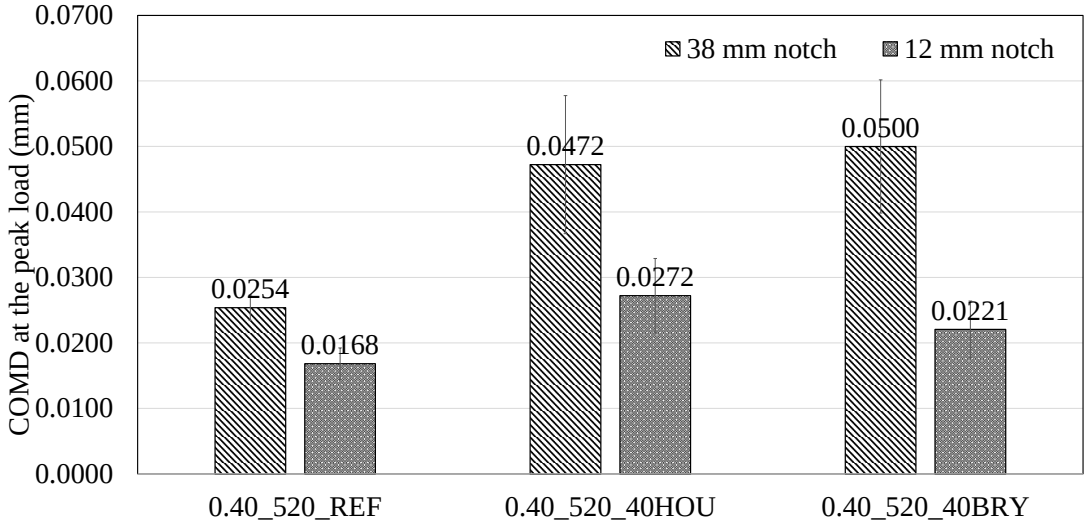

Figure 87 Comparison of CMOD at peak load

The fracture properties of the studied mixtures including K_{Ic}^{s}, $CTOD_c$, G_f and G_F are shown in Table 26. The results were calculated only using the data from the specimens with 38 mm notch because most of the specimens with the 12 mm notch had unstable failures. Brand et al. (2012) and Amirkhanian et al. (2015) obtained the fracture properties of the ternary blended RAP-PCC mixtures using the SEN(B) and DCT specimens, respectively. A summary of the test results from the current study in comparison with those from Brand et al. (2012) and Amirkhanian et al. (2015) is presented in Table 39.

From Table 39, although the SEN(B) and DCT test results showed that the RAP-PCC samples had slightly lower critical stress intensity factors, the current SCB test results indicated that the K_{Ic}^{s} values were approximately same between the control mixture and the two RAP-PCC mixtures. The K_{Ic}^{s} tested in this current study was significantly smaller than those using the other two testing methods, but the values were still within the range of typical stress intensity factor for the PCC material (Alam et al. 2010). The difference among different K_{Ic}^{s} measurements in

Table 39 is likely due to the specimens' age and mix design (The SEN(B) samples and DCT samples both used ternary blends, while the current study used a conventional mix design with fly ash). For the critical crack tip opening, almost all the tested RAP-PCC samples had higher values than their control samples, indicating that RAP-PCC is a more ductile material. Regarding the fracture energies, RAP-PCC generally had comparable or higher initial (G_f) and total fracture energy (G_F). The test results from this study invariably showed an increase in both initial and total facture energy in RAP-PCC relative to the control PCC. It is noted here that the BRY samples showed better fracture properties in terms of all tested parameters relative to the HOU samples. Since the 0.40_520_40BRY has a higher TAVF than the 0.40_520_40HOU, it appears that the higher the asphalt content, the more ductile the material. The better fracture properties of the PCC containing BRY RAP might be also attributed to the dense aggregate gradation.

Table 39 Summary of the RAP-PCC fracture properties from the current study in comparison with those from the available literature

Study	Test	RAP replacement level (%)	Age (days)	K_{Ic}^{s} ($MPa\sqrt{m}$)	$CTOD_c$(mm)	G_f(N/m)	G_F (N/m)
Brand et al. (2012)	SEN (B)	0	100	1.267 (5%)	0.016 (10%)	44.7(12%)	100.4 (15%)
		20	100	1.140 (3%)	0.016 (5%)	43.7 (13%)	86.4 (15%)
		35	100	0.974 (8%)	0.014 (36%)	35.8 (21%)	106.5 (15%)
		50	100	1.054 (9%)	0.019 (21%)	47.7 (11%)	113.5 (14%)
Amirkhanian et al. (2015)	DCT	0	142	1.33 (8%)	0.0167(8%)	49.1 (15%)	120.3 (30%)
		21	142	1.14 (10%)	0.0176 (15%)	42.2 (18%)	119.0 (17%)
Current	SCB	0	28	0.615 (12%)	0.0097 (20%)	15.2 (28%)	84.2 (14%)
		40 (HOU)	28	0.604 (11%)	0.0181(30%)	25.9 (17%)	91.9 (18%)
		40 (BRY)	28	0.674 (9%)	0.0244(21%)	30.4 (13%)	108.9 (24%)

Note: Mean of each test result followed by its coefficient of variance in the parentheses is presented in the table.

To eliminate the bias from the simple comparison among averaged values, an evaluation of data through statistical approaches was performed for the fracture properties tested in this

study. The two-sample t-test (by assuming equal variance) was carried out to evaluate the statistical significance between different comparisons of each two mixture types for the calculated K_{Ic}^{S}, $CTOD_c$, G_f and G_F, respectively. The p-values at a 95% confidence level for the null hypothesis that the calculated property between the compared two mixtures is equal to each other are presented in Table 40. From Table 40, the p-value for the K_{Ic}^{S} of any two-sample comparison is larger than 0.05, which means that there is no statistical evidence to reject the null hypothesis that the K_{Ic}^{S} values are equal. Therefore, the K_{Ic}^{S} for different mixtures tested in this study are statistically similar. This result matches the previous conclusion by comparing the averaged values. For the $CTOD_c$, p-values less than 0.05 are obtained for all the two-sample comparisons, indicating that there is a 95% confidence to reject the null hypothesis that the compared $CTOD_c$ values are equal. So, the tested values are indeed significantly different between the RAP-PCC and the plain PCC. It is noted that the p values of the $CTOD_c$ for the 0.40_520_REF VS 0.40_520_40HOU and the 0.40_520_REF VS 0.40_520_40BRY are extremely low. A lower p-value suggests that the difference is more pronounced, so the $CTOD_c$ of the RAP-PCC mixture (either with HOU RAP or BRY RAP) and the plain PCC are much more different, as compared to the difference between the RAP-PCC containing BRY RAP and the RAP-PCC containing HOU RAP. For the G_f, the difference between the RAP-PCC mixtures and the plain mixture is significant as well, but a same conclusion could not be drawn between the two RAP-PCC mixtures. It is interesting to see the p-values for the G_F comparisons are all above 0.05, indicating the calculated G_F of the studied mixtures do not have differences which are significant enough.

Table 40 Two-sample t-test results for the calculated fracture properties (p-values, two-tail)

Mixture comparison	K_{Ic}^{s}	$CTOD_c$	G_f	G_F
0.40_520_REF VS 0.40_520_40HOU	0.8294	0.0012	0.0075	0.4634
0.40_520_REF VS 0.40_520_40BRY	0.2227	0.0011	0.0008	0.1214
0.40_520_40HOU VS 0.40_520_40BRY	0.1226	0.0449	0.1250	0.2497

IV.6.2 Estimation of Other Properties of RAP-PCC

Theoretical Tensile Strength

Concrete theoretical material tensile strength f_t is the only strength parameter required in the cohesive zone model. It is a material property and is independent of size and structure of the specimen. There are two types of approaches to estimate the f_t of PCC. One approach is the direct tension test, whose application is impeded by the challenges and difficulties of grasping concrete specimen due to the brittle nature of concrete material. Instead, alternative test methods such as splitting tensile test (ASTM C496) and flexural bending test (ASTM C78 and ASTM C293) are more commonly used as indirect measurements of concrete tensile properties. However, these tests all tend to overestimate the f_t of PCC due to several reasons (Neville 1995). Besides, specimen size effect might also lead to a misinterpretation of concrete's theoretical tensile strength. Theoretically, f_t might be evaluated from the failure stress of an infinitely-large uniaxial tensile plate with double-edge crack. However, the size of the conventional lab specimen is not big enough as such the tested value (f_t') is always larger than the f_t.

Although it is hard or even impossible to obtain a close approximation of the f_t of PCC from either direct or indirect tension tests, f_t can be theoretically determined by substituting the values of K_{Ic}^{s} and $CTOD_c$ into the expressions for the stress intensity factor and the crack opening displacement for an infinitely-large uniaxial tensile plate with double-edge crack, which yields Equation (8).

Using Equation (8), the f_t of the 0.40_520_REF, 0.40_520_40HOU and 0.40_520_BRY are computed in Table 41. The f_t values are compared with the values from both the flexural test and the splitting tension test conducted in the previous section.

Table 41 Comparison of f_t and MOR and STS of the studied RAP-PCC mixtures

Mix	f_t (MPa)	COV	MOR (MPa)	COV	STS (MPa)	COV
0.40_520_REF	2.28	9%	4.46 (1.95)	6%	4.39 (1.92)	8%
0.40_520_40HOU	2.10	11%	3.39 (1.61)	4%	3.79 (1.80)	4%
0.40_520_40BRY	1.86	13%	3.67 (1.97)	7%	3.95 (2.12)	4%

Note: The (MOR or STS)/f_t ratio is included in the parentheses

Table 41 shows that the theoretically determined f_t values were invariably lower that the measured values from either flexural test or splitting tension test, which verified the statement that the measured PCC tensile strength from indirect approaches overestimates the f_t of PCC. For the conventional PCC, the directly measured tensile strength f_t is reported to be about 75% of the MOR or 85% of the STS. From Table 41, both MOR and STS are about twice of the f_t determined from the fracture test. The inconsistency is likely because that the f_t' in such relations might be obtained from a direct tension test, which naturally overestimates the theoretical tensile strength f_t due to the specimen size effect.

Material Length

The material length, Q, for the studied mixtures is calculated according to Equation (7) and is presented in Figure 88. It is indicated that the RAP-PCC mixtures had a higher material length than that of the plain PCC. Despite of suffering from a high variance, the averaged Q value of the 0.40_520_40BRY is almost twice of that of the 0.40_520_REF. A two-sample t-test was conducted and the result shows that the material length of the 0.40_520_40BRY is significantly higher than that of the 0.40_520_40HOU and the 0.40_520_REF (Table 42). Since

Q is an index for material brittleness, and the higher the Q the more ductile the material, the improvement of PCC ductility with the addition of RAP has been proved. According to Shah et al. (1995), the Q values for concrete range from 150-350 mm. The test results showed a very good agreement with this range and again validated the test results from this new SCB fracture test.

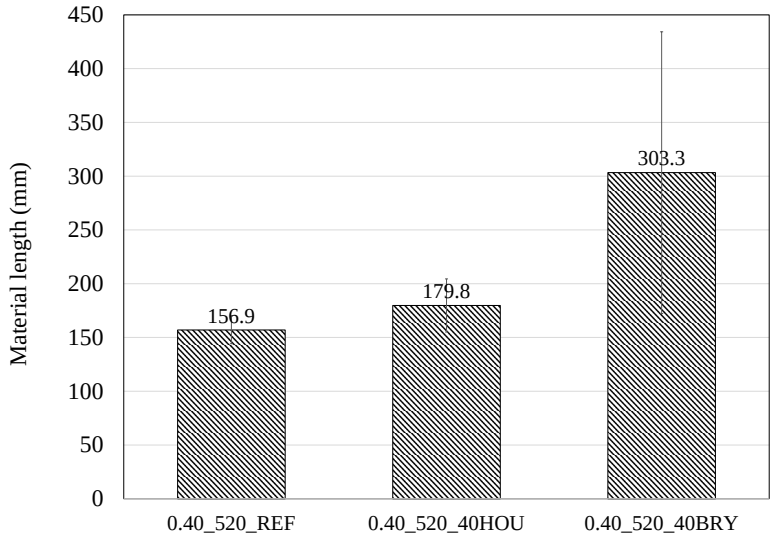

Figure 88 Material length of the studied RAP-PCC mixtures

Table 42 Two-sample t-test results for the calculated material length (p-values, one-tail)

Mixture comparison	Q
0.40_520_REF VS 0.40_520_40HOU	0.0702
0.40_520_REF VS 0.40_520_40BRY	0.0321
0.40_520_40HOU VS 0.40_520_40BRY	0.0360

Modulus of Elasticity

The modulus of elasticity of the studied mixtures can be evaluated through Equation (66). Figure 89 compares the MOE calculated from the SCB fracture testing using specimens with

both 38 mm notch and 12 mm notch, and the MOE tested from the compression test according to ASTM C469. It is found that the calculated MOE from the SCB fracture tests is dependent on the specimen notch size. The samples with the smaller notch length had higher calculated MOE values. The MOE estimation from the compression test was close to the calculated value using the SCB specimens with 12 mm notch. If the commonly accepted assumption that the tensile MOE and the compressive MOE are same for concrete material is considered, the SCB specimen with a notch length of 12 mm can provide a better estimation of MOE than that with a notch length of 38 mm. However, this assumption of the equivalence of tensile MOE and compressive MOE is not valid since the contact between matrix largely determines the tensile properties of PCC while the interaction of aggregate and matrix controls PCC's behavior under compression. As matrix is usually less stiff than aggregate, tensile MOE of PCC tends to be smaller than compressive MOE of PCC. It is noted that the use of Equation (66) to calculate E assumes that the specimen exhibits plain strain behavior. If the specimen exhibits plain stress behavior, the calculated MOE value equals to $\frac{E}{1-\nu^2}$. For the studied SCB geometries, the actual stress field in the specimen should be neither a plain stain nor plain stress, so the estimated value of MOE is within a range of E and $\frac{E}{1-\nu^2}$. It is reasonable to consider that the determined MOE is close to E because the difference between E and $\frac{E}{1-\nu^2}$ is less than 3% for a typically concrete material with a Poisson's ratio of 0.15.

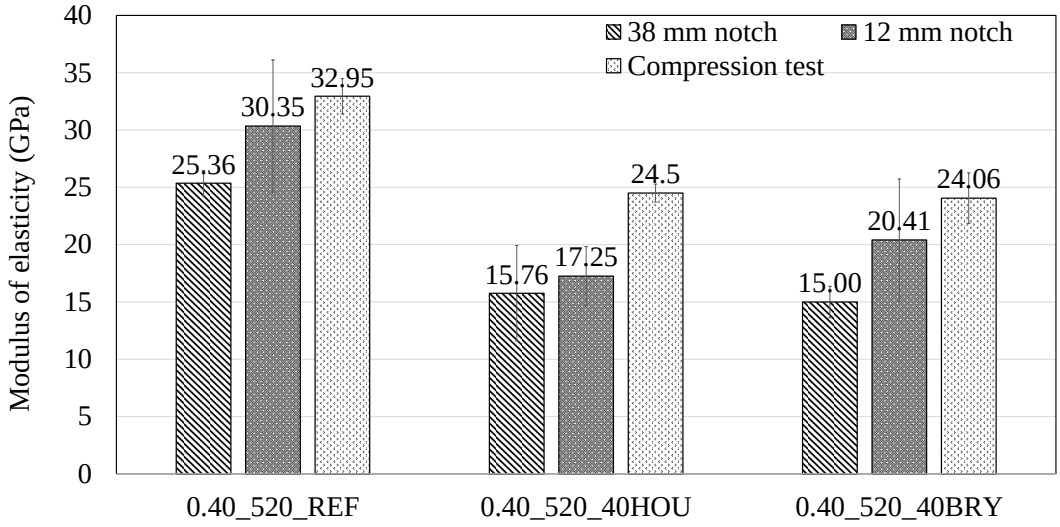

Figure 89 Comparions of the modulus of elasticity based on different tests

Parameters for the Cohesive Zone Model

The essential fracture parameters in the bilinear softening curve are calculated according to Equation (14)-(17). The results are shown in Table 43. Both of two RAP-PCC mixtures were reported to have higher displacement parameters (i.e., w_1, w_k and w_f) relative to the plain PCC mixture. This again manifested the ductile nature of the RAP-PCC material. The kink point stress ratio, ψ, turns out to be constant when substituting Equation (8) and (12) into Equation (15):

$$\psi = 1 - \frac{\mathrm{CTOD_c f_t}}{2\mathrm{G_f}} = 1 - \frac{(\mathrm{CTOD_c} \times 1.4705 \frac{(\mathrm{K_{ic}^s})^2}{\mathrm{E\ CTOD_c}})}{2 \times \frac{(\mathrm{K_{Ic}^s})^2}{\mathrm{E}}} = 0.265 \quad (90)$$

This current study might be the first one to show that a constant, ψ, should be used for the bilinear softening curve, while a considerable amount of the exiting work attempted to get a best estimate of ψ from different experimental approaches (Park et al. 2008).

Table 43 Parameters for the bilinear softening curve

Mix type	E (GPa)	υ	w_1 (mm)	w_k (mm)	w_f (mm)	f_t (MPa)	ψ
0.40_520_REF	33.0	0.151	0.0132	0.0097	0.2459	2.28	0.265
0.40_520_40HOU	24.5	0.176	0.0247	0.0181	0.2647	2.10	0.265
0.40_520_40BRY	24.1	0.190	0.0332	0.0244	0.3588	1.86	0.265

With all the parameters calculated in Table 43, the bilinear softening curves for the studied mixtures are plotted in Figure 90. These curves are inputs for the numerical modeling of RAP-PCC fracture behaviors in the future study.

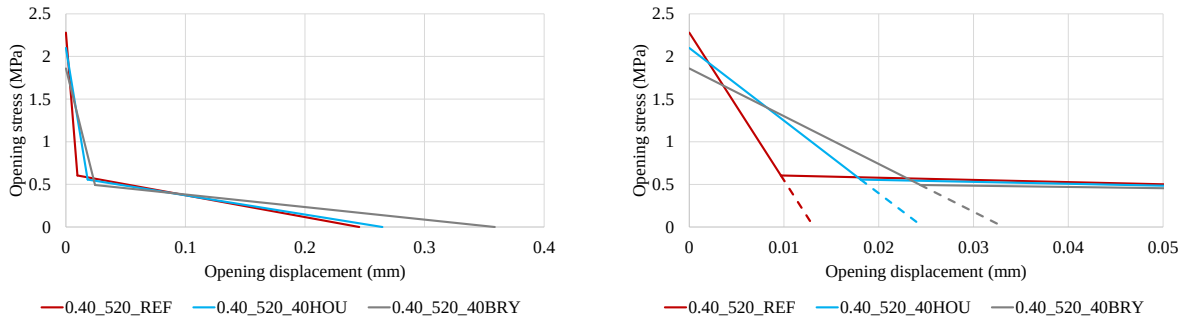

(a) Large x-axis scale (b)Small x-axis scale

Figure 90 Bilinear softening curves for the studied mixtures

IV.7 CONCLUSIONS

Based on the findings from this chapter, the addition of RAP into PCC invariably reduced the strength of the mixture, which might be a concern from pavement design's perspective. However, it is suggested that the reduction in MOR is the smallest among all the mechanical properties. Since the MOR is considered to be a more important and relevant parameter related to concrete performance, the negative effect of RAP on pavement performance might not be very significant if that was the only factor. Since asphalt cohesive failure is the primary mechanism responsible for the reduction in mechanical properties, the strength of the RAP-PCC mixture can

be designed by controlling the amount of asphalt in the mixture. The strength reduction of RAP-PCC can be mitigated by controlling the amount of agglomerated particles or achieving enhanced aggregate gradation with addition of considerable amounts of intermediate sized RAP particles.

The studied RAP-PCC mixtures appeared to have good durability characteristics. The only concern might be its reduced abrasion resistance, which is primarily due to the weak bonding of RAP particles in the mixture. On the other hand, the ring test suggested that the cementitious material containing RAP has considerably better cracking resistance compared to the conventional cement composites. This enhanced cracking resistance is likely attributed by the reduced MOE and stress relaxation due to the higher viscoelasticity.

Another potential advantage of RAP-PCC is the improved ductility and fracture properties. The findings that the existing field sections of PCCP containing RAP aggregates had equivalent performance as the conventional PCCP appeared to be interpretable given the fact that RAP-PCC has the improved ductility and fracture properties.

The effect of aforementioned changes in RAP-PCC properties with the addition of RAP on pavement performance is evaluated in the Chapter V.

CHAPTER V

EVALUATION OF RIGID PAVEMENT CONTAINING RAP-PCC*

The previous chapters evaluated the RAP-PCC material properties. The performance of the single-lift full-depth concrete pavement made of RAP aggregates is evaluated in this chapter. A pavement slab thickness design was performed through the TxDOT approved design tools in order to investigate whether using RAP in PCC would significantly increase slab thickness. To further understand the effect of RAP-PCC properties on pavement distresses, the effect of RAP-PCC on critical slab stress and deflection was conducted subsequently using a pavement finite element tool. A sensitivity analysis using Pavement ME software was performed to directly assess the effect of each RAP altered properties on pavement distresses. Based on the evaluation results, use of RAP-PCC in the lower lift of a two-lift concrete pavement has been justified. Evaluation of structural responses of using RAP-PCC in a two-lift pavement is not within the scope of this study.

Four rigid pavement evaluation tools/models were used in this chapter. The TxDOT approved slab thickness design tools are the AASHTO 1993 design equation for JPCP design and the TxCRCP-ME for CRCP design (Ha et al. 2012). The critical slab stress and deflection analysis was performed based on the ISLAB 2000 results. The effect of RAP altered property on pavement distress was directly evaluated through the sensitivity analysis via the Pavement ME software. Table 44 summarizes the types of material property needed for these four pavement evaluation tools. Because the aforementioned tools all adopted the U.S customary units, some of

*Part of the contents in this chapter is reprinted with permission from:
Validation of RAP and/or RAS in Hydraulic Cement Concrete: Technical Report by Mukhopadhyay, A., and Shi, X., 2017, Texas A&M Transportation Institute, Texas. Copyright [2017] by Texas A&M Transportation Institute.

the inputs and outputs presented in this chapter directly used the U.S customary units for the sake of convenience.

Table 44 Type of material property inputs needed for each evaluation tool

Tool	Evaluated pavement type	required inputs for PCC slab
AASHTO 1993	JPCP	MOE, MOR
TxCRCP-ME	CRCP	MOR
ISLAB 2000	JPCP/CRCP	Poisson's ratio, CoTE, unit weight, MOE
Pavement ME	JPCP	Poisson's ratio, CoTE, unit weight, thermal conductivity, heat capacity, MOE, MOR
	CRCP	Poisson's ratio, CoTE, unit weight, thermal conductivity, heat capacity, MOE, MOR, STS

SLFD pavements using five different PCC mixtures as the slab material were evaluated. The PCC mixtures were RAP-PCC mixtures with mix ID 0.40_520_20HOU, 0.40_520_40HOU, 0.40_520_20BRY, and 0.40_520_40BRY, and the plain PCC mixture (0.40_520_REF). The previously experimentally determined properties were assigned to the corresponding mixtures. The material property inputs are summarized in Table 45.

Table 45 Material property inputs

Mix ID	Poisson's Ratio	CoTE (10^{-6}/F)	Unit weight* (pcf)	Thermal conductivity (BTU/hr-ft-°F)	Heat capacity (BTU/lb-°F)	MOE (ksi)	MOR (psi)	STS (psi)
0.40_520_REF	0.151	4.463	147.07	1.570	0.192	4779	647	636
0.40_520_20HOU	0.162	4.847	146.25	1.434	0.179	4198	585	646
0.40_520_40HOU	0.176	4.950	143.91	1.376	0.187	3554	491	549
0.40_520_20BRY	0.180	5.085	146.32	1.460	0.168	4164	573	606
0.40_520_40BRY	0.190	5.670	143.99	1.411	0.174	3490	533	573

* Unit weight of hardened concrete was measured according to ASTM C138

V.1 EFFECT OF RAP-PCC ON SLAB THICKNESS

Chapter IV showed that the addition of RAP led to reductions in PCC's mechanical properties; the content of RAP in a class P concrete can be restricted by the material's strength requirements specified in (Texas 2014). The allowable RAP replacement level in a RAP-PCC mixture to satisfy the concrete strength requirements can be determined through the approaches developed in this study by controlling TAVF in the mixture. In this section, the exact effects of the RAP-PCC materials on slab thickness were evaluated.

V.1.1 AASHTO 1993 Results

The JPCP thickness design was performed according to the AASHTO 1993 procedure with the assistance of an online JPCP design service (Pavement Interactive 2017). The total design ESALs were 10 million. The reliability level of the design was 95 percent, and the combined standard error was set as 0.39. The initial serviceability index and the terminal serviceability index were set as 4.5 and 2.5, respectively. A drainage factor of 1.0 and a load transfer coefficient of 2.9 were assumed for all the design cases. A subgrade k value of 200 was used.

For different design cases, all of the aforementioned inputs remained constant, while the slab properties adopted the actual tested values for the studied mixtures (i.e., 28-day MOE and 28-day MOR, Table 45). The designed slab thickness was rounded to the nearest 1/2 inch after the calculated thickness was obtained. Table 46 presents the JPCP results for different cases. From Table 46, the use of RAP-PCC in JPCP requires the PCC slab to be slightly thicker. When 20% RAP aggregates were used, the slab thickness only increased by 0.5 inch, while 1.5 inch and 1 inch thicker slabs were needed for the 0.40_520_40HOU and 0.40_520_40BRY mixtures, respectively. All the design thicknesses were within the range of the specification (6-12 inch).

Table 46 JPCP design results

Mix ID	Calculated thickness (inch)	Design thickness (inch)
0.40_520_REF	10.005	10.5
0.40_520_20HOU	10.605	11
0.40_520_40HOU	11.505	12
0.40_520_20BRY	10.605	11
0.40_520_40BRY	11.005	11.5

V.1.2 TxCRCP-ME Results

The CRCP pavement design was completed using the TxCRCP-ME Excel® spreadsheet. The total design traffic was assumed as 20 million equivalent single axle loads (ESALs) in one direction, and the number of lanes in one direction was two. The pavement was assumed to be located in the Bryan District (Brazos County) with the environmental conditions automatically determined by the spreadsheet. The subgrade was classified as CL based on the Unified Soil Classification System (USCS) soil classification specification. A 6-inch cement treated base with a modulus of 500 ksi was used in the design. A 30-year design period was considered. In the design, all the inputs other than the concrete layer material properties remained constant among different cases. The concrete layer was assumed to be made with four different RAP-PCC materials and a plain PCC with material inputs listed in Table 45 (28-day MOR is the only input for TxCRCP-ME). The required pavement thickness was determined in which the predicted number of punchouts per mile was less than the design requirement (10 per mile). Table 47 shows the TxCRCP-ME design results for different mixture cases. The slab thickness requirement for the RAP-PCC increased very little (i.e., 0.5 inch) at 20 percent RAP replacement level. However, at 40 percent RAP replacement level, the increase of thickness requirement was slightly higher (i.e., 1-2 inch) than that at 20 percent replacement level. Since the simulation only requires to input MOR, the potential benefit of the reduced of MOE of RAP-PCC is omitted.

Based on the results, all the slab thickness remained within the range of the TxDOT specification for CRCP thickness as well (7-13 inch).

Table 47 CRCP design results

Mix ID	Design thickness (inch)	Punchout at design thickness (per mile)
0.40_520_REF	10	8.1
0.40_520_20HOU	10.5	9.3
0.40_520_40HOU	12	8.7
0.40_520_20BRY	10.5	9.7
0.40_520_40BRY	11	9.5

V.1.3 Pavement ME Results

The major distresses that determine JPCP's performance are transverse cracking and joint faulting, while a CRCP design is based on limiting punchout distress. Both of the aforementioned TxDOT approved tools suffer from limitations: (i) the AASHTO 1993 is an empirical method based on the AASHO road test results that are likely only valid for specific conditions and (ii) both the AASHTO 1993 and TxCRCP-ME require only a limited amount of material properties as inputs and ignore other PCC properties which can significantly affect the prediction (for example, the CoTE of the PCC material has a profound effect on pavement curling). The Pavement ME, developed under the National Cooperative Highway Research Program 1-37A project (AASHTO 2003), is considered a more advanced design tool to design pavements and predict pavement performance. Table 44 shows that the Pavement ME simulation requires much more inputs than the AASHTO 1993 and the TxCRCP-ME and therefore is able to evaluate the impact on pavement performance caused by the changes in a wide range of PCC properties with the addition of RAP. In this Pavement ME, a typical pavement structure from Texas was selected (Figure 91). College Station was selected as the climate station city for

inputting climate data. An average annual daily truck traffic (AADTT) of 30,000 was used as traffic input for the initial year of pavement life (i.e., 2017). All the other inputs adopted the default values. The pavement design life was set as 20 years.

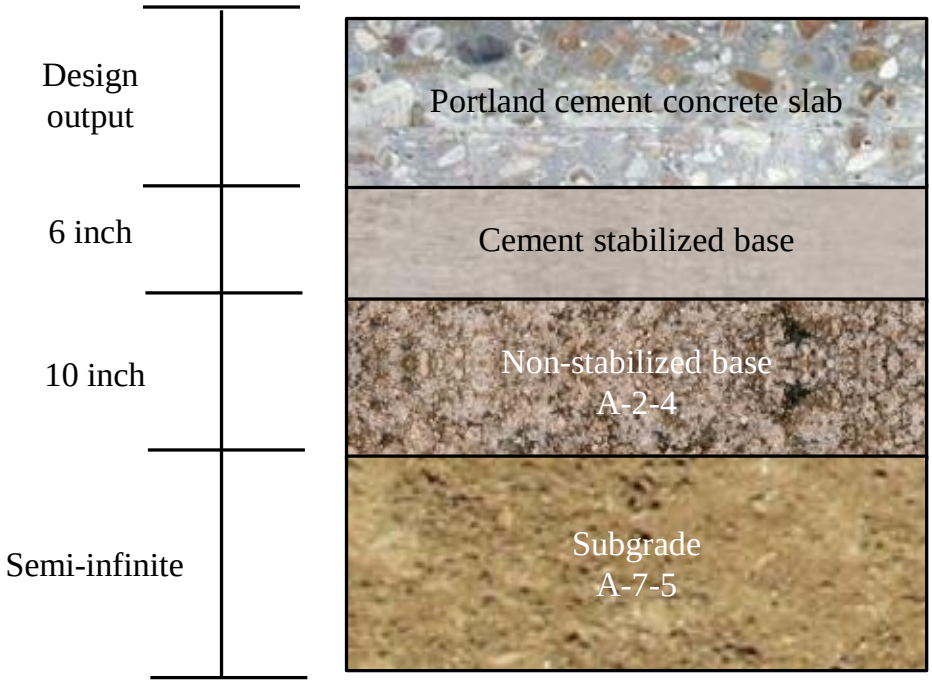

Figure 91 Pavement structure used in the Pavement ME simulations

The optimum slab thicknesses for JPCP and CRCP pavements containing different concrete materials were determined by the Pavement ME simulations. For the JPCP design, the pavement distress criteria are 172 inch/mile for terminal international roughness index (IRI), 0.12 inch for mean joint faulting, and 15 percent for slab transverse cracking (all default values). Table 48 lists the design results. The results again suggest that the use of RAP-PCC increased JPCP slab thickness. During the simulation, it was found that the primary failure distress was the joint faulting. The use of RAP-PCC caused slightly higher IRI, but appeared to have no effect on the transverse cracking distress for the studied cases.

Table 48 Pavement ME JPCP design results

Mix ID	Design thickness (inch)	IRI (inch/mile)	Mean joint faulting (inch)	Transverse cracking (%)
0.40_520_REF	8	133.15	0.1	0.96
0.40_520_20HOU	9	140.86	0.11	0.96
0.40_520_40HOU	10	148.06	0.12	0.96
0.40_520_20BRY	10	137.10	0.1	0.96
0.40_520_40BRY	11	144.52	0.11	0.96

The steel design of CRCP was based on the FHWA CRCP design and construction guideline (Roesler et al. 2016). The rebar was assumed to be placed at the depth of 4 inch from top surface of the slab. The steel design result is presented in Table 49. The design criteria for the CRCP Pavement ME are 172 inch /mile for terminal IRI and 10 per mile for punchout. The optimum slab thickness for each CRCP case is presented in Table 50. It is interesting to see that the CRCP built with RAP-PCC could yield reduced slab thickness. The minimum slab thickness for all the RAP-PCC cases were lower than the plain PCC pavement.

Table 49 Steel design of the CRCP

Rebar direction	Bar size	Bar spacing (inch)	Reinforcement percentage (%)	Bar depth (inch)
Longitudinal	0.63 (#5, deformed)	5	0.61	4
Transverse	0.5 (#4, deformed)	36	0.049	4

Table 50 Pavement ME CRCP design results

Mix ID	Design thickness (inch)	IRI (inch/mile)	Pounchout (per mile)
0.40_520_REF	10.0	87.96	0.66
0.40_520_20HOU	8.5	97.45	8.02
0.40_520_40HOU	9.5	98.4	8.48
0.40_520_20BRY	9.0	100.12	9.54
0.40_520_40BRY	8.5	98.94	8.77

To facilitate the understanding of the effect of RAP-PCC on pavement distresses, the models used for the Pavement ME predictions were extensively studied. A critical stress and deflection analysis for various distresses types was carried. The results with relevant discussion are presented below.

V.2 EFFECT OF RAP-PCC ON PAVEMENT STRUCTURAL RESPONSES

In the Pavement ME, rigid pavement stresses and deflections are determined by neural networks developed from a large number of finite element analysis results using the pavement finite element software ISLAB 2000. A similar analysis of slab critical stress and deflection was conducted using the ISLAB 2000 in this section in order to evaluate the performances of JPCP and CRCP containing RAP aggregates.

A typical PCC structure in Texas was used for both JPCP and CRCP in this critical stress and deflection analysis (Figure 92). For the PCC slab, the 0.40_520_HOU, 0.40_520_BRY mixture series, and the 0.40_520_REF were used in order to have a performance comparison between PCC slabs made of different RAP type and replacement level. All of the slab properties were directly obtained from the lab tests carried out in this research (Table 45). For the base and subgrade, some of the required input parameters were collected from the relevant literature, and the remaining parameters were based on reasonable assumptions. Table 51 shows the material property inputs for different layers. The subgrade used a Winker model, and the modulus of subgrade reaction (k-value) was assumed as 200 pci.

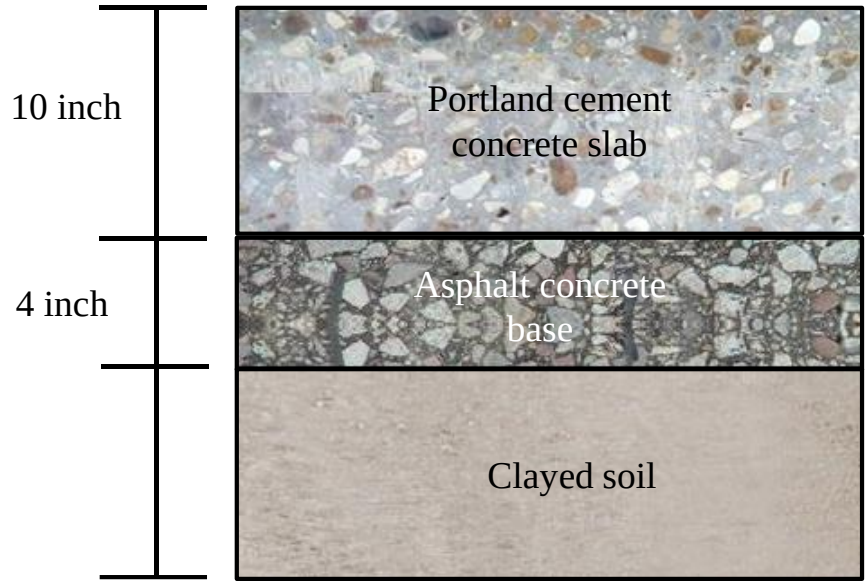

Figure 92 A typical PCC pavement structure in Texas

Table 51 ISLAB 2000 material property inputs

Structure		Modulus ($\times 10^6$ psi)	Poisson's ratio	Unit weight (pci)	CoTE (10^{-6}/°F)
PCC slab	0.40_520_REF	4.779	0.151	0.0851	4.463
	0.40_520_20HOU	4.198	0.162	0.0846	4.847
	0.40_520_40HOU	3.554	0.176	0.0833	4.950
	0.40_520_20BRY	4.164	0.180	0.0847	5.085
	0.40_520_40BRY	3.490	0.190	0.0833	5.670
Asphalt concrete base		0.25	0.35	0.0868	13.010
Clayed soil		k-value=200 pci	N.A	N.A	N.A

Stress and deflection of concrete slab are subject to temperature gradient in the slab. When the top of the slab is hotter than the bottom of the slab (a positive temperature gradient), the slab will form a downward curling shape. When a negative temperature gradient is developed, slab upward curling will happen. Because of the slab weight and contact with the base restrict movement, slab curling will result in considerable stress. In the ISLAB 2000, the temperature gradient of the PCC slab is a required input in order to perform a temperature related

stress and deflection analysis. Accordingly, a pavement heat transfer analysis (Shi 2014; Shi et al. 2017; Shi et al. 2015) was conducted using a one-dimensional finite difference heat transfer model to investigate the effect of slab mixture type on pavement temperature gradient. In this analysis, the same pavement structure in Figure 92 was assigned. The material properties (i.e., thermal properties) of the multiple layers inputted in this heat transfer model are summarized in Table 52. Both of the absorptivity and the emissivity of the surface layer were assumed as 0.85, irrespective of the PCC mixture type.

Table 52 Material property inputs for the pavement heat transfer model

Structure		**Thermal conductivity (W/m×K)**	**Heat capacity ($MJ/m^3×K$)**
PCC slab	0.40_520_REF	2.717	1.888
	0.40_520_20HOU	2.481	1.751
	0.40_520_40HOU	2.381	1.800
	0.40_520_20BRY	2.526	1.646
	0.40_520_40BRY	2.442	1.683
Asphalt concrete base		1.936	1.809
Clayed soil		1.000	2.850

The slabs' most positive temperature gradient and the most negative temperature gradient during a typical summer day were obtained from the simulation. The climate data inputs (i.e., air temperature, solar radiation, and wind speed) were collected from the National Solar Radiation Database using the actual measurements in College Station on August 01, 2015 (NSRDB 2017). The results are presented in Table 53. Table 53 indicates that the RAP-PCC slabs had higher magnitudes of temperature gradients relative to the plain PCC slab. This finding matches the one from the previous studies that lower thermal conductivity and lower heat capacity of the surface layer would cause a higher amplitude in temperature gradient (Shi 2014; Shi et al. 2017; Shi et al. 2015). However, for the studied mixtures, the difference in temperature gradient appeared to

be negligible. It is interesting to see even with a negative temperature gradient, the corresponding temperature gradient of the base layer was positive.

Table 53 Temperature gradients for the slabs containing different mixtures

PCC slab	Most positive temperature gradient (°F/inch)	Corresponding temperature gradient of the base (°F/inch)	Most negative temperature gradient (°F/inch)	Corresponding temperature gradient of the base (°F/inch)
0.40_520_REF	3.92	1.56	-1.24	0.48
0.40_520_20HOU	4.14	1.56	-1.27	0.47
0.40_520_40HOU	4.22	1.49	-1.27	0.53
0.40_520_20BRY	4.11	1.66	-1.28	0.39
0.40_520_40BRY	4.18	1.59	-1.28	0.44

It is worth mentioning that the moisture profile in the slab also induces slab curling. Since the surface of the slab dries faster, the slab usually curls upward after construction. The warping caused by a negative moisture gradient along with the permanent built-in curling during construction (the zero-stress temperature gradient) is expressed in terms of permanent curling/warping in Pavement ME. The Pavement ME uses a -10°F permanent curl/warp gradient based on the calibration for typical construction and mixture conditions. During each month, a transient moisture gradient is converted to an equivalent temperature difference for modeling the pavement transitory curling. The moisture effect was not included in this stress and deflection analysis.

V.2.1 Critical Stress and Deflection Analysis for JPCP

A JPCP pavement containing three slabs with 15 feet in length and 12 feet in width was modeled. Only a truck lane (outer lane) was modeled because a previous research found the effect of passing lane can be ignored (AASHTO 2003). A no load transfer shoulder was modeled in the analysis. The mesh size was selected as 2 inch. The effective temperature gradients

(permanent plus transitory) were assumed by adding the permanent curl/warp gradient (-10°F) to the simulated temperature gradients in Table 53, which yielded an approximate 3°F/inch gradient as the most positive case and an approximate -2.3°F/in gradient as the most negative case for the slab. The corresponding temperature gradient in the base referred to the values in Table 53 (i.e., 1.6 °F/inch for the most positive slab temperature gradient case and 0.5 °F/inch for the most negative slab temperature gradient case). A 18-kip single axle load with standard configuration (Buch et al. 2004) was used for all the simulations. The critical stress and deflection analysis for transverse cracking and faulting were conducted by referring to AASHTO (2003).

Transverse Cracking

According to AASHTO (2003), the transverse cracking in JPCP is correlated with the total fatigue damage to the pavement caused by repeated loading of heavy axles:

$$FD = \sum \frac{n_{i,j,k,l,m,n}}{N_{i,j,k,l,m,n}} \quad (91)$$

Where

FD= total fatigue damage (top-down or bottom-up)

$n_{i,j,k,l,m,n}$= applied number of load applications at condition i, j, k, l, m, n.

$N_{i,j,k,l,m,n}$= allowable number of load applications at condition i, j, k, l, m, n.

i= age (accounts for change in PCC modulus of rupture, layer bond condition, deterioration of shoulder load transfer efficiency (LTE)).

j= month (accounts for change in base and effective dynamic modulus of subgrade reaction)

k= axle type (single, tandem, and tridem for bottom-up cracking; short, medium, and long wheelbase for top-down cracking).

l= load level (incremental load for each axle type)

m= temperature difference

n = traffic path

The allowable number of load applications $N_{i,j,k,l,m,n}$ is determined in Equation (92):

$$\log(N_{i,j,k,l,m,n}) = C_1 \cdot \left(\frac{MR_i}{\sigma_{i,j,k,l,m,n}}\right)^{C_2} + 0.4371 \quad (92)$$

Where,

MR_i= PCC modulus of rupture at age i

$\sigma_{i,j,k,l,m,n}$= applied stress at condition i, j, k, l ,m, n

C_1= calibration constant = 2.0

C_2= calibration constant = 1.22

From Equation (92), the allowable number of load applications is determined by the strength to stress ratio in the slab. Therefore, the critical stress and deflection analysis for JPCP transverse cracking is essentially to compute the maximum tensile stress in the PCC slab under a combination of critical environmental and traffic loads. The transverse cracks in JPCP can initiate either from the top or from the bottom of concrete slab. On a hot sunny day, the temperature of the top surface of the slab is higher than that of the bottom surface of the slab (a positive temperature gradient), resulting in a downward curling. The critical traffic loading position is determined as the middle of the slab, which causes a high tensile stress at slab bottom (Figure 93(a)). To the contrary, a negative temperature gradient developed during nighttime causes slab to curl upward. When traffic loads are applied on the slab edges, a high tensile stress occurs at the top of the slab (Figure 93(b)).

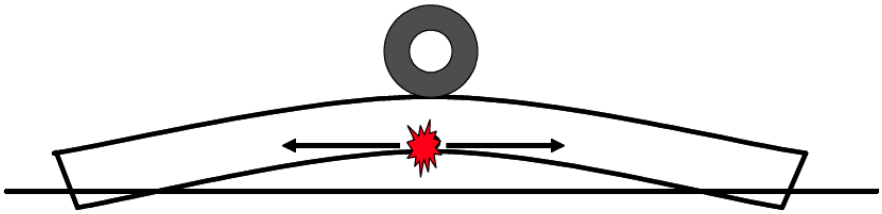

(a) Bottom-up cracking

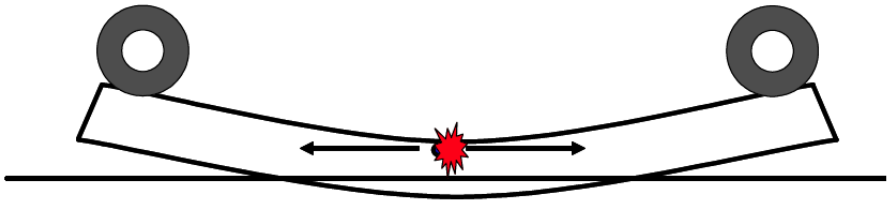

(b) Top-down cracking

Figure 93 Critical environmental and traffic loading for JPCP transverse cracking (Reprinted from AASHTO 2003)

The critical stress and deflection analysis was performed through the ISLAB 2000 based on the aforementioned two scenarios. The ISLAB 2000 interface for these two simulations are shown in Figure 94.

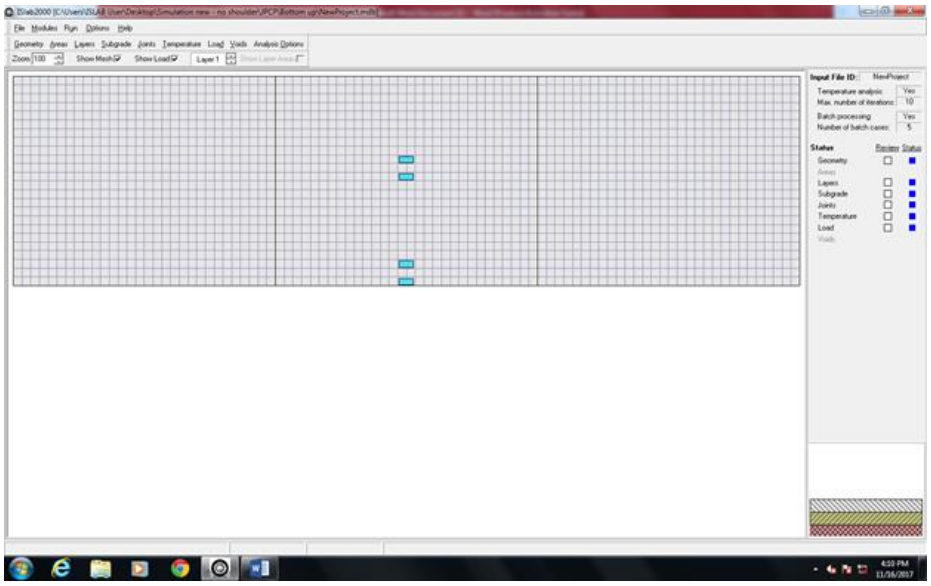

(a) Bottom-up

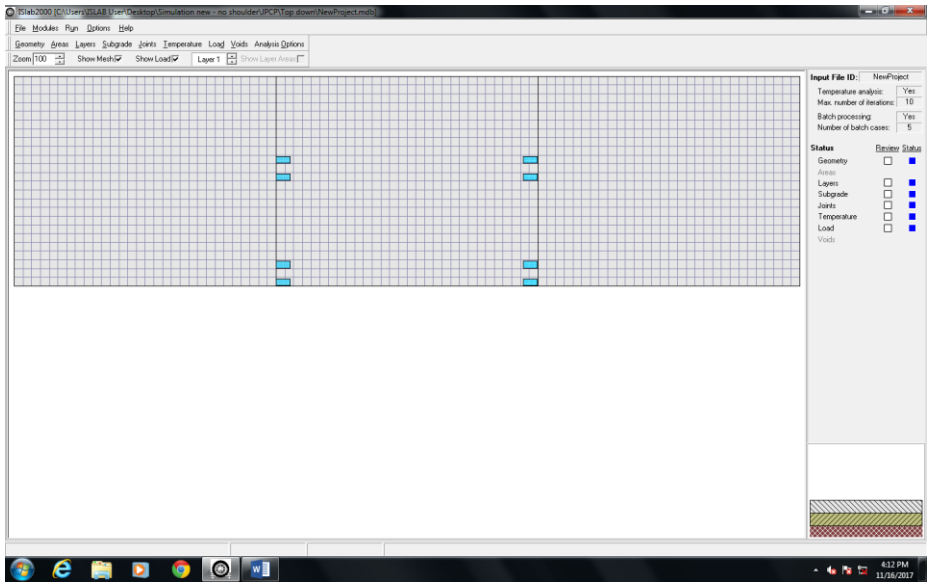

(b) Top-down

Figure 94 Modeling of stress and deflection for JPCP transverse cracking

Table 51 indicates that the addition of RAP has changed CoTE, MOE, Poisson ratio and unit weight of PCC. An analysis was carried out in order to evaluate the sensitivity of each of these altered PCC properties on transverse cracking development. With the conclusions from the sensitivity analysis, the critical stress and deflection results by simulating slabs containing the

studied mixtures could be better interpreted. The sensitivity analysis results are presented in Appendix E.

The maximum tensile stress and slab deflection in the RAP-PCC slabs for the bottom-up cracking scenario is presented in Figure 95. Figure 95(a) indicates that except for the 0.40_520_20BRY, other RAP-PCC slabs had lower maximum tensile stress compared to that in the plain PCC slab. This is because for the 0.40_520_20BRY case, the stress reduction caused by the MOE reduction was not sufficient to overcome the stress increase due to an increase in CoTE. For the maximum deflection in the slab, the RAP-PCC slabs all showed higher values compared to the plain PCC slab.

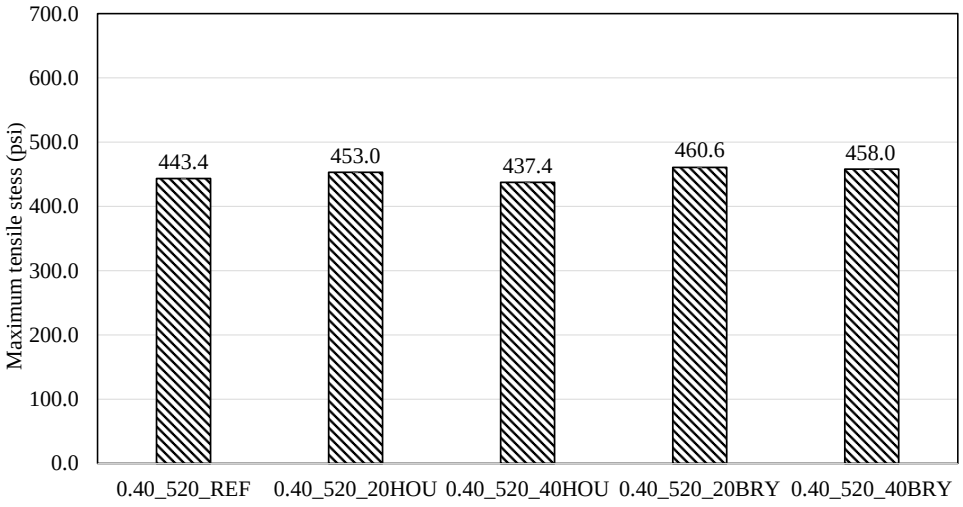

(a) Maximum tensile stress in PCC slab

Figure 95 Critical stress and deflection analysis for JPCP transverse cracking (bottom-up)

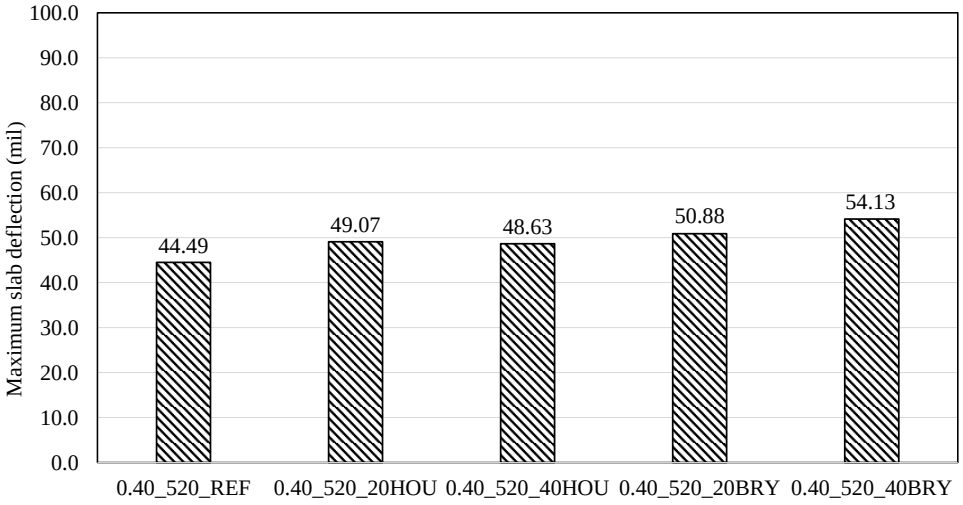

(b) Maximum deflection in PCC slab

Figure 95 Continued

The results for top-down cracking are presented in Figure 96. Similar to the bottom-up scenario, most of the RAP-PCC slabs showed a reduction in maximum tensile stress. Most the RAP-PCC slabs suffered from a higher maximum deflection relative to the plain PCC slab. The 0.40_520_40HOU had a slightly lower maximum deflection mainly because the mixture has a much lower MOE (contributing to a lower deflection) but the increase in CoTE (contributing to a higher deflection) was less significant relative to the plain PCC.

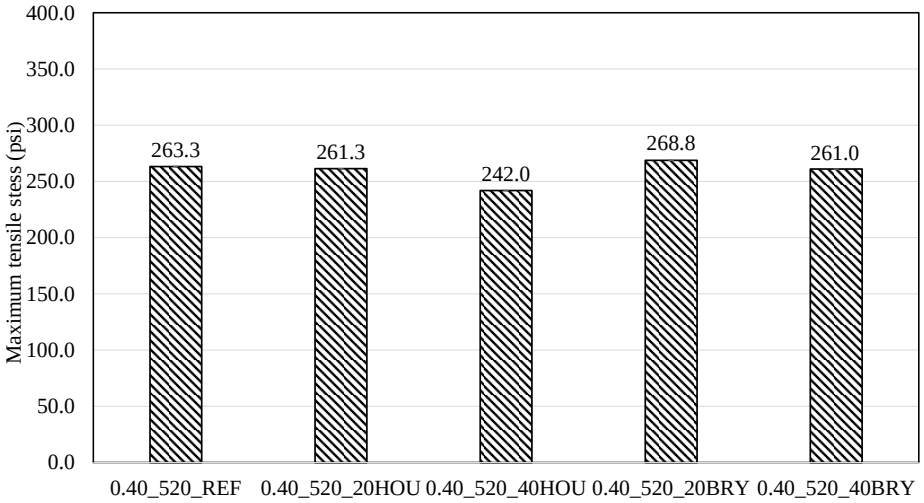

(a) Maximum tensile stress in PCC slab

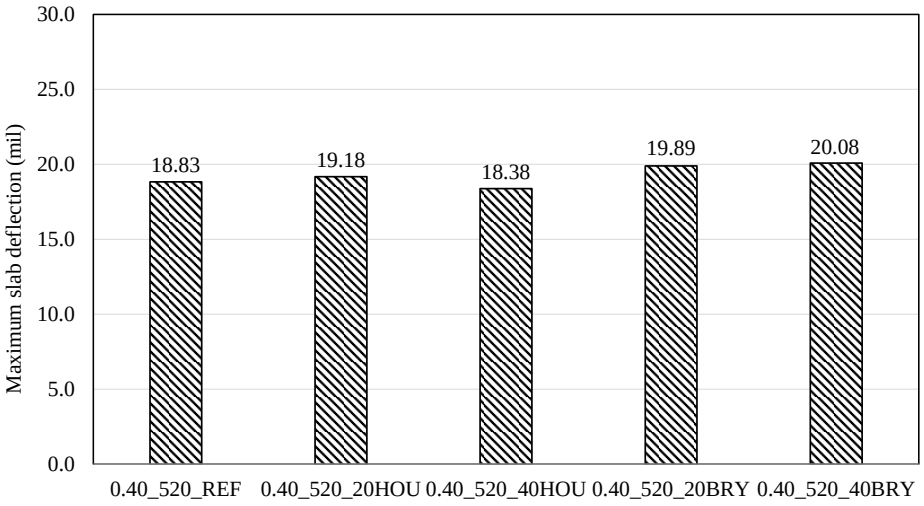

(b) Maximum deflection in PCC slab

Figure 96 Critical stress and deflection analysis for JPCP transverse cracking (Top-down)

From Equation (92), the fatigue damage of the JPCP is controlled by the stress to strength ratio in the slab. The stress to strength ratio for the studied cases is shown in Figure 97. Although a reduction in maximum tensile stress was reported for most of the RAP-PCC cases, the stress to strength ratio for all of the RAP-PCC slabs was higher than that for the plain concrete slab,

which is simply because the addition of RAP yielded reduced tensile strength. According to Equation (92), a higher stress to strength ratio leads to a lower allowable number of load applications N (assumes that calibration constants are same for RAP-PCC pavements). Therefore, the RAP-PCC slabs may have a lower fatigue life.

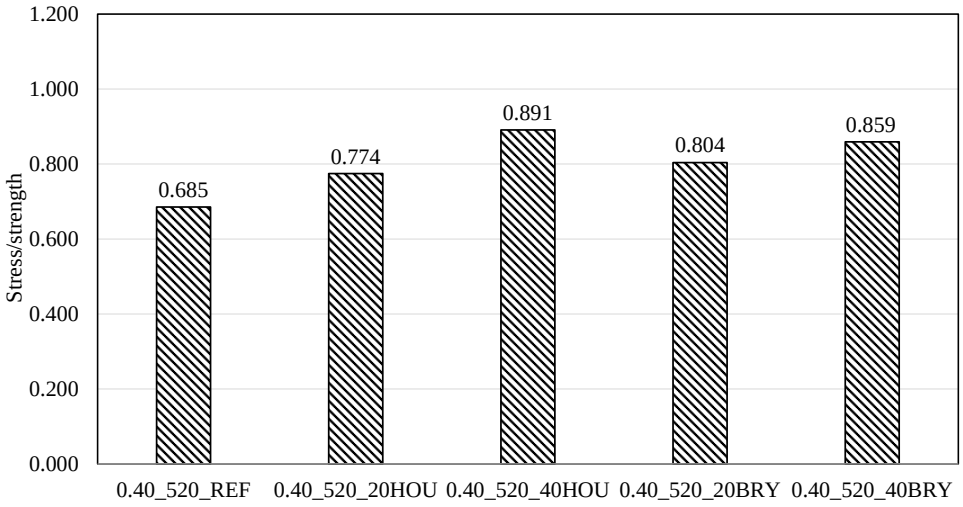

(a) Bottom-up

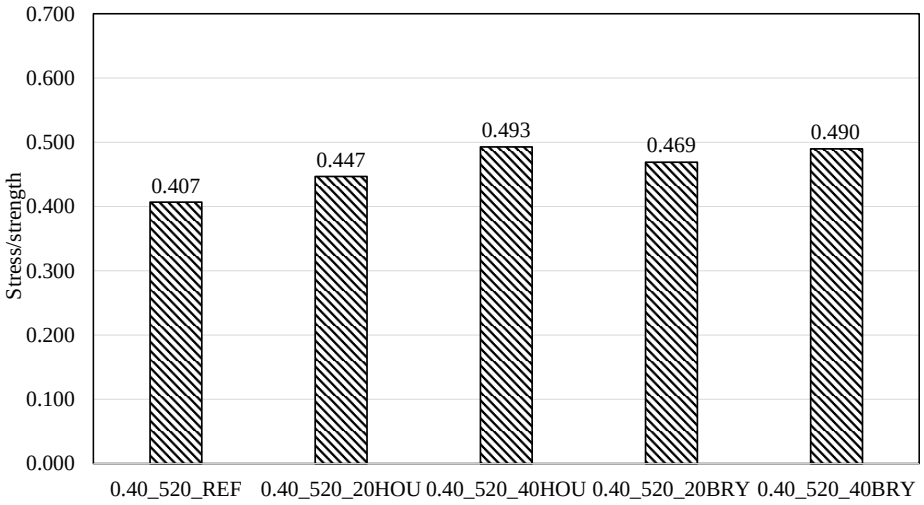

(b) Top-down

Figure 97 Comparison of stress/strength for the studied mixtures (JPCP)

Faulting

The faulting model in the Pavement ME is shown in Equation (93)-(96):

$$\text{Fault}_m = \sum_{i=1}^{m} \Delta\text{Fault}_i \tag{93}$$

$$\Delta\text{Fault}_i = C_{34} \times (\text{FAULTMAX}_{i-1} - \text{Fault}_{i-1})^2 \times \text{DE}_i \tag{94}$$

$$\text{FAULTMAX}_i = \text{FAULTMAX}_0 + C_7 \times \sum_{j=1}^{m} \text{DE}_j \times \text{Log}(1 + C_5 \times 5.0^{\text{EROD}})^{C_6} \tag{95}$$

$$\text{FAULTMAX}_0 = C_{12} \times \delta_{curling} \times [\log(1 + C_5 \times 5.0^{\text{EROD}}) \times \text{Log}(\frac{P_{200} \times \text{WetDays}}{P_s})]^{C_6} \tag{96}$$

Where

Fault_m= mean joint faulting at the end of month m

ΔFault_i= incremental change (monthly) in mean transverse joint faulting during month i

FAULTMAX_i= maximum mean transverse joint faulting for month i

FAULTMAX_0= initial maximum mean transverse joint faulting

EORD= base/subbase erodibility factor

DE_i=differential deformation energy accumulated during month

$\delta_{curling}$= maximum mean month slab corner upward deflection PCC due to temperature curling and moisture warping

P_s= overburden on subgrade

P_{200}= percent subgrade material passing #200 sieve

WetDays= average annual number of wet days (greater than 0.1 inch rainfall)

In the Pavement ME model, the difference in corner deflection (difference between the loaded and non-loaded side of the joint) is a critical parameter that affects faulting. The

difference in corner deflection is used to calculate the differential energy (DE), shear stress of slab corner, τ, and maximum dowel bearing stress, σ_b with the following equations:

$$DE = \frac{k}{2}(\delta_{loaded}^2 - \delta_{unloaded}^2) \quad (97)$$

$$\tau = \frac{AGG \times (\delta_{loaded} - \delta_{unloaded})}{H} \quad (98)$$

$$\sigma_b = \frac{D_d \times (\delta_{loaded} - \delta_{unloaded})}{d \times dsp} \quad (99)$$

Where

DE= differential energy

δ_{loaded}= loaded corner deflection

$\delta_{unloaded}$= unloaded corner deflection

AGG= aggregate interlock stiffness factor

k= coefficient of subgrade reaction

D_d= dowel stiffness factor

dsp= dowel spacing

As shown in Equation (94) and (95), DE directly relates to determining maximum mean transverse joint faulting for each month, while τ, σ_b are used to evaluate loss of joint shear capacity and dowel-concrete interface damage, respectively. The loss of joint shear capacity and dowel-concrete interface damage reduce the LTEs provided by the aggregate interlock and the dowel respectively, and as a result, affecting the prediction of the difference in the corner deflection for the next time increment. Accordingly, the critical stress and deflection analysis for JPCP faulting is to determine the difference in corner deflection through the ISLAB 2000 simulations. A lower difference in corner deflection is desirable not only because it produces less

incremental change in mean transverse joint faulting (Equation (94) and (95)), but also induces less loss of joint shear capacity and damage to dowel-concrete interface (Equation (98) and (99)).

Since the maximum faulting development occurs during nighttime when the slab undergoes an upward curling and joints are open (AASHTO 2003), the negative temperature gradient (-2.3°F/inch) was used in the simulation. A screenshot of the ISLAB 2000 interface for the faulting prediction is shown in Figure 98. A standard loading was applied in the corner of the second slab. In order to get the actual corner deflections (δ_{loaded} and $\delta_{unloaded}$), an additional reference case with only temperature gradient built in the slab but no traffic loading (unloaded) was paired for each loaded case. The actual corner deflection was calculated by subtracting the deflection value reported from the loaded case from the deflection value for the unloaded case.

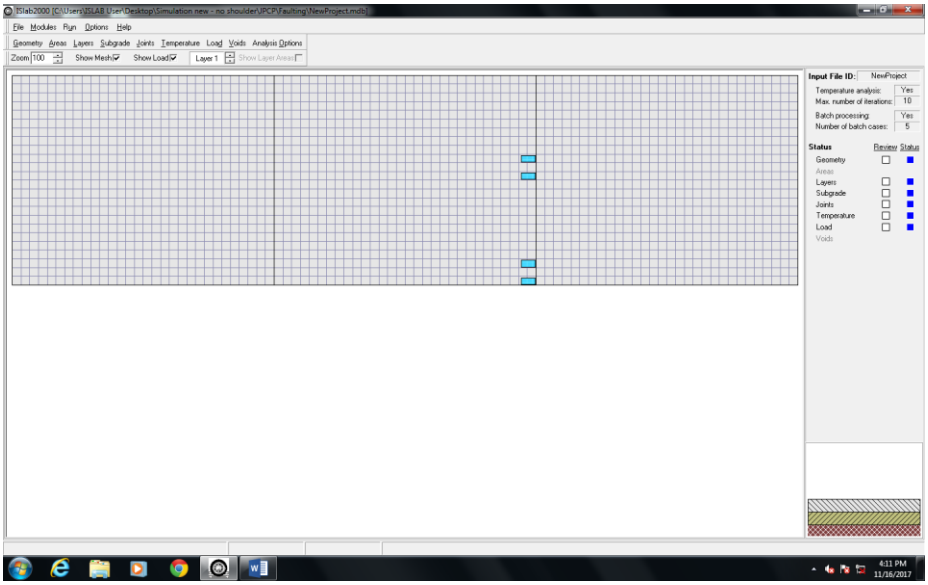

Figure 98 Modeling of stress and deflection for JPCP faulting

The results for the slabs containing the studied mixtures are presented in Figure 99. The sensitivity analysis presented in Appendix E shows decreasing MOE would cause a higher difference of corner deflection, so achieving a higher difference of corner deflection value for all

the RAP-PCC cases is reasonable (Figure 99 (a)). According to Equation (98) and (99), the difference of corner deflection causes loss of joint shear capacity and dowel-concrete interface damage, and ultimately reduces joint LTE. A reduced LTE would cause a higher difference in corner deflection in the next time step. Besides, all the RAP-PCC mixtures would have a considerable increase in differential energy (calculated based on Equation (97)) due to an increase of $\delta_{\text{loaded}}^2 - \delta_{\text{unloaded}}^2$, which would induce higher incremented faulting. The higher CoTE of the RAP-PCC materials could also lead to higher initial faulting (FAULTMAX_0) caused by maximum mean month slab corner upward deflections (δ_{curling}) according to Equation (96), which would worsen the RAP-PCC faulting performance further. All in all, the pavement containing RAP-PCC is anticipated to have a worse faulting performance.

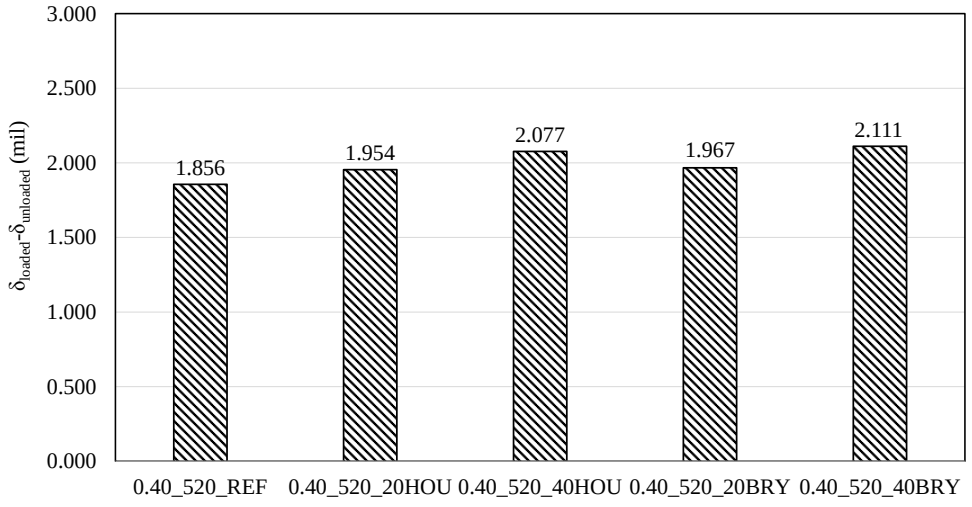

(a) Difference of corner deflection

Figure 99 Critical stress and deflection analysis for JPCP faulting

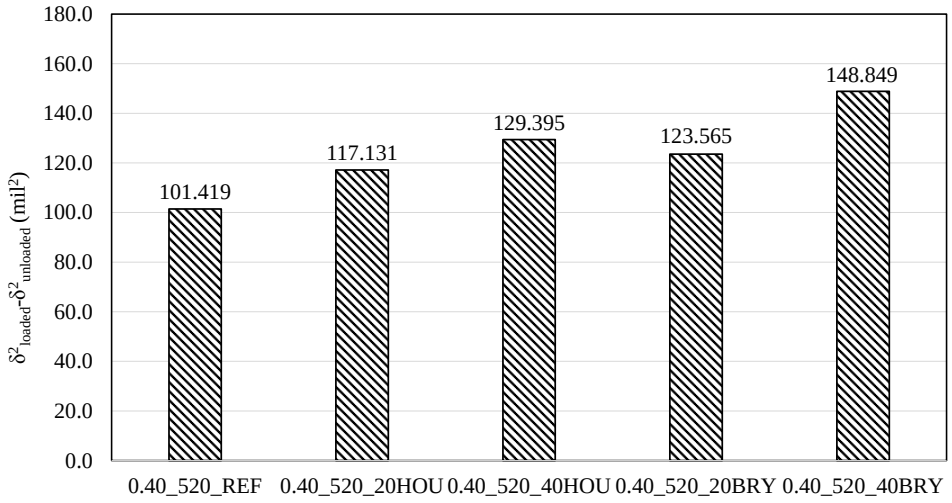

(b) Difference of the square of corner deflection

Figure 99 Continued

V.2.2 Critical Stress and Deflection Analysis for CRCP

The major distress for CPCP pavement is punchout. The punchout development is governed by the maximum tensile stress (bending stress) at the top surface of the concrete slab. The tensile stress is highly influenced by loss of load transfer of transverse cracks and erosion beneath the edge of slab (AASHTO 2003). In this section, the critical stress and deflection analysis for CRCP punchout was performed through the ISLAB 2000 simulations.

The CRCP simulation used the same pavement structure as the JPCP pavement (Figure 92). The finite element simulations were established based on 12-slab assembly (two 12 feet traffic lanes and 6 slabs in each lane). The effects of the shoulder and rebar were ignored. A uniform 48 inch (4 feet) transverse cracking spacing was fixed for all the simulated cases because the previous works showed the bending stresses are typically not significant if the crack spacing is greater than 4 feet (Zollinger et al. 1999). The mesh size was selected as 2 inch. An effective slab temperature gradient with the most negative case (-2.3°F/in) was simulated. Crack

opens when the slab has an upward curling; the crack is supposed to have the highest opening width when the slab undergoes the most negative temperature gradient. The crack with the highest width yields the lowest LTE, which is the most critical condition of the CRCP. The 18-kip single axle load with standard configuration was used for all the simulations.

Punchout

In the Pavement ME, punchout is controlled by the fatigue damage caused by repeated loading of heavy axles. The fatigue of slab first results in micro-cracks at the transverse crack and then drives micro-cracks propagate longitudinally across the slab to the adjacent transverse crack. The CRCP punchout is predicted using the following equation (AASHTO 2003):

$$PO = \frac{A}{1 + \alpha \times FD^{\beta}} \tag{100}$$

Where,

PO= total predicted number of punchouts per mile

FD= accumulated fatigue damage (due to slab bending in the transverse direction)

A, α, β= calibration constants (105.26, 4.0, -0.38, respectively)

The fatigue damage is determined in a similar manner as the JPCP transfer cracking calculation. The form of the expression to determine allowable number of load application is same but the calibration constants are different:

$$\log(N_{i,j,k,l,m,n}) = C_1 \cdot \left(\frac{MR_i}{\sigma_{i,j,k,l,m,n}}\right)^{C_2} + 1 \tag{101}$$

Where,

MR_i= PCC modulus of rupture at age i

$\sigma_{i,j,k,l,m,n}$= applied stress at condition i, j, k, l ,m, n

C_1= calibration constant = 2.0

C_2= calibration constant = 1.22

The critical stress for the punchout is the high tensile stress at the top of the slab when truck axles pass along near the edge of the slab between two closely spaced transverse cracks according to the Pavement ME (Figure 100). It is worth mentioning that this loading position could hardly evaluate the effect of the crack spacing and a load placed in the middle of the slab might be more appropriate for the simulation. However, the edge loading position was still adopted in order to ensure the consistency with the original Pavement ME simulation used in AASHTO (2003). To simulate the loss of support under the slab, voids were modeled beneath the area of the slab where the load was placed. It is assumed that the voids occupied 48 inch long in the longitudinal direction and 48 inch wide in the transverse direction. A fixed LTE (90%) was assigned to all the longitudinal and transverse joints/cracks.

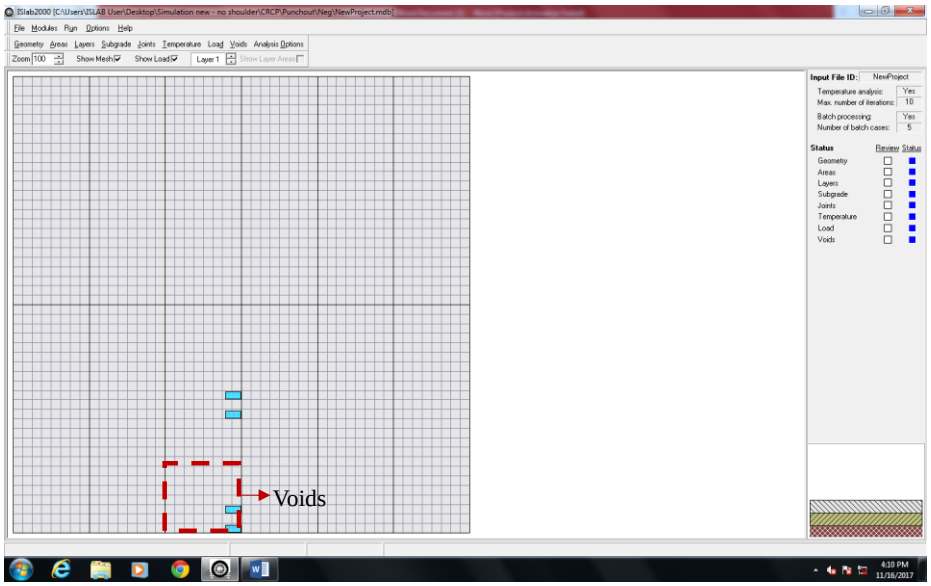

Figure 100 Modeling of stress and deflection for CRCP punchout

A similar sensitivity analysis was performed in order to acquire ideas of the effect of each concrete property on the critical stress and deflection of the CRCP slab. Since the slabs made of

RAP-PCC might have different crack pattern and crack width (CW), which ultimately have different transverse cracking LTE, an additional sensitivity analysis with the varying transverse cracking LTE was carried to evaluate its effect on structure responses. The effect of cracking spacing is not evaluated in the sensitivity analysis because the simulated load position (placed at the edge) is not able to pick up such sensitivity. The sensitivity analysis results are presented in Appendix E. The effect of the altered PCC properties resulted from the addition of RAP on LTE is investigated in a later section.

The critical stress and deflection for the CRCP slabs containing varying RAP contents and different RAP types are presented in Figure 101. The results show that using RAP-PCC to build CRCP concrete slab slightly increased the maximum tensile stress in general. The slab deflection also became larger. The stress to strength ratio for the all studied RAP-PCC mixture was invariably higher than that for the plain PCC, indicating that RAP-PCC slab may be more vulnerable to punchout development. However, it is also noted that the use of RAP in CRCP slab could generate tighter transverse cracks. A smaller crack width could potentially provide higher LTEs (presented later). Since the LTE is the most dominating factor in controlling the tensile stress at the top surface of the slab, the use of RAP in CRCP could potentially yield some benefits.

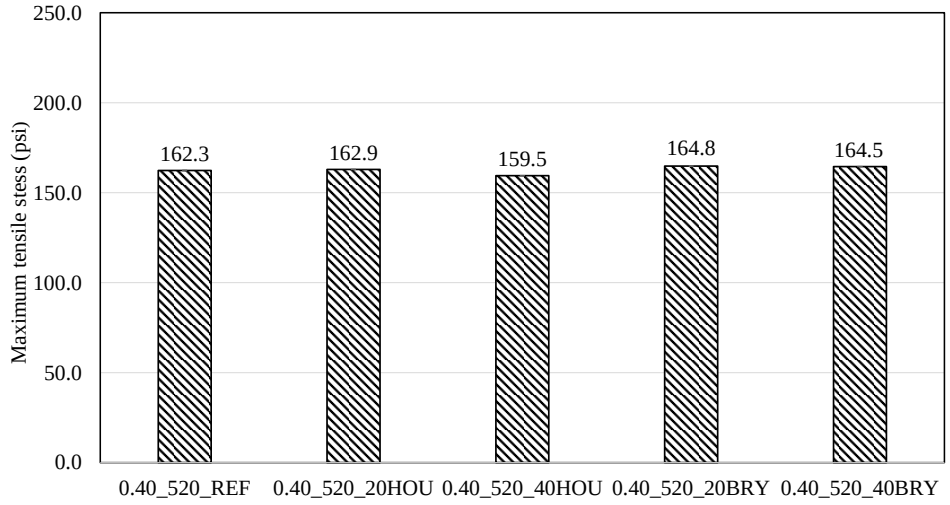

(a) Maximum tensile stress

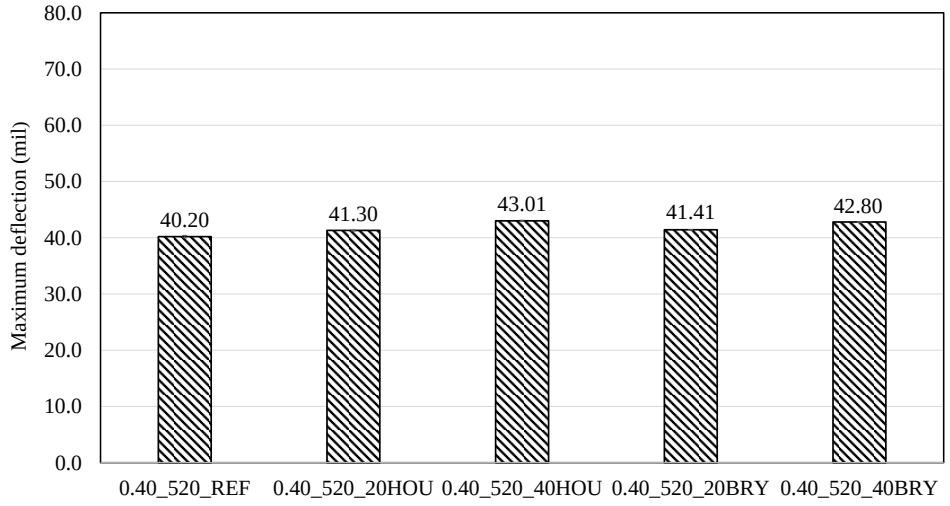

(b) Maximum deflection

Figure 101 Critical stress and deflection analysis for CRCP punchout

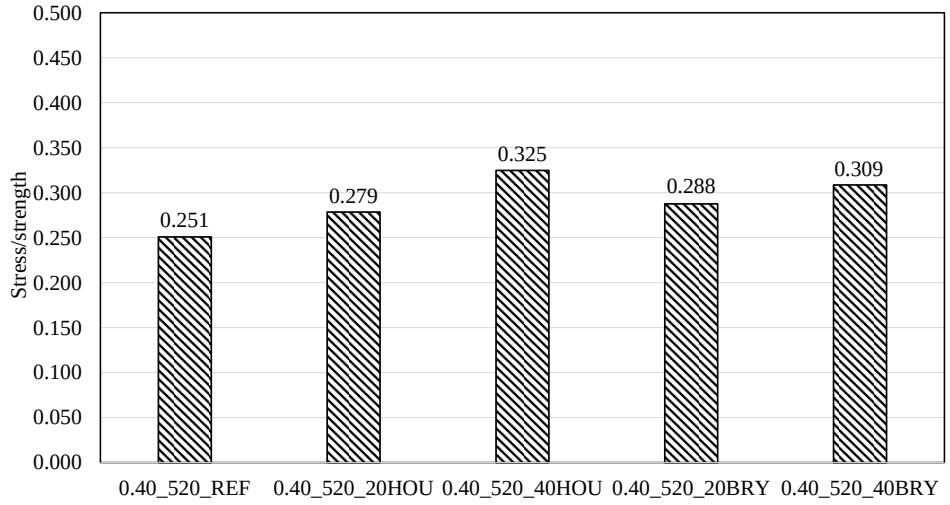

Figure 102 Comparison of stress/strength for the studied mixtures (CRCP)

V.3 EFFECT OF RAP-PCC ON LTE OF CRCP TRANSVERSE CRACK

The load transfer of the CRCP transverse crack can be provided by aggregate interlock, steel reinforcement and base support. The load transfer efficiency is one of the most critical factors in controlling CRCP pavement performance. There are two components contributed to the LTE due to aggregate interlock: one is the transverse crack width and the other is the aggregate interlock wear-out. Maintaining load transfer of 92% or greater will minimize the loss of the aggregate interlock. Prior to wear-out of the aggregate interlock and significant loss of load transfer, the development of punchout distress is limited because the contributions of bending stresses to fatigue damage is negligible.

The ability of a transverse crack to carry load is defined as its shear capacity, which is expressed in Equation (102) (a modified version from (AASHTO 2003)):

$$s_0 = \left(\frac{7.9h^2}{9000}\right)^{0.723} \times e^{-(0.039)\frac{cw}{D}} \quad (102)$$

Where

s_0= dimensionless shear capacity

h = thickness of the slab to sustain shear (inch)

cw = crack width (mils)

D = nominal coarse aggregate size (inch)

According to Equation (102), the shear capacity is a related to crack width, thickness of the slab to sustain shear and nominal coarse aggregate. In the following sections, the effects of RAP-PCC on CRCP transverse crack width and the thickness of the slab to sustain shear are analyzed and discussed.

V.3.1 Crack Spacing and Crack Width

The effect of each RAP altered PCC property on CRCP crack spacing and crack width was investigated using the crack spacing and CW prediction models in the Pavement ME. In this study, the crack spacing and CW of the CRCP slabs containing the aforementioned four different RAP-PCC mixtures and the plain PCC mixture were calculated. The steel design followed Table 49. Although the rebar depth could significantly affect crack spacing and crack width, research on the effect of rebar depth on crack spacing and CW is out of the scope of this study.

In order to determine the transverse crack spacing, the following equations are used:

$$\bar{L} = \frac{[f_t - C\sigma_0\left(1 - \frac{2\zeta}{H}\right)]}{\frac{F}{2} + \frac{U_m P_b}{c_1 d_s}} \quad (103)$$

Where

$\bar{L}$= mean crack spacing

f_t= concrete tensile strength (MOR is used in this study)

f= AASHTO subbase friction coefficient (7.5 is used in this study)

U_m= peak bond stress

P_b= steel content

c_1= first bond stress coefficient

The expressions for the bond related coefficients c_1 and U_m are obtained from Kohler and Roesler (2006b):

$$c_1 = 0.577 - 9.499 \times 10^{-9} \frac{\ln \varepsilon_{tot-\zeta}}{\left(\varepsilon_{tot-\zeta}\right)^2} + 0.00502\bar{L}\ln(\bar{L}) \quad (104)$$

$$U_m = 0.2344 f'_{c28} \quad (105)$$

Where

$\varepsilon_{tot-\zeta}$= total strain at the depth of the steel from shrinkage and temperature drop

$$\varepsilon_{tot-\zeta} = \varepsilon_\infty [1 - rh^3_{PCC}(\zeta)] + \alpha_{PCC}[T_{set} - T(\zeta)] \quad (106)$$

ε_∞= ultimate shrinkage of PCC

$rh_{PCC}(\zeta)$= relative humidity at the depth of the steel

α_{PCC}= PCC coefficient of thermal expansion

T_{set}= temperature at time of concrete set, assume 70 °F, irrespective to mixture type

$T(\zeta)$= temperature at the depth of the steel, assume 32 °F, irrespective to mixture type

H= slab thickness

ζ= depth to steel layer

C= Bradbury's curling/warping stress coefficient:

$$C = 1 - \frac{2\cos\lambda\cosh\lambda(\tan\lambda + \tanh\lambda)}{\sin 2\lambda + \sinh 2\lambda} \quad (107)$$

$$\lambda = \frac{\bar{L}}{l\sqrt{8}} \quad (108)$$

l= radius of relative stiffness

$$l = \sqrt[4]{\frac{E_{PCC}H^3}{12(1-\nu_{PCC})k}} \quad (109)$$

σ_0= Westergaard's nominal stress factor

$$\sigma_0 = \frac{E_{PCC}\Delta\varepsilon_{tot}}{2(1-\nu_{PCC})} \quad (110)$$

ν_{PCC}= PCC Poisson's ratio

$\Delta\varepsilon_{tot}$= unrestrained curling and warping strain

$$\Delta\varepsilon_{tot} = \alpha_{PCC}\Delta t_{eqv} + \varepsilon_\infty(1 - rh^3_{PCC})_{eqv} \quad (111)$$

Δt_{eqv}= equivalent temperature (temperature difference between top surface and bottom surface of the slab)

$(1 - rh^3_{PCC})_{eqv}$= equivalent relative humidity coefficient, difference between top surface and bottom surface of the slab

The only PCC material property which was not tested in this study is the ultimate shrinkage of the concrete. The ultimate shrinkage is not practical to measure in the lab. Field studies have indicated that it could take at least 5 years to reach a stable maximum drying shrinkage value (AASHTO 2003). The ultimate shrinkages for the studied PCC mixtures were estimated through the following equation presented in Bazant and Baweja (1995):

$$\varepsilon_\infty = C_1 \times C_2 \times [26w^{2.1}(f'_{c28})^{-0.28} + 270] \quad (112)$$

Where

C_1= cement type factor: 1.0 for type I cement used in this study

C_2= type of curing factor: 1.0 for 100% relative humidity curing used in this study

w= water content, lb/ft^3

Despite the fact that Equation (112) was originally developed based on the data from conventional concrete mixtures, it is assumed that the ultimate shrinkages for the RAP-PCC

would not differ too much from the estimated values using Equation (112), as the previous research showed that the addition of RAP did not change the free shrinkage of concrete significantly (Brand et al. 2012).

Another concern is that the temperature and moisture profile of the PCC slab might be altered when RAP aggregates are added. The temperature and moisture profile in PCC layer not only depends on material properties (i.e., thermal properties, absorptivity, and diffusivity), but also are significantly influenced by ambient environment conditions. Based on the thermal properties test results for the studied mixtures, the addition of RAP reduced PCC's thermal conductivity and heat capacity, but the influences appeared to be insignificant. The neglectable effect of the changes of the thermal properties of PCC with addition of RAP on pavement temperature distribution was also manifested in the heat transfer analysis presented in Section 5.2. Regarding the diffusivity of the RAP-PCC, no such data is available in the literature, nor has the diffusivity of the RAP-PCC been tested in this study. It is assumed that RAP-PCC and plain PCC have comparable diffusivity since their electrical resistivities were similar (refer to Chapter IV). In accordance with the above assumptions, a same temperature and moisture profile was used for all the cases, irrespective to RAP type and content. The temperature profile was assumed to have a 1°F/inch gradient with the temperature at the depth of steel of 32°F. The temperature at time of concrete set was assumed to be 70°F for all cases. The moisture profile was modeled after reviewing the actual field reported in Kohler and Roesler (2006a). Figure 103 shows the temperature and moisture gradient along the concrete slab depth in this study.

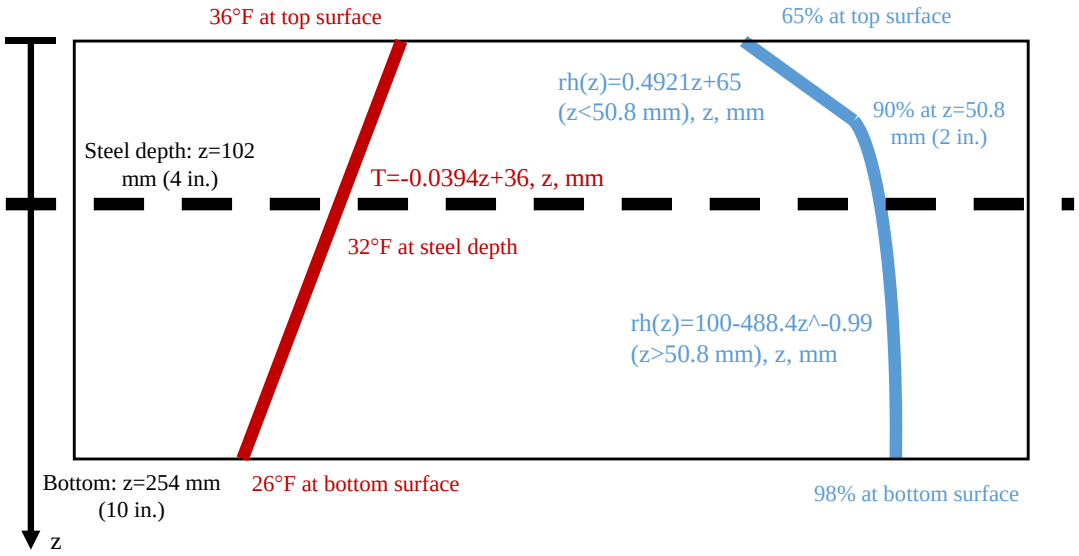

Figure 103 Temperature and moisture gradient for calculating crack spacing and CW

Once the crack spacing for the slabs made with different mixtures was determined, the cracking width at the depth of steel can be computed according to Equation (113) listed in AASHTO (2003).

$$cw = CC\bar{L}(\varepsilon_{tot-\zeta} - \frac{c_2 f_\sigma}{E_{PCC}}) \quad (113)$$

Where

$$f_\sigma = \frac{\bar{L} U_m P_b}{c_1 d_b} + C\sigma_0(1 - \frac{2\zeta}{H}) + \frac{\bar{L}}{2}F \quad (114)$$

$$c_2 = a + \frac{b}{117.2 f'_{c28}} + \frac{c}{\bar{L}^2} \quad (115)$$

$$a = 0.7606 + 1772.5(\varepsilon_{tot-\zeta}) - 2 \times 10^6 (\varepsilon_{tot-\zeta})^2 \quad (116)$$

$$b = 9 \times 10^8 (\varepsilon_{tot-\zeta}) + 149.486 \times 10^3 \quad (117)$$

$$c = 3 \times 10^9 (\varepsilon_{tot-\zeta})^2 - 5 \times 10^6 (\varepsilon_{tot-\zeta}) + 2020.4 \quad (117)$$

The Pavement ME formula only calculates CW at the depth of steel, which can be misleading when comparing cases with steel located in various depths. By assuming that concrete tensile stress caused by the steel restraint is uniform through the slab depth, Kohler and

Roesler (2006b) modified Equation (113) and came up with an equation which can predict CW at any depth in the slab:

$$cw(z) = CC\bar{L}[\varepsilon_{\infty}[1 - rh_{PCC}^{3}(z)] + \alpha_{PCC}[T_{set} - T(z)] - \frac{c_2}{E_{PCC}} \times [\frac{\bar{L}U_m P_b}{c_1 d_b} + C\sigma_0\left(1 - \frac{2z}{H}\right) + \frac{\bar{L}}{2}F]] \quad (118)$$

With all the formulas identified from the previous literature, a sensitivity analysis was performed to evaluate the effect of the RAP altered PCC properties on crack spacing and CW at surface. The studied concrete properties were CoTE, MOE, Poisson' ratio, compressive strength and flexural strength. The same CoTE, MOE and Poisson's varying ranges as in the previous sensitivity analysis were studied (Section V.2). The compressive strength of the PCC varied from 2000 psi to 9000 psi with an increment of 1000 psi while the flexural strength of PCC varied from 200 psi to 900 psi with an increment of 100 psi. All the other properties were fixed constant by assigning the values from the plain PCC's testing results. The sensitivity analysis results are presented in Figure 104. It is concluded that the properties that can significantly affect the crack spacing are CoTE, fc and MOR. Both of the CoTE and fc have a negative effect on crack spacing (i.e., the higher the CoTE/fc value, the smaller the crack spacing), while the crack spacing is correlated positively with the MOR. For the crack width at the top surface of the slab, the higher the CoTE or MOE, the higher the CW. Increasing the concrete strength (either fc or MOR) would cause the CW first to increase and then decrease. The significance of each property is shown in Figure 105. It is suggested that the crack spacing is most sensitive to MOR, followed by fc and CoTE. For the crack width at the top surface, only monotonically decreasing portion of Figure 104(d) and Figure 104(e) are manifested. The change of MOR and MOE can significantly affect the predicted CW. The effects of CoTE and fc are less critical than those for MOR and MOE.

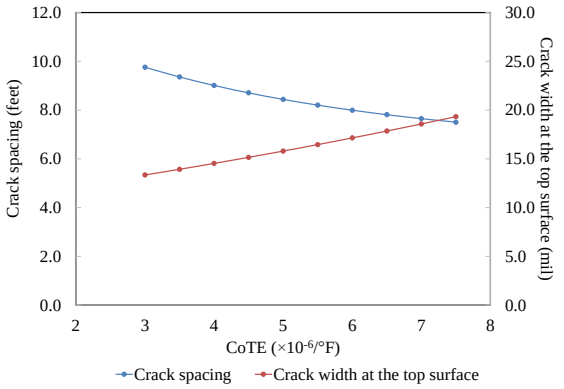

(a) Effect of CoTE

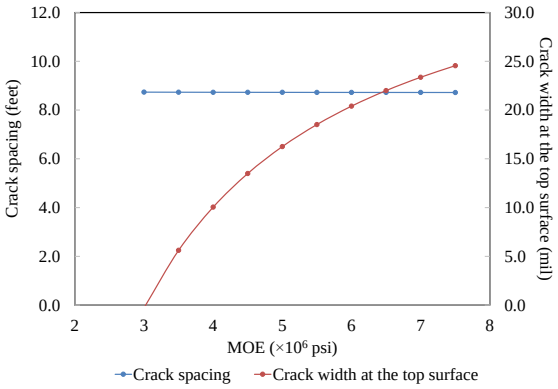

(b) Effect of MOE

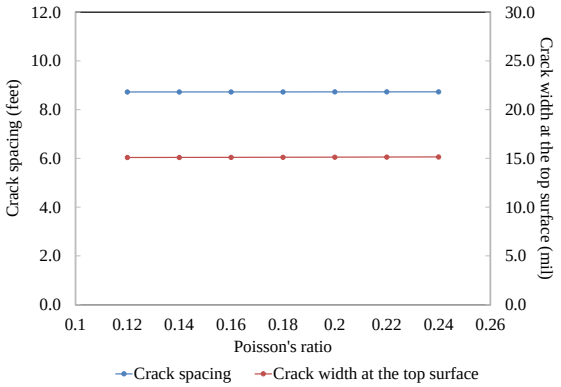

(c) Effect of Poisson's ratio

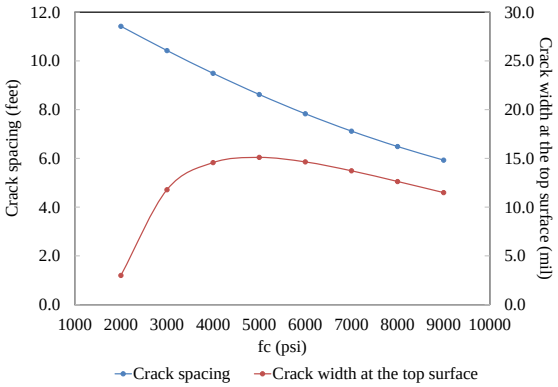

(d) Effect of CS

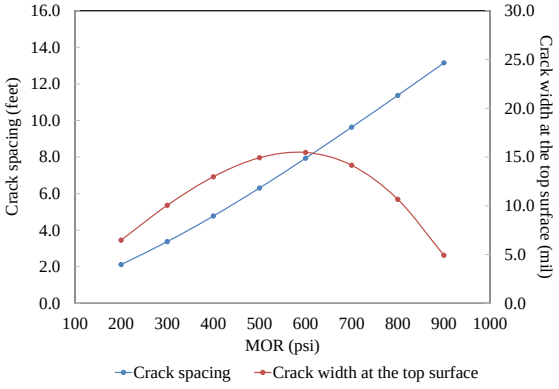

(f) Effect of MOR

Figure 104 Sensitivity analysis results for CRCP crack spacing and CW

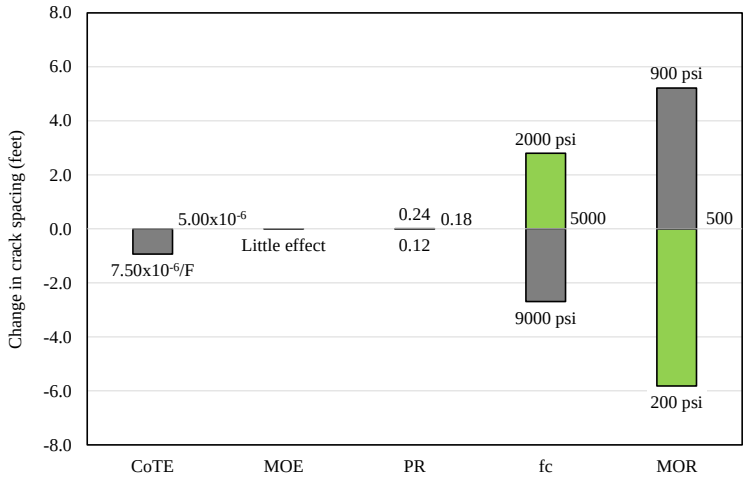

(a) Change in crack spacing

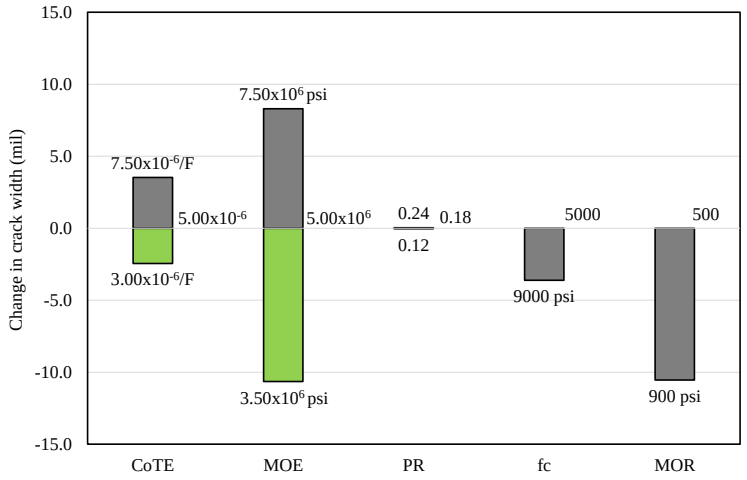

(b) Change in crack width

Figure 105 Comparison of effects of different properties for crack spacing and CW

The calculated values for the mean crack spacing and crack width of the CRCP slabs containing different mixtures are presented in Table 54. Table 54 shows that the addition of RAP reduces crack spacing. The higher the RAP content, the smaller the crack spacing. This is mainly due to the fact that the RAP-PCC has lower tensile strength (MOR). The CW at top surface of

the RAP-PCC slab is smaller than that for the plain PCC slab. Since a lower CW usually produces a higher LTE according to Equation (102) and LTE is considered the one of the most dominating factors for concrete punchout development, the addition of RAP to PCC slab could potentially limit punchout development by providing tighter transverse cracks. It is found that the crack didn't propagate to the steel depth (i.e., 4 inch) for any of the cases. By assuming $cw(z) = 0$ in Equation (118), the deepest point where crack can reach was calculated and summarized in Table 54. The results indicate that the depth of the crack is lower for the RAP-PCC slabs than that for the plain PCC slab.

Table 54 Crack spacing and CW for PCC containing different mixtures

Mix ID	Crack spacing (feet)	Crack width at top surface (mils)	Crack width at steel depth (mils)	Deepest point crack can reach (inch)
0.40_520_REF	8.7	15.1	0	2.3
0.40_520_20HOU	8.3	12.7	0	1.9
0.40_520_40HOU	7.3	9.4	0	1.6
0.40_520_20BRY	8.0	13.1	0	2.0
0.40_520_40BRY	7.6	8.8	0	1.5

V.3.2 Thickness of the Slab to Sustain Shear

Another parameter in Equation (102) which can be affected by RAP addition is the thickness of the slab to sustain shear (h). Chapter IV indicated that the RAP aggregates had poor shear resistance due to the presence of asphalt films, therefore the thickness of the slab to sustain shear should be reduced in the case of the slabs containing RAP-PCC mixtures. It is assumed that the shear capacity of the RAP aggregates is negligible compared to that of the virgin coarse aggregate, so the volume of the RAP aggregates in the slab can be deducted in the h calculation for Equation (102). Based on the mix design information, the adjusted thickness of the slab to

sustain shear (h_{adj}) is computed and summarized in Table 55. The calculated dimensionless shear capacity near the top surface of the slab is also presented in Table 55 based on the predicted crack width at top surface for different cases.

Table 55 Shear capacity of the CRCP transverse crack

Mix ID	Original slab thickness (inch)	Adjusted thickness (inch)	Crack width at top surface (mils)	s_0
0.40_520_REF	10	10	15.1	0.0955
0.40_520_20HOU	10	9.11	12.7	0.0917
0.40_520_40HOU	10	8.28	9.4	0.0907
0.40_520_20BRY	10	9.08	13.1	0.0900
0.40_520_40BRY	10	8.22	8.8	0.0919

From Table 55, while all the slabs made with RAP-PCC have smaller crack width, their shear capacity is lower because of the lower adjusted thickness. A lower shear capacity would lead to a less stiff transverse crack, which ultimately yield lower crack LTE.

V.4 SENSITIVITY ANALYSIS BY PAVEMENT ME

A sensitivity analysis for the studied JPCP and CRCP cases was performed using the Pavement ME software to directly assess the effect of RAP altered PCC property on JPCP and CRCP distresses. The significance of each varying PCC property with the addition of RAP for JPCP is summarized in Table 56. Table 56 shows that coefficient of thermal expansion, thermal properties (i.e., thermal conductivity, heat capacity), MOE and MOR of the RAP-PCC play important roles on JPCP performances. An increase in CoTE and a decrease in MOR resulted from the addition of RAP in PCC would cause a rougher pavement (higher IRI values), higher joint faulting and more transverse cracking. The decreased MOE of RAP-PCC could compensate

for such changes in pavement performance to some extent. The thermal properties of RAP-PCC appear to have effect on slab cracking, but the effect of thermal conductivity and heat capacity could be somewhat cancelled out. Taking all the factors into account, JPCP containing RAP-PCC would have slightly reduced performance relative to the control pavement.

Table 56 Effect of RAP-PCC properties on JPCP pavement performance

Properties	Studied range	Effect of adding RAP on properties in this study (maximum % difference relative to control)	Effect of RAP-PCC on pavement performance parameters with nature of significance					
			IRI		Mean joint faulting		Transverse cracking	
Poisson's ratio	0.121-0.212	Increase (26%)	Increase	IS	Increase	IS	NE	n.a
CoTE ($\times \frac{10^{-6}}{°C}$)	4.820-11.247	Increase (27%)	Increase	S	Increase	VS	Increase	S
Unit weight (kg/m^3)	2323-2403	Decrease (-2%)	Increase	IS	Increase	IS	NE	n.a
Thermal conductivity (W/mK)	1.630-3.803	Decrease (-10%)	Unclear	n.a	Unclear	n.a	Increase	S
Heat capacity (J/kgK)	481-1122	Decrease (-9%)	Increase	IS	Increase	IS	Decrease	S
MOE (GPa)	19.77-46.13	Decrease (-27%)	Decrease	VS	Decrease	VS	Decrease	VS
MOR (MPa)	2.677-6.245	Decrease (-37%)	Increase	VS	Increase	VS	Increase	VS

IS: insignificant
S: significant
VS: very significant
NE: no effect (with the studied varying range)
n.a: not applicable

The results for CRCP are summarized in Table 57**.** Similar to the JPCP case, CoTE, thermal properties, MOE and MOR of the PCC material have significant effects on CRCP performance (i.e., IRI and punchout). While MOE and MOR are significantly related to both IRI

and punchout prediction, it appears that CoTE has a more profound effect on punchout than on IRI. Since transverse crack width is one of the most dominating factors for determining load transfer of CRCP, which ultimately affects CRCP performance, the sensitivity of each property on crack width is also presented in Table 57 (It is not possible to adjust the slab thickness for calculating shear capacity of the crack in the Pavement ME software, so the sensitivity analysis of the dimensionless shear capacity was not performed). Although thermal properties of PCC have some effect on crack width (CW), the increase in CW by a decrease of thermal conductivity probably could be balanced by its reduced heat capacity for RAP-PCC slab. Reducing MOE is extremely effective to control crack width, which helps RAP-PCC pavement maintain a good load transfer efficiency for a longer service period. It turns out that the positive effect by reducing MOE is much more significant than the negative effect due to reduced MOR. Because of the dominating effect by the reduced MOE, CRCP containing RAP-PCC could potentially outperform its control pavement according to the Pavement ME prediction results.

Table 57 Effect of RAP-PCC properties on CRCP pavement performance

Properties	Studied range	Effect of adding RAP on properties (maximum % difference relative to control)	Effect of RAP-PCC on pavement performance parameters with nature of significance					
			IRI		Punchout		CW at the end of design life	
Poisson's ratio	0.121-0.212	Increase (26%)	Increase	IS	Increase	IS	NE	n.a
CoTE ($\times \frac{10^{-6}}{°C}$)	4.820-11.247	Increase (27%)	Increase	S	Increase	VS	Increase	S
Unit weight (kg/m^3)	2323-2403	Decrease (-2%)	Increase	IS	Increase	IS	NE	n.a
Thermal conductivity (W/mK)	1.630-3.803	Decrease (-10%)	Unclear	n.a	Unclear	n.a	Increase	S
Heat capacity (J/kgK)	481-1122	Decrease (-9%)	Increase	IS	Increase	IS	Decrease	S
MOE (GPa)	19.77-46.13	Decrease (-27%)	Decrease	ES	Decrease	ES	Decrease	ES
MOR (MPa)	2.677-6.245	Decrease (-37%)	Increase	VS	Increase	VS	Increase	VS

ES: extremely significant

To verify that CRCP containing RAP aggregates could possibly yield lower CW and maintain higher LTE for a longer time, two CRCP simulations with a longer design year (i.e., 60 year) were conducted through the Pavement ME software. The CRCPs were made with a 9.5 inch slab using the 0.40_520_REF mixture and a 9.5 inch slab using the 0.40_520_40BRY, respectively. All of the other design parameters remained same as the previous Pavement ME studies in Section V.2.2. The analysis results are compared in Figure 106. The results show that the pavement life of the plain CRCP was less than 20 years, while that for the RAP-PCC case could be more than 40 years. A peruse of the crack width development with pavement age (Figure 107) suggests that the CRCP containing RAP aggregates had much tighter cracks compared to the plain CRCP. These tighter cracks were very effective in maintaining a high LTE

for a longer time period for the RAP CRCP (Figure 108), therefore yielding a longer pavement life. However, all of conducted Pavement ME simulations failed to take into account of the lack of shear resistance of RAP aggregates on crack shear capacity. As has been demonstrated in Section V.3.2, the shear capacity of the crack might be lower given the assumption that the RAP aggregates could sustain negligible shear stress.

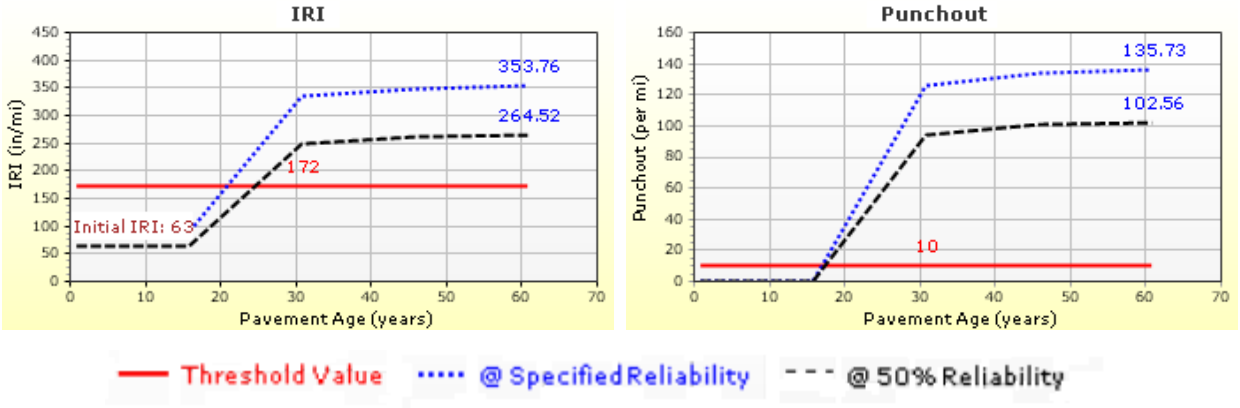

(a) CRCP made with the 0.40_520_REF mixture

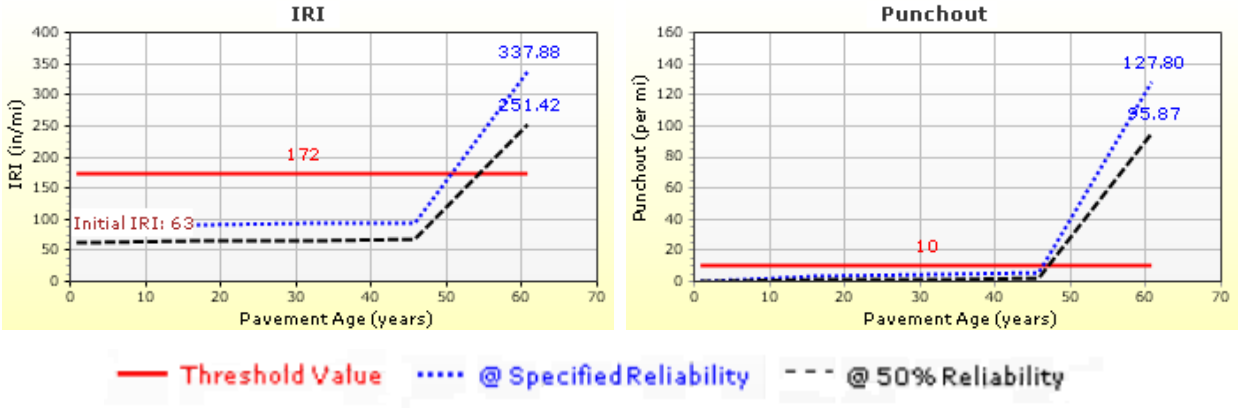

(b) CRCP made with the 0.40_520_40BRY mixture

Figure 106 Comparison between CRCP made with the 0.40_520_REF mixture and CRCP made with the 0.40_520_40BRY mixture

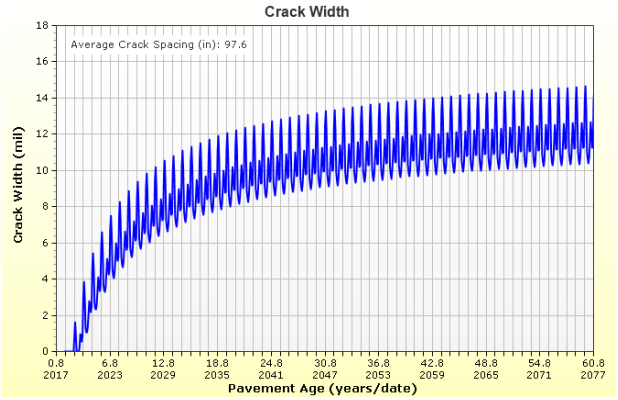

(a) CRCP made with the 0.40_520_REF

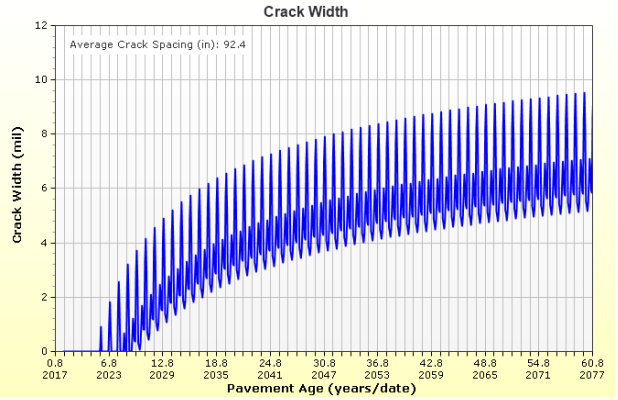

(b)CRCP made with the 0.40_520_40BRY

Figure 107 Crack width with pavement age

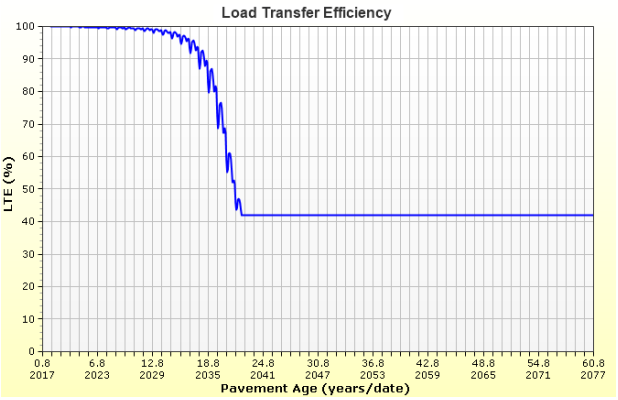

(a) CRCP made with the 0.40_520_REF

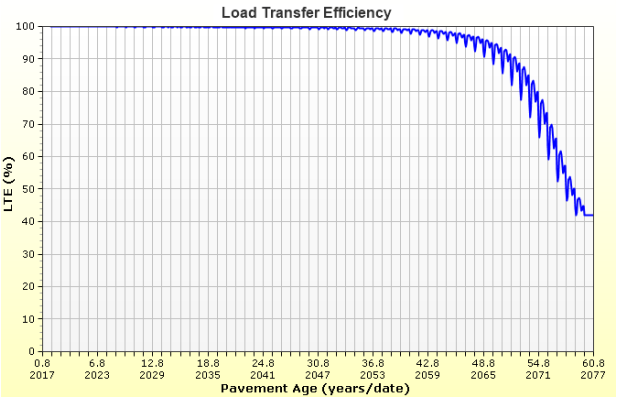

(b) CRCP made with the 0.40_520_40BRY

Figure 108 LTE with pavement age

Based on the extensive studies in this chapter, use of RAP-PCC to construct conventional JPCP may lead to some deviation from achieving favorable transverse cracking and faulting performance. RAP-PCC's lower modulus may balance the negative effects caused by its higher CoTE, but a reduction in tensile strength causes a higher stress/strength ratio and leads to increasing chances of occurring fatigue cracking. The RAP-PCC pavement is anticipated to have a worse faulting performance relative to the plain PCC pavement due to a higher differential

energy component ($\delta^2_{\text{loaded}} - \delta^2_{\text{unloaded}}$)and a higher difference of corner deflection ($\delta_{\text{loaded}} - \delta_{\text{unloaded}}$). The higher differential energy would cause a higher accumulative faulting value, while the higher difference of corner deflection between the unloaded and loaded slab would cause higher loss of joint shear capacity and higher damage to dowel-concrete interface, which consequently would lead to higher differential energy in the following time increment. With regard to the CRCP performance, the major drawback for the RAP CRCP is the reduced tensile strength. However, the RAP-PCC slab is anticipated to have tighter transverse crack. A decrease in crack width could potentially provide a higher LTE. The decrease in crack width is very significant for CRCP made with slab containing higher RAP content. This is largely due to the fact that the positive effect caused by the MOE reduction is much more significant than the negative effect caused by the MOR reduction for RAP-PCC. Although the Pavement ME simulations indicated that the RAP CRCP, which has tighter cracks, is able to maintain a higher LTE for a much longer time and ultimately leads to a longer pavement service life compared to the plain CRCP, the simulations failed to evaluate of RAP on the shear capacity of the cracks. The poor shear resistance of RAP aggregates caused by the presence of asphalt films could damage the shear capacity of the crack, which casts doubts on whether using RAP-PCC in CRCP could indeed yield higher crack LTE.

V.5 FIELD INVESTIGATION OF PAVEMENTS CONTAINING RCA-PCC

In order to assess the simulative analysis performed in the previous sections of this chapter, field data from evaluating single-lift pavement built with PCC containing RCA (RCA-PCC) from two pavement sections in Oklahoma was used due to the lack of RAP-PCC field sections. Pavement built with RCA-PCC slab is analogical to pavement built with RAP-PCC,

because RCA-PCC has been reported to have similar effect on PCC properties such as reducing MOE (Gress et al. 2009), increasing CoTE (Gress et al. 2009), and improving ductility and fracture properties (Brand et al. 2014). The information about these two pavements is summarized in Table 58.

Table 58 Information about the two existing pavements built with RCA-PCC in Oklahoma

Location	Pavement type	Length	Construction date	RCA-PCC Slab information	Base information
I-40, Oklahoma County, OK	JPCP	7.75 mile	1983	10” slab Both control and 100% coarse RCA	6" soil asphalt base
I,35, Logan County, OK	CRCP	5.77 mile	1989	10” slab Both control and 100% coarse RCA	Existing 8" subbase

The two existing pavements are JPCP and CRCP, respectively; they both have RCA and control sections (i.e., normal PCC slab). The pavements were both reconstructed in the 1980s, and are still in service, which offered a unique opportunity to assess long-term performance of the PCCP made of RCA aggregates by comparing with the control PCCP. The pavement assessment was carried through the mechanical property testing and the pavement structure evaluation via FWD testing.

V.5.1 Mechanical Property Test Results

Field core samples were obtained and underwent different mechanical property tests including CS, MOE and STS. The tested mechanical properties of the core samples are summarized in Figure 109. The MOE and STS of RCA section were invariably lower than its control section for both JPCP and CRCP pavements, and their percent reduction relative to control properties was close between the JPCP and CRCP pavements. The test results was inconsistent in terms of CS though. The JPCP pavement indicated that the RCA section had

higher averaged CS compared to the control section, while an opposite conclusion was made for the CRCP. A possible increase in the compressive strength of PCC with addition of RCA has been reported by several investigations (Gress et al. 2009). It is noted that due to the limited amount of testing data, statistical significances could not be established.

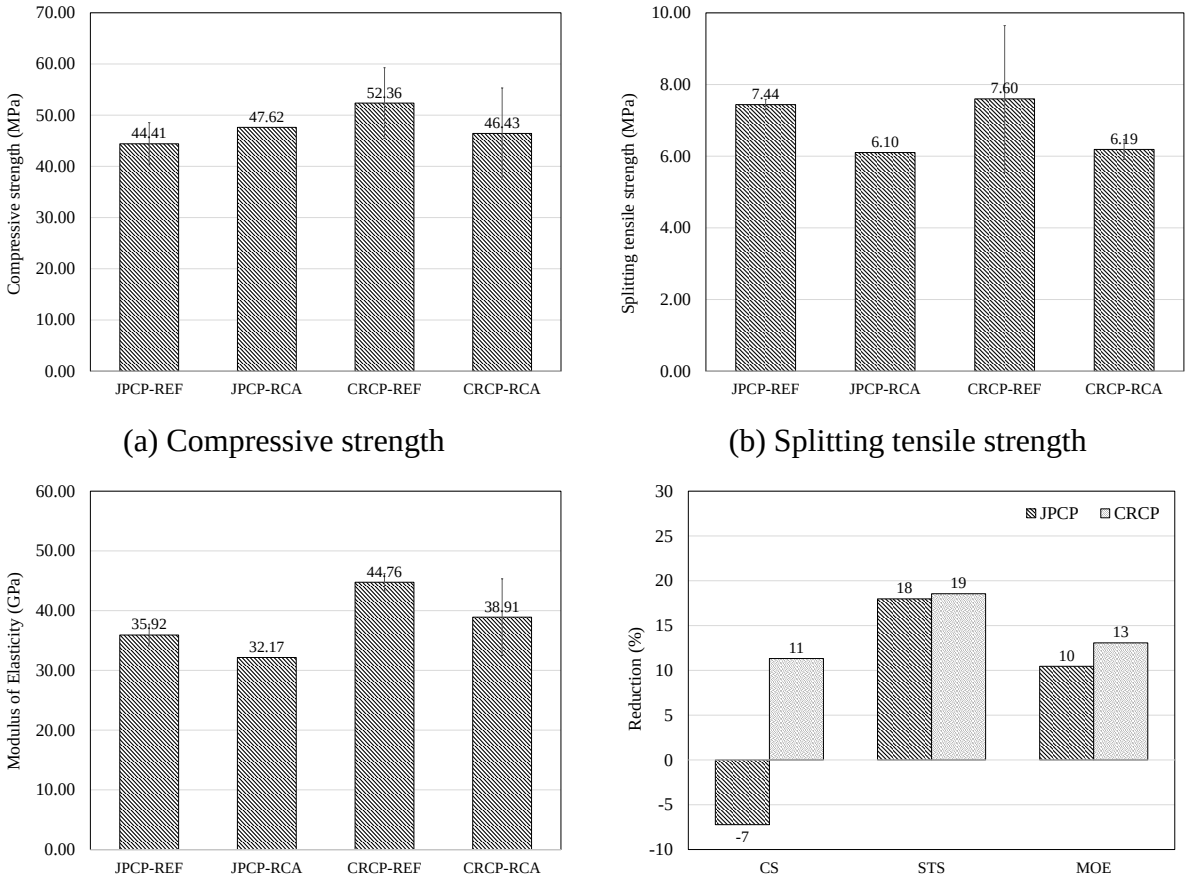

(a) Compressive strength

(b) Splitting tensile strength

(c) Modulus of elasticity

(d) Reduction of RCA-PCC in comparison with control

Figure 109 Mechanical property test results of the field cores

V.5.2 FWD Test Results

The FWD data for testing these two pavements covering both of the RCA and control sections were collected and analyzed. The sensor locations were 0, 12, 24, 36, 48 and 60 inches

away from the loading plate; an additional rear sensor which was located as a distance of 12 inch back of the loading plate was used in order to get additional data point when the FWD is leaving the joint/crack.

Different pavement structural parameters including the pavement load transfer efficiency (LTE), equivalent thickness (h_{e-p}), coefficient of friction (μ) and differential energy (DE) were computed based on the following equations.

Load Transfer Efficiency

Load transfer efficiency is a term used to quantify the transfer load across discontinuities (e.g., joint for JPCP, transverse crack for CRCP). If the joint/crack is performing perfectly, the LTE equals to 1. On the contrary, a 0 LTE means there is no integrity between the two pavement segments. The LTE is defined as:

$$\mathrm{LTE}(\%) = \frac{w_{\mathrm{unload}}}{w_{\mathrm{loaded}}} \tag{119}$$

Where w_{unload}=unloaded deflection

w_{loaded}= loaded deflection

In the FWD data analysis, if the FWD is approaching a joint/crack, the LTE is calculated as:

$$\mathrm{LTE_A}(\%) = \frac{w_1}{w_0} \tag{120}$$

Where w_0= sensor deflection 0 inch away from the loading point

w_1= sensor deflection 12 inch away from the load point

And if the FWD is leaving a joint/crack, the LTE is calculated as:

$$\mathrm{LTE_L}(\%) = \frac{w_7}{w_0} \tag{121}$$

Where w_7= sensor deflection -12 inch away from the load point (rear sensor)

The LTE of a particular joint/crack can be determined by averaging $\mathrm{LTE_A}$ and $\mathrm{LTE_L}$:

$$\mathrm{LTE}(\%) = \frac{\mathrm{LTE_A} + \mathrm{LTE_L}}{2} \tag{122}$$

Equivalent Thickness

The concept of equivalent or effective PCC thickness is applied to evaluate the structure integrity of the PCC and base as a whole, which is shown in Figure 110.

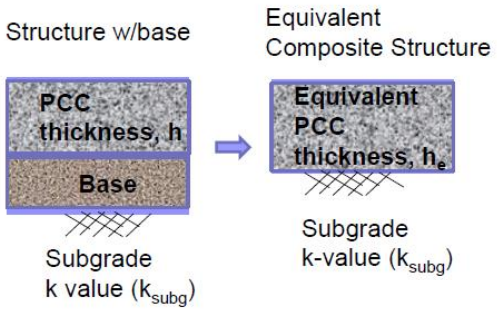

Figure 110 Equivalent PCC thickness

To determine the equivalent PCC thickness, the pavement basin area (BA) is computed based on measured FWD deflections:

$$\mathrm{BA} = \frac{\mathrm{SS}}{2 \times \mathrm{w_0}}[\mathrm{w_0} + 2(\mathrm{w_1} + \mathrm{w_2} + \mathrm{w_3} + \mathrm{w_4}) + \mathrm{w_5}] \tag{123}$$

Where

SS=FWD sensor spacing (12 inch)

w_i= sensor deflection (i=0 to 5)

The effective relative stiffness (RSS) is then computed using the following regression model.

$$\mathrm{l_{e-p}} = \mathrm{a} + \mathrm{b} \times (\mathrm{BA}) + \mathrm{c} \times (\mathrm{BA})^2 \tag{124}$$

Where a, b, c are coefficients obtained from the field correlation. a=0.992, b=-0.2891, c=0.0284

The RRS along with the center plate deflection is useful to determine the foundation modulus of the subgrade reaction. Since the deflection data is associated with a rather high frequency loading cycle, the resulting calculation is assumed to result in a dynamic foundation modulus (k_{dyn}) as:

$$k_{dyn} = \frac{w_0^* P}{w_0 {l_{e-p}}^2} \tag{125}$$

Where

P= wheel load

w_0= center plate deflection

$$w_0^* = \frac{1}{8}\left[1 + \left(\frac{1}{2\pi}\right)\left(\ln\left(\frac{a}{2l_{e-p}}\right) + \gamma - 1.25\right)\left(\frac{a}{l_{e-p}}\right)^2\right] \tag{126}$$

a=5.9055 inch

γ= 0.5772156649

The equivalent thickness is then obtained using the following equation:

$$h_{e-p} = \sqrt[3]{\frac{12k_{dyn}(1-\nu^2){l_{e-p}}^4}{E_c}} \tag{127}$$

Where

ν= Poisson's ratio (0.15)

E_c= concrete modulus of elasticity

Coefficient of Friction (μ)

The coefficient of friction is determined as:

$$\mu = \frac{\sigma_{e-u} - \sigma_e\left[\frac{2h_{e-u}}{h_{e-p}} - 1\right]}{\frac{h_c}{12} + \sigma_v} \tag{128}$$

Where

h_{e-u} is the unbonded equivalent thickness

$$h_{e-u} = [\left(h_c^3 + \frac{E_{base}}{E_c} h_{base}^3\right)]^{1/3} \quad (129)$$

σ_{e-u} is the unbonded effective stress:

$$\sigma_{e-u} = \frac{S_{e-u} P}{h_{e-u}^2} \quad (130)$$

And S_{e-u} is the unbonded dimensionless stress

$$S_{e-u} = a + bl_u + cl_u{}^2 \quad (131)$$

$$(a = 0.0006, b = 0.0403 \text{ and } c = -0.0002)$$

$$l_u = \sqrt[4]{\frac{E_c h_u^3}{12 k_{DCP}(1-\nu^2)}} \quad (132)$$

k_{DCP}=DCP modulus of the subgrade reaction (assumed to be 120 pci for this study)

h_u= Unbonded PCC slab thickness

σ_v= load induced vertical pressure (0.7 psi)

$$\sigma_e = \frac{S_{e-p} P}{h_{e-p}^2} \quad (133)$$

$$S_{e-p} = a + bl_{e-p} + cl_{e-p}{}^2 \quad (134)$$

$$(a = 0.0006, b = 0.0403 \text{ and } c = -0.0002)$$

When the calculated μ is a negative value, $\mu = 0$ is adopted.

Differential Energy (DE)

The differential energy is computed as

$$DE = \frac{k_{dyn}}{2}(w_{loaded}^2 - w_{unloaded}^2) \quad (135)$$

Same as the LTE calculation, if the FWD is approaching a joint/crack, $w_{unload} = w_1$ and $w_{loaded} = w_0$. If FWD is leaving a joint/crack, $w_{unload} = w_7$ and $w_{loaded} = w_0$

The FWD analysis results are shown in Figure 111 and Figure 112 for the JPCP and CRCP, respectively. Figure 111 compares the averaged values for equivalent thickness,

coefficient of friction, LTE and differential energy for the JPCP testing sections. The REF-1-T is an additional FWD test which was performed in the afternoon on the same slab of the REF-1. The pavement tested in the afternoon had a higher temperature, so the effect of pavement temperature could be evaluated by comparing the results of the REF-1 with those of the REF-1-T. As expected, the RCA section shows a slightly worse overall field performance compared to the control sections. The worse overall performance of the control section was manifested by lower equivalent thicknesses for interior and edge loadings, lower coefficient of frictions for interior loading and higher differential energies for edge and corner loadings. For the corner loading, the RCA section turned out to have higher equivalent thickness and higher coefficient of friction compared to all the control sections though. As expected the corner area always had lowest structural integrity (i.e., lower equivalent thicknesses, lower coefficient of friction and higher differential energy), followed by pavement edge and interior region, respectively. This finding confirmed the presence of separation between the slab and the base at the corner. From Figure 111(d), the difference between the differential energy of the edge loading and that of the corner loading appeared to be negligible for the RCA section, while the REF-1 and REF-1-T both manifested a much lower differential energy for the edge loading than that for the corner loading. For the REF-2, although the differential energy for the edge loading was similar with that for the corner loading, it exhibited a high coefficient of variance. The findings from Figure 111(d) suggest that the structural integrity at the edge of the slab for the REF-1 was still good, while the REF-2 has started to loss such structural integrity. Regarding RCA section, it is believed that the structural integrity has already lost from the results.

To eliminate the bias from the simple comparison among the averaged values, an evaluation of data through statistical approaches was performed. Two-sample t-test results (by

assuming unequal variance) are shown in Table 59. From Table 59, the P-values lower than 0.05 for equivalent thickness (h_{e-p}) comparison are REF-2 & RCA for the interior loading and REF-1 & RCA for the corner loading, which indicates that the equivalent thickness of REF-2 is significantly higher than that of RCA at interior of the slab and the equivalent thickness of RCA is significantly higher than that of REF-1 at corner. For the coefficient of friction, the significantly different comparison is REF-1 & RCA and REF-2 & RCA at interior, which means the coefficients of friction for both REF-1 and REF-2 are significantly higher than that of RCA at slab interior location. With regard to the LTE, the only significant comparison is the REF-1 & REF-1-T at edge loading, which indicates the REF-1-T has a statistically higher LTE than the REF-1. Also, the differential energy comparisons show that the results for the REF-1 is statistically lower than the RCA, and the REF-1-T is statistically lower than the REF-1. The statistical analysis confirmed the previous conclusion that the RCA section had an overall worse performance compared to the control sections. Also, the change in temperature did result in a considerable difference in stiffness of the pavement. The higher the pavement temperature, the stiffer the pavement.

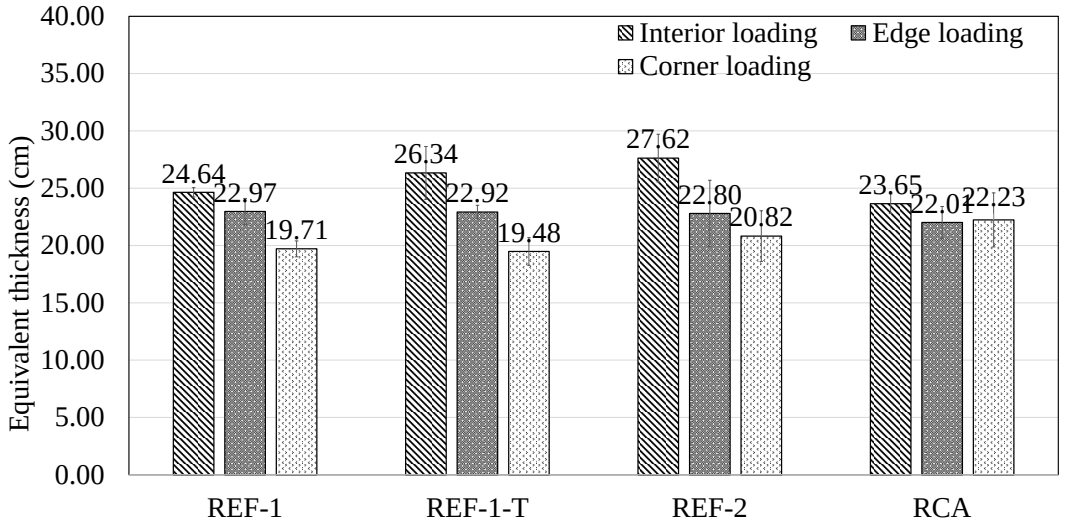

(a) Equivalent thickness

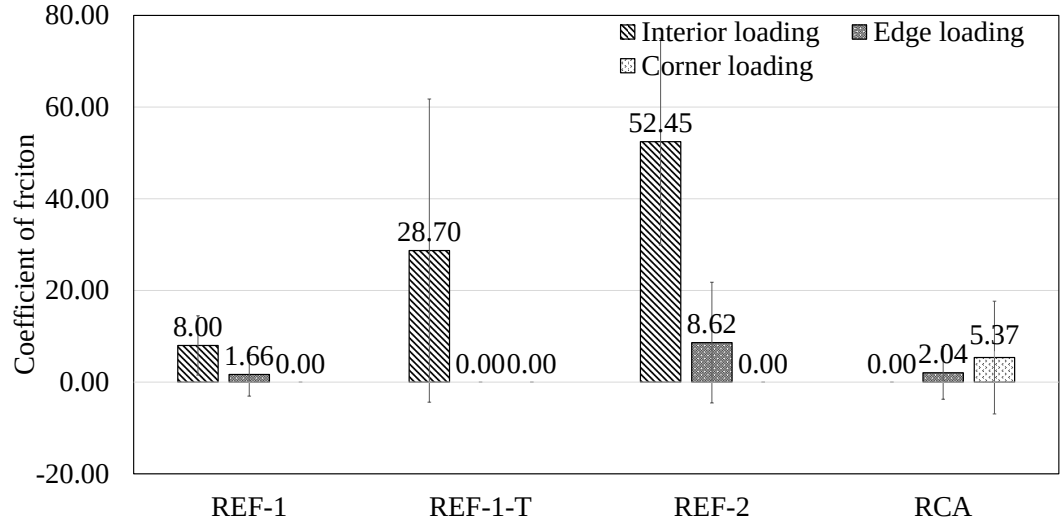

(b) Coefficient of friction

Figure 111 FWD results for JPCP sections

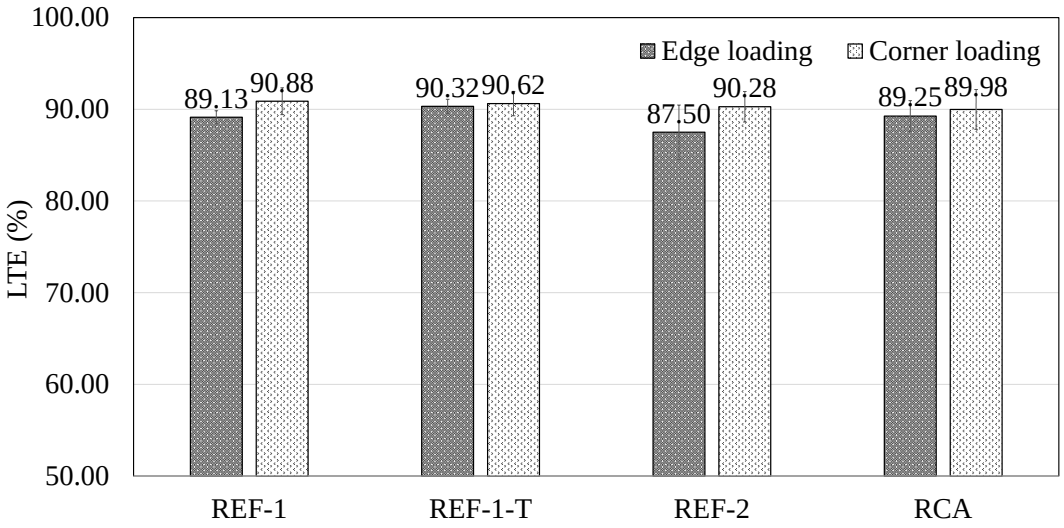

(c) LTE

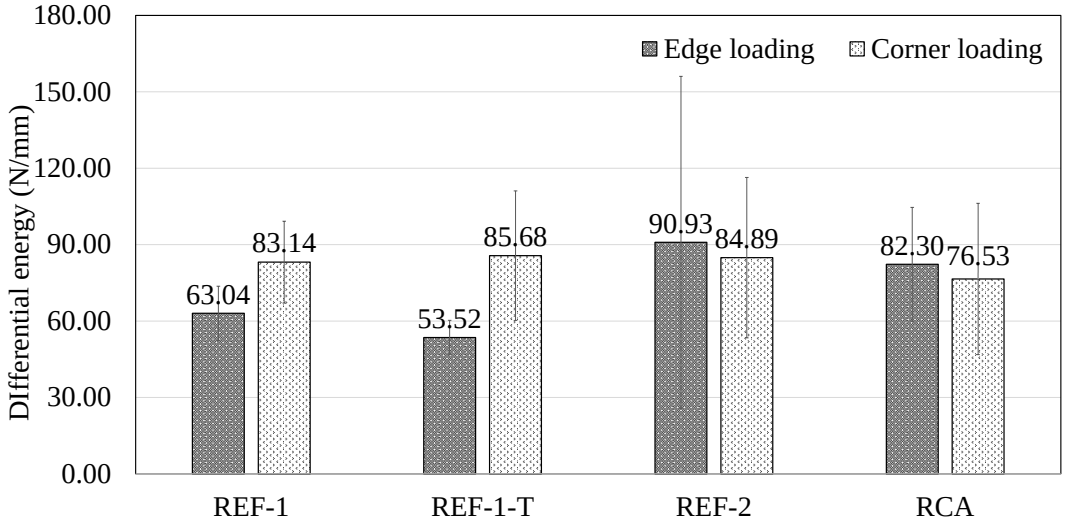

(d) Differential energy

Figure 111 Continued

Table 59 Two-sample t-test results (by assuming unequal variance) for JPCP with a significance level of 0.05

Parameter	FWD loading position	REF-1 & RCA	REF-2 & RCA	REF-1 & REF-1-T
P-value for h_e	Interior	0.08158	0.02771	0.12164
	Corner	0.00964	0.10773	0.31918
P-value for μ	Interior	0.04490	0.02823	0.14307
	Corner	0.12843	0.12843	-
P-value for LTE	Edge	0.42793	0.06804	0.00302
	Corner	0.16845	0.37883	0.35004
P-value for DE	Edge	0.02619	0.35128	0.02699
	Corner	0.29186	0.28585	0.40511

Note: the null hypothesis is the property between two segments is equal. A less than 0.05 P-value means that there is 95% confidence to reject the null hypothesis, which suggests that the property of the two segments is significantly different.

The averaged values for equivalent thickness, coefficient of friction, LTE and differential energy for the CRCP testing sections are shown in Figure 112. The results for the equivalent thickness and coefficient of friction indicate that the second RCA segment (RCA-2) outperformed the control section (REF) while the first RCA segment (RCA-1) had slightly lower structural integrity than the control one. For the LTE and differential energy, it appeared that

both the RCA sections had lower LTE and higher differential energy than the control section. The two-sample t-test results are shown in Table 60. For the equivalent thickness comparison, the difference between REF and RCA-1 is significant for the edge loading (i.e., the equivalent thickness of REF is significantly higher than that of RCA-1). The P-value for RCA-1&RCA-2 is also below 0.05, suggesting RCA-2 had significantly higher equivalent thickness than that of RCA-1 at edge. Based on the P-values for μ, REF and RCA-2 both had significantly higher coefficient of friction than the RCA-1 section at pavement edge while the coefficient of friction of RCA-2 section was significantly lower than that of either REF or RCA-1 at pavement corner. The DE and LTE results generally indicate that the crack of REF is significantly stiffer than that of the RCA sections.

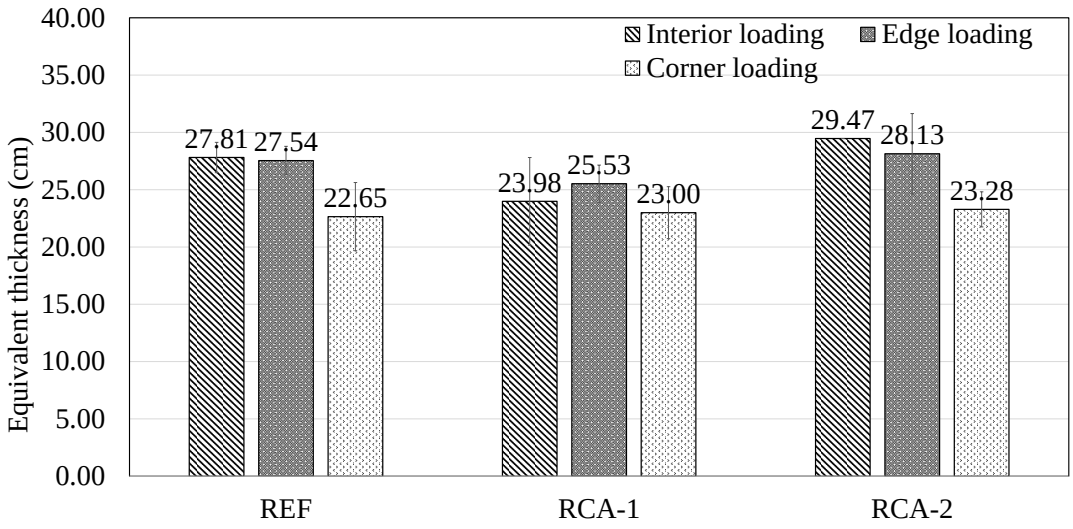

(a) Equivalent thickness

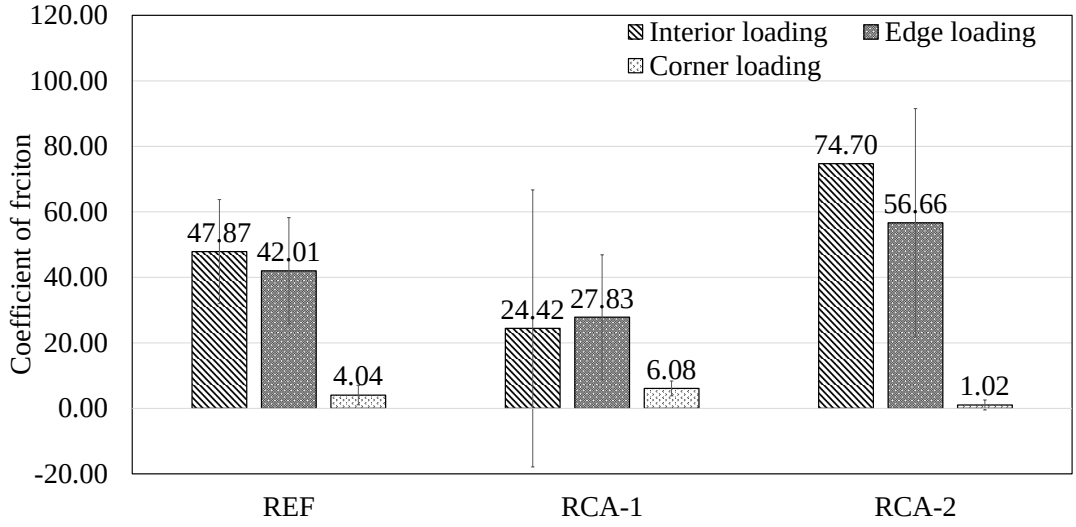

(b) Coefficient of friction

Figure 112 FWD results for CRCP sections

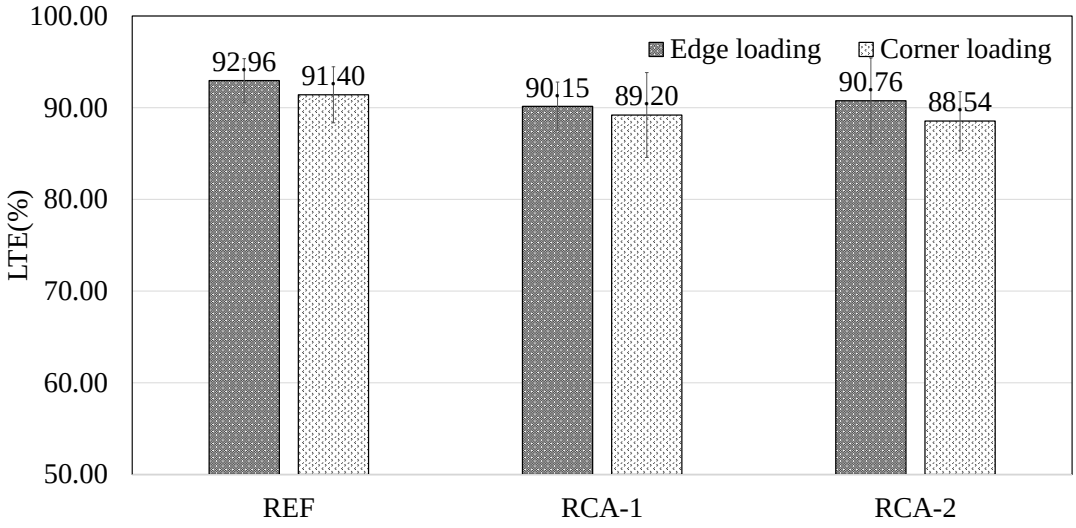

(c) LTE

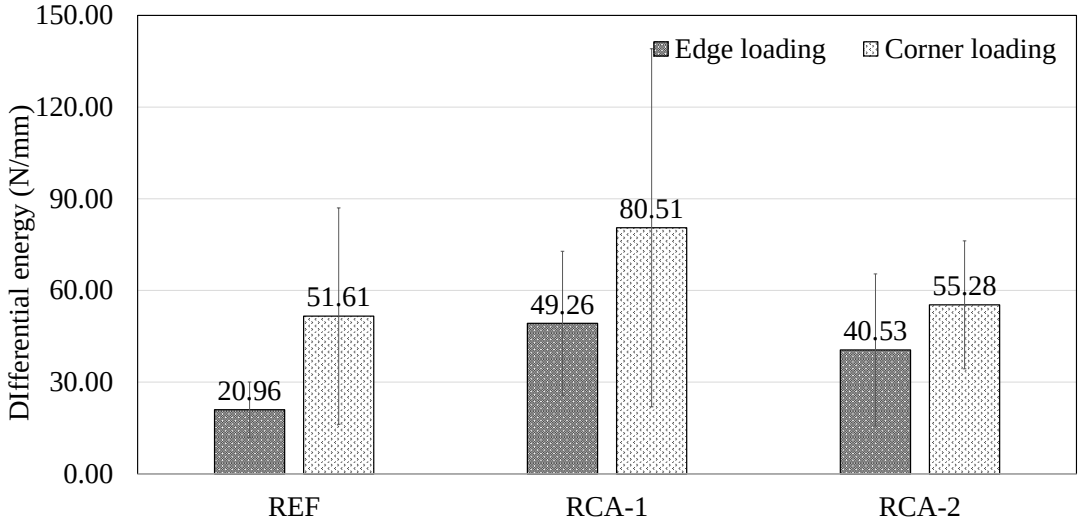

(d) Differential energy

Figure 112 Continued

Table 60 Two-sample t-test results (by assuming unequal variance) for CRCP with a significance level of 0.05

Parameter	FWD loading position	REF & RCA-1	REF & RCA-2	RCA-1 & RCA-2
P value for h_e	Edge	<0.00001	0.49632	0.02621
	Corner	0.24382	0.13832	0.30545
P value for μ	Edge	<0.00001	0.17123	0.01719
	Corner	0.17606	0.02752	0.01045
P value for LTE	Edge	<0.00001	0.07723	0.34061
	Corner	0.003419	0.00588	0.28840
P value for DE	Edge	<0.00001	0.01370	0.14850
	Corner	0.00234	0.31227	0.01136

Note: the analysis for the interior loading was not performed because the data points were not sufficient

The field test results presented in this section generally match the findings from the simulative works conducted in the previous sections: the performance of JPCP containing RCA-

PCC (analogical to RAP-PCC) is worse than that of the control, while the CRCP containing RCA-PCC can potentially yield better performance than the control.

V.6 OTHER CONSIDERATIONS FOR RAP-PCC PAVEMENT PERFORMANCE

Satisfying the requirements of allowable surface characteristics (e.g., skid, abrasion, and noise reduction properties) of the PCC slab is another important area to ensure safe and durable PCCP field performances. Based on the limited abrasion resistance test presented in Chapter IV, the RAP-PCC showed slightly reduced abrasion resistance characteristic in comparison with the control, but the effect of this reduced abrasion resistance on pavement performance has not been well understood. The effect of RAP on PCC's skid resistance and noise generation is not well studied and needs further research as well. It has been shown that the introduction of polymer admixtures can help improve concrete damping (Amick and Monteiro 2005). As addition of RAP introduces asphalt (similar to polymer) in RAP-PCC system, exploring the possibility of achieving favorable damping properties of RAP-PCC can be a promising area of future investigation. Additionally, the presence of asphalt makes PCC more viscoelastic. Slabs containing RAP-PCC will have a higher creep relative to the conventional PCC slabs. The high creep of RAP-PCC slab could potentially bring some additional benefits such as reduce the long-term permanent curl/warp gradient.

RAP-PCC showed equivalent or even better fracture properties with higher ductility relative to the conventional PCC based on the findings from Chapter IV and some other previous researches (Brand et al. 2014). Fracture mechanics based explanation is considered more appropriate to understand RAP-PCC pavement performance (Shi et al. 2017). The development

of a fracture based criterion in designing PCCP has been identified as an important area of future research.

V.7 USE OF RAP-PCC TO CONSTRUCT TWO-LIFT PAVEMENT

As shown in the previous sections, SLFD pavement built with RAP-PCC may cause some problems. It is still a premature concept and needs further research and implementation through field test section construction before allowing for field applications. On the other hand, two-lift paving using RAP-PCC as bottom lift opens up opportunities for implementation followed by suitable applications. A two-lift concrete pavement contains a thinner top lift which uses high-quality concrete and aggregate to ensure durability, skid resistance improvement and noise reduction and a thicker bottom lift made of lower quality concrete and aggregate (such as RAP-PCC material). Applying RAP-PCC in the bottom lift can help mitigate the issues related to strength reduction and increase of CoTE with no need to satisfy the requirements of skid resistance or noise reduction. The existing two-lift PCC pavement field sections have been reported in the United States (Hu et al. 2014), and those field cases using RAP-PCC are summarized in Chapter II.

Although the two-lift pavement has been routinely applied in some of the Europeans countries, it has not been widely adopted in the United States. It is important to address the following challenges and difficulties in order to successfully implement the two-lift paving construction practice:

- A robust approach with clearly specified procedures to design two-lift PCC pavement is not available. Tompkins et al. (Tompkins et al. 2009) suggested to incorporate their modifications for PCC-PCC (a bonded PCC overlay over existing PCC pavement) modeling into the publicly available version of the Pavement ME for designing two-lift

pavements. However, further work related to model validation and calibration is needed in order to validate this approach.

- The material properties for both top and bottom lifts shall be specified: While Illinois has developed some requirements (Hu et al. 2014), detailed specifications for mix design and material properties have yet to be developed nationwide.
- The nature of bonding between top and bottom lift and its effect on pavement performance needs further evaluation: the two-lift concrete paving requires placing a top lift on a bottom lift which is still wet. This wet-on-wet contact could facilitate good bonding between the two layers. More work is needed both in the lab and field to determine the optimum time lag between the two lifts under different conditions, allowable bond strength and the effect of CoTE on de-bonding issues (Hu et al. 2014).
- Ensuring two-lift pavement construction is practical and cost effective: the two-lift concrete paving requires a consistent effort, especially in handling additional equipment, placing and scheduling (Hu et al. 2014). A good project scheduling and jobsite management not only ensures paving quality, but also makes the two-lit paving project more cost-effective.

CHAPTER VI

CONCLUSIONS

Over 90% of the U.S highways and roads are constructed with HMA, and the increasing maintenance and rehabilitation actions result in a considerable amount of RAP left in stockpiles. The possible use of RAP in PCC as aggregate replacement not only helps dispose of excess RAP stockpiles, but also provides a reduction in virgin aggregate consumption in PCC, which brings significant benefits from economic, social and environmental standpoints. In this dissertation, various aspects including mechanical properties, durability, microstructures and crack pattern, fracture properties, and pavement evaluation related to the use of RAP-PCC in pavement applications were evaluated through robust experimental, analytical, and simulative approaches. The mechanical properties and durability of the RAP-PCC were tested through an extensive experimental program, followed by sufficient discussions of the results. An effective method using the total asphalt volumetric fraction to determine the optimum RAP replacement level in a RAP-PCC mixture was developed. The microstructures and crack pattern in the RAP-PCC system were subsequently investigated through several advanced techniques such as optical microscope, X-ray CT, and SEM in order to provide scientific evidence and explanation of RAP-PCC's behaviors observed in the lab. The fracture properties of the RAP-PCC were experimentally determined through an innovative approach using specimens with semi-circular geometry. Finally, evaluation of the performance of rigid pavements containing RAP-PCC was carried out. The major conclusions of each aspect of this research are drawn below.

VI.1 MECHANICAL PROPERTIES AND DURABILITY OF RAP-PCC

One of the major tasks of this dissertation was to validate the earlier findings on mechanical properties and durability of PCC containing coarse RAP from Texas. The 0.40_520_HOU, the 0.40_520_AMA, the 0.40_520_BRY, and the 0.40_520_SA RAP-PCC mixture series were evaluated through a detailed testing program. A regression analysis was performed to correlate the RAP-PCC mechanical properties with the total asphalt volumetric fraction. Based on the regression equations, an effective method using the total asphalt volumetric fraction to determine the optimum RAP replacement level in a RAP-PCC mixture was developed. The benefits of attaining dense combined aggregate gradation due to the replacement of a certain percentage of coarse virgin aggregate by coarse RAP were demonstrated by comparing the dense-graded mixtures and the gap-graded mixtures. The following conclusions are made:

- Replacing virgin coarse aggregate by RAP in a typical PCC pavement mixture has caused considerable reductions in CS, MOE, MOR and STS. The percentage reduction in flexural strength for all the PCC mixtures containing different types of RAPs remain the lowest compared to the other tested mechanical properties. RAP replacement exceeding 40 percent was considered to be impractical for formulating Class P concrete mixture as the percentage reduction of different strengths may not be allowed.
- A proper use of coarse RAP with a suitable gradation containing sufficient intermediate sized particles can facilitate formation of dense graded concrete not only because it contains a large amount of intermediate particles but also due to the fact that these particles are less flat and elongated. The presence of aged asphalt layer in the RAP aggregates provides some additional smoothness, which facilitates better flowability.

- The dense-graded RAP-PCC mixtures showed better workability and mechanical properties compared to the gap-graded RAP-PCC mixtures.
- Both of the RAP-PCC's compressive strength and flexural strength can be linearly related to the TAVF, provided the TAVF is not very high. This finding enables the prediction of the properties based on regression equations and the development of an approach to determine optimum RAP replacement level in a RAP-PCC mixture.
- Based on the durability test data, PCC made of a certain percentage of coarse RAP (≤40 percent RAP replacement) manifested good durability characteristics in terms of freeze-thaw resistance and permeability. The ring tests suggested that the addition of RAP postpone the cracking occurrence. An innovative abrasion testing and analysis approach was developed and is anticipated to be useful for predicting the concrete pavement service life under erosion damage.

VI.2 MICROSTRUCTURE AND CRACK PATTERN OF RAP-PCC

An evaluation of the microstructures and crack pattern in RAP-PCC was carried out. Three advanced tools, namely the optical microscope, X-ray CT and SEM, were used in a combined manner to investigate the mechanisms responsible for the earlier observations on RAP-PCC's mechanical properties. The major findings from the microstructure and crack pattern study are:

- Based on the findings from the RAP-PCC thin section examination, the presence of a clean asphalt layer (i.e., asphalt layer alone without any other particulate materials) around RAP particles was not observed in any of the studied RAP materials. In general, the asphalt layer contains varying amounts of fine aggregates and air voids.

- The presence of RAP clumps (i.e., agglomerated RAP particles) in RAP-PCC specimens containing big sized RAP particles is a common feature. The agglomerated RAP particles appeared to be a single particle by visual observation but their agglomerated nature was clearly identified under a microscope.
- Adding RAP into PCC yielded porous ITZ, but the effects on the size and nature of distribution of CH crystals in the ITZ are minimal.
- The major weak zone of the RAP-PCC system is the asphalt. Asphalt cohesive failure (i.e., crack easily propagate through the asphalt layer around the RAP particles) is the major mechanism responsible for the strength reduction of RAP-PCC. The presence of RAP clumps is also found to be another weak zone in RAP-PCC. These observations are able to explain the previous mechanical properties testing results.
- The presence of RAP has caused higher amounts of air voids in the studied RAP-PCC mixtures compared to the reference PCC sample, which can be another reason for strength and stiffness reductions.

VI.3 FRACTURE PROPERTIES OF RAP-PCC

The critical stress intensity factor (K_{Ic}^{s}) and critical crack tip opening displacement ($CTOD_c$) of concrete are considered two size-independent fracture properties and can be used to predict concrete fracture behavior. The existing test methods using a single-edge notch beam or a disk-shaped compact tension geometry suffer from some limitations. An easy but effective method using specimens with SCB geometry to characterize the RAP-PCC fracture properties has been developed. The important findings are summarized as below:

- The SCB specimen with a 76 mm radius and a 38 mm notch length (A/R=0.5) was selected as a feasible specimen dimension for an effective SCB fracture test. The specimen with the 0.16 A/R ratio suffered from a sudden failure after the peak load as such applying an unloading process when the loading was still within 95% of the maximum load was not possible.
- The comparisons of the means of the fracture properties indicated that the RAP-PCC mixtures had similar K_{Ic}^{s}, but higher $CTOD_c$, G_f, and G_F relative to the plain PCC. An evaluation of the data through statistical approaches showed the K_{Ic}^{s} and G_F for different mixtures are statistically similar. However, the differences for the $CTOD_c$ and G_f between the RAP-PCC and the plain PCC are statistically significant.
- The theoretical tensile strength, f_t, of the studied mixtures was determined using the tested fracture properties and then compared with the conventional measurements from the flexural strength and splitting tensile strength tests. It was confirmed that the conventionally measured PCC tensile strength, f_t', overestimates the f_t of PCC.
- The material length, Q, of the PCC containing BRY RAP was statistically higher than that of the plain PCC, indicating that RAP-PCC is a more ductile material.
- The MOE determined from the SCB fracture test was invariably lower than that obtained from a conventional compression test, despite the fact the MOE is notch size dependent. It is hypothesized that tensile MOE of PCC is smaller than compressive MOE of PCC based on this finding.
- The bilinear softening curves for the studied mixtures were generated for future fracture behavior modeling. The RAP-PCC mixtures had higher displacement parameters relative to the plain PCC, which again manifested the ductile nature of RAP-PCC material. For

the first time, the kink point stress ratio, ψ, was theoretically determined as a constant value 0.265.

VI.4 EVALUATION OF RIGID PAVEMENT CONTAINING RAP-PCC

Finally, the RAP-PCC pavement performance was evaluated through a number of case studies using some relevant pavement design tools. The following conclusions are made from the findings:

- The RAP-PCC has reduced thermal conductivity, heat capacity, and unit weight, and increased Poisson's ratio and CoTE, relative to plain PCC.
- Use of the conventional pavement design tools (i.e., AASHTO 1993 and TxCRCP ME) yielded a slightly higher slab thickness for SLFD pavement containing RAP-PCC relative to control pavement. The Pavement ME analysis showed that SLFD JPCP containing RAP-PCC required a thicker slab compared to plain JPCP, but was not necessarily the case for the CRCP. The CRCP slabs made with the RAP-PCC exhibited a decrease in required slab thickness.
- Use of RAP-PCC to construct JPCP is likely to lead to some deviation from achieving favorable performance. RAP-PCC's lower modulus may balance the negative effects caused by its higher CoTE, but a reduction in tensile strength causes a higher stress/strength ratio and leads to increasing chances of occurring fatigue cracking. Additionally, use of RAP-PCC may cause higher differential corner deflections and consequently lead to higher faulting.
- Use of RAP-PCC to construct CRCP could potentially improve pavement performance due to the chances of occurrence of tighter cracks. The reduced MOE is beneficial in

tightening CRCP transverse cracking together and maintaining a higher LTE for a much longer pavement service life according to the Pavement ME simulations. However, poor shear resistance of RAP aggregates might lower the overall shear capacity of the crack and cast doubts on the improvement of LTE.

- The findings from the field investigation on the concrete pavements containing RCA-PCC generally supported the findings from the simulative analysis of the pavement containing RAP-PCC.
- The idea of using RAP-PCC as a bottom lift material in a two-lift PCC pavement can maximize the RAP usage with little compromise of the pavement performance. Use of RAP-PCC in two-lift pavement is considered one of the feasible approaches to implement RAP-PCC for the time being.

In conclusion, RAP-PCC is a construction material with higher ductility and better fracture properties relative to conventional PCC. It meets the increasing need for sustainability and therefore should be greatly advocated. It is feasible to use RAP-PCC material to construct SLFD pavement with up to 40-50% coarse RAP replacement level under current strength based specifications. The RAP usage is anticipated to be increased by applying RAP-PCC in a two-lift pavement.

The important future work is to generate more lab and field data to verify that RAP-PCC has adequate durability and surface characteristics. Besides, research to develop a fracture based material criterion for applying on RAP-PCC pavements is highly warranted; the application of RAP-PCC could be further facilitated thanks to its good fracture properties. The addition of RAP into PCC makes PCC more viscoelastic, which causes PCC slab to creep more in the field. Slabs

with higher creep can have some potential benefits such as those from a reduced permeant curl and warp gradient. Research to address the creep of RAP-PCC is needed.

REFERENCES

AASHTO (1993). AASHTO Guide for Design of Pavement Structures, American Association of State Highway and Transportation Officials, Washington, D.C

AASHTO (2003). Guide for Mechanistic-Empirical Design of New and Rehabilitated Pavement Structures, American Association of State Highway and Transportation Officials, Washington, D.C.

AASHTO T161. Standard Method of Test for Resistance of Concrete to Rapid Freezing and Thawing, American Association of State Highway and Transportation Officials, Washington, D.C, 2008

AASHTO T164. Standard Method of Test for Quantitative Extraction of Asphalt Binder from Hot Mix Asphalt (HMA), American Association of State Highway and Transportation Officials, Washington, D.C, 2016.

AASHTO T277. Standard Method of Test for Electrical Indication of Concrete's Ability to Resist Chloride Ion Penetration, American Association of State Highway and Transportation Officials, Washington, D.C, 2011.

AASHTO T308. Standard Method of Test for Determining the Asphalt Binder Content of Hot Mix Asphalt (HMA) by Ignition Method, American Association of State Highway and Transportation Officials, Washington, D.C, 2011.

AASHTO T336. Standard Method of Test for Coefficient of Thermal Expansion of Hydraulic Cement Concrete, American Association of State Highway and Transportation Officials, Washington, D.C, 2011.

AASHTO TP105. Standard Method of Test for Determining the Fracture Energy of Asphalt Mixtures Using the Semicircular Bend Geometry (SCB), American Association of State Highway and Transportation Officials, Washington, D.C, 2013.

Abrams, D. (1918). "The Basic Principles of Concrete Mixes." Mining and Scientific Press.

ACI 211.1:62. Standard Practice for Selection of Proportions for Nomral, Heavywieght, and Mass Concrete, American Concrete Institute, Farmington Hills, MI, 1985.

ACI 318. Building Code Requirements for Structural Concrete and Commentary, American Concrete Institute, ACI 318, Farmington Hills, MI, 2008.

Al-Oraimi, S., Hassan, H. F., and Hago, A. (2009). "Recycling of Reclaimed Asphalt Pavement in Portland Cement Concrete." *The Journal of Engineering Research*, 6(1), 37-45.

ASTM C1202. Standard Test Method for Electrical Indication of Concrete's Ability to Resist Chloride Ion Penetration, ASTM International, West Conshohocken, PA, 2012.

ASTM C127. Standard Test Method for Relative Density (Specific Gravity) and Absorption of Coarse Aggregate, ASTM International, West Conshohocken, PA, 2015.

ASTM C128. Standard Test Method for Relative Density (Specific Gravity) and Absorption of Fine Aggregate, ASTM International, West Conshohocken, PA, 2015.

ASTM C136/C136M. Standard Test Method for Sieve Analysis of Fine and Coarse Aggregates, ASTM International, West Conshohocken, PA, 2014.

ASTM C138/C138M. Standard Test Method for Density (Unit Weight), Yield, and Air Content (Gravimetric) of Concrete, ASTM International, West Conshohocken, PA, 2017.

ASTM C143/C143M. Standard Test Method for Slump of Hydraulic Cement Concrete, ASTM International, West Conshohocken, PA, 2015.

ASTM C1581/C1581M. Standard Test Method for Determining Age at Cracking and Induced Tensile Stress Characteristics of Mortar and Concrete under Restrained Shrinkage, ASTM International, West Conshohocken, PA, 2016

ASTM C173/C173M. Standard Test Method for Air Content of Freshly Mixed Concrete by Volumetric Method, ASTM International, West Conshohocken, PA, 2016.

ASTM C192/C192M. Standard Practice for Making and Curing Concrete Test Specimens in the Laboratory, ASTM International, West Conshohocken, PA, 2016.

ASTM C29/C29M. Standard Test Method for Bulk Density (“Unit Weight’) and Voids in Aggregate, ASTM International, West Conshohocken, PA, 2017

ASTM C295/C295M. Standard Guide for Petrographic Examination of Aggregates for Concrete, ASTM International, West Conshohocken, PA, 2012

ASTM C33/C33M. Standard Specification for concrete aggregates, ASTM International, West Conshohocken, PA, 2016.

ASTM C39/C39M. Standard Test Method for Compressive Strength of Cylindrical Concrete Specimens, ASTM International, West Conshohocken, PA, 2016.

ASTM C457/C457M. Standard Test Method for Microscopical Determination of Parameters of the Air-Void System in Hardened Concrete, ASTM International, West Conshohocken, PA, 2016.

ASTM C469/C469M. Standard Test Method for Static Modulus of Elasticity and Poisson's Ratio of Concrete in Compression, ASTM International, West Conshohocken, PA, 2014.

ASTM C496/C496M. Standard Test Method for Splitting Tensile Strength of Cylindrical concrete specimens, ASTM International, West Conshohocken, PA, 2011.

ASTM C666/C666M. Standard Test Method for Resistance of Concrete to Rapid Freezing and Thawing, ASTM International, West Conshohocken, PA, 2015.

ASTM C779/C779M. Standard Test Method for Abrasion Resistance of Horizontal Concrete Surfaces, ASTM International, West Conshohocken, PA, 2012.

ASTM C78/C78M. Standard Test Method for Flexural Strength of Concrete (Using Simple Beam with Third-Point Loading), ASTM International, West Conshohocken, PA, 2016.

ASTM C856. Standard Test Method for Petrographic Examination of Hardened Concrete, ASTM International, West Conshohocken, PA, 2017.

ASTM C944/C944M. Standard Test Method for Abrasion Resistance of Concrete for Mortar Surfaces by the Rotating-Cutter Method, ASTM International, West Conshohocken, PA, 2012.

ASTM D2172/D2172M. Standard Test Method for Quantitative Extraction of Bitumen from Bituminous Paving Mixtures, ASTM International, West Conshohocken, PA, 2011.

ASTM D6307. Standard Test Method for Asphalt Content of Asphalt mixture by Ignition Method, ASTM International, West Conshohocken, PA, 2016

Adamson, R., Dempsey, J., and Mulmule, S. (1996). "Fracture Analysis of Semi-circular and Semi-circular-bend Geometries." *International Journal of Fracture*, 77(3), 213-222.

Asphalt Institute (2001). *Superpave Mix Design Series No.2 (SP-2).*

Al-Oraimi, S., Hassan, H. F., and Hago, A. (2009). "Recycling of Reclaimed Asphalt Pavement in Portland Cement Concrete." *The Journal of Engineering Research*, 6(1), 37-45.

Alam, M., Azad, M., and Kadir, M. (2010). "Fracture Toughness of Plain Concrete Specimens Made with Industry-burnt Brick Aggregates." *Journal of Civil Engineering (IEB)*, 38(1), 81-94.

Amick, H., and Monteiro, P. J. (2005). "Modification of Concrete Damping Properties for Vibration Control in Technology Facilities." *Proceedings of the SPIE Conference*.

Amirkhanian, A., Spring, D., Roesler, J., and Paulino, G. (2015). "Forward and Inverse Analysis of Concrete Fracture Using the Disk-Shaped Compact Tension Test." *Journal of Testing and Evaluation*, 44(1), 625-634.

Bari, M. E., and Zollinger, D. G. (2016). "New Concepts for the Assessment of Concrete Slab Interfacial Effects in Pavement Design and Analysis." *International Journal of Pavement Engineering*, 17(3), 233-244.

Bažant, Z. P. (1989). "Fracture Energy of Heterogeneous Materials and Similitude." *Fracture of Concrete and Rock*, Springer, 229-241.

Bazant, Z. P., and Baweja, S. (1995). "Creep and Shrinkage Prediction Model for Analysis and Design of Concrete Structures-model B3." *Materials and Structures*, 28, 357-365.

Bažant, Z. P., and Kazemi, M. (1990). "Determination of Fracture Energy, Process Zone Longth and Brittleness Number from Size Effect, with Application to Rock and Conerete." *International Journal of Fracture*, 44(2), 111-131.

Bažant, Z. P., and Oh, B. H. (1983). "Crack Band Theory for Fracture of Concrete." *Materials and Structures*, 16(3), 155-177.

Bentsen, R. A., Vavrik, W. A., Roesler, J. R., and Gillen, S. L. (2013). "Ternary Blend Concrete with Reclaimed Asphalt Pavement as an Aggregate in Two-Lift Concrete Pavement." *Proceedings of the 2013 International Concrete Sustainability Conference*, 6-8.

Bentur, A., and Odler, I. (1996). "Development and Nature of Interfacial Microstructure." *RILEM Report*, 18-44.

Bergren, J. V., and Britson, R. A. (1977). "Portland Cement Concrete Utilizing Recycled Pavements." *Proceedings of the International Conference on Concrete Pavement Design*.

Berry, M., Dalton, K., and Murray, F. (2015). "Feasibilty of Recalimed Asphalt Pavement as Aggregate in Portland Cement Concrete Pavement Phase II: Field Demonstration." *Report FHWA/MT-15-003/8207*, U.S. Dep. of Transportation, Montana.

Berry, M., Stephens, J., Bermel, B., Hagel, A., and Schroeder, D. (2013). "Feasibility of Reclaimed Asphalt Pavement as Aggregate in Portland Cement Concrete." *Report FHWA/MT-13-009/8207*, U.S. Dep. of Transportation, Montana.

Besson, F. (1935). "Case Against Surface Area and Fineness Modulus." *Engineering New Record*, 114(7).

Bilodeau, K., Sauzeat, C., Di Benedetto, H., Olard, F., and Bonneau, D. (2011). "Laboratory and In Situ Investigations of Steel Fiber-Reinforced Compacted Concrete Containing Reclaimed Asphalt Pavement." *Proceedings of the Transportation Research Board 90th Annual Meeting*.

Brand, A. (2012). "Fractionated Reclaimed Asphalt Pavement as A Coarse Aggregate Replacement in A Ternary Blended Concrete Pavement." Thesis, University of Illinois at Urbana-Champaign, in Partial Fulfillment of the Requirements for the Degree of Master of Science.

Brand, A., Amirkhanian, A., and Roesler, J. (2014). "Flexural Capacity of Full-depth and Two-lift Concrete Slabs with Recycled Aggregates." *Transportation Research Record: Journal of the Transportation Research Board*, 2456, 64-72.

Brand, A. S., and Roesler, J. R. (2015). "Expansive and Concrete Properties of SFS–FRAP Aggregates." *Journal of Materials in Civil Engineering*, 28(2), 04015126.

Brand, A. S., and Roesler, J. R. (2017a). "Bonding in Cementitious Materials with Asphalt-coated Particles: Part I–The Interfacial Transition Zone." *Construction and Building Materials*, 130, 171-181.

Brand, A. S., and Roesler, J. R. (2017b). "Bonding in Cementitious Materials with Asphalt-coated Particles: Part II–Cement-asphalt Chemical Interactions." *Construction and Building Materials*, 130, 182-192.

Brand, A. S., Roesler, J. R., Al-Qadi, I. L., and Shangguan, P. (2012). "Fractionated Reclaimed Asphalt Pavement (FRAP) as a Coarse Aggregate Replacement in a ternary Blended Concrete Pavement." *Report ICT-12-008*, Illinois State Toll Highway Authority, Downers Grove.

Buch, N., Gilliland, D., Vongchusiri, K., and Van Dam, T. J. (2004). "A Preliminary Mechanistic Evaluation of PCC Cross-Sections Using ISLAB2000–A Parametric Study." *Report RC-1441*, Michigan State University, East Lansing, Michigan.

Chesner, W. H., Collins, R. J., and MacKay, M. (1998). "User Guidelines for Waste and By-Product Materials in Pavement Construction." *Report FHWA-RD-97-148*, U.S. Dep of Transportation, Federal Highway Administration.

Copeland, A. (2011). "Reclaimed Asphalt Pavement in Asphalt Mixtures: State of the Practice." *Report FHWA-HRT-11-021*, Turner-Fairbank Highway Research Center, Federal Highway Administration.

Daniel, J. S., and Lachance, A. (2005). "Mechanistic and Volumetric Properties of Asphalt Mixtures with Recycled Asphalt Pavement." *Transportation Research Record: Journal of the Transportation Research Board*, 1929(1), 28-26.

Delwar, M., Fahmy, M., and Taha, R. (1997). "Use of Reclaimed Asphalt Pavement as an Aggregate in Portland Cement Concrete." *ACI Materials Journal*, 94(3).

Dempsey, J. P., Adamson, R. M., and Defranco, S. J. (1995). "Fracture Analysis of Base-edge-cracked Reverse-tapered plates." *International Journal of Fracture*, 69(4), 281-294.

Dong, Q., and Huang, B. (2013). "Laboratory Evaluation on Resilient Modulus and Rate Dependencies of RAP Used as Unbound Base Material." *Journal of Materials in Civil Engineering*, 26(2), 379-383.

Dumitru, I., Smorchevsky, G., and Caprar, V. (1999)."Trends in the Utilisation of Recycled Materials and By-products in the Concrete Industry in Australia." *Proceedings of the Concrete Institute of Australia 19th Biennial Conference, Sydney,* 289-301.

Edwards, L. (1918). "Proportioning the Materials of Mortoars and Concretes by Surface Areas of Aggregates." *ASTM, Proceedings of the 21st Annual Meeting,* 18, Part II, pp. 235-302

Gates, L., Masad, E., Pyle, R., and Bushee, D. (2011). "Aggregate Imaging Measurement System 2 (AIMS2): Final Report." *FHWA-HIF-11-030,* Pine Instrument Company.

Gillen, S. L., Brand, A. S., Roesler, J. R., and Vavrik, W. R. (2012). "Sustainable Long-Life Composite Concrete Pavement for the Illinois Tollway." *Proceedings of the International Conference on Long-Life Concrete Pavements*, 2.

Grasley, Z. C., and Matthew, D. (2011). "Viscoelastic Properties and Drying Stress Extracted from Concrete Ring Tests." *Cement and Concrete Composites*, 33(2), 171-178.

Gress, D., Snyder, M., and Sturtevant, J. (2009). "Performance of Rigid Pavements Containing Recycled Concrete Aggregate: Update for 2006." *Transportation Research Record: Journal of the Transportation Research Board*, 2113, 99-107.

Ha, S., Yeon, J., Won, M. C., Jung, Y. S., and Zollinger, D. G. (2012). "User's Guide for TxCRCP-ME Design Software: Volume I-User's Guide and Volume II-Software Architecture." *Report FHWA/TX-12/0-5832*, U.S. Dep. of Transportation, Texas.

Hansen, K. R., and Copeland, A. (2017). "Annual Asphalt Pavement Industry Survey on Recycled Materials and Warm-Mix Asphalt Usage: 2015.", *Report IS-138*, National Asphalt Pavement Association, Lanham, MD.

Harrison, P. J. (2004). "For the Ideal Slab-on-ground Mixture." *Concrete International Detroit*, 26(3), 49-55.

Hassan, K., Brooks, J., and Erdman, M. (2000). "The Use of Reclaimed Asphalt Pavement (RAP) Aggregates in Concrete." *Waste Management Series*, 1, 121-128.

Hillerborg, A., Modéer, M., and Petersson, P.-E. (1976). "Analysis of Crack Formation and Crack Growth in Concrete by Means of Fracture Mechanics and Finite Elements." *Cement and concrete research*, 6(6), 773-781.

Hogancamp, J., and Grasley, Z. (2017). "The Use of Microfine Cement to Enhance the Efficacy of Carbon Nanofibers with respect to Drying Shrinkage Crack Resistance of Portland Cement Mortars." *Cement and Concrete Composites*, 83, 405-414.

Holland, J. (1990). "Mixture Optimization." *Concrete International*, 12(10), 10.

Hossiney, N., Tia, M., and Bergin, M. J. (2010). "Concrete Containing RAP for Use in Concrete Pavement." *International Journal of Pavement Research and Technology*, 3(5), 251-258.

Hu, J., Fowler, D. W., Siddiqui, M. S., and Whitney, D. P. (2014). "Feasibility Study of Two-lift Concrete Paving: Technical Report." *Report FHWA/TX-14-0-6749-1*, U.S. Dep. of Transportation, Texas.

Hu, J., Siddiqui, M. S., and David Whitney, P. (2014). "Two-Lift Concrete Paving–Case Studies and Reviews from Sustainability, Cost Effectiveness and Construction Perspectives." *Proceedings of the Transportation Research Board 93rd Annual Meeting.*

Huang, B., Shu, X., and Burdette, E. (2006). "Mechanical Properties of Concrete Containing Recycled Asphalt Pavements." *Magazine of Concrete Research*, 58(5), 313-320.

Huang, B., Shu, X., and Li, G. (2005). "Laboratory Investigation of Portland Cement Concrete Containing Recycled Asphalt Pavements." *Cement and Concrete Research*, 35(10), 2008-2013.

Huang, B., Shu, X., and Tang, Y. (2005). "Comparison of Semi-circular Bending and Indirect Tensile Strength Tests for HMA Mixtures." *Advances in Pavement Engineering*, 1-12.

Jenq, Y., and Shah, S. P. (1985). "Two Parameter Fracture Model for Concrete." *Journal of Engineering Mechanics*, 111(10), 1227-1241.

John, R., and Shah, S. P. (1989). "Fracture Mechanics Analysis of High-strength Concrete." *Journal of Materials in Civil Engineering*, 1(4), 185-198.

Kandhal, P. S., and Mallick, R. B. (1998). "Pavement Recycling Guidelines for State and Local Governments Participant's Reference Book." *Report FHWA-SA-98-042*, National Center for Asphalt Technology, Auburn, AL.

Katsakou, M., and Kolias, S. (2007). "Mechanical Properties of Cement-bound Recycled Pavements." *Proceedings of the ICE-Construction Materials*, 160(4), 171-179.

Kennedy, C. T. (1940). "The Design of Concrete Mixes." *ACI Journal Proceedings*, ACI.

Kim, D.-H., and Won, M. C. (2008). "Pilot implementation of Optimized Aggregate Gradation for Concrete Paving." *Report FHWA/TX-09/5-9026-01-1*, U.S. Dep. of Transportation, Texas

Kohler, E., and Roesler, J. (2006a). "Accelerated Pavement Testing olf Extended Life Continuously Reinforced Concrete Pavement Sections." *FHWA-IL-UI-289*, Illinois Cooperative Highway and Transportation.

Kohler, E., and Roesler, J. (2006b). "Crack Spacing and Crack Width Investigation from Experimental CRCP Sections." *International Journal of Pavement Engineering*, 7(4), 331-340.

Kolias, S. (1996). "Mechanical Properties of Cement-Treated Mixtures of Milled Bituminous Concrete and Crushed Aggregates." *Materials and Structures*, 29(7), 411-417.

Li, X.-J., and Marasteanu, M. (2010). "Using Semi Circular Bending Test to Evaluate Low Temperature Fracture Resistance for Asphalt Concrete." *Experimental Mechanics*, 50(7), 867-876.

Li, X., Marasteanu, M. O., Williams, R. C., and Clyne, T. R. (2008). "Effect of Reclaimed Asphalt Pavement (Proportion and Type) and Binder Grade on Asphalt Mixtures." *Transportation Research Record: Journal of the Transportation Research Board*, 2051(1), 90-97.

MAPA. (2007). "Asphalt Pavement FAQ's." <http://www.texasasphalt.org/content.asp?contentid=155> (Jan. 1, 2017)

Maso, J. (1980). "The Bond Between Aggregates and Hydrated Cement Pastes." *Proceedings of the 7th international Cement Congress*, 3-15.

Mathias, V., Sedran, T., and de Larrard, F. (2004). "Recycling Reclaimed Asphalt Pavement in Concrete Roads." *Proceedings of the PRO 40: International RILEM Conference on the Use of Recycled Materials in Buildings and Structures (Volume 1)*, RILEM Publications, 66.

McGarrah, E. J. (2007). "Evaluation of Current Practices of Reclaimed Asphalt Pavement/Virgin Aggregate as Base Course Material." *Report FHWA/WA-RD 713.1*, U.S. Dep. of Transportation, Washington.

Mirsayar, M., Shi, X., and Zollinger, D. (2017). "Evaluation of Interfacial Bond Strength Between Portland Cement Concrete and Asphalt Concrete Layers using Bi-Material SCB Test Specimen." *Engineering Solid Mechanics*, 5(4), 293-306.

Moaveni, M., Cetin, S., Brand, A. S., Dahal, S., Roesler, J. R., and Tutumluer, E. (2016). "Machine Vision Based Characterization of Particle Shape and Asphalt Coating in Reclaimed Asphalt Pavement." *Transportation Geotechnics*, 6, 26-37.

Mukhopadhyay, A., and Shi, X. (2017a). "Validation of RAP and/or RAS in Hydraulic Cement Concrete: Guidelines and Implementation Recommendations." *Report FHWA/TX-17/0-6855-P1*, U.S. Dep. of Transportation, Texas.

Mukhopadhyay, A., and Shi, X. (2017b). "Validation of RAP and/or RAS in Hydraulic Cement Concrete: Technical Report." *Report FHWA/TX-17/0-6855-1*, U.S. Dep. of Transportation, Texas.

Neville, A. M. (1995). *Properties of Concrete*, Longman London.

Nguyen, M., Balay, J., Sauzéat, C., Di Benedetto, H., Bilodeau, K., Olard, F., and Ficheroulle, B. (2012). "Accelerated Pavement Testing Experiment of Pavement Made of Fiber-Reinforced Roller-Compacted Concrete." *Advances in Pavement Design Through Full-Scale Accelerated Pavement Testing*, 299-311.

NSRDB. (2017). "National Solar Radiation Database 1998-2014 Update." < http://rredc.nrel.gov/solar/old_data/nsrdb/> (Aug. 15, 2017)

Okafor, F. O. (2010). "Performance of Recycled Asphalt Pavement as Coarse Aggregate in Concrete." *Leonardo Electronic Journal of Practices and Technologies*, 9(17), 47-58.

Park, K., Paulino, G. H., and Roesler, J. R. (2008). "Determination of the Kink Point in the Bilinear Softening Model for Concrete." *Engineering Fracture Mechanics*, 75(13), 3806-3818.

Patankar, V., and Williams, R. (1970). "Bitumen in Dry Lean Concrete." Highways and Traffic Engineering. 38, 1721.

Pavement Interactive. (2017). "1993 AASHTO Rigid Pavement Structural Design Application." < http://www.pavementinteractive.org/1993-aashto-rigid-pavement-structural-design-application/> (Sep. 1, 2017)

Ramezanianpour, A. A., Pilvar, A., Mahdikhani, M., and Moodi, F. (2011). "Practical Evaluation of Relationship between Concrete Resistivity, Water Penetration, Rapid Chloride Penetration and Compressive Strength." *Construction and Building Materials*, 25(5), 2472-2479.

Rao, S. P., Darter, M., Tompkins, D., Vancua, M., Khazanovich, L., Signore, J., Coleri, E., Wu, R., and John, H. (2013). "Composite Pavement Systems: Volume 2: PCC/PCC Composite Pavements. " Transportation Research Board.

Richardson, D. N. (2005). "Aggregate Gradation Optimization-Literature Search." *Report RDT 05-001*, University of Missouri-Rolla.

Riding, K. A., Poole, J. L., Schindler, A. K., Juenger, M. C., and Folliard, K. J. (2008). "Simplified Concrete Resistivity and Rapid Chloride Permeability Test Method." *Materials Journal*, 105(4), 390-394.

Robinson, G. R., Menzie, W. D., and Hyun, H. (2004). "Recycling of Construction Debris as Aggregate in the Mid-Atlantic Region, USA." *Resources, Conservation and Recycling*, 42(3), 275-294.

Roesler, J. R., Hiller, J. E., and Brand, A. S. (2016). "Continuously Reinforced Concrete Pavement Manual: Guidelines for Design, Construction, Maintenance, and Rehabilitation." *Report FHWA-HIF-16-026,* U.S. Dep. of Transportation Federal Highway Administration.

Sachet, T., Balbo, J., and Bonsembiante, F. (2013). "Rendering The Loss of Strength in Dry Concretes with Addition of Milled Asphalt Through Microscopic Analysis." *Revista IBRACON de Estruturas e Materiais*, 6(6), 933-954.

Saïd, S. E. E. B., Khay, S. E. E., Achour, T., and Loulizi, A. (2017). "Modelling of the Adhesion Between Reclaimed Asphalt Pavement Aggregates and Hydrated Cement Paste." *Construction and Building Materials*, 152, 839-846.

Shah, S. P., Swartz, S. E., and Ouyang, C. (1995). *Fracture Mechanics of Concrete: Applications of Fracture Mechanics to Concrete, Rock and Other Quasi-Brittle Materials*, John Wiley & Sons.

Shi, X. (2014). "Controlling Thermal Properties of Asphalt Concrete and its Multifunctional Applications." Thesis, Texas A&M University, in Partial Fulfillment of the Requirements for the Degree of Master of Science.

Shi, X., Mukhopadhyay, A., and Liu, K.-W. (2017). "Mix Design Formulation and Evaluation of Portland Cement Concrete Paving Mixtures Containing Reclaimed Asphalt Pavement." *Construction and Building Materials*, 152, 756-768.

Shi, X., Rew, Y., Ivers, E., Shon, C.-S., Stenger, E. M., and Park, P. (2017). "Effects of Thermally Modified Asphalt Concrete on Pavement Temperature." *International Journal of Pavement Engineering*, 1-13.

Shi, X., Rew, Y., Shon, C., and Park, P. (2015). "Controlling Thermal Properties of Asphalt Concrete and Their Effects on Pavement Surface Temperature." *Proceedings of the Transportation Research Board 94th Annual Meeting*. No. 15-3651.

Shilstone, J. (1990). "Mixture Optimization for Fast-Track." *Proceedings of the 69th Annual Transportation Research Board Meeting*, Washington, DC.

Shilstone, J. (1993). "Research for Smartplant ", 24.

Shilstone, J. S. (1990). "Concrete Mixture Optimization." *Concrete International*, 12(6), 33-39.

Singh, S., Debbarma, S., and Kumar, P. (2017). "Utilization of Reclaimed Asphalt Pavement Aggregates Containing Waste from Sugarcane Mill for Production of Concrete Mixes." *Journal of Cleaner Production*.

Singh, S., Ransinchung, G., and Kumar, P. (2017). "Feasibility Study of RAP Aggregates in Cement Concrete Pavements." *Road Materials and Pavement Design*, 1-20.

Smith, D. (2006). "The Development of A Rapid Test for Determining the Transport Properties of Concrete." Thesis, University of New Brunswich, in Partial Fulfillment of the Requirements for the Degree of Master of Science.

Su, Y.-M., Hossiney, N., and Tia, M. (2013). "The Analysis of Air Voids in Concrete Specimen Using X-Ray Computed Tomography." *Proceedings of the SPIE Smart Structures and Materials+ Nondestructive Evaluation and Health Monitoring*, International Society for Optics and Photonics.

Su, Y.-M., Hossiney, N., Tia, M., and Bergin, M. (2014). "Mechanical Properties Assessment of Concrete Containing Reclaimed Asphalt Pavement Using the Superpave Indirect Tensile Strength Test." *Journal of Testing and Evaluation*, 42(4), 1-9.

Talbot, A. N., and Richart, F. E. (1923). "The Strength of Concrete-Its Relation to the Cement, Aggregates and Water." *Illinois Univ Eng Exp Sta Bulletin 137*.

Texas Department of Transportation (2014). "Standard Specifications for Construction and Maintenance of Highways, Streets, and Bridges." Texas Department of Transportation, Austin, TX.

Thompson, B. (2007). "Shoulder Rehabilitation Using Portland Cement and Recycled Asphalt pavement." *Report 03-09*, U.S. Dep. of Transportation, Maine.

Tia, M., Hossiney, N., Su, Y.-M., Chen, Y., and Do, T. A. (2012). "Use of Reclaimed Asphalt Pavement in Concrete Pavement Slabs." *Report 00088115*, U.S Dep. of Transportation, Florida.

Tompkins, D., Khazanovich, L., Darter, M., and Fleischer, W. (2009). "Design and Construction of Sustainable Pavements: Austrian and German Two-Layer Concrete Pavements." *Transportation Research Record: Journal of the Transportation Research Board*, 2098, 75-85.

Topcu, I. B., and Isikdag, B. (2009). "Effects of Crushed RAP on Free and Restrained Shrinkage of Mortars." *International Journal of Concrete Structures and Materials*, 3(2), 91-95.

Townsend, T. (1998). "Leaching Characteristics of Asphalt Road Waste." *Report 98-2*, Florida Center for Solid and Hazardous Waste Management, University of Florida, Gainsville, FL.

Wee, T., Suryavanshi, A. K., and Tin, S. (2000). "Evaluation of Rapid Chloride Permeability Test (RCPT) Results for Concrete Containing Mineral Admixtures." *Materials Journal*, 97(2), 221-232.

Weymouth, C. (1933). "Effects of Particle Interference in Mortars and Concretes." *Rock Products*. 36(2), 26-30.

Wojakowski, J. (1998). "High Performance Concrete Pavement." *Report FHWA-KS-98/2,* U.S. Dep. of Transportation, Kansas.

Wu, X.-R., and Carlsson, J. (1991). *Weight Functions and Stress Intensity Factor Solutions*, Pergamon.

Wu, Z., Mohammad, L. N., Wang, L., and Mull, M. A. (2005). "Fracture Resistance Characterization of Superpave Mixtures Using the Semi-Circular Bending Test." *Journal of ASTM International*, 2(3), 1-15.

Yamada, M., Ninomiya, T., and Mise, T. (1987). "Recycled Asphalt Mixtures in Osaka and Their Performance." *Memoirs of the Faculty of Engineering, Osaka City University*, 28, 197-201.

Young, R. (1919). "Some Theoretical Studies on Proportioning Concrete: By the Method of Surface Area of Aggregates. " *Proceedings of the ASTM 19(Part II)*, 444-509.

Zhou, F., Button, J. W., and Epps, J. A. (2012). "Best Practice of Using RAS in HMA. " *Report FHWA/TX-12/0-6614-1*. U.S. Dep. of Transportation, Texas.

Zollinger, D., Buch, N., Xin, D., and Soares, J. (1999). "Performance of Continuously Reinforced Concrete Pavements. Volume VI-CRC Pavement Design, Construction, and Performance." *Report FHWA-RD-97-151,* U.S. Department of Transportation, Federal Highway Administration.

APPENDIX A

METHODS FOR CONCRETE AGGREGATE GRADATION OPTIMIZATION

Aggregates are impartible parts of PCC, and they generally occupy 70 percent to 80 percent of the volume of the total mixtures. While numerous investigations have been completed to improve concrete performances by using additives like fibers, supplementary cementitious material, chemical admixtures etc., efforts have also been made to optimize aggregate gradation, and the benefits turned out to be very significant. Because the main purpose of the use of the RAP in this study is as an aggregate replacement for concrete, it is of great importance to review the methods for optimizing aggregate gradation and apply these theories to the mix design in this study. It is noted here that this section is largely based on Richardson (2005) as he did very good job in searching and summarizing the literature on aggregate gradation optimization.

MAXIMUM DENSITY THEORY

Around 100 years ago, initial researches about gradation optimization were conducted to develop an ideal shape of the gradation curve. The authors at that time believed that aggregate should be graded in size and combined with water and cement to yield the maximum density. This concept could result in mixtures containing fewer voids to be filled with cement paste, leading to higher concrete strength. Talbot and Richart developed the famous equation (Equation (136)) and suggested using n=0.5 to produce maximum density. However, several researches

reported difficulties in dealing with concrete made via this method, and eventually the maximum density theory fell into disfavor (Talbot and Richart 1923).

$$P = (\frac{d}{D})^n \quad (136)$$

Where

P = amount of material in the system finer than size d.

d = size of the particular group in question.

D = largest particle in the system.

n = exponent governing the distribution of sizes.

SURFACE AREA AND FINENESS MODULUS

Edwards (1918) believed that the surface area of aggregates was a crucial factor to calculate the amount of water required for a workable concrete. Young (1919) further developed this concept and stated that the amount of water is related to the quantity and consistency of cement and the total area of the aggregate. Almost at the same time, Abrams (1918) developed concept for fineness modulus and used this parameter to represent aggregate gradation. Although Abrams insisted his theory was useful and he believed concrete with same fineness modulus would have the same strength, he was continuously being challenged by various researchers (Besson 1935; Edwards 1918; Kennedy 1940; Young 1919).

ACI MIX DESIGN

The ACI method (ACI 1985) was developed largely based on Goldbeck and Grey's work. The controlling principle stated that workability depends on particle interferences among coarse aggregates. Weymouth developed his theory based on the relationship that one size of particles

of one size group are just under the opening provided by the next larger group (Weymouth 1933). The equation can be expressed as Equation (137):

$$t = [\left(\frac{do}{da}\right)^{\frac{1}{3}} - 1] \times D \quad (137)$$

Where

T = average distance between particles of diameter D.

do = density of the size group.

da = ratio of the absolute volume of a size group to the space available t that size in concrete.

D = average diameter of the particles in the size group.

SHILSTONE'S METHOD

Shilstone started to work on concrete aggregate optimization in the 1970s. He believed concrete properties can be controlled by changing aggregate gradation. Shilstone used three fractions different from the definition of coarse and fine aggregates in traditional mix design, namely the coarse fraction (Q) (material retained on the 9.5-mm sieve), the intermediate fraction (I) (material passing the 9.5-mm sieve and retained on the 2.36-mm sieve), and the fine fraction (W) (material passing the 2.36-mm sieve and but coarse than 0.075-mm sieve).

IPR Chart

Shilstone promoted to use IPR versus sieve size chart to characterize aggregate gradation (Shilstone Sr 1990). In his theory, a haystack shape curve indicates an ideal gradation, while curves with a double hump may have problems. Figure 113 and Figure 114 show examples of an ideal gradation and a problematic gradation, respectively.

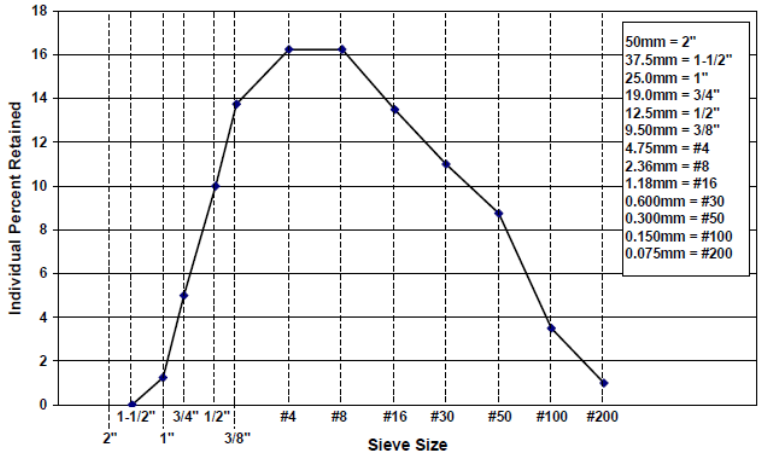

Figure 113 Ideal haystack gradation, IPR (Reprinted from Richardson 2005)

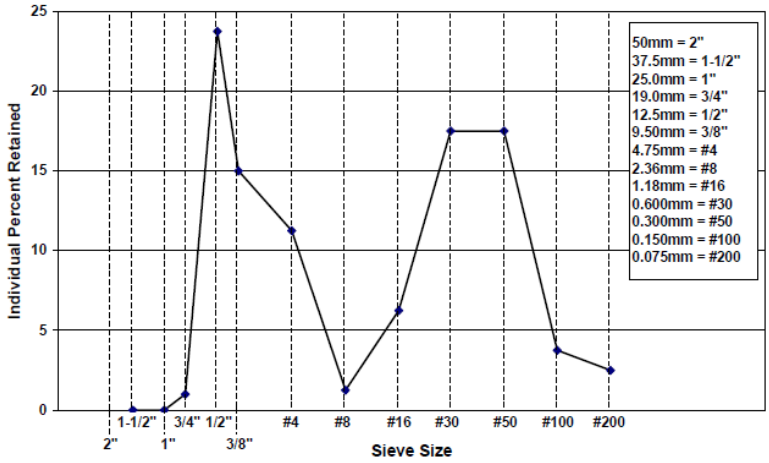

Figure 114 Problematic gradation, IPR (Reprinted from Richardson 2005)

CF Chart

Two factors were derived from aggregate gradation to predict the workability of concrete mix by Shilstone. CF is defined as Equation (138), which can be used to represent the proportion of #8 (2.36 mm) to 3/8 inch (9.5 mm) aggregate in the total coarse aggregate:

$$\mathrm{CF} = \left(\frac{\mathrm{Q}}{\mathrm{Q}+1}\right) \times 100 \tag{138}$$

Another term is workability factor (WF), and this is simply percentage aggregate smaller than #8 sieve (2.36 mm) but coarser than #200 sieve (0.075 mm). Based on these two factors,

Shilstone developed the famous CF chart, and this chart is used to characterize the mix properties, such as hardness, sandiness, excessive shrinkage, degree of gap-grading. Figure 115 presents a revised Shilstone CF Chart. As shown in Figure 115, the chart is divided into five zones representing concrete mixtures of different properties (Richardson 2005):

Bar: optimum but excellent control required.

Zone I: coarse, gap graded, tends to segregate.

Zone II: 1-1/2 inch (38 mm) well graded, best spot for everyday mixes.

II-1: excellent but caution.

II-2: excellent paving but slipform.

II-3: high quality slab.

II-4: good general.

II-5: varies to material and construction needs.

Zone III: ¾ inch (19 mm) and finer.

Zone IV: oversanded, sticky.

Zone V: rocky.

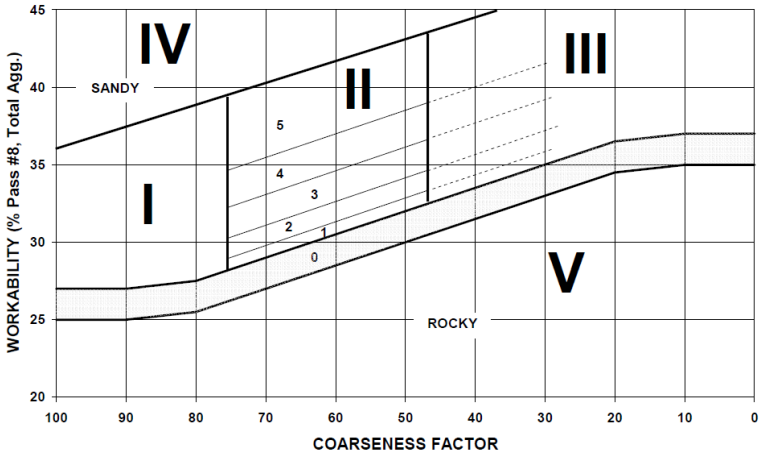

Figure 115 Revised Shilstone CF chart (Reprinted from Richardson 2005)

0.45 Power Chart

Shilstone also plotted the aggregate gradation on a 0.45 power plot, as shown in Figure 116.

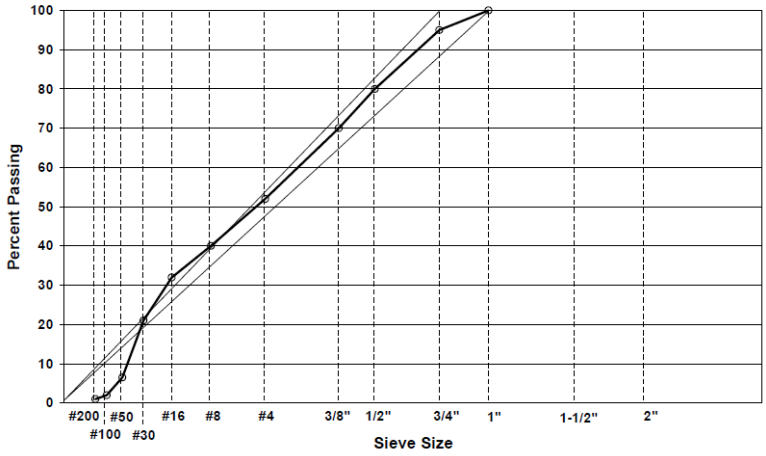

Figure 116 Shilstone's 0.45 power chart (Reprinted from Richardson 2005)

In the chart, the maximum density line is drawn from the origin to the intersection of the 100 percent passing line with either the nominal maximum size or the maximum size. A gradation following the maximum density line down to either the 2.36-mm (Shilstone 1990) sieve or the 1.18-mm (Shilstone 1993) sieve where it dips below the reference line is considered to be optimum.

Recommendations Based on Shilstone Method

Holland (1990) first came up with the ideas to specify an "8-18" band in the IPR chart, meaning the total percentage of fine and coarse aggregate on any size should be between 8 and 18 percent. Harrison (2004) suggested to use the IRP and CF charts for optimization. He developed an optimum location on the CF chart for slabs-on-ground (Figure 117).

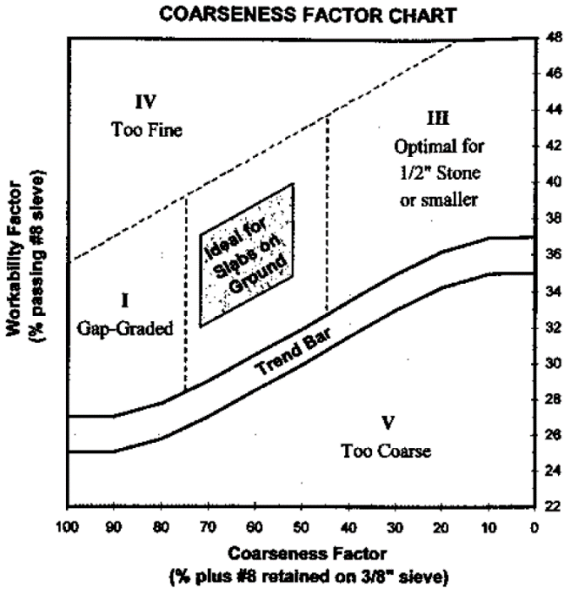

Figure 117 Optimum location on CF chart for slabs-on-ground (Reprinted from Harrison 2004)

The U.S. Air Force adopted Shilstone's design concepts and developed a specification guide. In the guide, the IPR chart with 8-18 band, modified CF chart, and 0.45 power chart are required to be used. The intention to use the band in the IPR chart is to control individual retained percent between 8 and 18 for sieve #30 (0.6 mm) through one size below nominal maximum size, and to keep other sizes below 18 percent. Also, a significant valley (one has more than two sieve sizes between two peaks) is not allowed in the plot. Figure 118 and Figure 119 show examples for an acceptable plot and an unacceptable one, respectively. For the CF chart with construction-related areas (Figure 120), the U.S. Air Force concentrates the Shilstone chart between CF value 30 and 80. They modified Zone II in Shilstone's chart and replaced the five strip areas with three circular areas, which are recommended locations for slip from (A) paving, (B) form and place mechanical paving, and (C) hand replacement. The 0.45 chart (Figure 121) in the design manual is used to check the gradation if doubts still remain after the use of the

IPR and CF chart. Three references line are plotted in the chart, and a good gradation should meander along the top size line.

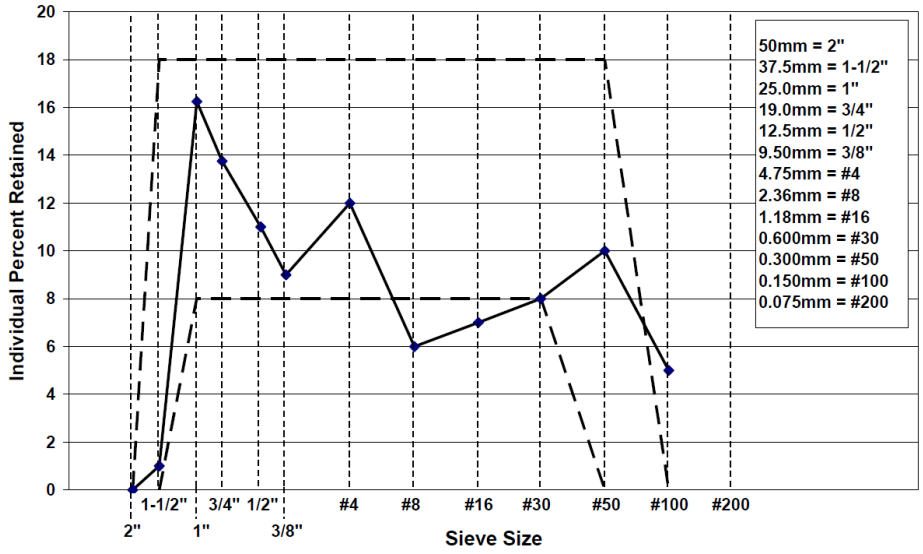

Figure 118 Example of an acceptable mix for U.S. Air Force design (Reprinted from Richardson 2005)

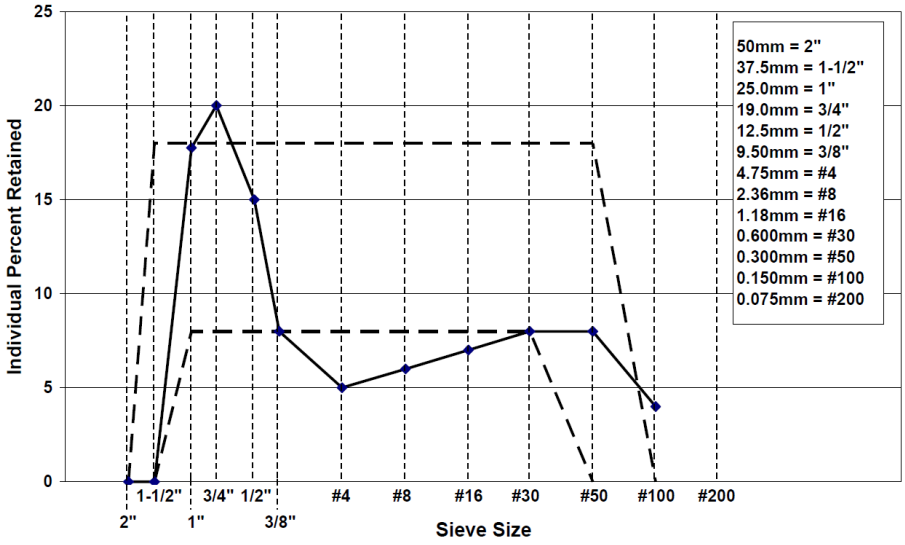

Figure 119 Example of an unacceptable mix for U.S. Air Force Design (Reprinted from Richardson 2005)

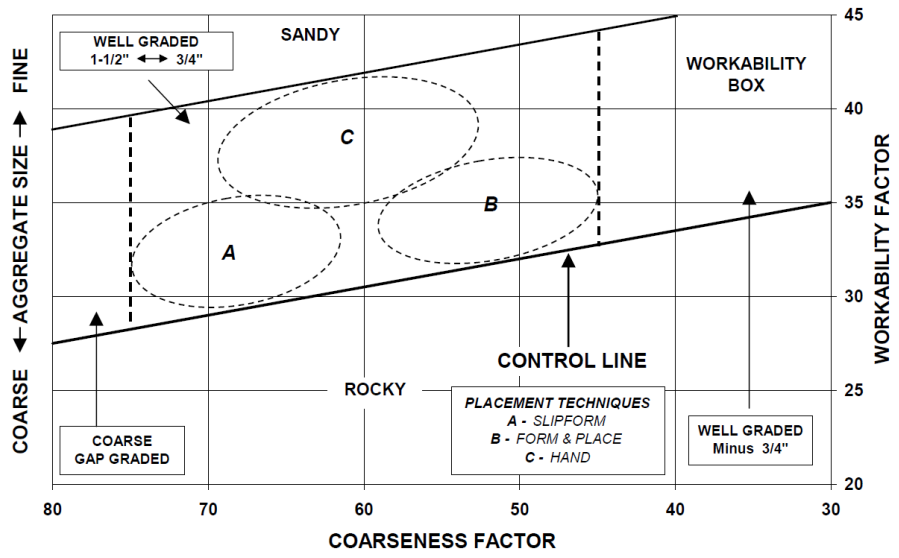

Figure 120 U.S. Air Force aggregate proportioning guide with construction related areas (Reprinted from Richardson 2005)

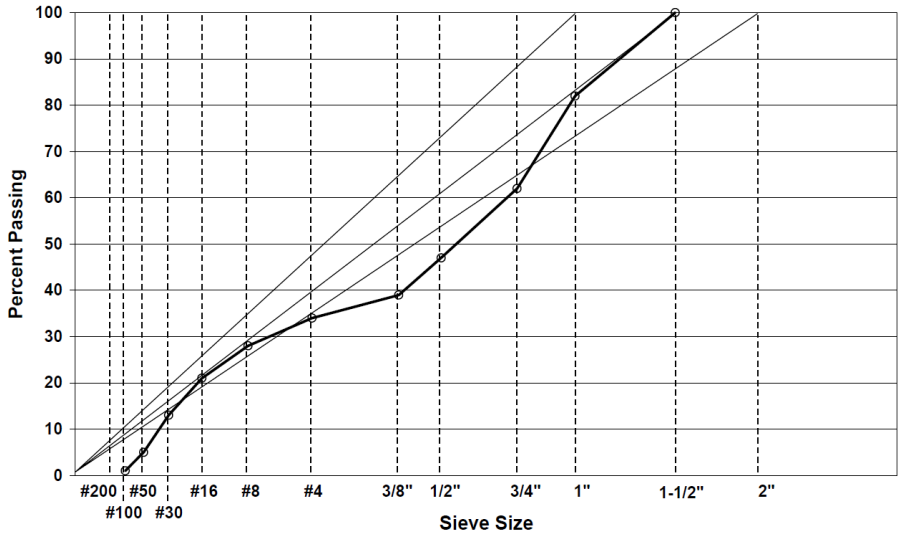

Figure 121 U.S. Air Force 0.45 power chart (Reprinted from Richardson 2005)

APPENDIX B

REVIEW OF FRACTURE MECHANICS OF CONCRETE

The concrete fracture mechanics theory relevant to this study is reviewed below.

NONLINEAR FRACTURE MECHANICS THEORY FOR CONCRETE

Concrete is a quasi-brittle material. In a typical tensile stress-elongation curve for concrete (Figure 122), the first portion of the curve that within a proportional limit is considered linearly elastic. A substantial nonlinearity exists before the load reaches the peak. Within this nonlinearity zone, randomly distributed microcracks have been initiated and developed. These microscracks are localized into a marcocrack which critically propagates at the peak load. After the peak load, strain softening is observed and the crack propagates in a stable manner.

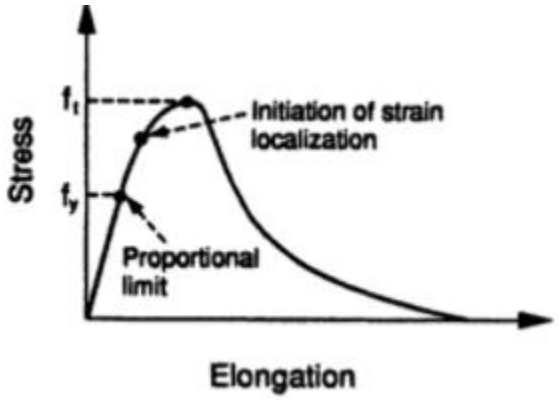

Figure 122 Tensile stress-elongation for a quasi-brittle material (Reprinted from Shah et al. 1995)

The complexity of the constitutive behavior of PCC lies in its nonlinearity. Cracks begin at a crack tip. Although linear elastic fracture mechanics allows the stress to approach to infinitely, a certain range of inelastic zone must exist at the crack tip because infinite stress

cannot be allowed in a real material. The inelastic zone is termed as fracture process zone (FPZ). For metallic materials, the fracture process zone is a yielding zone and is always small. The small FPZ of metallic material allows LEFM to be applied. For a quasi-brittle material such as concrete, the FPZ is fairly big because of the heterogeneous natural of concrete material. For a massive concrete structure like a dam, LEFM might still be valid because the FPZ is negligibly small compared to the size of the structure. However, the FPZ cannot be ignored for those smaller structures like pavement, and especially, the conventional laboratory sized specimens. Therefore, nonlinear fracture mechanics (NLFM) theory is needed to explain the fracture behaviors of those concrete structures.

Consider an effective quasi-brittle crack with an initial crack length of A_0 in Figure 123. Ahead of the initial crack tip presents the FPZ where the toughening mechanisms are modeled by a cohesive pressure acting on the crack surfaces. Some toughening mechanisms in fracture zone are crack shielding, crack deflection, aggregate bridging, crack surface roughness-induced closure, crack tip blunted by void and crack branching (Shah et al. 1995) The cohesive pressure is a function of crack separation displacement w. At the end of the fracture process zone the cohesive pressure is the theoretical tensile strength f_t. When the crack in Figure 123 is subjected to loading, the energy release rate G_q at the tip of the crack may be divided into two portions: (i) the energy rate consumed for creating new fracture faces and (ii) the energy rate to overcome the cohesive pressure during crack opening. The expression can be written as:

$$G_q = G_{Ic} + G_\sigma \tag{139}$$

Where G_{Ic} is called the critical energy release, which can be calculated based on LEFM.

And

$$G_\sigma = \int_0^{w_t} \sigma(w)dw \tag{140}$$

Where w_t is the crack separation displacement at the initial crack tip.

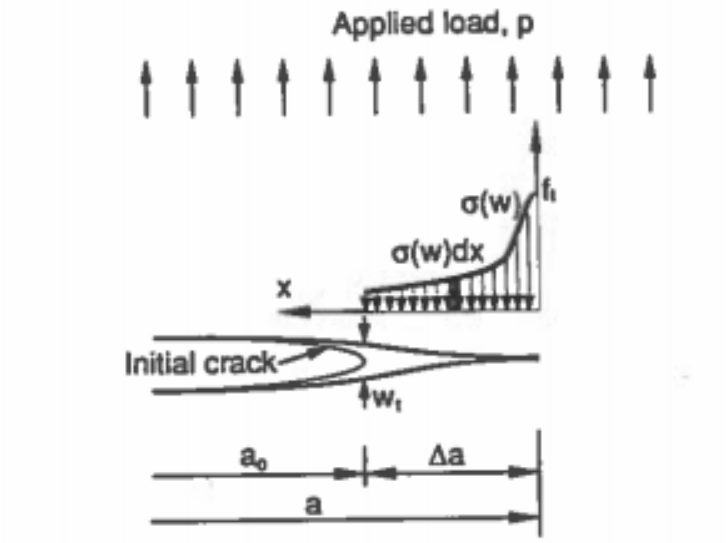

Figure 123 Modeling of quasi-brittle crack (Reprinted from Shah et al. 1995)

The existing nonlinear fracture mechanics models can be classified into two categories based on which term in Equation (139) is ignored. A fictitious crack approach is based on the Dugdale-Barenblatt mechanism by neglecting G_{Ic} term, while an effective-elastic crack approach uses the Griffith-Irwin mechanism by assuming $\sigma(w) = 0$.

Fictitious Crack Approach

The fictitious crack approach assumes that the energy for creation of new fracture surfaces is negligibly small compared to that for overcoming the cohesive pressure. Therefore, in Equation (139) the G_{Ic} term can be discarded. Equation (139) is reduced to:

$$G_q = G_\sigma = \int_0^{w_t} \sigma(w)dw \qquad (141)$$

The existing models using a fictitious crack approach for concrete are fictitious crack model by Hillerborg et al. (1976) and crack band model by Bažant and Oh (1983), which are reviewed below.

Fictitious Crack Model by Hillerborg

Hillerborg et al. (1976) were the very first ones to use a fictitious crack approach to model fracture of concrete. In their model, the post peak fracture softening can be characterized with a stress-crack opening curve when a concrete plate is subjected to uniaxial tension (Figure 124). The area under the entire curve is denoted as G_F. G_F is given by

$$G_F = \int_0^{w_c} \sigma(w)dw \tag{142}$$

Where w_c is the crack opening displacement associated with 0 stress in the stress-crack opening curve.

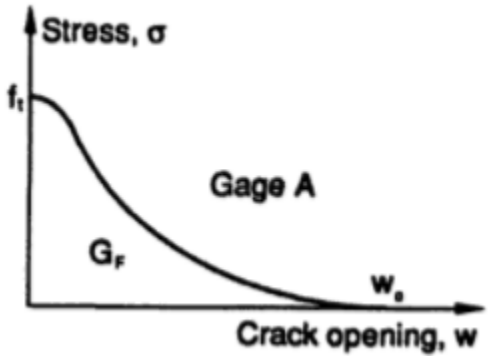

Figure 124 Stress-crack opening curve (Reprinted from Hillerborg et al. 1976)

The softening stress-crack opening curve is assumed to be independent of structural geometry and can be completely determined when the theoretical tensile strength, f_t, the facture toughness G_F and shape of the curve are known. The softening stress-crack opening curve is

considered a material property. Hillerborg et al. (1976) defined another concrete material fracture property, characteristic length l_{ch}, by combining f_t and G_F:

$$l_{ch} = \frac{EG_F}{f_t^2} \tag{143}$$

From their observations, the l_{ch} value for concrete approximately ranges from 100 mm to 400 mm while the length of the fracture process zone when the initial crack tip is fully separated (i.e., $w_t = w_c$) in concrete is between $0.3l_{ch}$ and $0.5l_{ch}$. The developed fictitious crack model was used in a finite element analysis to successfully predict fracture behavior concrete (Hillerborg et al. 1976).

Crack Band Model by Bažant and Oh

Bažant and Oh (1983) used a band of uniformly and continuously distributed microcracks to model the fracture process zone of concrete (Figure 125(a)). The crack band has a fixed width, which is denoted as h_c. During the crack propagation, the microcrack progressively develops within the band with a stress-strain curve in Figure 125(b).

The energy consumed due to the crack propagation per unit area of the crack band G_f is expressed:

$$G_f = h_c(1 + \frac{E}{E_t})\frac{f_t^2}{2E} \tag{144}$$

Where E is the modulus of elasticity, E_t is the strain-softening modulus and f_t is theoretical tensile strength

To estimate h_c, Bažant and Oh (1983) used an empirical equation:

$$h_c = n_a d_a \tag{145}$$

Where d_a is the maximum aggregate size in concrete, and n_a equals to 3 for concrete

The crack band model successfully explained the size effect: the failure stress of a concrete structure was predicted to decrease with an increase in structure size. Finite element

approach has also been applied in prediction of fracture response of concrete using the crack band model (Bažant and Oh 1983).

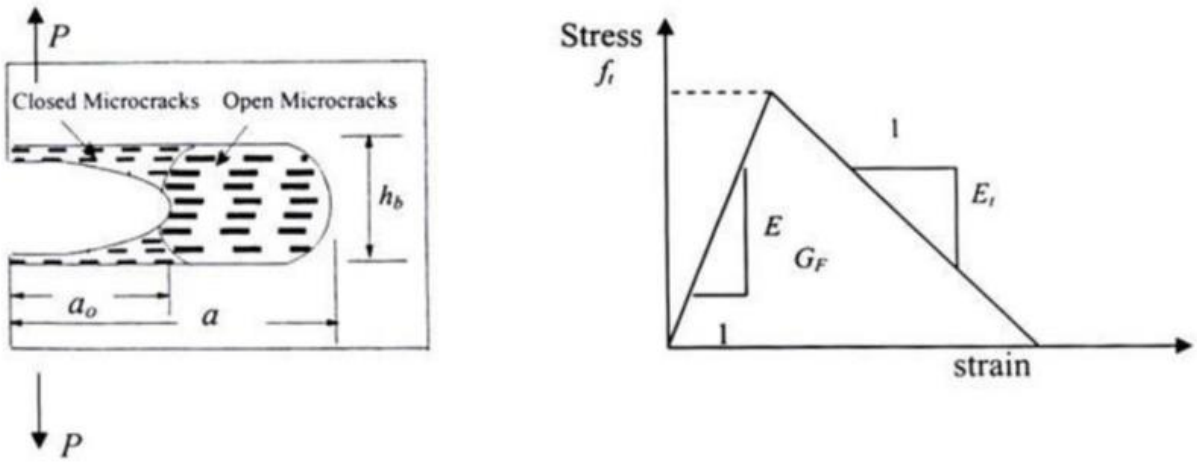

(a) A microcrack band fracture (b) Stress-strain curve for the microcrack band

Figure 125 Crack band model of concrete (Reprinted from Shah et al. 1995)

Effective Elastic Crack Approach

The effective crack approach neglects the G_σ term in Equation (139) by assuming the cohesive pressure is zero: $\sigma(w) = 0$. In this approach, an equivalent, traction-free elastic crack is used to model the fracture process zone through linear elastic fracture mechanics. The equivency between the effective elastic crack and the actual crack is prescribed explicitly in each model. The energy release rate for an effective-elastic crack is expressed as:

$$G_q = G_{Ic} \tag{146}$$

Most of the effective elastic crack approaches use two fracture parameters as the fracture criterion because the structural size and geometry dependent nature of the effective elastic crack. Those effective elastic crack approaches are summarized as below.

Size Effect Model by Bažant and Kazemi

Bažant and Kazemi (1990) considered a series of geometrically similar structures with a constant ratio of initial crack length A_0 to characteristic dimension of a structure D and an unchanged the third dimension (i.e., thickness). The nominal stress at failure (i.e., normal strength) for the geometrically similar structure is expressed:

$$\sigma_{Nc} = \frac{c_n P_c}{tD} \tag{147}$$

Where P_c is the peak load, t is the thickness of the structure, and c_n is the structure type coefficient. For a beam, $c_n = 1.5\frac{S}{D}$ (S is the span and D is the depth).

Bažant and Kazemi (1990) assumed that the fracture energy dissipated at failure is associated with structural dimensions and size of fracture process zone, so they further proposed:

$$\sigma_{Nc} = Bf_t[\frac{D}{D_0} + 1 + L_1\left(\frac{D}{D_0}\right)^{-1} + L_2\left(\frac{D}{D_0}\right)^{-2} + \cdots]^{-1/2} \tag{148}$$

Where, D_0, L_1, $L_2 \cdots$ are constants and f_t is the theoretical tensile strength of the material

When $\frac{D}{D_0} < \frac{1}{20}$, Equation (148) can be reduced to:

$$\sigma_{Nc} = \frac{Bf_t}{\sqrt{1 + \frac{D}{D_0}}} \tag{149}$$

The constants B and D_0 can be determined based on the effective-elastic crack approach using the following approach:

The critical energy release rate G_{IC} is obtained from LEFM:

$$G_{IC} = \frac{K_{Ic}^2}{E} = \frac{\sigma_{Nc}^2 \pi A_c}{D} g_1^2\left(\frac{A_c}{D}\right) = \frac{\sigma_{Nc}^2 D}{E{c_n}^2} g(\frac{A_c}{D}) \tag{150}$$

Where A_c is the critical crack length: $A_c = A_0 + \Delta A_c$ (ΔA_c is the effective crack extension) and $g(\frac{A_c}{D})$ is the geometric function.

The critical energy release rate and the critical crack extension for an infinitely large structures are used as fracture parameters for a quasi-brittle material, which are defined:

$$G_f = \lim_{D\to\infty} G_{IC} \tag{151}$$

$$c_f = \lim_{D\to\infty} \Delta A_c \tag{152}$$

Where G_f and c_f represent the critical energy release rate and the critical crack extension for an infinitely large structure, respectively.

After some algebra:

$$G_f = \frac{B^2 f_t^2 D_0}{E c_n^2} g(\frac{A_0}{D}) \tag{153}$$

And:

$$c_f = \frac{g(\frac{A_0}{D})}{g'(\frac{A_0}{D})} D_0 \tag{154}$$

The nominal strength of structures can be obtained by replacing B and D_0 with Equation (153) and Equation (154):

$$\sigma_{Nc} = c_n[\frac{EG_f}{g'\left(\frac{A_0}{D}\right) c_f + g\left(\frac{A_0}{D}\right) D}]^{1/2} \tag{155}$$

Equation (155) is effective in explaining the size effect on nominal failure stress by Bažant (1989)(Figure 126). When the structure size is small, the nominal strength is conventionally specified by a strength criterion. When the structure size is very large, the single parameter failure criterion based on LEFM can be applicable. Equation (155) predicts the failure strength of intermediate sized structures, which is within the size range to apply nonlinear fracture mechanism. Bažant and Kazemi (1990) defined a brittleness number β_b

$$\beta_b = \frac{D}{D_0} \tag{156}$$

When $\beta_b < 0.1$, the strength criterion may be used. For $0.1 < \beta_b < 10$, the NLFM equation should be use. The LEFM criterion may be used when $\beta_b > 0.1$.

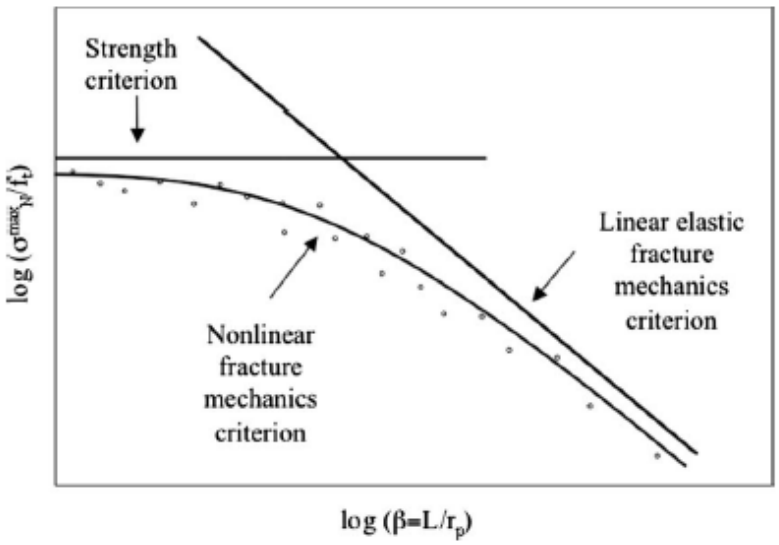

Figure 126 Size effect on nominal failure stress by Bažant (1989)

APPENDIX C

SELECTIVE TESTS TO COMPARE MORE RIGOROUS CLASS P MIXES AND LESS RIGOROUS CLASS P MIXES

The designed class P concrete in this research (the 0.40_520 series) adopted a #4 coarse aggregate gradation instead of using a #2 or #3 gradation which is specified in Texas (2014). Because there is a little difference between the #3 and #4 gradation, it was expected that the difference in terms of mechanical properties (i.e., compressive strength, flexural strength) between mixes made with #3 coarse aggregate (considered as more rigorous class P mixes) and those made with #4 coarse aggregate (considered as less rigorous class P mixes) is not significant. To verify this assumption, a set of RAP-PCC samples made with #3 virgin aggregate gradation was tested. Table 61 shows the strength comparison between the mixes made with #3 coarse aggregate and those made with #4 coarse aggregate. Table 61 clearly shows the difference between the two sets of mixes was insignificant (with a same order of coefficient of variance of the tests). Therefore, what has been concluded regarding the RAP-PCC strengths analysis is considered valid for the more rigorous class P mixes.

Table 61 Comparison of selected mechanical properties between RAP-PCC made with #3 virgin coarse aggregate and RAP-PCC made with #4 virgin coarse aggregate

Sample	Slump (mm)	Air void (%)	fc (MPa)		MOE (GPa)		MOR (MPa)		STS (MPa)	
			7-day	28-day	7-day	28-day	7-day	28-day	7-day	28-day
0.40_520_40SA (#4)	65	3.0	18.60 (7%)	26.97 (4%)	22.61 (3%)	26.13 (3%)	3.28(8%)	3.96 (2%)	3.19 (3%)	3.92 (7%)
0.40_520_40SA-(#3)	75	3.5	18.83 (5%)	25.39 (2%)	22.79 (2%)	24.48 (7%)	3.45(4%)	3.98 (0.1%)	3.05 (6%)	3.85 (0.4%)
Difference (%)	-	-	-1.22%	+ 6.20%	-0.76%	+ 6.73%	-5.10%	-0.46%	+ 4.29%	+1.91%

The coefficient of variance is shown in the parenthesis.

APPENDIX D

RAP-PCC TRIAL MIXES TEST (THE 0.45_656_HOU SERIES)

A series of trial mixes with 0.45 water/cementitious (w/cm) ratio and 389 kg/m^3 cementitious content was initially designed. Table 62 presents the mix designs for the trial mixes. The 389 kg/m^3 cementitious content was still within the TxDOT specification for class P concrete. The class F fly ash was added to replace 20 percent of cement on the weight basis. The amount of mid-range water reducer added was 1.3 ml per 1kg cementitious materials, and the amount of air entraining agent was selected as 0.2 ml per 1kg of cementitious to get an air content of 5.0 percent. In this trial mixes, only HOU was introduced into the mixture as a virgin coarse aggregate replacement. The replacement levels for the trial mix were selected as 20 percent, 40 percent, 70 percent, and 100 percent, and all of them were based on the volumetric fraction of the total coarse aggregate.

Table 62 Mix design for the 0.45_656 mixes

Ingredient	0.45_656_ REF	0.45_656_ 20HOU	0.45_656_ 40HOU	0.45_656_ 70HOU	0.45_656_ 100HOU
Cement (kg/m^3)	311	311	311	311	311
Fly Ash (kg/m^3)	78	78	78	78	78
Virgin coarse aggregate (kg/m^3)	1058	827	606	292	0
Coarse RAP (kg/m^3)	0	207	404	682	939
FA (kg/m^3)	554	570	586	610	635
Water Reducer (ml/m^3)	503	503	503	503	503
Air Entraining Agent (ml/m^3)	76	76	76	76	76
Water (kg/m^3)	175	175	175	175	175

The fresh concrete properties (i.e., slump and percent air content) and the 7-day, 28-day and 56-day hardened concrete properties (i.e., CS, MOE, MOR and STS) were tested according to the corresponding standards. The test results are presented below:

FRESH CONCRETE TEST RESULTS

Figure 127 shows the results for the slump and percent air voids of the 0.45_656 series. From Figure 127(a), replacing virgin coarse aggregate by HOU with varying replacement levels increased the mixture slump significantly. When the RAP replacement level ≥40 percent, the slump became extremely high. There is no doubt that such a high slump would result in serious segregation problems, so more reasonable w/cm ratio (0.40) and cementitious content (520 lb/cy) were used in the modified mix design for the detailed testing. Figure 127(b) shows a decreasing trend of air content with increasing levels of RAP replacement in the mix.

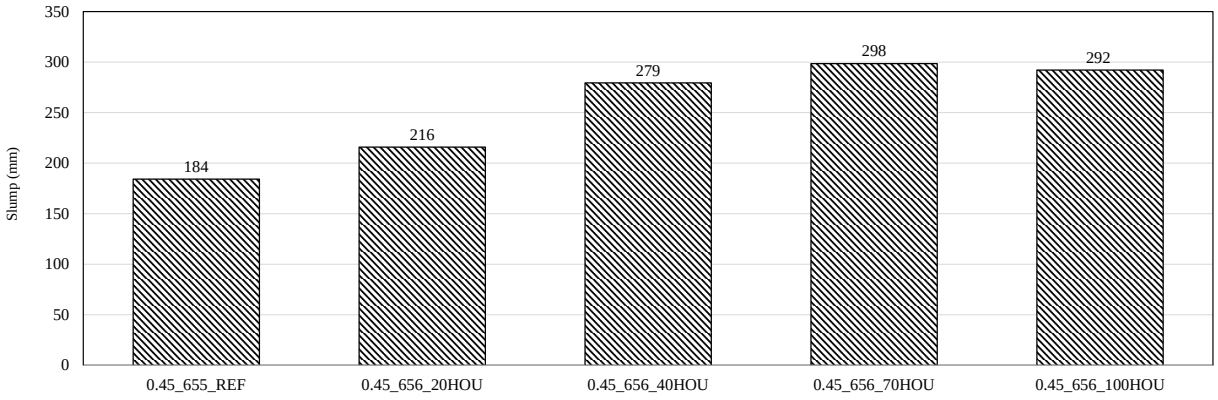

(a) Slump

Figure 127 Fresh properties of the 0.45_656_HOU mixture series

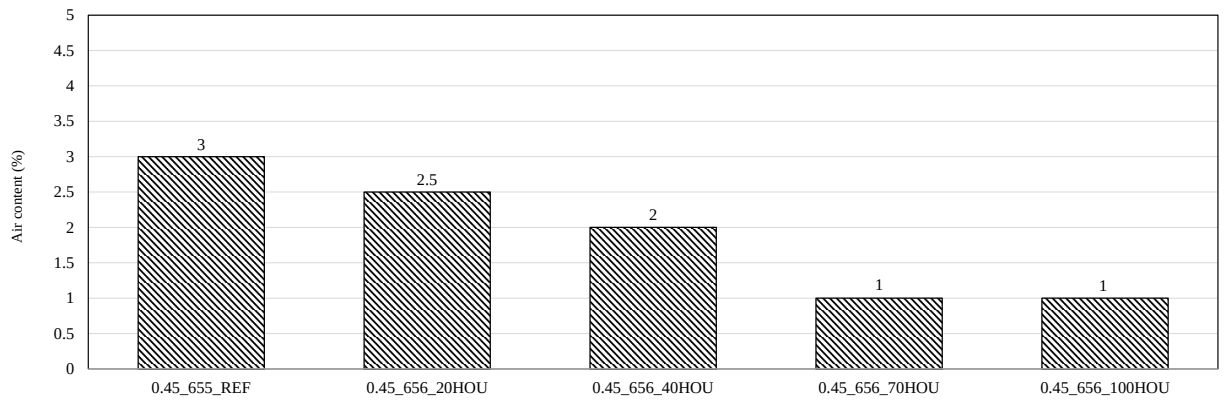

(b) Percent air content

Figure 127 Continued

HARDENED CONCRETE TEST RESULTS

Compressive Strength

Figure 128 plots the absolute compressive strength values, the percentage reduction of strength in comparison with reference mix and the rate of increase of strength over time. Results show that the higher the amount of RAP in the mix, the higher the reduction of the compressive strength is, irrespective of testing age. Figure 128(b) shows that RAP replacement of 70 percent and 100 percent has caused more than 50 percent reduction in compressive strength in comparison with the reference mix. Therefore, RAP replacement more than 40 percent is considered to be impractical in the field. Based on the literature review on previous research (presented in Chapter II), the other researchers have also recommended the similar practical level of RAP replacement (Brand et al. 2012). As a result, it was decided to limit the RAP replacement level to no more than 40% for all the follow-up detailed testing. Regarding the rate of strength increase (Figure 128(c)), almost all the samples had higher strength improvement from 7 day to 28 day than 28 day to 56 day, and when the RAP replacement were at high levels (i.e., 70–100 percent), the strength increase from 28 days to 56 days became negligible. The rate of

compressive strength increase over time (7 to 56 days) for the RAP concrete (irrespective of replacement level) is invariably lower than that at reference concrete.

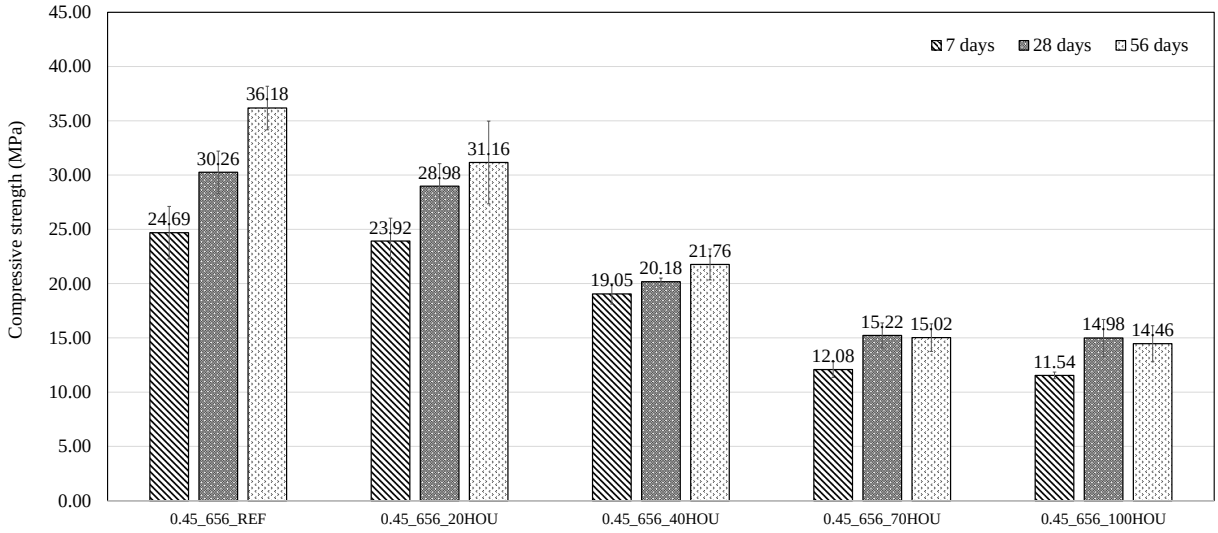

(a) Compressive strength

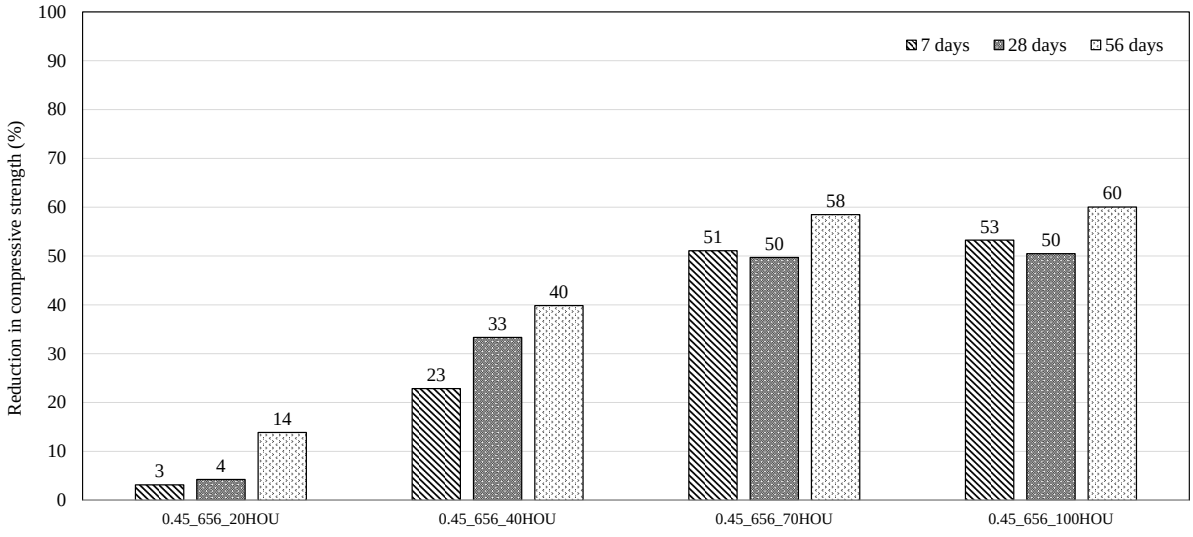

(b) Percentage reduction in comparison with the reference mix

Figure 128 Compressive strength results for the 0.45_656_HOU mixes

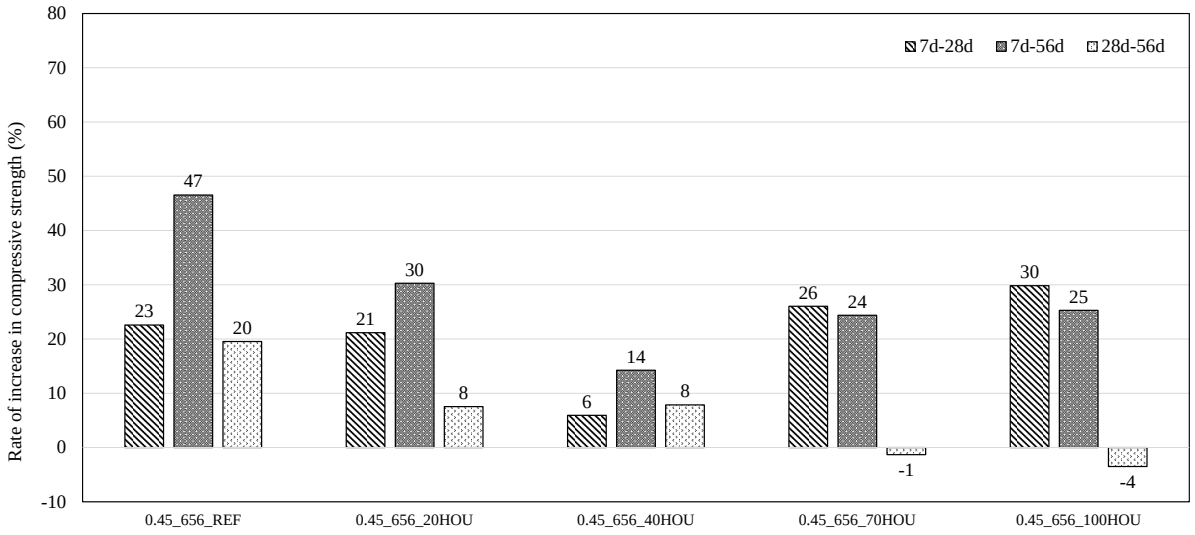

(c)Rate of increase over different time intervals

Figure 128 Continued

Modulus of Elasticity

Figure 129 plots the absolute MOE values, the percentage reduction of MOE in comparison with the reference mix, and the rate of increase of MOE over time. The inclusion of RAP with varying replacement levels in the concrete mix reduced the MOE dramatically (Figure 129(a)). Especially when the replacement level exceeded 40 percent, the reduction of MOE was found to be more than 35 percent (Figure 129(b)). For the rate of increase of MOE over time, a clear trend was not obtained. Although the absolute value of RAP concrete MOE is lower than reference concrete, the rate of increase of MOE over time is either comparable or even greater in RAP concrete than the reference concrete.

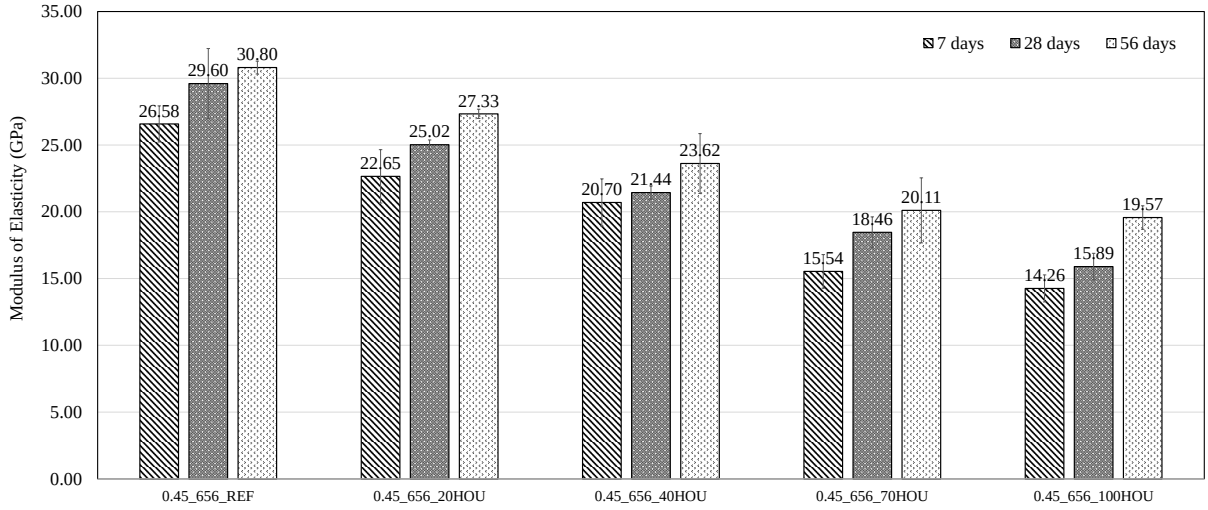

(a) MOE

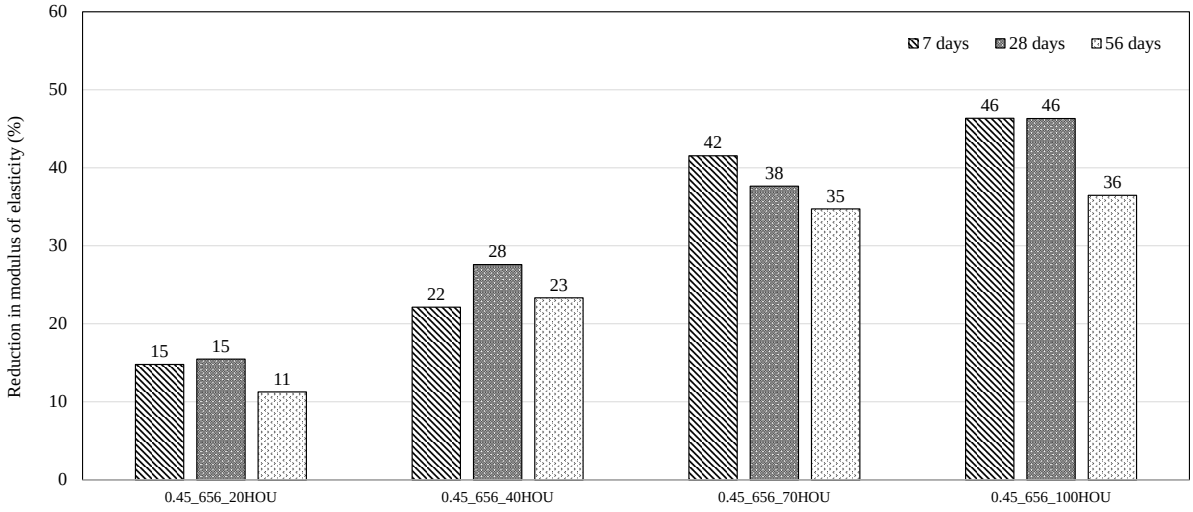

(b) Percentage reduction in comparison with the reference mix

Figure 129 MOE results for the 0.45_656_HOU mixes

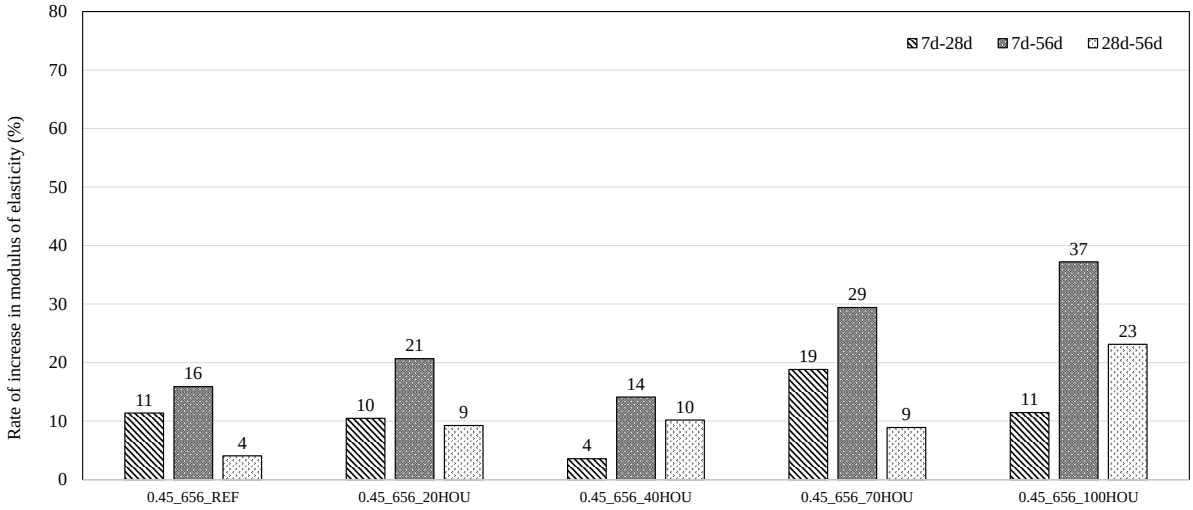

(c) Rate of increase over different time intervals

Figure 129 Continued

MOR

Figure 130 shows the absolute values of MOR, the percentage reduction of MOR in comparison with the reference mix, and the rate of increase of MOR over time. Unlike other mechanical properties, the reduction of MOR for concrete containing RAP was not very significant. The flexural strength of the concrete mixture with the RAP replacement level of 70 percent was similar with that of the concrete mixture with the 100 percent RAP replacement. This indicates the flexural strength may not be significantly affected by the RAP content when the replacement level exceeded a limit. Figure 130(c) shows that a higher flexural strength improvement occurred in the time period of 7 day to 28 days than that between 28 days and 56 days. The rate of increase in MOR of RAP-PCC (7-28 and 7-56 days irrespective of replacement levels) is in general higher than that at the reference concrete.

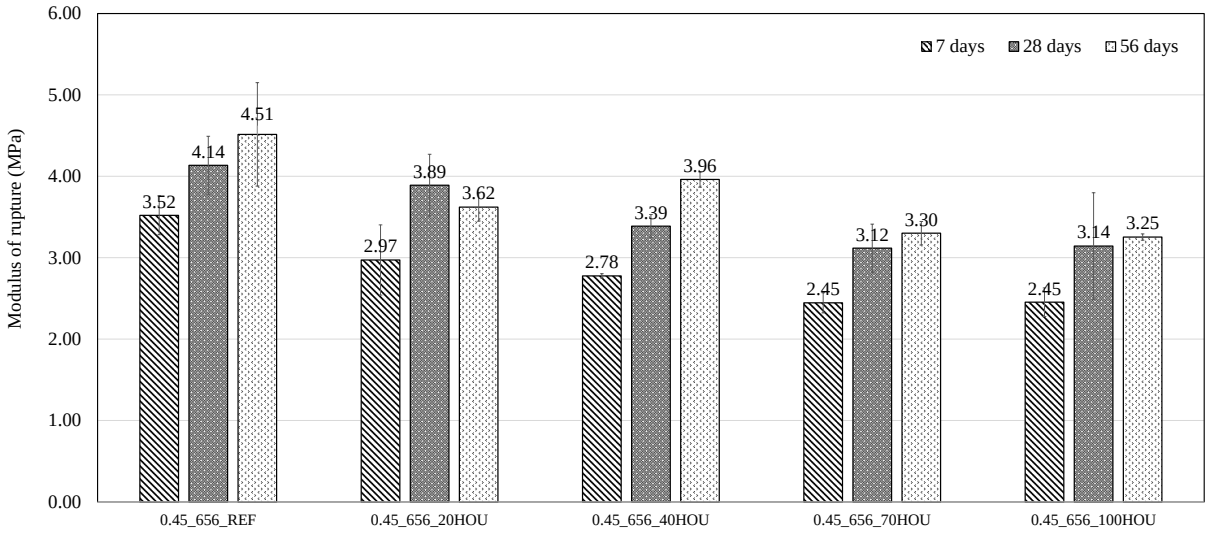

(a) MOR

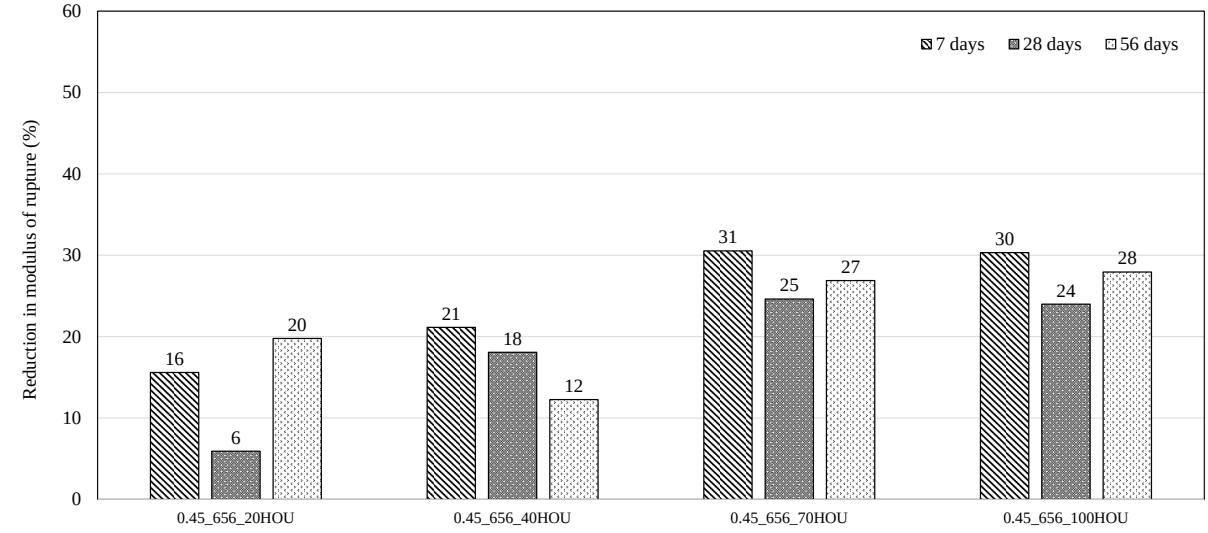

(b) Percentage reduction in comparison with the reference mix

Figure 130 MOR results for the 0.45_656_HOU mixes

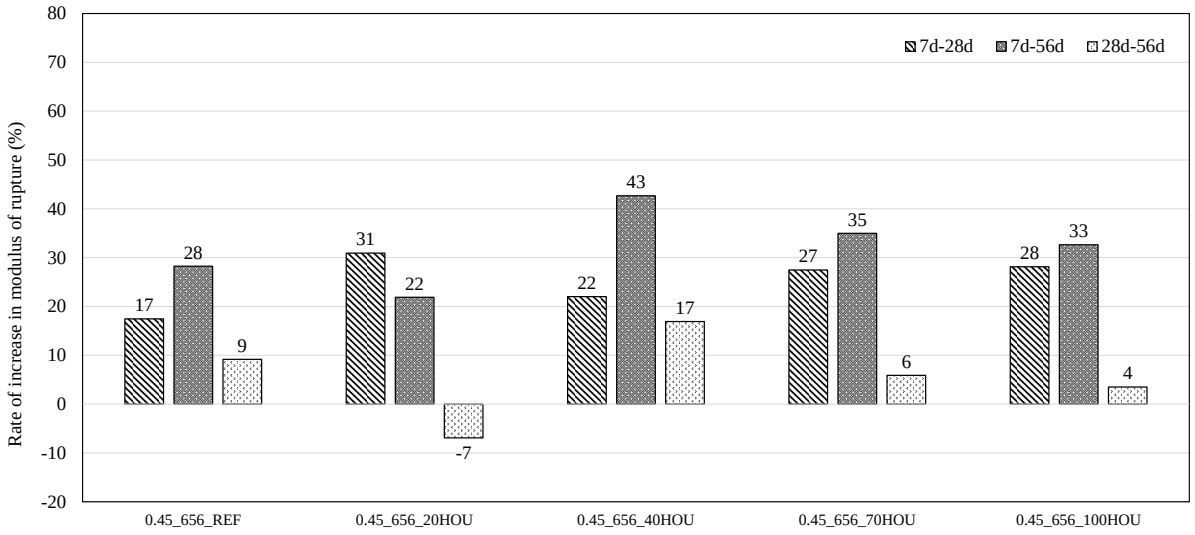

(c) Rate of increase over different time intervals

Figure 130 Continued

STS

Figure 131(a) compares the absolute values of STS, and Figure 131(b) shows the rate of reduction of STS in comparison with the reference concrete. Similar to the results for the compressive strength and MOE, the reduction in STS was significant, especially at the high replacement levels (i.e., 70 percent and 100 percent). Figure 131(c) indicates the STS improved faster during a short term curing process than it did during a long term one. The rate of increase of STS for the RAP concrete mixes (7-28 and 7-56 days, irrespective of level of replacement) is greater than that at the reference concrete (Figure 131(c)).

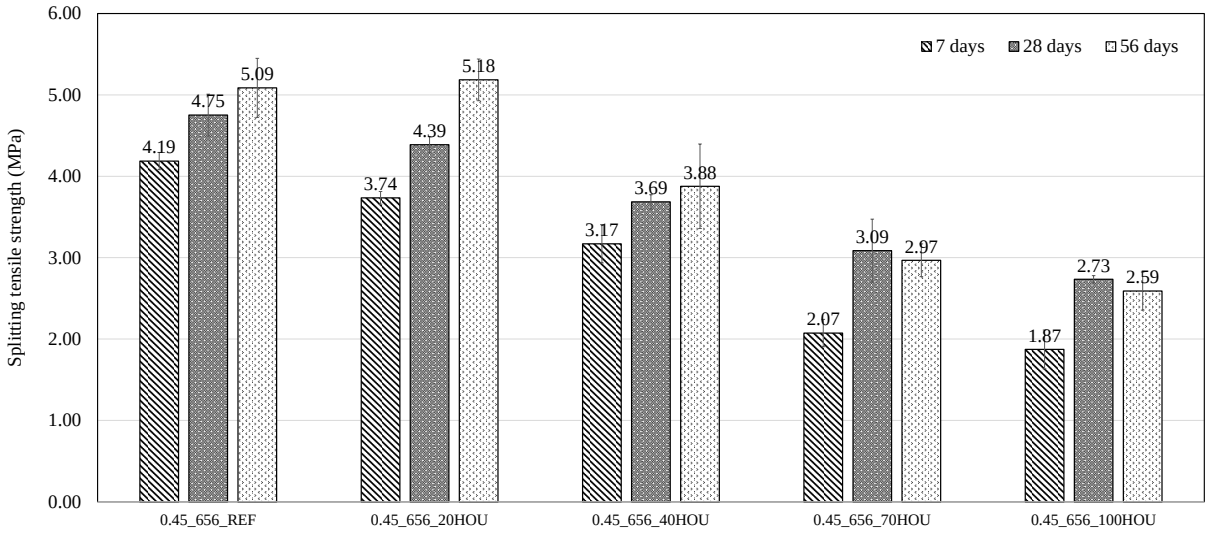

(a) STS

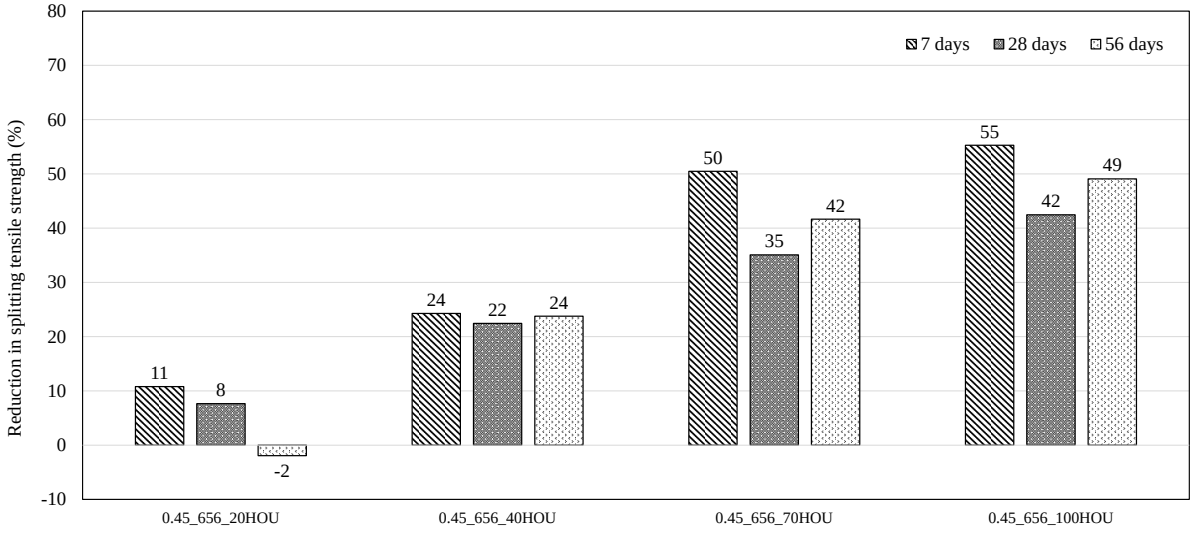

(b) Percentage reduction in comparison with the reference mix

Figure 131 STS for the 0.45_656_HOU mixes

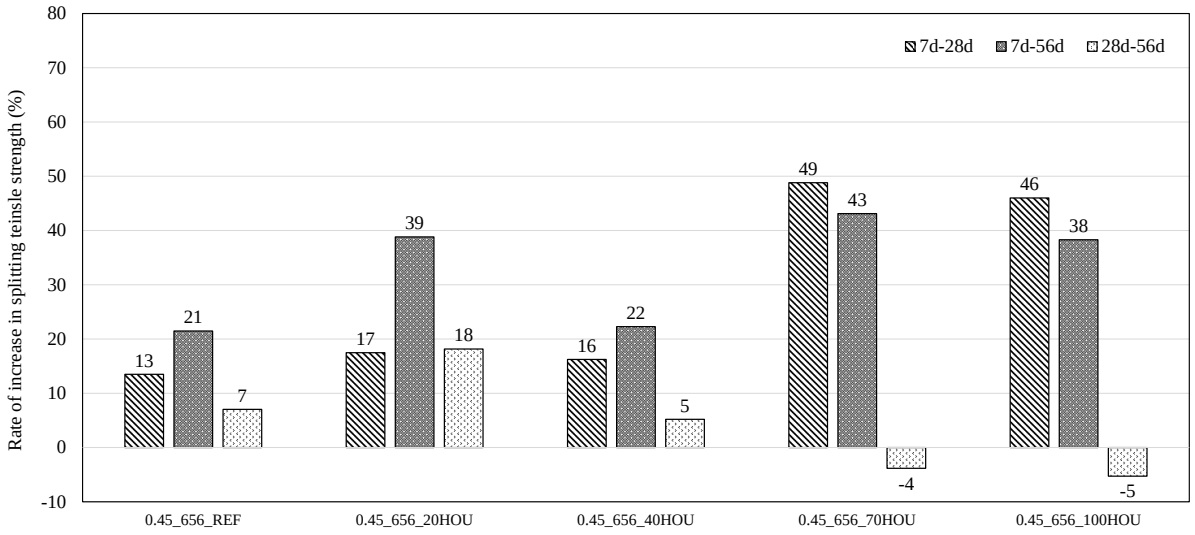

(c) Rate of increase over different time intervals

Figure 131 Continued

FINDINGS FROM THE TRIAL MIXES

The following conclusions are made based on the results from the 0.45_656_HOU series:

- A combination of 0.45 w/cm and 389 kg/cm^3 cementitious content led to extremely high slumps for the RAP-PCC mixes, especially at high RAP replacement level, causing potential segregation issues.
- RAP replacement exceeding 40 percent caused very significant reduction in concrete mechanical properties.
- Unlike other mechanical properties, the reduction of MOR for concrete containing RAP was not that significant.
- The rate of increase of MOR, MOE, and STS for the RAP concrete mixes (7–28 and 7–56 days, irrespective of level of replacement) is greater than that at the reference concrete

It was recommended that reduction of w/cm and cementitious content to 0.40 and 520 lb/cy (389 kg/m^3) respectively will facilitate to overcome the above limitations. Therefore, a 0.40_520 RAP-PCC series with RAP replacement level up to 40% warranted further detailed testing in this dissertation.

APPENDIX E

SENSITIVITY ANALYSIS FOR THE CRITICAL STRESS AND DEFLECTION CALCULATION OF RIGID PAVEMENT

The sensitivity analysis of the critical stress and deflection for different pavement distress is presented in this appendix.

CRITICAL STRESS AND DEFLECTION FOR JPCP CRACKING

Figure 132 presents the results for the bottom-up cracking. The effects of the CoTE and MOE on the maximum stress (occurred at the bottom of the slab) and deflection turn out to be significant. As the CoTE increases, the maximum tensile stress and maximum deflection both increase. When concrete become stiffer (i.e., higher MOE), the maximum tensile stress and maximum deflection increase as well. The effect of the change of CoTE and MOE is more significant within lower varying ranges. The Poisson's ratio and unit weight of the slab material have little effect on the slab tensile stress and deflection. A comparison of each material property on change of stress and deflection is shown in Figure 133. It is concluded that both CoTE and MOE have a very profound effect on maximum tensile stress. The effect of MOE on slab deflection is not as significant as that of CoTE, especially when the MOE values are close to the upper limit of the MOE varying range.

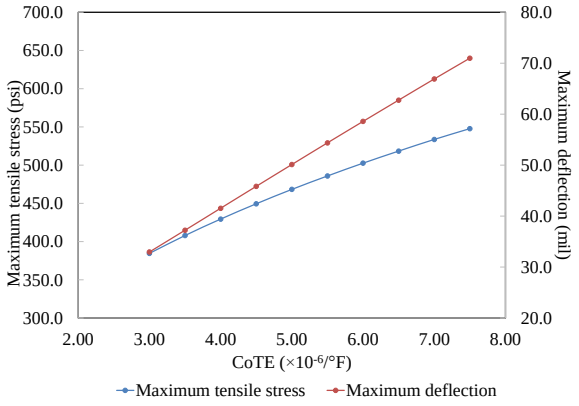

(a) Effect of CoTE

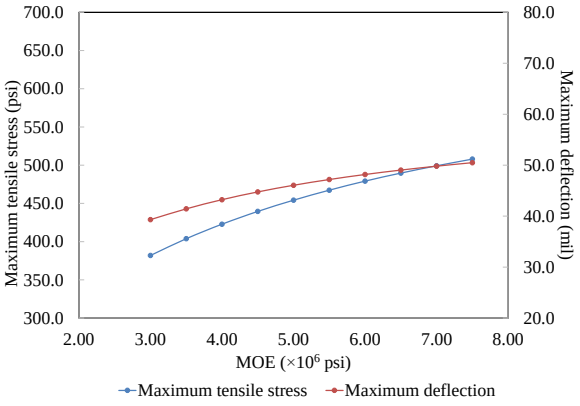

(b) Effect of MOE

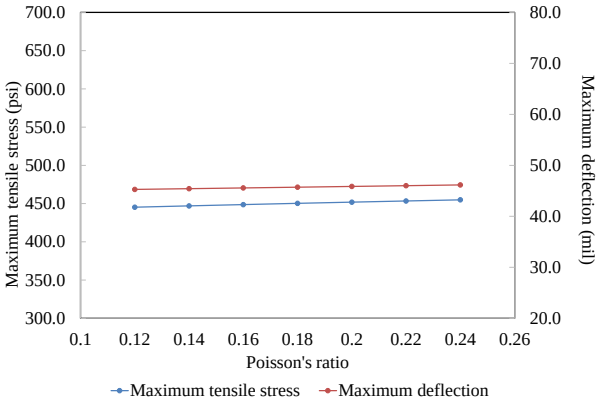

(c) Effect of Poisson's ratio

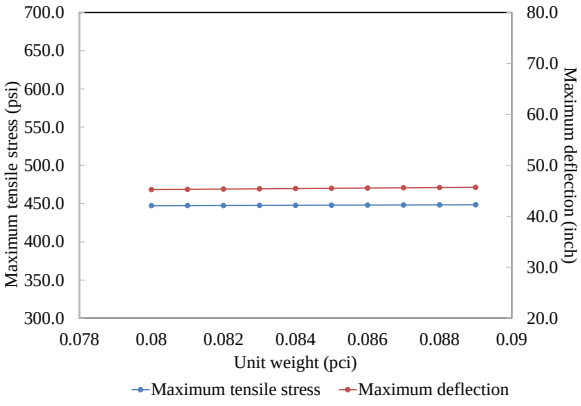

(d) Effect of unit weight

Figure 132 Sensitivity analysis results for JPCP bottom-up cracking

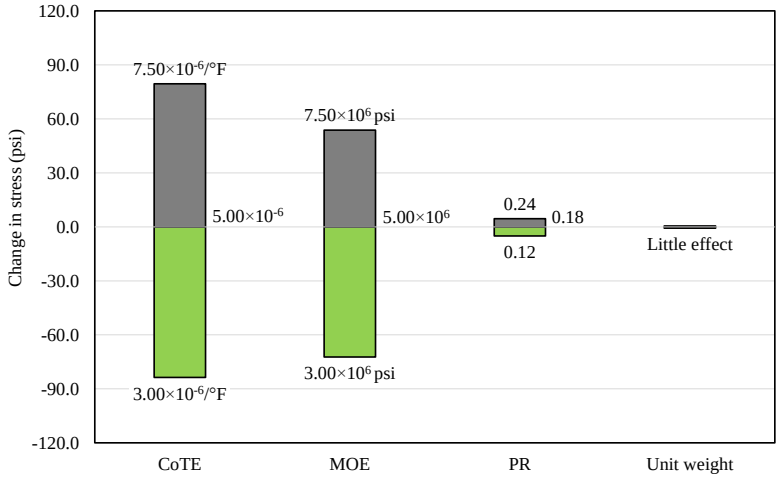

(a) Change in stress

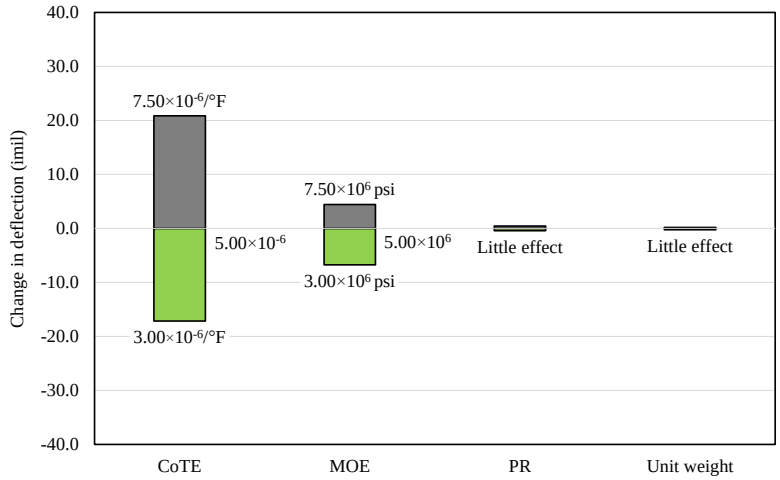

(b) Change in deflection

Figure 133 Comparison of effects of different properties for JPCP bottom-up cracking

The sensitivity analysis results for the top-down cracking are shown in Figure 134. For the maximum tensile stress (occurred at the top of the slab), an increase of CoTE and MOE both cause a higher value. The trend line for the CoTE is linear while that for the MOE is nonlinear (the effect is more significant within lower range of MOE). Regarding the maximum deflection,

increasing CoTE or MOE also increases the deflection nonlinearly. The effect of Poisson's ratio and unit weight on slab maximum tensile stress and deflection is negligible. Figure 135 compares the effect of different properties. The maximum tensile stress in the slab is very sensitive to both CoTE and MOE of the slab material, while the maximum deflection is more related to the CoTE than the MOE.

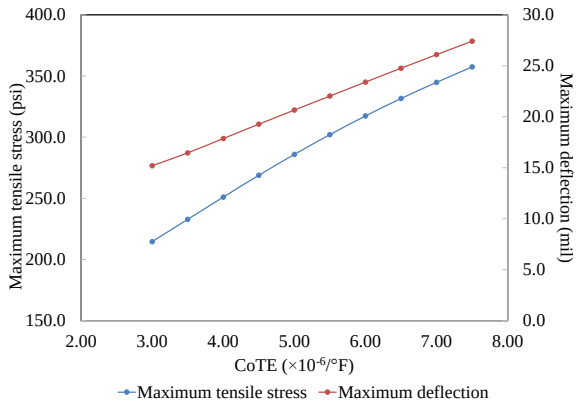

(a) Effect of CoTE

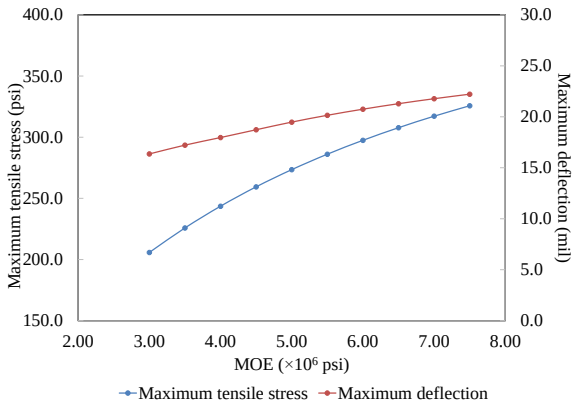

(b) Effect of MOE

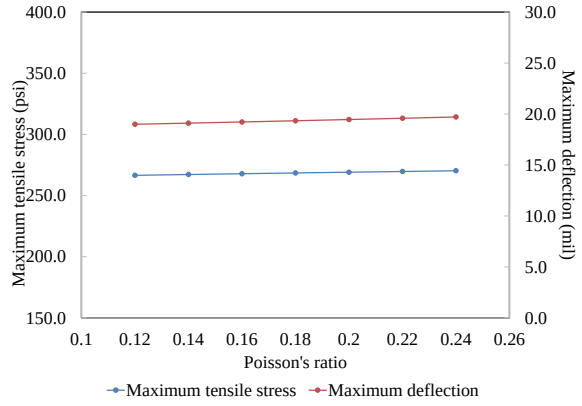

(c) Effect of Poisson's ratio

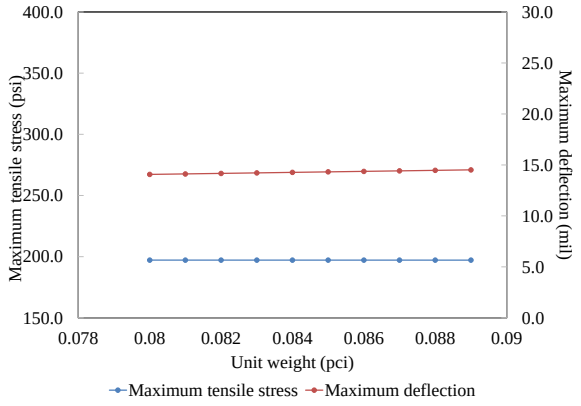

(d) Effect of unit weight

Figure 134 Sensitivity analysis results for JPCP top-down cracking

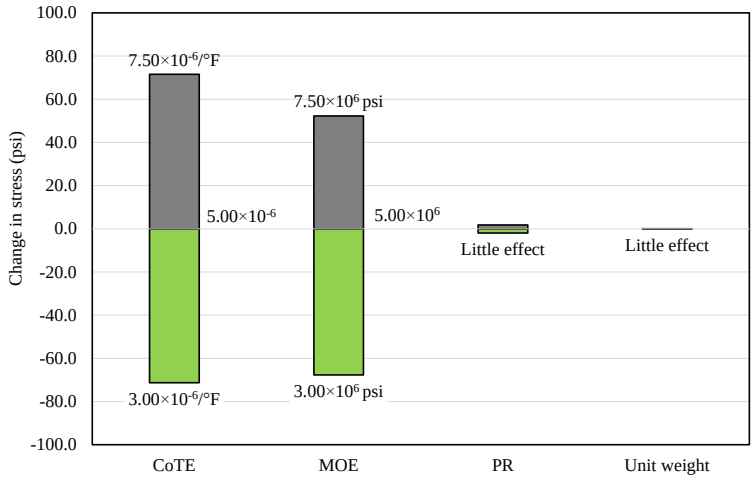

(a) Change in stress

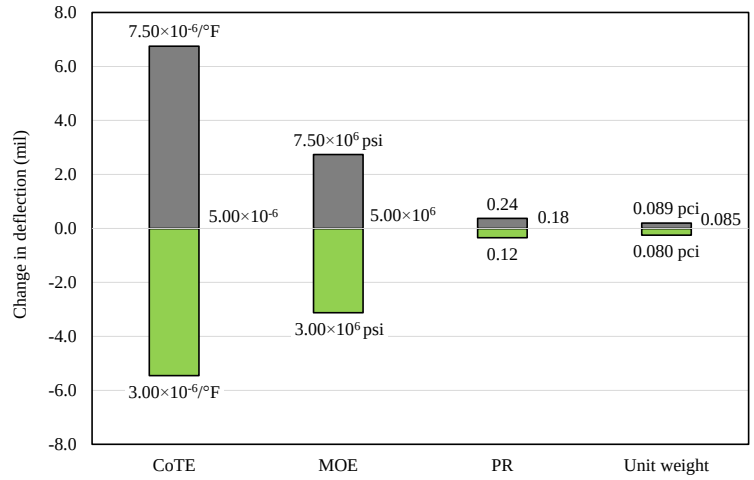

(b) Change in deflection

Figure 135 Comparison of effects of different properties for JPCP top-down cracking

CRITICAL STRESS AND DEFLECTION FOR JPCP FAULTING

The sensitivity analysis results for the faulting are presented in Figure 136 and Figure 137. The results indicate that the difference in corner deflection ($\delta_{loaded} - \delta_{unloaded}$) is only slightly sensitive to MOE; the higher the MOE, the lower the corner deflection difference

between the loaded and unloaded slab. Regarding difference in the square of corner deflection ($\delta^2_{loaded} - \delta^2_{unloaded}$), either decreasing CoTE or increasing MOE would decrease the value. Poisson's ratio and unit weight have negligible effect on both of the difference terms.

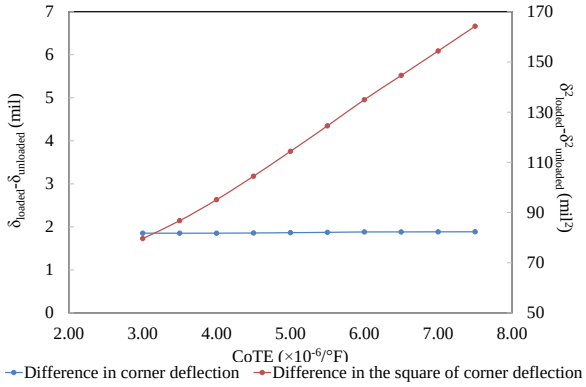

(a) Effect of CoTE

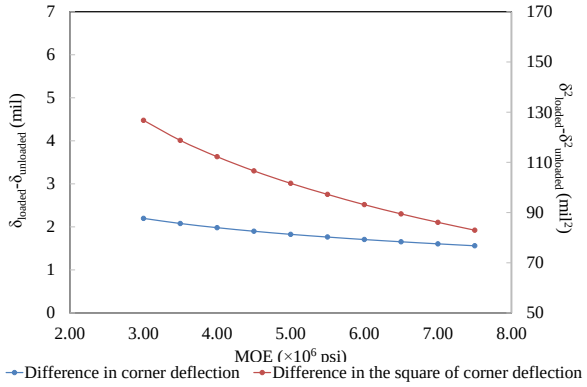

(b) Effect of MOE

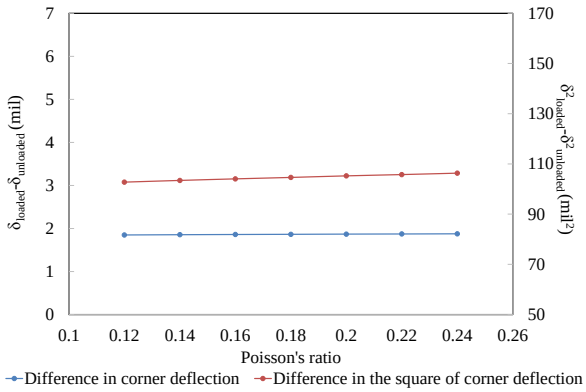

(c) Effect of Poisson's ratio

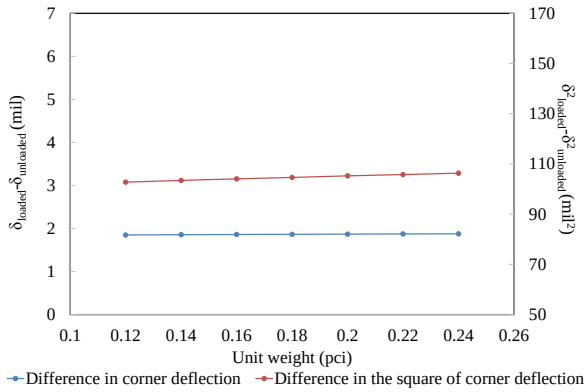

(d) Effect of unit weight

Figure 136 Sensitivity analysis results for JPCP faulting

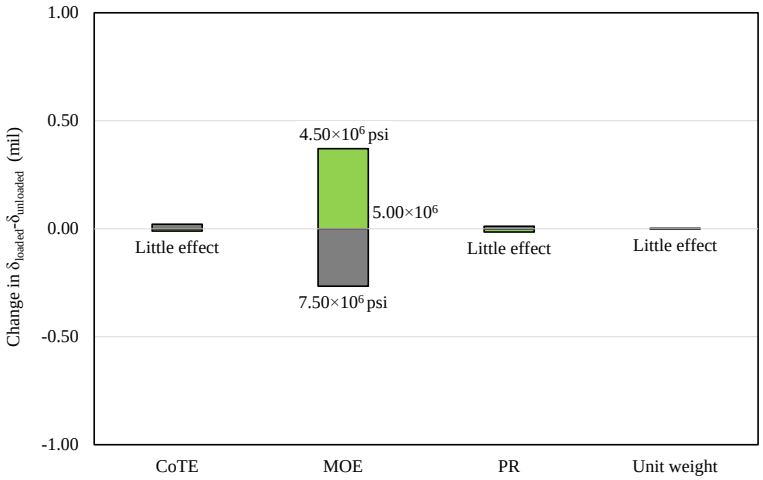

(a) Change in difference of corner deflection

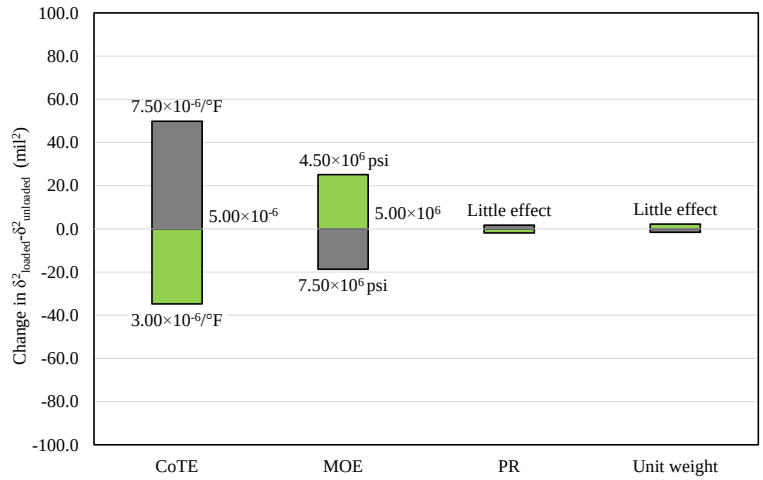

(b) Change in difference of the square of corner deflection

Figure 137 Comparison of effects of different properties for JPCP faulting

CRITICAL STRESS AND DEFLECTION FOR CRCP PUNCHOUT

The results of the sensitivity analysis for the critical stress and deflection related to CRCP punchout are shown in Figure 138. Figure 138 shows that the maximum tensile stress and maximum deflection are not very sensitive to concrete properties (i.e., CoTE, MOE, Poisson's

ratio and unit weight); an increase in either CoTE or MOE would lead to a slightly higher tensile stress but a slightly lower slab deflection. The tensile stress and deflection are, however, dramatically influenced by the LTE. When LTE dropped below 40%, both the slab tensile stress and deflection suffer from a rapid increase. The comparison of each parameter in Figure 139 confirms that the LTE is the dominating factor for CRCP punchout.

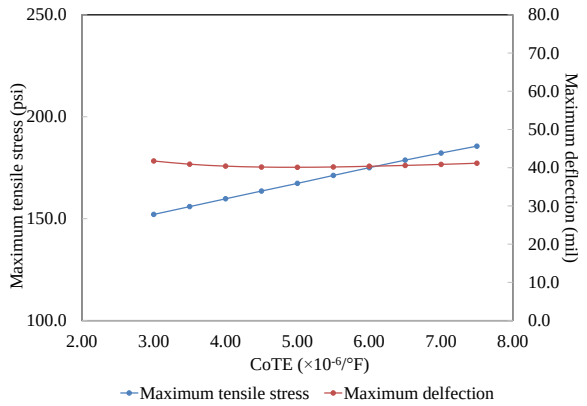

(a) Effect of CoTE

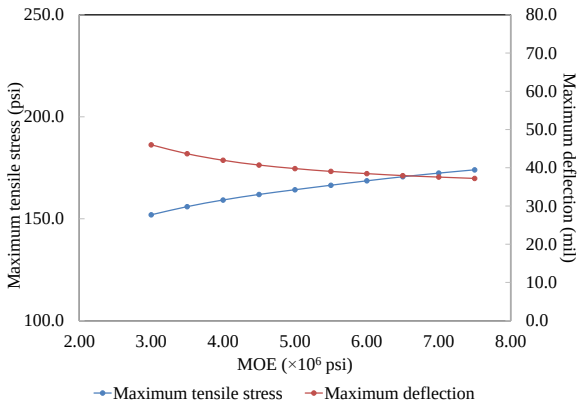

(b) Effect of MOE

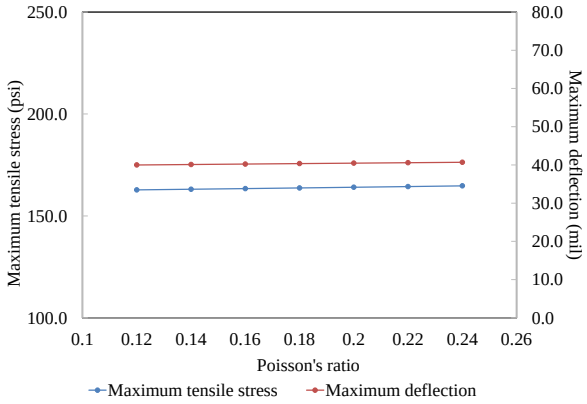

(c) Effect of Poisson's ratio

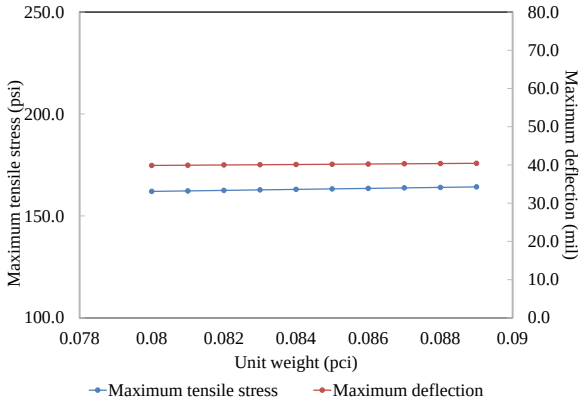

(d) Effect of unit weight

Figure 138 Sensitivity analysis results for CRCP punchout

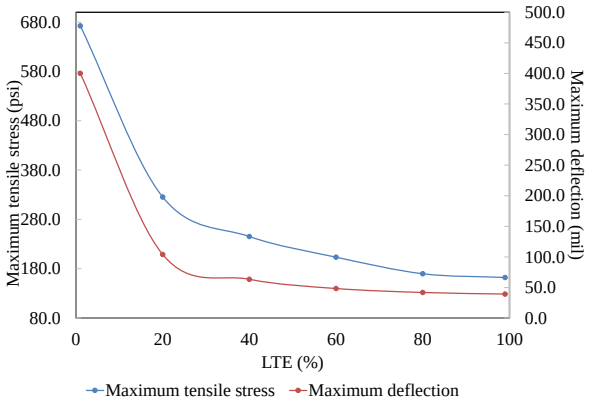

(f) Effect of LTE

Figure 138 Continued

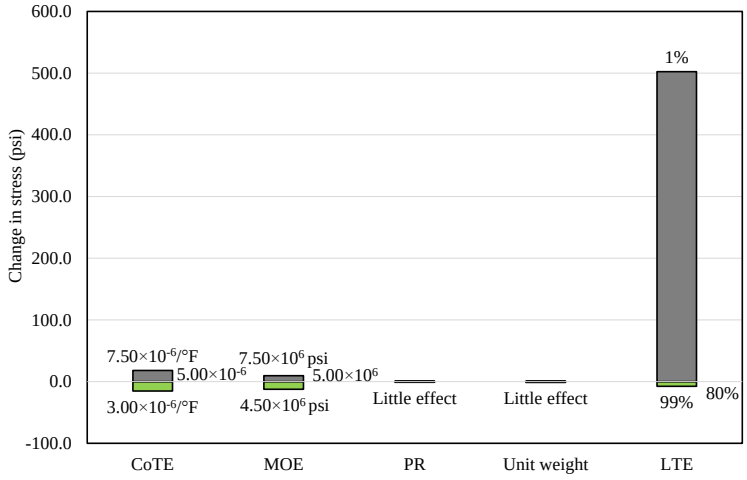

(a) Change in stress

Figure 139 Comparison of effects of different properties for CRCP punchout

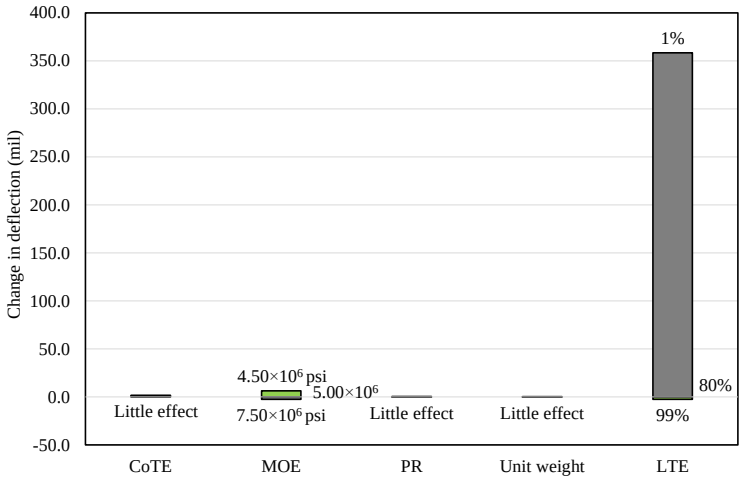

(b) Change in deflection

Figure 139 Continued